“Deciphering the role of RBM10 in development and cancer using a genetic mouse model”

Ana Margarita Maldonado Barragán
Master in Science

Tesi doctoral UPF/2020
Biomedical Sciences Program
Health and Life Science Department

Thesis Directors:
Dr. Francisco X. Real
Dr. Miriam Marqués

Epithelial Carcinogenesis Group
Cancer Cell Biology Program
Centro Nacional de Investigación Oncológicas (CNIO)

Universitat Pompeu Fabra Barcelona

Madrid, 2020.

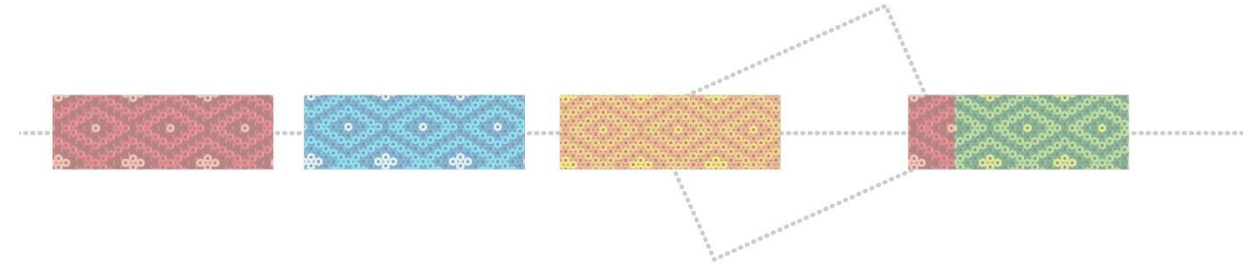

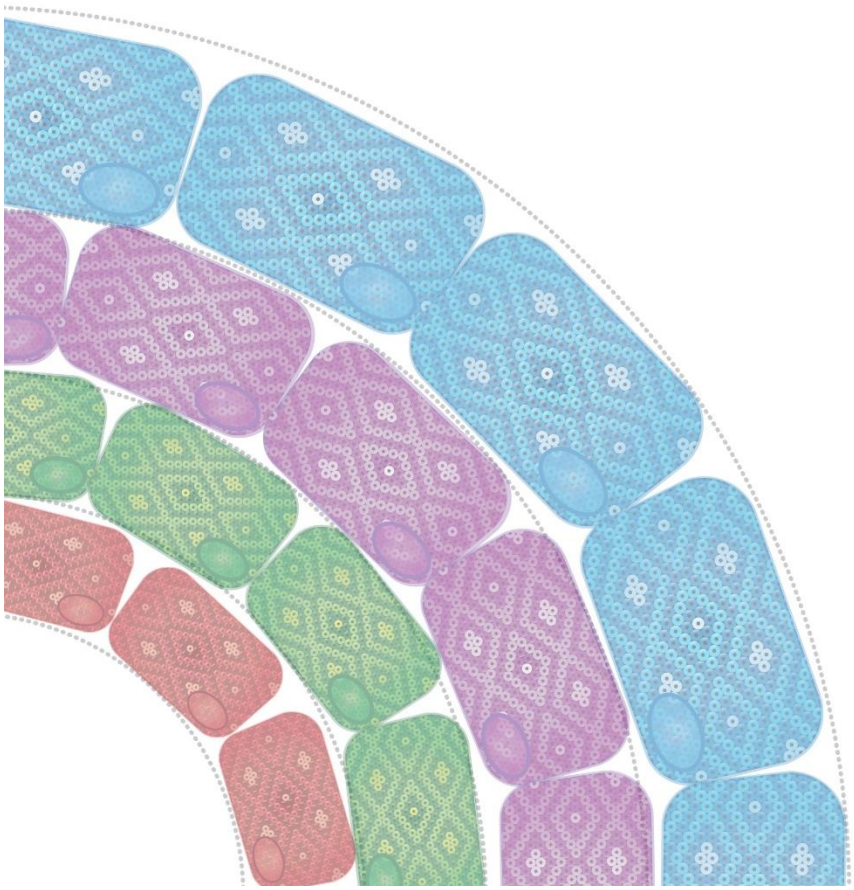

The work conducted as part of this doctoral thesis was carried out in the Epithelial Carcinogenesis Group, at the Spanish National Cancer Research Centre (CNIO), under the supervision of Dr. Francisco X. Real and Dr. Miriam Marqués

Ana M. Maldonado Barragán was supported, in part, by a *Beca de estudios doctorales en el extranjero -CONCYTEP/CONACYT,* awarded by Consejo Nacional de Ciencia y Tecnología, in Puebla, Mexico

“Success is not the absence of failure; it’s the persistence through failure.” – Aisha Tyle

ACKNOWLEDGEMENTS

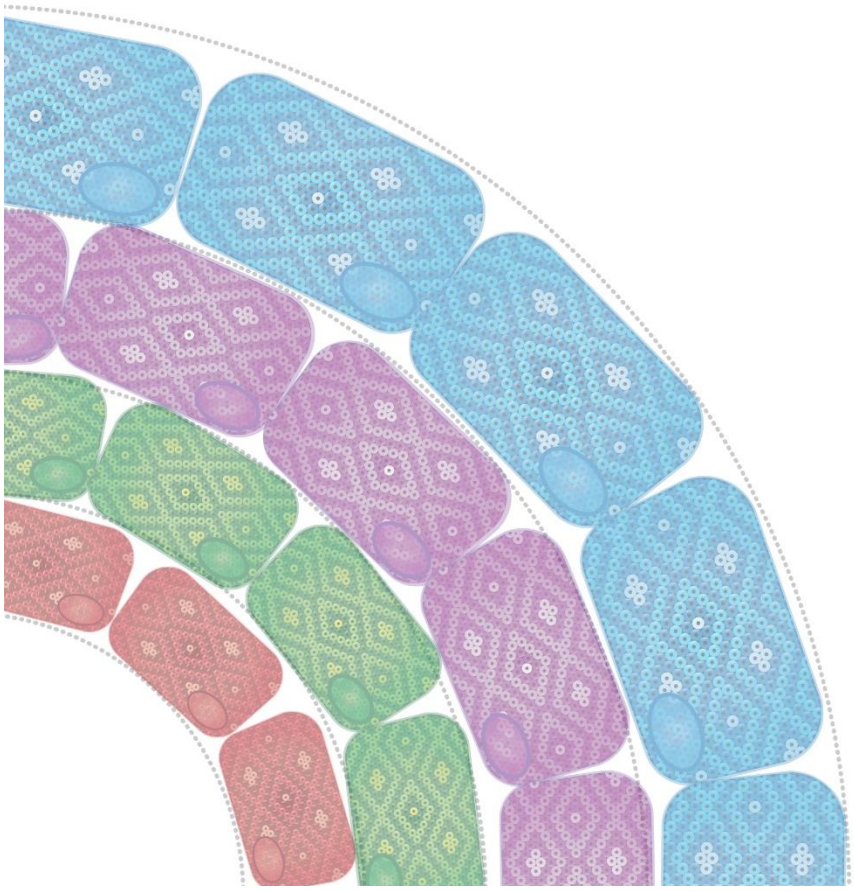

¡Mi parte favorita de la tesis!

¡Ni los tacos de todos los restaurantes mexicanos de Madrid alcanzarían para dar las gracias a tantas personas! No es mentira cuando te dicen que el doctorado es duro, pero definitivamente lo más valioso que me han dejado estos cuatro años y medio ha sido la gente con la que he tenido la oportunidad de compartir risas, lágrimas, chelas, abrazos, cantos, bailes, mucha buena vibra y cariño.

A Paco, gracias por darme la oportunidad de unirme al labo, por todo el tiempo y trabajo invertido en mi proyecto, mis cosas y hasta mis papeles, y porque aunque con dureza siempre trataste de sacar lo mejor de mi y hacer que valga la pena.

A Miri, mi jefecita santa, la jefa más cool y chingona del universo. Tuve la suerte de terminar bajo tu supervisión, eres un modelo a seguir para un científico en muchos aspectos, conservas la parte más importante que tenemos, nuestra parte humana, cercana, cálida, y a la vez, no compras cualquier cosa, eres lo máximo. Hacer el doctorado con tu guía ha sido uno de los factores más determinantes para llegar a este punto, gracias por siempre poner buena cara y por aguantar todos mis audios, cantos, fotos, preguntas, crisis, memes y gifs con tanta paciencia (o eso parecía). Gracias por creer en mí y siempre motivarme en los momentos difíciles.

A Estrella, mi apoyo constante e inagotable para todas las crisis derivadas del doctorado, de esta tesis y de la vida. Gracias por la increíble paciencia y empatía para entender y sentir mi mundo como pocas personas hacen, por creer en mí e impulsarme a mejorar. No podría haber escogido mejor persona para compartir mi camino.

Por supuesto, no hubiera sido lo mismo sin mis primeras compañeras del labo: Mónica, la güera y Cata. Desde el primer momento han estado ahí constantemente, en las buenas y en las malas. Monicus siempre con su contagiosa actitud positiva y planeando viajes ante la menor sugerencia, la güera (querido Sr. Árbol) siguiéndome la corriente con cada tontería que inventara y relajando el ambiente, y Cata, siempre dando el consejo más oportuno en el momento preciso. ¡Ha sido un placer coincidir tantos años! Pero claro, luego llego Sonia, que se le agarra cariño rápido cuando hace favores de tan buena gana y encima deja dibujitos en mis placas y tubos, bien jugado, Sonia, bien jugado, incluso aunque no sepas quién es Juan Gabriel ¡Gracias por ser tan buenas amigas!

A Natalia, aunque se haga la dura y no haya ido por una cerveza conmigo en 4 largos años… ¡Sé que en el fondo me quiere y que le caigo bien! ¡Y obviamente a Yoli también! A las dos, gracias por ser buen pedo conmigo a pesar de todos mis desmadres. A Irene, que tiene elevados niveles de acelerina en sangre y aun así siempre tiene tiempo de preguntarme cómo estoy y qué tal va todo. ¡Qué grande! A Ele, el bladder team, gracias por ayudarme siempre que necesitara consejos sobre el mundo de los organoides. A Elena, un gusto tener platicas rojillas y feministas. ¡Te voy a extrañar en el labo! A Jaime, siempre de buen rollo y echándome la mano a la menor dificultad bioinformática, por cierto, jamás olvidaré la despensa de comida mexicana ¡jamás! A Miguelin, gracias por cooperar con la noble causa migrante y ayudarme cuando más lo necesitaba, tampoco lo olvidaré. Mark, thanks for being Mark, you're really fun to be around and always keen to help, I really appreaciate. Gabriel, aunque hemos convivido poco, siempre estás disponible para ayudar, gracias por la disposición. Luis, ¡siempre es agradable coincidir contigo! Gracias por corregir mi intro. Y por supuesto, las nuevas adquisiciones: Lavinia, la italiana menos italiana, pero siempre agradable, buen rollo y echándome la mano a la menor oportunidad, muchas veces sin que lo pida… ¡ya iremos a bailar! Auba, la intensidad andante, bájale carnal, aún te queda pa' largo! Roma no se hizo en un día! (pregúntale a Ele, seguro que ella sabe mejor). Catalina, ¡da gusto tener otra latina en el grupo! Además, que sea así de buen pedo. A Martina, aunque ya no esté en el labo, lo que estuvo bastó para hacerse un huequito en estos agradecimientos por ser tan sweet y cariñosa conmigo. Sladjana, Cristina S, María y Jake, a pesar de que hemos coincidido poco, el ambiente

que suman al laboratorio es genial. En resumen, más que mis compañeros, ustedes se han convertido en mi familia, ¡gracias a todos!

Raquel, Jess y Clau, desde el 8 de marzo de 2019 supe que ya no había vuelta atrás, que habíamos hecho match y que esto era para siempre. No podría pedir más de estas amigas, siempre al pendiente de mí y listas para salir por un café ante la menor señal de agobio. Y claro, luego se nos unió Thelmi, que sólo lo hizo mejor y con comida griega incluida.

A Marta, Naiara, Xavi y Vicky, por todas las beer hours en las que me colaron, todos los postres que me llevaron, los ánimos, por mi hijo (Potatsio), por rapar a mis ratones y las fiestas que compartimos.

A Vero que se tomó más en serio mi cloning que su vida misma, bendita intensidad la tuya ¡you know you're the best! A Tati, mi quasi paisana, por más chelas y cumbias. A Sergio, mi dealer favorito, gracias a él todos los análisis de esta tesis están hechos con las versiones más actualizadas de todos los programas (no te incluí en materiales y métodos, lo siento).

A Raúl, mi paisano, por las todas las pláticas en cultivos, ¡nunca aprendiste a tocar el yembé, güey! A Simone, un placer compartir cafés en el pasillo y tocar canciones de los Beatles acompañados de unas chelas.

A Sarai y Génesis, mi espalda no habría sobrevivido esta tesis sin su trabajo, pero sobretodo, mi día a día no hubiera sido tan alegre y divertido sin ustedes y nuestro querido aquelarre con mis teenagers salvajes e Iván.

A Raúl Torres por ayudarme con el cloning y siempre facilitar una que otra enzima de restricción, con una buena plática incluida.

A Diego Megias, ¡ojalá hubiera más jefes como tú! ¡Eres súper chido!

To Tobias, the German counterpart of this story, it has been tough but also a nice trip!

A mi familia:

A mis papás por darme alas, a lo mejor de más, para ir a buscar lo que quería, aunque eso implicará estar lejos. Por todo el apoyo, siempre incondicional, para lograr lo que me propongo y siempre motivarme y repetirme que todo tiene solución. A Gaby por siempre estar ahí, literal desde el primer momento, en las buenas y en las malas, por hacer el diseño de mi portada (que está súper chido), por toda la despensa de comida mexicana de apoyo a falta de México (y a Romi) y por todos los viajes durante este tiempo y por los que nos faltan por hacer. A Erandi y Pepe por estar pendientes de cómo van las cosas, platicar un rato y apoyarme. A toda mi familia en Guadalajara, Puebla, Zacapu, Morelia, Celaya, Toluca y Ciudad de México, que siempre me está echando porras. Los amo mucho.

A mis amigos en México y por allá en lugares lejanos, a Helena y Nathalie, gracias por escucharme, enrollarse y por no perder el contacto después de tanto tiempo. A Potro, mi apá, la neta es que sin tu noble colaboración esta tesis no hubiera sido posible, gracias por rifárterla apostillando papeles en la gran ciudá. A mi querida ex roomie, Erika Paola, me hace falta llegar a la casa, ponerte a Juan Gabriel, cantar como locas y echarnos unos mezcalitos. A mis amigos Groningeanos, Juarenses, Poblanos, Chilangos y derivados de múltipes encuentros del 3er tipo.

1. SUMMARY

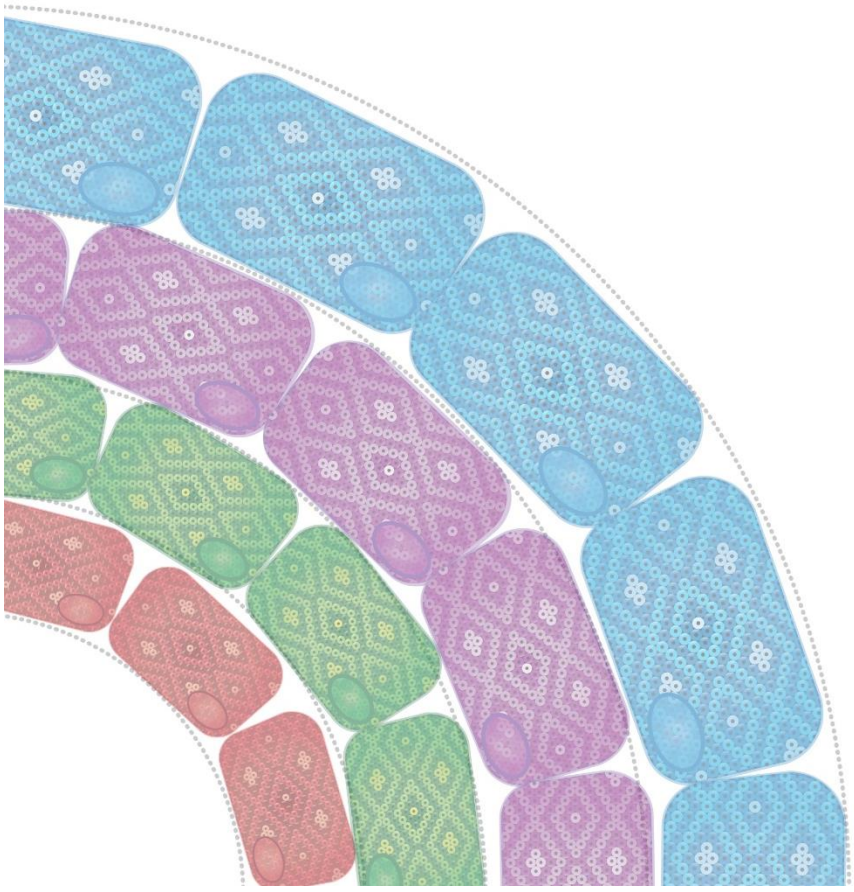

SUMMARY

Bladder cancer represents a high economic burden for the health systems since patients frequently relapse. Most BC are urothelial tumors; these are clinically and molecularly heterogeneous and are characterized by a high mutational burden, including mutations in several genes coding for proteins involved in splicing. *RBM10* was found by our laboratory as a recurrently mutated gene in BC, although at low frequency (2-5%). *RBM10* mutations have also been reported in lung (7-9%), pancreatic, and colorectal cancers. *RBM10* maps to the X chromosome and encodes an RNA-binding protein involved in alternative splicing. The majority of *RBM10* somatic mutations lead to a premature stop codon and loss of protein expression, supporting the notion that it is a tumor suppressor gene. In addition, germline *RBM10* mutations cause TARP syndrome, a severe developmental condition with early male lethality.

To reveal how *RBM10* loss contributes to development and cancer we have established *Rbm10* constitutive and conditional knockout mouse models and have analyzed phenotypes at the organismal and cellular level. Constitutive inactivation of *Rbm10* in the mouse germline results in partial male embryonic lethality and partially recapitulates TARP syndrome, although some mutant mice survive into adulthood. Tissue-wide *Rbm10* inactivation in young mice is well tolerated, indicating that the protein is dispensable in adulthood. I have established normal urothelial organoids to induce *Rbm10* inactivation *in vitro* and show that, compared to their wild type counterparts, their growth is partially EGF-independent. *Rbm10 KO* organoids acquire more prominent cystic features, related to urothelial differentiation. RNA-Seq analysis of the organoids in proliferative conditions revealed significant up-regulation of luminal and stratified epithelium signatures. Down-regulation of cell cycle and translation-related signatures were observed in proliferation, while translation was up-regulated in differentiation conditions. Several splicing events associated with *RBM10* inactivation in bladder tumors have been validated using the mouse organoids models. The analysis of human tumors reveals that *RBM10* inactivation is an early genetic alteration in bladder carcinogenesis.

I have also generated several tools to further analyze the molecular mechanisms through which RBM10 loss-of-function contributes to bladder cancer. Altogether, the results validate the newly developed strain as a valuable model to study TARP syndrome and urothelial cancer, allowing the identification of RBM10-related splicing targets and molecular mechanisms relevant to disease progression.

RESUMEN

El cáncer de vejiga representa una alta carga económica para los sistemas de salud debido a la alta frecuencia de recurrencias. La mayor parte de los tumores son uroteliales, siendo clínica y molecularmente heterogéneos y caracterizándose por tener una alta carga mutacional, incluyendo mutaciones en varios genes codificantes de proteínas involucradas en el procesamiento del ARN . Nuestro laboratorio, identificó mutaciones recurrentes de *RBM10* en tumores uroteliales aunque con una frecuencia relativamente baja (2-5%). Las mutaciones en *RBM10* también han sido descritas en cáncer de pulmón (7-9%), páncreas y colorectal. El gen *RBM10* se encuentra en el cromosoma X y codifica una proteína de unión al ARN involucrada en procesamiento alternativo. La mayoría de las mutaciones somáticas en *RBM10* generan un codón de parada prematuro y la pérdida de la expresión de la proteína, apoyando la noción de que este es un gen supresor de tumores. Adicionalmente, las mutaciones germinales en *RBM10* causan el síndrome de TARP, una enfermedad rara que asocia anomalías congénitas severas que conllevan a la muerte temprana en varones.

Para revelar cómo la pérdida de *RBM10* contribuye al desarrollo embrionario y al cáncer, hemos establecido modelos de ratón *Rbm10* knockout condicionales y constitutivos, y hemos analizado sus fenotipos a nivel celular y de organismo. La inactivación constitutiva de *Rbm10* en la línea germinal resulta en letalidad embrionaria en machos y parcialmente recapitula las malformaciones asociadas al síndrome TARP, aunque algunos mutantes son capaces de sobrevivir hasta la etapa adulta. La inactivación de *Rbm10* ubicua en ratones jóvenes es bien tolerada, indicando que la proteína es dispensable en la etapa adulta. También, he establecido organoides uroteliales normales para inducir la inactivación de *Rbm10 in vitro* y mostrar que, comparados a su contraparte silvestre, su crecimiento es parcialmente independiente de EGF. Los organoides *Rbm10 KO* adquieren características císticas más prominentes, relacionadas con la diferenciación urotelial. Nuestro análisis de secuenciación de ARN en estos organoides en condiciones proliferantes reveló la sobreexpresión de firmas genéticas de diferenciación luminal y de epitelio estratificado. Además, firmas genéticas relacionadas con ciclo celular y la traducción mostraban una menor expresión en organoides KO proliferantes comparados con organoides WT, mientras que genes asociados a traducción y síntesis de proteínas estaban sobreexpresados en organoides KO en condiciones de diferenciación. Además, numerosos eventos de procesamiento alternativo asociados con la inactivación de *RBM10* en tumores de vejiga han sido validados en estos modelos de organoides de ratón. Asimismo, el análisis de los tumores humanos reveló que la

inactivación de *RBM10* es una alteración genética temprana en la carcinogénesis de vejiga.

Finalmente, he generado numerosas herramientas para continuar analizando los mecanismos moleculares a través de los cuales la pérdida de función de RBM10 contribuye al cáncer de vejiga. Estos resultados validan nuestros modelos para el estudio del síndrome de TARP y de cáncer de vejiga, permitiendo la identificación de dianas de splicing y mecanismos moleculares mediados por RBM10 relevantes para la progresión de la enfermedad.

2. INDEX

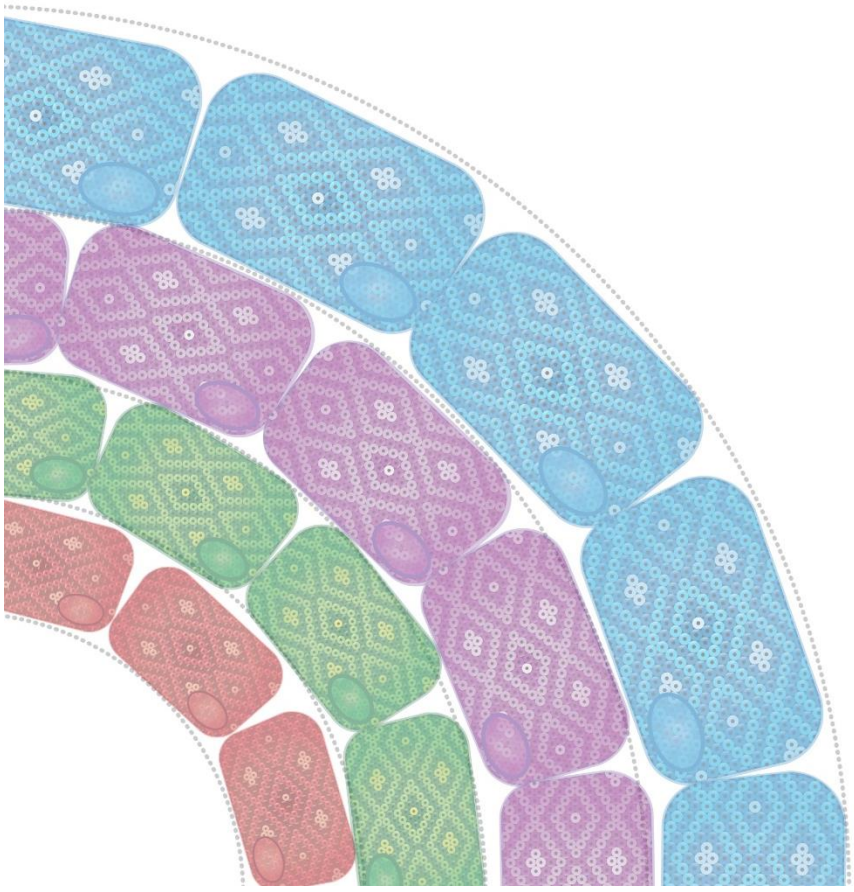

INDEX

3. INTRODUCTION

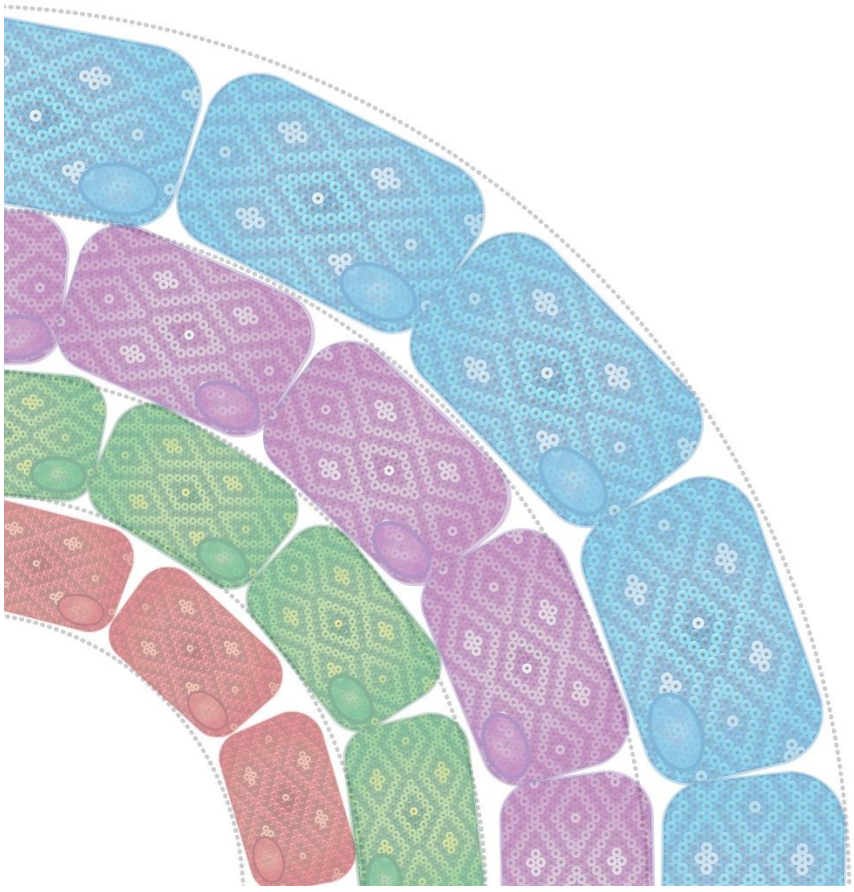

INTRODUCTION

3.1. Bladder Cancer

3.1.1. Epidemiology

Bladder cancer (BC) is the 10th most frequent cancer worldwide with an estimated 549,393 new cases in 2018. The highest incidence rates are observed in Southern and Western Europe, North America, Northern Africa, and Western Asia (Bray et al., 2018; GLOBOCAN, 2018; Antoni et al., 2017). It is the 7th most common cancer in males worldwide, having an incidence that is 3-7 times greater than in women. Women tend to be diagnosed with more advanced disease and face less favorable outcomes after treatment. This gender-bias might be caused by environmental/lifestyle factors, hormonal, and enzymatic differences that impact carcinogen metabolism (Dobruch et al., 2015).

BC ranks 14th in mortality rates according to GLOBOCAN 2018, with 200,000 estimated deaths, most occurring in developing countries. The main risk factor associated with BC is tobacco smoking, although many other factors contribute to the disease, including occupational exposures to chemicals (e.g. aromatic amines and polycyclic hydrocarbons), water contaminants (e.g. arsenic), obesity, age, and diet, among others (Al-Zalabani et al., 2016; Bray et al., 2018; Knowles and Hurst, 2014). Familial aggregation of BC is rare but there is strong evidence that inherited genetic factors contribute to disease risk (Malats & Real, 2015) and it is a paradigm of cancer where gene-environment interactions play a significant role (García-Closas et al., 2005).

BC represents a high economic burden due to its relatively low death rate and frequent recurrence of the disease, requiring continued and long-term follow-up, leading to the highest cost among all cancer types on a per-patient basis (Hong and Loughlin, 2008; Ploeg et al.,2009).

The tumor is commonly diagnosed due to the presence of blood in the urine (haematuria). However, emergency admission is also usual and is associated with poor prognosis (Knowles and Hurst, 2014).

3.1.2. Classification

BC is a heterogeneous disease: approximately 90% of tumors are urothelial carcinomas (Warrick et al., 2019) and the remaining tumors are classified as squamous-cell carcinomas, adenocarcinomas, and small cell carcinomas, among others (Willis &

Kamat, 2015; Knowles and Hurst, 2015; Humphrey et al., 2016). According to histopathology, urothelial cancers can be categorized as “conventional” or “variant” (Kamat et al., 2016; Damrauer et al., 2014; Humphrey et al., 2016). Depending on the level of invasion, tumors are classified as non-muscle-invasive bladder cancer (NMIBC) or muscle-invasive bladder cancer (MIBC); the latter infiltrate the muscularis propria or muscle wall **(Fig. 1)**.

Table 1: **TNM pathological classification of bladder cancer** (modified from the International Union Against Cancer, UICC in TNM, 2009).

Stage	Substage	Description
Ta		Non-invasive papillary carcinoma
Tis		Carcinoma in situ, “flat tumor”
T1		Tumor invades subepithelial connective tissue
T2		Tumor invades muscle
	T2a	Tumor invades superficial muscle (inner half)
	T2b	Tumor invades Deep muscle (outer half)
T3		Tumor invades perivesical tissue
	T3a	microscopically
	T3b	macroscopically (extravesical mass)
T4		Tumor invades prostate stroma, seminal vesicles, uterus, vagina, pelvic wall, or/and abdominal wall
	T4a	Tumor invades prostate stroma, seminal vesicles, uterus, or vagina
	T4b	Tumor invades pelvic wall or abdominal wall
Grade		**Description**
G1		Well-differentiated
G2		Moderately differentiated
G3-G4		Poorly differentiated/undifferentiated

The main histopathological parameters considered for patient management are stage (T) and grade (G). There has been a lot of debate regarding the staging/grading of urothelial carcinomas. The stage is determined by using the Tumor-Node-Metastasis

system (TNM system) which describes the level of invasion of the bladder wall (Tis-T4); grading is based on the nuclear morphology and cell differentiation (Table 1) (International Union Against Cancer, UICC in TNM, 2009; Humphrey et al., 2016). The International Agency for Research on Cancer from the World Health Organization (WHO) has proposed classifications alternating between a three- (1-3) and two-grade (low-high) system. Low-grade tumors generally include grade 1 and 2 tumors with well-differentiated cells and few mitoses. High-grade tumors include grade 3 tumors - displaying poor differentiation, aberrant nuclei, and frequent mitoses - and a subset of grade 2 tumors (Humphrey et al., 2016). Nowadays, a combination of T and G is used to classify BC patients in the clinic to determine the treatment.

BC can present two growth patterns: papillary and solid. Papillary tumors arise from urothelial hyperplasia and represent 70-80% of NMIBC **(Fig. 2)**. These are subclassified as papillary urothelial proliferations of low malignant potential (PUNLMP) and low- or high-grade papillary carcinomas. Low-grade papillary tumors have not yet penetrated the basement membrane (stage Ta) whereas high-grade tumors have invaded the basement membrane but not the muscle (stage T1) (Knowles and Hurst, 2015; Humphrey et al., 2016).

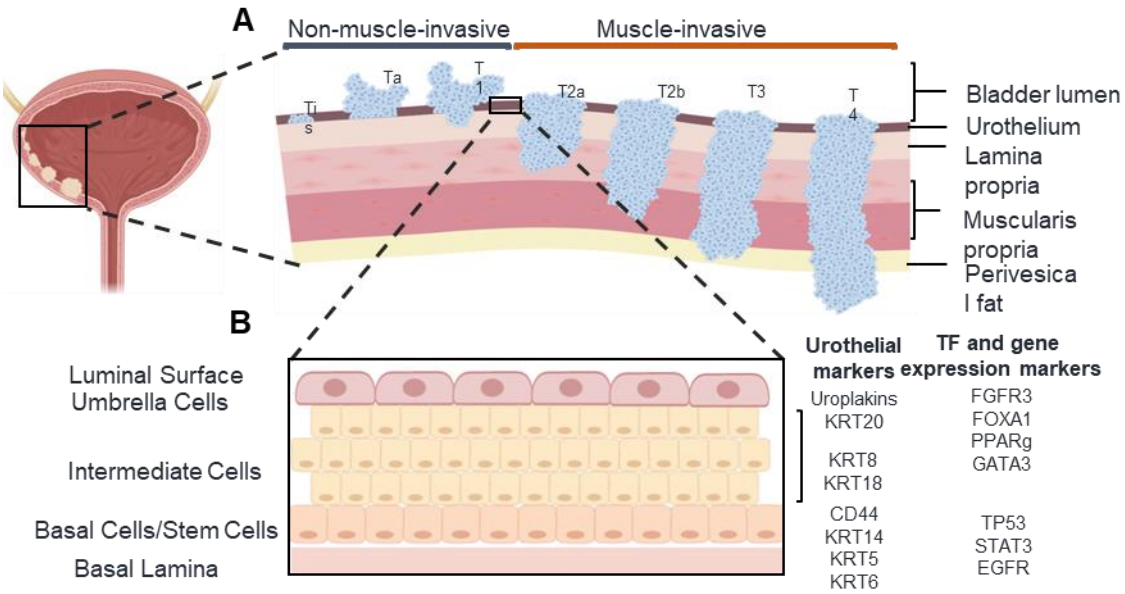

Figure 1: Bladder cancer staging and grading. A. 1973 WHO classification and 2004 WHO/International Society of Urological Pathology (ISUP) classification. **B.** Urothelial cell layers and markers of the various cell types (Modified from Knowles and Hurst, 2015).

The remaining 20 to 30% are urothelial tumors arising from carcinoma *in situ* (CIS), a high-grade flat lesion that can progress to invade the lamina propria and further to become muscle-invasive; 50% of patients with MIBC develop distant metastases

(Knowles and Hurst, 2015; Cheng et al., 2009; Smith et al., 2014). Of note, 10 to 15 % of NMIBC progress to become MIBC (NICE, 2017; Knowles and Hurst, 2015).

Patients with NMIBC tend to have a long life expectancy with a 5-year survival of approximately 90% (Knowles and Hurst, 2015); they are usually treated by transurethral resection of the tumor followed by intravesical chemotherapy. Regular cystoscopies are required o identify recurrences (Woldu, et al., 2017). Patients with high-grade tumors also receive immunotherapy with intravesical Bacille Calmette-Guérin (BCG) to avoid recurrence/progression. Despite this treatment, approximately 70% of the tumors recur and some patients eventually require a radical cystectomy (NICE, 2017; Babjuk et al., 2017; Meeks & Lerner, 2017). The standard treatment for patients with MIBC is radical cystectomy with perioperative cisplatin-based chemotherapy (either neoadjuvant or adjuvant). There is an increasing interest in the use of bladder-preserving therapies. Patients with distant metastasis require systemic therapy. However, 50% of them are not eligible for cisplatin-based chemotherapy, exhibiting a five-year survival of less than 15%. Patients with metastatic BC have a poor prognosis with a 5-year survival of less than 50% (NICE, 2017; Knowles and Hurst, 2015). Over the last 5 years, there has been substantial progress in the treatment of metastatic BC through the introduction of immune checkpoint inhibitor antibodies and targeted therapies (Wolacewicz et al., 2020; Godwin et al., 2018).

3.1.3. Molecular genetics

Urothelial carcinoma has a high degree of mutational heterogeneity and a high frequency of somatic mutations (7.7 per megabase) when compared to other solid tumors. NMIBC is more genetically stable than MIBC, which commonly presents with aneuploidy, gene copy number changes, and other alterations such as chromothripsis, mediated by nonhomologous end-joining DNA repair (Morrison et al., 2014) (Knowles and Hurst, 2015). Currently, two genetic pathways have been proposed to contribute to bladder tumor initiation and progression, largely matching the two morphological patterns **(Fig. 2)**.

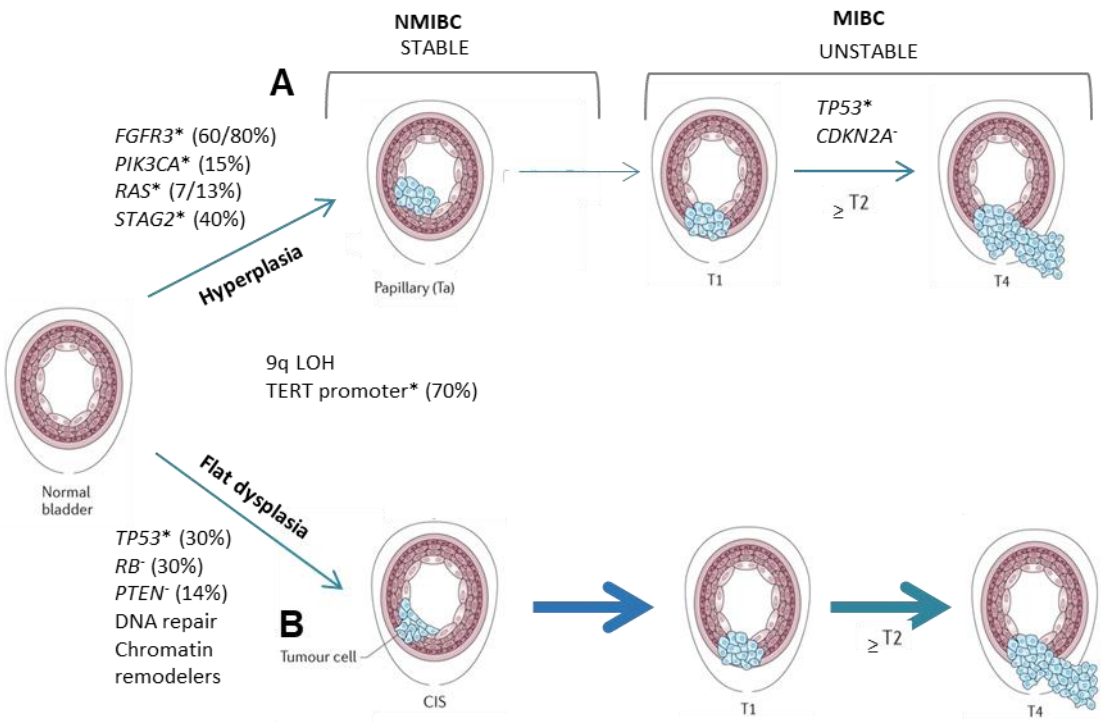

Figure 2: Proposed genetic pathways of BC progression. Both pathways share losses of chromosome 9 and mutations on the *TERT* promoter. **A.** The papillary pathway frequently involves activating mutations in oncogenes, leading to the development of NMIBC low-stage tumors. A small proportion of these tumors acquire additional genetic alterations, such as *CDKN2A* loss and mutations in *TP53,* resulting in invasive high-stage tumors. **B.** The non-papillary pathway involves predominantly inactivating mutations in tumor suppressor genes, with a high frequency of mutations in *TP53* and *RB*.

Tumors arising from both pathways share hotspot mutations in the promoter of *TERT*, which encodes the telomerase catalytic subunit, conferring enhanced TERT expression. *TERT* mutations are considered an early event during tumorigenesis since they can be found in approximately 70% of the tumors regardless of stage and grade (Hurst et al., 2014; Allory et al., 2014; Kinde et al., 2013). Moreover, both pathways share chromosome 9 deletions (9p, 9q, or both) which occur in more than 50% of the NMIBC and MIBC tumors (Knowles and Hurst, 2015; Platt et al., 2009).

3.1.3.1. The Papillary pathway

The papillary pathway involves mainly activating mutations in oncogenes, such as *FGFR3*, *PIK3CA*, and the *RAS* oncogene family, being the most commonly altered genes leading to the development of low-stage/grade tumors (Pietzak et al., 2017). Papillary tumors that progress to MIBC are characterized by a high genomic instability (Sjodahl et al., 2019), exhibiting the acquisition of *CDKN2A* homozygous deletions (Rebouissou et al., 2012) and mutations in *TP53* (Mitra et al., 2006; TCGA Network, 2014), likely causing this progression **(Fig. 2B)**.

FGFR3 mutations occur in up to 80% of Ta low-grade tumors, including activating point mutations, gene translocations, and gene amplification (Zieger et al., 2005; Juanpere et al., 2012; Marqués and Real, 2017). The frequency of *FGFR3* mutations progressively decreases from Ta to T1 tumors and MIBC, mutant tumors being associated with an overall better prognosis (Hernandez et al., 2006; Billerey et al., 2001; Zieger et al., 2005). *FGFR3* mutations have been found to significantly co-occur with *PIK3CA* mutations, which are present in 15 to 20% of low-grade bladder tumors (Kompier et al., 2010; Juanpere et al., 2012; López-Knowles et al., 2006). *FGFR3*, but not *PIK3CA,* mutations are mutually exclusive with *RAS* mutations, probably due to the redundancy in the RAS-MER-ERK signaling pathway. Conversely, combined *PIK3CA*-*RAS* mutations are associated with high-grade tumors (Juanpere et al., 2012; Jebar et al., 2005). *RAS* genes are mutated in approximately 13% of all bladder tumors (Kompier et al., 2010).

In recent years, mutations in several novel tumor suppressor genes have been described in BC, including *ARID1A* and *STAG2* (Balbas-Martínez et al., 2013). This last gene codes for a cohesin complex component that is frequently mutated in NMIBC (40%) and its alterations are associated with an improved outcome (Balbás-Martínez et al., 2013). Cohesin plays an important role in chromatid segregation (Carretero et al., 2010), DNA double-strand break repair (Kong et al., 2014), and genomic organization (Baranello et al., 2014), supporting the role of *STAG2* as a tumor suppressor.

3.1.3.2. The Non-Papillary pathway

The non-papillary pathway involves predominantly tumor suppressor genes, including a high frequency of mutations in *TP53, RB*, *PTEN,* and genes involved in DNA repair and chromatin remodeling **(Fig. 2B)**. These tumors are high-grade, aggressive, genomically unstable, and have a high likelihood of progression and muscle invasion (Cordon-Cardo and Reuter, 1997; Puzio-Kuter et al., 2009)

TP53 is mutated in 24-56% of the MIBC exhibiting inactivating mutations and loss of function (Esrig et al., 1994; Hartmann et al., 2002; Knowles and Hurst, 2015). P53, known as the guardian of the genome, is a transcription factor involved in many cellular processes, such as the cell cycle, stress response, senescence, DNA repair, and induction of apoptosis, highlighting its role in tumor progression (Lane, 1992). The *PTEN* tumor suppressor is inactivated in approximately 24% of MIBC bladder tumors, generally exhibiting loss of heterozygosity, and its down-regulation is associated with

TP53 mutations and poor outcomes in patients and aggressive tumors in mice (Aveyard et al., 1999; Platt et al., 2009; Puzio-Kuter et al., 2009). The RB pathway is also commonly altered in MIBC (Mitra et al., 2007) and is associated with aggressive tumors with poor prognosis (Cordon-Cardo et al., 1992).

The advent of massive parallel sequencing has allowed identifying novel genes mutated in many cancer types in an agnostic manner through several international consortia. In BC, the Tumor Cell Genome Atlas (TCGA) focused on MIBC. The TCGA analysis highlighted three main pathways as frequently dysregulated: cell cycle (93%), MAPK and *PI3K* signaling (72%), and chromatin remodeling/histone-modifying genes (64%). In MIBC, 76% of the tumors harbor mutations in genes coding for proteins involved in chromatin function. Among them are *KMT2D*, *ARID1A*, *KDM6A,* and *EP300.* Additionally, frequent mutations in DNA repair genes, including *ERCC2* (Balbás-Martínez, Sagrera, et al., 2013; Van Allen et al., 2014), a member of the nucleotide excision repair pathway, *ATM* (Balbás-Martínez, Sagrera, et al., 2013), and *FANCC*, involved in post replication repair, have been found in MIBC (Plimack et al., 2015).

Other important genetic alterations are found in receptors of signaling pathways and include, besides FGFRs, the ERBB receptors (*EGFR/ERBB1, HER2*/*ERBB2, and ERBB3)*. High *EGFR* expression has been associated with non-papillary tumors; overexpression of *EGFR* and *HER2* has been reported in high-grade and invasive tumors, having an impact on overall survival and recurrence-free survival (Kassouf et al., 2008; Kruger et al., 2002). In addition, gene amplifications are more common in metastases than in primary tumors (Fleischmann et al., 2011).

EGFR activation is mechanistically linked to PI3K and RAS pathways, which also have been described as mutated in BC. Other receptor tyrosine kinases, including MET, and RON (MST1R) are up-regulated in aggressive non-papillary tumors (Cheng et al., 2005; Sanchez-Carbayo et al., 2006). Deregulated expression of downstream targets of these pathways has been reported, where more than half of tumors exhibit high levels of pERK1/2 and pAKT or PI3K/AKT/mTOR pathway activation, independently of the stage or grade (Juanpere et al., 2012; Hedegaard et al., 2016; Rebouissou et al, 2014).

Other pathways, such as PPARγ signaling, are frequently altered with *PPARγ* amplifications occurring in 12-17% of MIBC and 10% of NMIBC (Biton et al., 2014; Rochel et al., 2019; Lui et al., 2019).

3.1.3.3. Molecular Taxonomy

In the last decade, transcriptomics analyses using Next Generation Sequencing (NGS) have allowed the establishment of molecular taxonomies highlighting the molecular heterogeneity of BC. These subtypes are associated with distinct clinical outcomes and response to treatment. One of the first studies was performed by Sjödahl and colleagues (Lund cohort) in NMIBC and MIBC, identifying 5 major molecular groups: Urobasal A (UroA), Urobasal (UroB), genomically unstable (GU), squamous cell carcinoma-like (SCCL) and infiltrated (Sjödahl et al., 2012). In this classification, UroA are mainly NMIBC tumors; UroB includes NMIBC and MIBC. Both UroA and UroB express high levels of an *FGFR3* associated signature and are related with good prognosis and poor prognosis respectively. The majority of UroB tumors present mutations in *TP53* and *FGFR3*, suggesting evolution from UroA. These tumors also harbor alterations in *CDKN2A*, which is associated with progression to MIBC **(Fig. 2A)**. The SCCL group exhibits basal-like features, expressing *KRT5, KRT6, KRT14, EGFR,* and *P-cadherin,* and is associated with a poor prognosis. Finally, GU tumors express low levels of *FGFR3*, *CCDN1,* and *p63*, and high levels of *HER2* and *E-cadherin,* being associated with an intermediate prognosis (Sjödahl et al., 2012). Subsequent studies have focused on MIBC or NMIBC selectively, the latter having been studied less extensively.

All classifications of MIBC converge on the identification of two major tumor subgroups having urothelial/luminal- or basal-like characteristics (Biton et al., 2014; Damrauer et al., 2012; Choi et a., 2014; TCGA Research Network, 2014; TCGA Research Network, 2017; Tan et al., 2019; Kamoun et al., 2020). The TCGA Network and Kamoun and colleagues (The Bladder Cancer Molecular Taxonomy Group) performed the most extensive initiatives. The study performed by the TCGA Network proposed 5 clusters according to gene expression profiles: luminal-papillary, luminal-infiltrated, luminal, basal-squamous, and neuronal. The Bladder Cancer Molecular Taxonomy Group reached an international consensus classification, proposing 6 tumor subtypes: Luminal Papillary (LumP), Luminal Non-Specified (LumNS), Luminal Unstable (LumU), Stroma-rich, Basal/Squamous (Ba/Sq), and Neuroendocrine-like (NE-like). There are several other classifications **(Fig. 3)** considering different clusters and subgroupings.

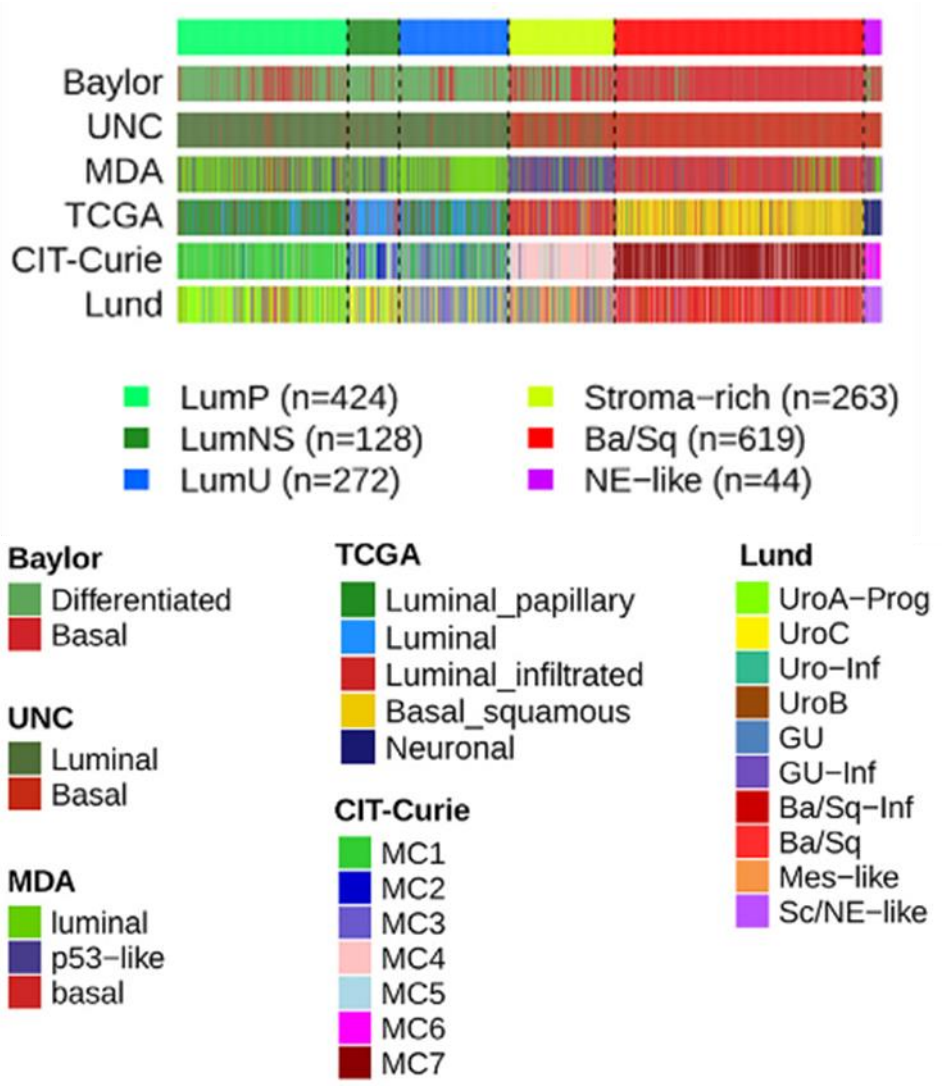

Figure 3: Comparison of the 6 consensus classes of urothelial carcinoma and the derived molecular subtypes. Major classifications of MIBC over the last decade (Modified from Kamoun et al., 2020).

Most of the studies agree that luminal-like tumors are enriched in a papillary morphology, having a higher rate of *FGFR3* up-regulation/activating mutations and expressing uroplakins, *KRT20*, *HER2*, *FOXA1*, *GATA3,* and *PPARγ*. Similarly, they agree that basal-like tumors can be defined based on the expression of *KRT5*, *KRT6, KRT14,* and *CD44* and the lack of *GATA3* and *FOXA1* (Alifrangis et al., 2019; Lerner & Robertson, 2016). It has been suggested that the molecular subgroups proposed are relevant to the prediction of treatment response (Choi et al., 2014b; Damrauer et al., 2014; TCGA Research Network, 2014; Kamoun et al., 2020).

Regarding NMIBC, the number of studies dealing with them is much lower than those related to MIBC. For that reason, it is necessary to provide novel tools to generate a deeper understanding of the behavior, progression, and treatment response of the

early-stage disease. In the first large-scale study focused on NMIBC (n=406), Hedegaard and colleagues (UROMOL consortium) classified these tumors into 3 major groups with significant overlaps with the Lund cohorts: class 1 and 3 tumors overlapped with UroA and class 2 fitted into the infiltrated or GU groups (Hedegaard et al., 2016; Sjödahl et al., 2012). Class 3 tumors showed some basal-like features. More recently, this classification has been expanded through a large integrative analysis of 834 tumors from the UROMOL consortium (Lindskrog et al., 2020). In this study, 4 transcriptomic classes are proposed: class 1, class 2a, class 2b, and class 3, analogous to the previous classification from 2016. Interestingly, 91% of the tumors overlapped with the UroA classification and 4% with the GU classification from the Lund cohorts (Sjödahl et al., 2012). In agreement with this, and according to the classification of Kamoun and colleagues, 93% of the tumors were classified as Luminal Papillary (LumP) (Kamoun et al., 2020).

In this new classification, class 1 and 3 tumors exhibited similar regulon activity patterns and high expression of early cell cycle genes, high *FGFR3* expression, and alterations. Specifically, class 1 tumors presented the best recurrence-free survival, showing high expression of uroplakins and intermediate expression of cytokeratins, also displaying alterations in *RAS* along with high *HIF1A, KAT5,* and *HDAC3* regulon activity. Class 3 tumors were characterized by high *KRT5/15* and low uroplakin expression*,* along with high *GATA3, KMT2E, KAT2A, HDAC10,* and *AR* regulon activity*,* and overall these tumors had less immune infiltration. On the other hand, class 2a tumors expressed genes related to late cell cycle, DNA replication, cell differentiation, and uroplakins, with high activity of *FOXM1, RARB, STAT3, ERBB2*, and *ERBB3* regulons. These tumors also showed alterations in the p53 pathway, copy number gains in *PPARγ and E2F3,* and losses in *CDKN2A* and *RB1,* displaying the worst recurrence-free survival and high intra-tumoral heterogeneity. Finally, class 2b tumors were associated with high expression of genes involved in epithelial-mesenchymal transition (EMT) and cancer stem cell markers, low expression of genes related to cell proliferation, and high *ESR1, FGFR1,* and *PGR* regulon activity, also exhibiting high immune cell infiltration and an intermediate recurrence-free survival **(Fig. 4)** (Lindskrog et al., 2020).

In addition to a transcriptomic classification, Lindskrog and colleagues have proposed tumor classes considering the genomic stability: genomic class (GC) 1, 2, and 3, showing low, intermediate, and high instability, respectively. These subclasses were significantly associated with the above mentioned transcriptomic classes, where class 2a included the highest fraction of GC3, whereas class 1 and 3 included nearly half of

the tumors that belong to GC1, with smaller fractions of GC2. Finally, class 2b presented similar fractions of tumors of the GC1, GC2, and GC3 subgroups **(Fig. 4)**.

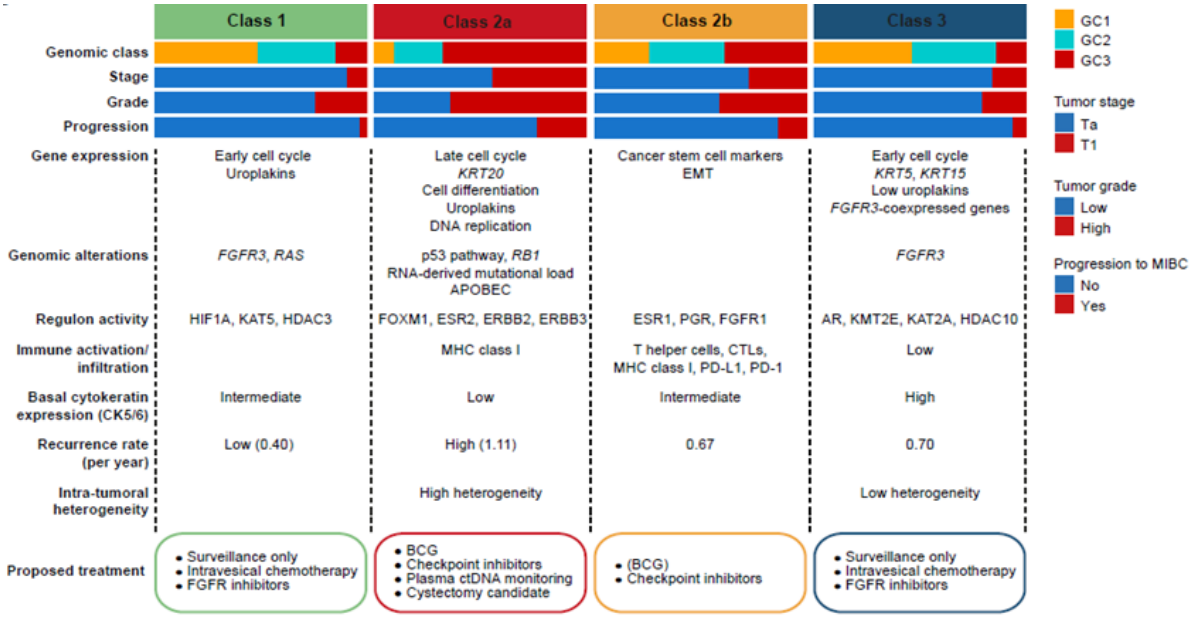

Figure 4: NMIBC subtypes and association with mutational profile and clinical features. Frequently mutated genes observed in urothelial carcinoma by Lindskrog and classified into four transcriptomic and three genomic classes (Modified from Lindskrog et al., 2020).

Similarly, another study from Hurst and colleagues classified 140 NMIBC tumors in two genomic subtypes, considering whether these are chromosomally stable or unstable. The first group was characterized by a high frequency of mutations in chromatin modifier genes. The second group was distinguished by up-regulated mTORC1 signaling and an altered metabolic profile, where females presented a higher frequency of mutations in the *KDM6A* gene (Hurst et al., 2017). Another two studies identified 5 molecular subtypes across luminal tumors that were mainly NMIBC (Bernardo et al., 2019) and 5 subtypes across stage T1 BC according to its transcriptomic profile; T1-LumGU, T1-TLum, T1-Inflam, T1-Myc, and T1-Early (Robertson et al., 2020).

3.2. Models to study bladder cancer

Different approaches have been used to study urothelial biology and BC development. These models should recapitulate the diversity of this tumor.

3.2.1. 2D cell cultures

The first attempts to culture human urothelial normal and cancer cells can be dated to >40 years ago (Logethethou-Rellaa et al., 1988; Bubeník et al., 1973; Berky and Zolotor, 1977; Rasheed et al., 1977; Elliott et al., 1974). More than 50 bladder cancer lines, and a few non-tumoral lines, have been established over the last decades. One of the main advantages of these models is that cells cultured in 2D are quite practical to handle. They have proven useful to perform pharmacological screenings due to the ease of performing large-scale experiments. However, cell lines do not reflect the genetic and phenotypic diversity of BC and they show a strong bias toward aggressive tumor subtypes (Earl et al., 2015). Cell lines undergo substantial changes as they are passed in culture and the selection pressure on tumor cells can result in a misrepresentation of the original tumor (Weeber et al., 2017). In addition, the standard 2D cultures do not include components of the tumor microenvironment such as fibroblasts and inflammatory cells.

3.2.2. 3D organoid models

In the last decade, there has been a major interest in developing 3D models to overcome some of the caveats of cell lines. While the first attempts to use such models date back to the 80's, the Clevers laboratory has pioneered their study in recent times. 3D cultures originating from stem or progenitor cells proliferate and recapitulate some of the features of the tissue they are derived from, thus receiving the name of organoids.

Using organoids as experimental models has many advantages. Organoids derived from primary tissue have proven to better preserve the tumor identity than cell lines after passing and they even provide the opportunity to culture strictly normal cells. Their self-renewal and self-organizing capacities allow them to differentiate under specific conditions, expressing markers of fully differentiated tissues (Pauli et al., 2017; Van de Wetering et al., 2015; Weeber et al., 2017; Duarte et al., 2017; Lee et al., 2018). However, their expansion is more cumbersome and is dependent on the use of natural matrices and a variety of growth factors, making them more expensive and less amenable to screenings (Weeber et al., 2017). Organoids tend to display greater heterogeneity in growth patterns than 2D cultures. In addition, the microenvironment is generally lacking, although there are several studies introducing co-cultures with

stromal and immune cells to overcome this limitation (Bertaux-Skeirik et al., 2016; Chakrabarti et al., 2018; Cattaneo et al., 2019; Neal et al., 2019).

The first experiments with organoids used intestinal cells and identified Wnt ligands, R-spondin1, EGF, and Noggin as growth factors required to maintain a stem-like state (Sato et al., 2009). Ever since, organoids have been established from healthy and malignant colon (Sato et al., 2011), prostate (Gao et al., 2014; Karthaus et al., 2014), pancreas (Boj et al., 2015; Huang et al., 2015), stomach (Bartfeld et al., 2015), breast (Pauli et al., 2017; Byrne et al., 2017), liver (Huch et al., 2013; Huch et al., 2015), and - recently - bladder (Santos et al., 2019; Mullenders et al., 2018; Lee et al., 2018), using different growth factors depending on the tissue of origin. The ability to expand organoids uninterruptedly facilitates their use for gene editing (Nie and Hashino et al., 2017; Drost et al., 2015), personalized medicine (i.e. living biobanks) (Van de Wetering et al., 2015), *ex vivo* mouse xenografts, drug discovery, and screening **(Fig. 5)** (Jabs et al., 2017; Lee et al., 2018; Byrne et al., 2017; Weeber et al., 2017), but also to understand normal and tumor physiology, growth factor requirements, stem cell characterization, and differentiation requirements.

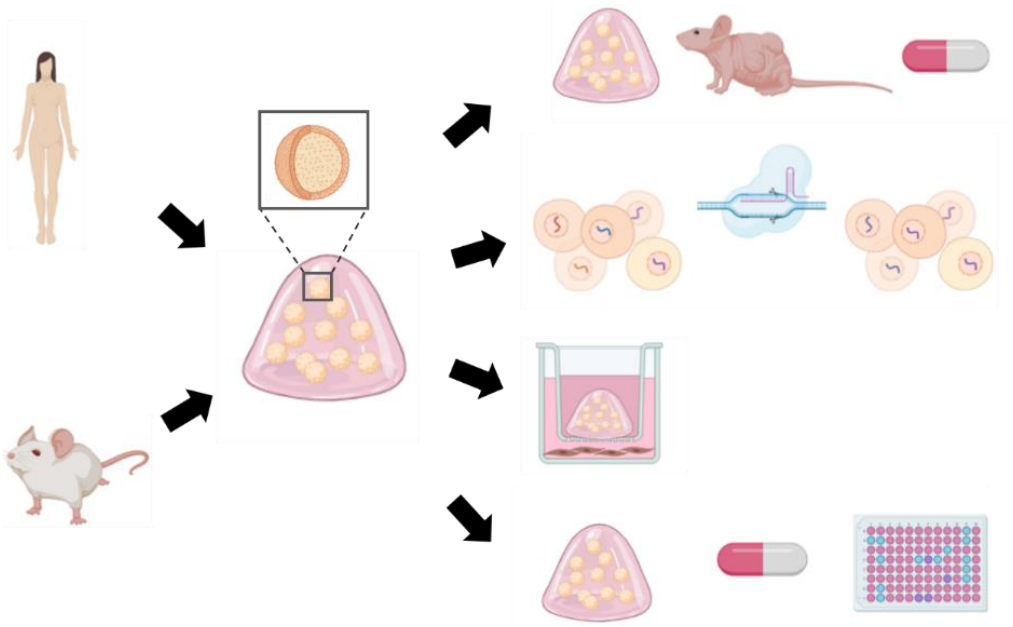

Figure 5: Organoid technology. Stem cells derived from human and mouse tissues are isolated and embedded in Matrigel or hydrogels to generate organoids. Organoids can be used for mouse xenografts, gene editing, co-culture, and drug screenings, among others.

Our laboratory has shown that normal mouse urothelial organoids depend on EGF and Wnt activators and their growth in medium containing these factors results in the deployment of a default squamous-like program that can be replaced by the activation

of a urothelial program upon growth factor depletion, EGFR inhibition, and PPARγ activation. Under the latter conditions, luminal urothelial markers are expressed, and organoids acquire barrier function. Additionally, these studies have demonstrated a role of Notch signaling in urothelial differentiation since its inhibition resulted in increased basal marker expression (Santos, et al., 2019).

As of BC, patient-derived organoid lines have been recently described and shown to largely recapitulate the features of the original tumor. Most organoids were established from low-grade NMIBC. Such organoids have been used for drug testing, gene editing, and orthotopic xenografting to study tumor evolution and treatment (Lee et al., 2018; Mullenders et al., 2018). Nevertheless, the field regarding BC organoids is just starting to be exploited.

In summary, organoids are a powerful tool to perform functional assays since they recapitulate better the genetic and morphological heterogeneity of tumors and there is a promise that they will be more useful to predict response to therapy.

3.2.3. Mouse models

There are several ways in which the study of BC in mice has been approached:

a) Chemical carcinogenesis: chemical carcinogens have been used to induce tumors in mice. The most commonly used carcinogen to induce BC is BBN (N-butyl-N-4-hydroxybutylnitrosamine) which is considered a genotoxic molecule. BBN belongs to the nitrosamine family of alkylating agents that can induce hyperplasia, dysplasia, CIS, NMIBC, MIBC, and metastasis in mice. BBN is metabolized to N-butyl-N-(3-carboxypropyl) nitrosamine, the main mutagen (Vasconcelos-Nóbrega et al., 2012). The lesions and tumors generated in the bladder are histologically and genetically similar to basal human BC; tumors show a high mutational burden, commonly exhibiting mutations in *Trp53*, the p53 pathway, *Kmt2d* and *Kmt2c* (Fantini et al., 2018), and less frequently in *Hras* and *Kras* (Yamamoto et al., 1995). The type of lesions observed in mice depends on the sex, strain, age, and time of exposure to BBN (Vasconcelos-Nóbrega et al., 2012).

b) Xenografts of cancer cell lines and tumors: both cancer cell lines and patient-derived xenografts (PDXs) are commonly used to study the effects of the tumor microenvironment on disease progression by using nude mice as recipients, although the latter lack an immune system. Cancer cells can be injected orthotopically into the bladder to investigate tumor growth and therapeutic effects in the native tissue/hormonal environment. Cell take rate is variable, ranging from 50

to 100% (Gunther et al., 1999; Dobek and Godbey, 2010). However, cells are often undifferentiated, derived from aggressive tumors, and have a poor relation to the tissue of origin (Park et al., 2013; Hidalgo et al., 2015).

On the other hand, PDXs are generated by orthotopically or heterotopically implanting patient's primary tumor cells or biopsies into immune-deficient or humanized mice. Usually, PDXs retain better the genomic alterations, morphology, and architecture of the original tumor, making them useful to study tumor heterogeneity (Park et al., 2013; Ben-David et al., 2017). Some of the caveats of PDXs are a relatively low tumor take, the long time required to establish and propagate tumors, and the absence of an immune system. Nonetheless, PDXs are useful for drug discovery and screening, predicting clinical outcomes, personalized medicine, and biomarker identification (Hidalgo et al., 2015). There are few studies in BC but these have proven to retain a good correlation with the patient tumor at the genomic level and treatment response (Blinova et al., 2019; Lee et al., 2018; Pan et al., 2015).

c) Genetically engineered models: the mouse is the most experimentally tractable mammalian system to study cancer to date and the use of genetically engineered mouse models (GEMMs) has been one of the major breakthroughs in this field. The basis of GEMMs consists of heritably modifying gene expression, by either inserting extra DNA encoding a specific gene or sequence into the mouse genome, or knockout/knock-in technology in which a specific sequence of the mouse genome is altered. Models have evolved to become more and more sophisticated, including multiple allele modifications, gene editing, and xenograft approaches, adding up a wide range of possibilities (Kersten et al., 2017). One of the many advantages of GEMMs is the ability to direct oncogene and/or tumor suppressor gene activation/inactivation in a temporally and spatially controlled manner. The ability to concomitantly express a reporter marker along with the selected cancer gene modification facilitates lineage tracing, the isolation of transduced cell populations, the identification of biomarkers and to reversibly control cancer gene expression, allowing to assess tumor generation or regression, study the interactions and cooperation between genes, and even, the discovery of cancer-associated mutations (Kersten et al., 2017).

There has been relatively little research on BC GEMMs **(Table 2)**, compared with other tumor types. The earliest models were transgenic mice expressing SV40 large

T antigen under the control of tissue-specific promoters, such as *Upk2* and *Krt19*, where the mice developed CIS, MIBC, and metastasis (Zhang et al., 1999; De la Peña et al., 2011; Grippo and Sandgren, 2000; Ruan et al., 2018). Among the oncogenes tested in GEMMs are *Hras*, *Egfr*, and *CyclinD1,* which lead to urothelial hyperplasia and - when combined with mutant *p53* - promote the progression to dysplasia and NMIBC (Zhang et al., 2001; Cheng et al., 2002; García-España et al., 2005; Gao et al., 2004).

Tissue-specific conditional models have also been used, using gene targeting combined with the Cre recombinase system. Studies that have used a urothelial-specific promoter, the luminal marker *Upk2*, along with knock-in mutations in *Ras*, *Pten* loss, or activating mutations in *Fgfr3* and *β-catenin* as driver mutations. Individual alterations have not led to bladder tumors but combinations thereof have led to a variety of urothelial phenotypes (Ahmad, Patel, et al., 2011; Ahmad, Morton, et al., 2011; Ahmad, Singh, et al., 2011). Other approaches have used non-tissue-specific promoters, for example, by constitutively activating *β-catenin* in *Msx2* expressing cells with doxycycline-inducible transgenes or inactivation of *Notch* by using a conditional line targeting *Nctsn* lead to the same outcome (Lin et al., 2013; Rampias et al., 2014). A version of GEMMs has used Adeno-Cre delivery into the bladder, leading to simultaneous inactivation of *Pten* and *Tp53,* promoting invasive bladder cancer (Abate-Shen et al., 2009). In this regard, the generation of better mouse models to study both non-invasive and invasive bladder cancer is needed, particularly to deliver genetic alterations selectively to basal cells.

Table 2: Current mouse models of MIBC. Compilation of BC mouse models showing the molecular subtype and markers that are promoted in each of them. PDX = patient-derived xenograft; EET = earliest established time reported (after induction); BBN N-butyl-N-4-hydroxybutyl nitrosamine. Adapted from Ruan et al., 2018.

Model	Host	Induction source	EET	Molecular subtype	Molecular markers	Reference
Xenotransplant						
Subcutaneous	Immunocompromised	Human bladder cancer cell lines or PDX	Depends on inoculated cells			**Earl 2015**
PDX	Immunocompromised					**Lee 2018**
Orthotopic	Immunocompromised					**Jäger 2018**

Humanised	Severely				Immune markers	**Gong 2015**
	immunodeficient					
Allograft	C3H	MBT-2		Basal-squamous	KRT5, KRT14, HIF1a	**Huang 2017**
	C57/B6	MB49		Basal-squamous	CD44	**Chade 2008**
Autochthonous						
Hedgehog	*Gli1*$^{CreER/WT}$; *Smo*$^{flox/flox}$	BBN	12 wk	Basal-squamous	KRT14, SHH, PTCH1, GLI1, BMP4,BMP5, ID2, ID3, ID4	**Shin 2014**
Notch	*R26rtTA*; *tetO-Cre*; $_{Ncstn}$flox/flox		2 wk (2 mo)	Basal-squamous	KRT5, pERK, Ki67, cyclin D1, p63	**Rampias 2014**
STAT3	*K5-Stat3C*	BBN	2 wk	Basal-squamous	STAT3, KRT14	**Ho 2012**
p53 and others	*UPII-Cre*; $_{p53}$flox/flox$_{RB1}$flox/flox *CK19-Tag* *UPII-SV40T*^{high} *UPIIIa-Cre*; $_{p53}$flox/flox$_{Pten}$flox/flox	BBN	10 wk	Basal-squamous	KRT5, KRT14, Ki67	**He 2009**
			6 wk	Neuronal?	KRT19	**Grippo 2000**
			12 wk	Neuronal?	UPK2	**Cheng 2003**
			~58 wk	Luminal	UPK3	**Saito 2018**
	p53$^{+/-}$	BBN	16 wk	Basal-squamous	Ki67, KRT20	**van Batavia 2015**
Carcinogen-induced	**C57/B6**		**20 wk**	**Basal-squamous**	**CD44, CDH3, KRT14, KRT5**	**Fantini 2018**

Most of the available bladder cancer GEMMs have perturbed the "classical" cancer genes. However, the genomic projects described above led to the identification of novel BC genes whose function in tumorigenesis has not been studied. Our laboratory discovered mutations in *STAG2* and *RBM10* in BC and set out to explore the role of these genes by generating GEMMs through their conditional inactivation. In this work, I will focus on the study of *RBM10*.

3.3. The *RBM10* gene

3..3.1. Alternative splicing: importance in homeostasis and cancer

3.3.1.1. **Constitutive and alternative splicing**

In 1978, Walter Gilbert first described that the DNA sequence of protein-coding genes contains regions that will be ultimately translated into protein (i.e. exons), interrupted by “silent”, non-translated, DNA (i.e. introns). Coding sequences that are found between introns are called exons and are defined by two main sequence elements: the 5’ splice site and the 3’ splice site (Kelemen et al., 2013). RNA polymerase II transcription leads to a pre-mRNA that contains introns that will later be excised to generate the mature mRNA, a process designated as "splicing" that takes place in the nucleus. Intronic DNA has been roughly estimated to be 5-10 times more abundant than exons (Gilbert, 1978).

Two types of splicing events have been described: constitutive and alternative **(Fig. 6)**. Constitutive splicing involves intron removal and joining of exons from pre-mRNA transcripts. In alternative splicing, exons are differentially included or excluded leading to a variety of mature mRNA isoforms (Wang et al., 2015). Alternative splicing generates protein diversity, with >95% of human genes undergoing some level of splicing (Pan et al., 2009; Wang et al., 2008). In this manner, alternative splicing is considered to be one of the main sources of proteomic diversity in multicellular eukaryotes (Nilsen & Gravaley, 2010). Alternative splicing is a very complex molecular process that is regulated through multiple mechanisms, including the concentration or activity of splicing regulatory factors, depending on diverse physiological or pathological conditions (Wang et al., 2015). Alternative splicing plays a key role in almost every aspect of protein function; from protein binding to proteins, nucleic acids, and ligands to enzymatic properties, having profound functional effects (Irimia et al., 2007; Kelemen et al., 2013; Wang et al., 2015). Notably, distinct alternative splicing patterns have been observed in different cell types, suggesting this process can be tissue-specific, dictated by developmental (Sánchez, 2008) or differentiation-specific cues (Makeyev et al., 2007).

Although most changes caused by alternative splicing are structurally subtle, at a functional level the protein isoforms derived from a given gene can have different or even opposing functions (Kelemen et al., 2013; Leoni et al., 2011; David and Manley, 2010). Of note, splicing is subject to multiple levels of regulation and can vary in response to multiple environmental cues. The outcome of this process generates diverse transcripts that are involved in many cellular processes, such as cell

proliferation and cell survival, highlighting the importance of understanding alternative splicing and how its disruption can eventually lead to disease (Kelemen et al., 2013).

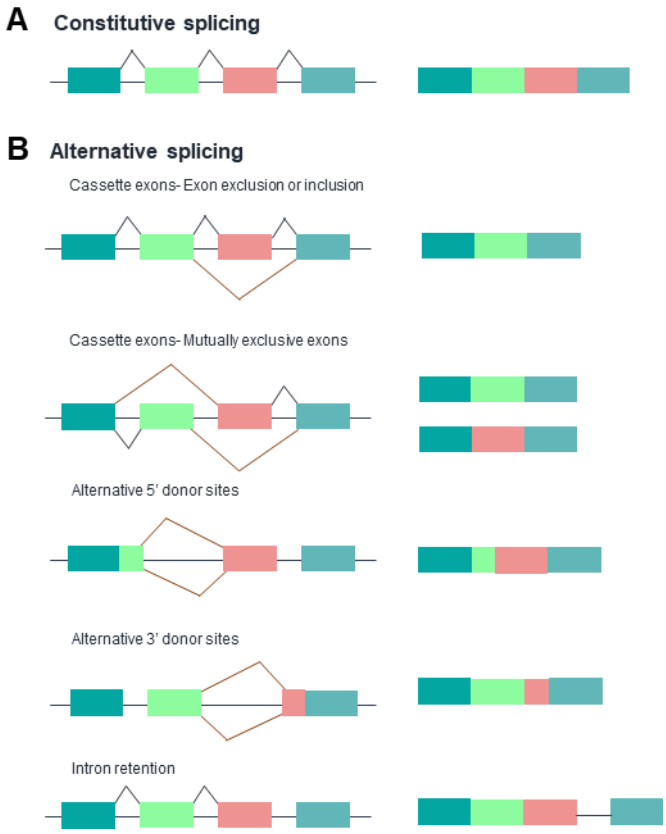

Figure 6. Constitutive and alternative splicing. A. Constitutive splicing takes place by removing intronic sequences from the pre-mRNA transcripts leading to the mature mRNA. **B.** Alternative splicing takes place in diverse ways by including or excluding exons, using alternative 5' or 3' donor sites, and intron retention.

Alternative splicing is achieved by the interaction between cis-acting mRNA elements and trans-acting factors. Cis-acting elements consist of 3´ and 5´- splice sites and intronic or exonic enhancer or silencer splicing sequences. These sequences also participate in constitutive splicing, where enhancer sequences play a more dominant role (Wang et al., 2015). Trans-acting factors are mainly RNA binding proteins that constitute the spliceosome and its regulators and can have both positive and negative effects (Wang et al., 2015; Nilsen & Gravaley, 2010). The spliceosome is a large and specialized machinery of approximately 170 proteins that will be discussed below. Besides the spliceosome, the other best-known regulators of alternative splicing are the SR proteins (serine/arginine-rich family of nuclear phosphoproteins) and heterogeneous nuclear ribonucleoproteins (hnRNPs). SR proteins recruit the components of the core splicing machinery (the spliceosome) by binding to exonic sequences (Zhou & Fu, 2014). By contrast, hnRNPs can either repress or promote splicing by binding to exonic or intronic sequences. The collaboration of both types of

regulators results in the promotion or inhibition of spliceosome protein binding to splice sites (Wang et al., 2015).

3.3.1.2. **The spliceosome**

The main regulator of alternative splicing is the spliceosome, a large macromolecular complex that recognizes exons, assembles in a stepwise manner, and removes introns from the pre-mRNA. The spliceosome is composed of approximately 170 proteins and 5 snRNA (small nuclear RNAs) complexes (U1, U2, U4, U5, and U6). The U1 snRNP is the first protein to bind the pre-mRNA recognizing the 5' splice sites **(Fig. 7)**. Then, splicing factor 1 (SF1) binds to the branch point, allowing the binding of the U2AF factor in the 3' splice site and generating the early complex. Later, SF1 is substituted by U2 snRNP leading to the pre-spliceosomal A complex. After this step, a series of exchanges and recruitments of more factors take place to transform the A complex into the spliceosomal B complex where introns are removed and exons joined in a trans-esterification reaction (Kelemen et al., 2013).

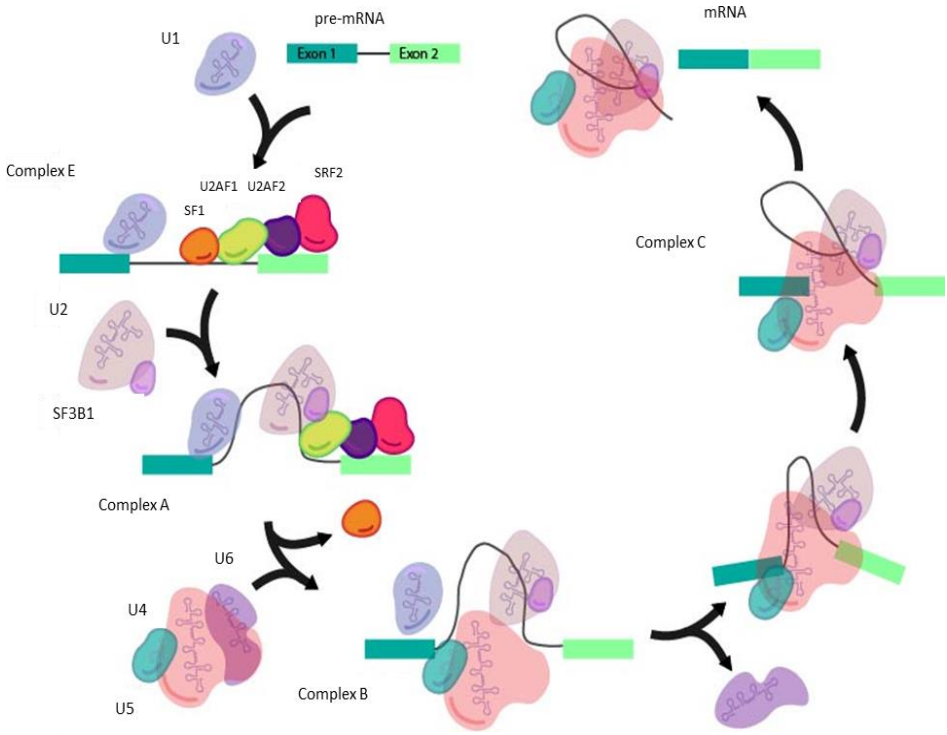

Figure 7: Spliceosome function. The U1 snRNP binds the pre-mRNA by recognizing the 5' splice sites. Then, splicing factor 1 (SF1) binds to the branch point, allowing the binding of non-snRNP associated factors as the U2AF1 and 2 factors in the 3' splice site and generating the early complex (E complex). Later, U2 snRNP and SF3B1 bind to the branch region by interacting with the U2AF proteins leading to the pre-spliceosomal A complex. Then, U4, U5, and U6 tri-snRNP are recruited to transform the A complex into the spliceosomal B complex, after which U6 is removed and the intronic region forms a laureate and forms the complex C. This intronic laureate is then removed and exons joined in a transesterification reaction to form mature mRNA.

3.3.1.3. **Splicing factor alterations in cancer**

The wide role played by alternative splicing in cell proliferation, differentiation, metabolism, apoptosis, motility, invasion, and angiogenesis accounts for the fact that changes in splicing occur during tumorigenesis. There is evidence that altered alternative splicing is a hallmark of cancer and has been implicated in almost all aspects of the disease, with substantial variation among tumor types (Wang et al., 2014; Cooper et al., 2009; David and Manley, 2010; Seiler et al., 2018).

The first studies supporting the role of alternative splicing in cancer described a wide number of cancer-associated changes leading to increased cell proliferation, survival, EMT, and invasion (Venables et al., 2008; Klinck et al., 2008; He et al., 2009; Shapiro et al., 2011). This led to the question of which specific protein isoforms are cancer-associated and which mechanisms are responsible for their generation. Among the main cancer-associated splicing events reported are those affecting transcripts coding for proteins involved in apoptosis such as *Caspase-3* (Vegran et al., 2006), *BCL2L1 (BCL-X)* (Xerri et al., 1996), *FAS* (Izquierdo & Valcarcel, 2007; Corsini et al., 2007), and *BIRC5 (*Sampath & Pelus*, 2007)*, genes involved in the ubiquitination of *TP53* tumor suppressor as *MDM2* (Sigalas et al., 1996; Manfredi et al., 2010), genes related to immortality as *TERT* and angiogenesis (*VEGF-A*) (Biselli-Chicote et al 2012; Lapuk et al., 2014).

Some of these alterations result from somatic mutations in genes coding for trans-acting splicing regulatory genes. They were first described in *SRSF1* (Serine/Arginine-rich splicing factor 1), which encodes a protein affecting alternative splicing of many transcripts that are known to contribute to tumorigenesis (Ghigna et al., 2005). Additional mutations were reported in *SRSF3* (Serine/Arginine-rich splicing factor 3) (Kurokawa et al., 2014; Tang et al., 2013) and in *SRSF2* (Serine/Arginine-rich splicing factor 2), *SF3B1*, *U2AF1*, and *ZRSR2*, all involved in U2 complex function (Yoshida et al., 2011). These core machinery factors are involved in the recognition of 3' splice sites of introns and, therefore, mutations therein lead to defects in RNA recognition/splicing (Hicks et al 2010).

Importantly, splicing factor gene alterations occur in a wide range of tumors (Makishima et al., 2012; Papaemmanuil et al., 2013; Haferlach et al., 2014; Lindsley et al., 2015; Jeromin et al., 2013; Ferreira et al., 2014; DeBoever et al., 2015; Darman et al., 2015) and the genome sequencing consortium studies have highlighted their prevalence

across tumor types (Seiler et al., 2018; Obeng et al., 2019). Mutations can be either gain- or loss-of-function. Hotspot mutations in *SRSF2*, *SF3B1*, and *U2AF1* have been described in a wide variety of cancer types. Other genes are *RBM10,* encoding an RNA-binding protein (RBP), and *FUBP1* which encodes a DNA-binding protein; the first presents loss-of-function mutations in lung adenocarcinoma, bladder cancer, among others; the latter, in low-grade glioma (Seiler et al., 2018).

3.3.2. RBM10, a regulator of alternative splicing

RBM10 is an RNA-binding motif-containing protein that belongs to the RBP family, regulating the nature, quantity, and function of transcripts (Tessier et al., 2015; Loiselle et al., 2017; Glisovic et al., 2008). *RBM10* is located on Xp11.23 (Thiselton et al., 2002). The gene contains 24 exons and is subject to alternative splicing, yielding two transcripts: the predominant transcript leads to a protein of 930 residues and the second to a protein of 835 amino acids (Johnston et al., 2011). The long and short isoforms differ in the inclusion of exon 4. Recently, a GTC RNA triplet located at the end of RBM10v1 exon 10 was identified as encoding a Val residue, thus generating further variation in the structure in both RBM10v1 and RBM10v2. Hence, 4 main alternative splice variants have been reported: 1) RBM10v1 (V354); 2) RBM10v1 (V354del), lacking the GTG RNA triplet; 3) RBM10v2 (V277), lacking exon 4 of RBM10v1; and 4) RBM10v2 (V277del), lacking exon 4 of RBM10v1 and the GTG RNA triplet **(Fig. 8)** (Sutherland et al., 2005; Loiselle et al., 2017).

RBM10 is expressed in most, if not all, human cells (Human Protein Atlas, https://www.proteinatlas.org/) and it regulates its own alternative splicing (Sun et al., 2017). As expected, one of the *RBM10* alleles is silenced in somatic cells of females through X chromosome inactivation (Thiselton et al., 2002). RBM10 contains characteristic domains that confer regulatory features on RNA metabolism and pre-mRNA splicing **(Fig. 8)**. Its functional domains include two RNA recognition motifs (RRM) on the N-terminus, a RanBP2-type zinc finger motif, a C2H2 Zn finger that binds to 5'- splice sites, an arginine/serine-rich domain, an OCtamer REpeat (OCRE) domain that regulates its interaction with other molecules of the spliceosomal complex, three nuclear localization signals (NLSs) (NLS2 and NLS3 are within the RRM1 and OCRE regions, respectively), and a C-terminal glycine(G)- patch domain (Sutherland et al., 2005); most of these features are also found in snRNPs and hnRNPs (Glisovic et al., 2008).

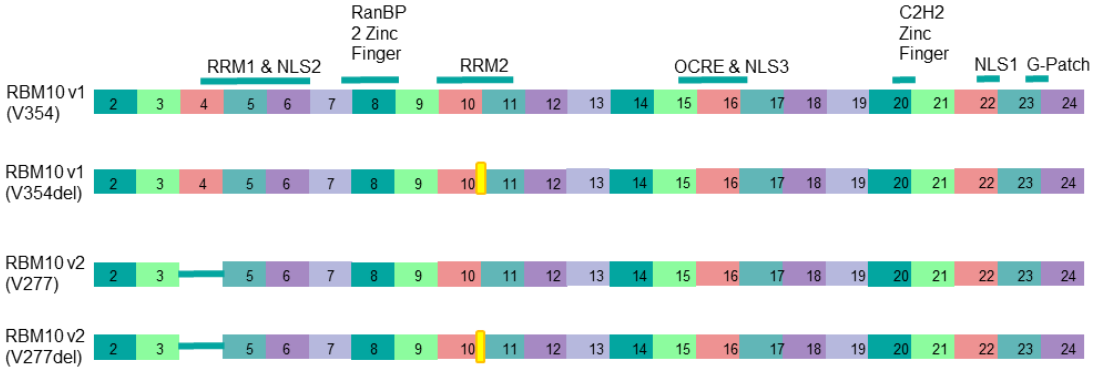

Figure 8: RBM10 structure and functional domains in reported variants. Principal RBM10 alternative splice variants, where yellow line represents the absence of a GTG RNA triplet at the end of exon 10 which leads to two additional variants having or lacking a Val residue (Modified from Sutherland et al., 2017).

The first studies on the spliceosome revealed that RBM10 is part of the pre-spliceosomal A and B complexes (Behzadnia et al., 2007; Bessonov et al., 2008; Deckert et al., 2006; Hegele et al., 2012) and that it preferentially binds to G- and U-rich RNA sequences (Inoue et al. 1996). Later, thousands of RBM10 new binding sites were discovered near 3'- and 5'- splice sites both upstream and downstream introns, where the main role of RBM10 was revealed: promoting exon skipping **(Fig. 9)** (Wang et al., 2013; Rodor et al., 2017). Importantly, RBM10 was found to have antagonistic effects to RBM5 and RBM6 on the alternative splicing of a wide range of transcripts related to apoptosis and proliferation (Bechara et al. 2013).

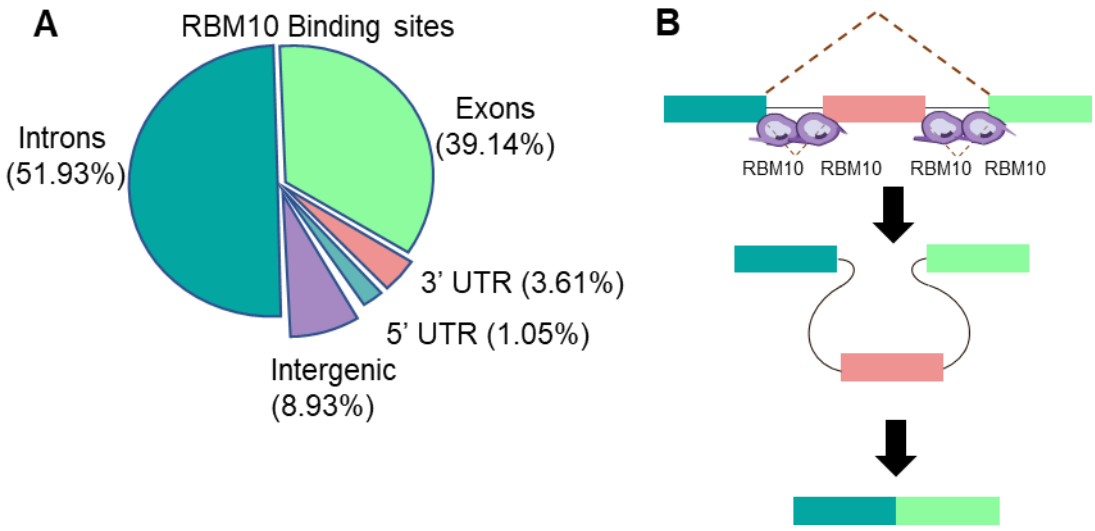

Figure 9: RBM10 function. A. RBM10 preferential binding sites on pre-mRNA, **B.** RBM10 binding to splicing sites in the flanking regions of introns, delaying the splicing choice, and promoting exon skipping.

The first RBM10-mediated splicing events identified were in the pre-mRNA of the apoptosis-related genes *Fas* receptor, and *Bcl-x* (Inoue et al. 2014). Later, the splicing

of *Dlg4* (Zheng et al., 2013), *NUMB* (Bechara et al., 2013), *RBM5* (Sun et al., 2017), and *SMN2* (Sutherland et al., 2017) were discovered, highlighting its importance in the regulation of essential cellular processes.

3.3.3. RBM10 somatic mutations

The TCGA studies have reported somatic mutations in *RBM10* in lung adenocarcinoma (7-9% of the tumors), bladder, pancreatic, colorectal, and kidney cancer (2-5%), among others (Collison et al., 2014; Brooks et al., 2014, TCGA consortium). In BC, *RBM10* mutations occur in 16% of NMIBC (cBioportal, MSK Eur Urol, 2017; Pietzak et al., 2017) and 5% of MIBC (cBioportal, TCGA PanCancer Atlas, Hoadley et al., 2018), in both papillary and non-papillary pathways.

RBM10 somatic mutations are distributed across the gene, following the pattern of a tumor suppressor **(Fig. 10)** (cBioportal, TCGA 2014). Approximately, 30% of the mutations described in the TCGA are predicted to lead to premature stop codons, causing protein-truncating loss-of-function variants. The remaining mutations are mainly missense (>50%) and synonymous (14%) mutations (TCGA, 2014); their effect on splicing depends on the type and location of the alteration and its effect on protein structure or RNA binding (Wang et al., 2013; Tessier et al., 2015).

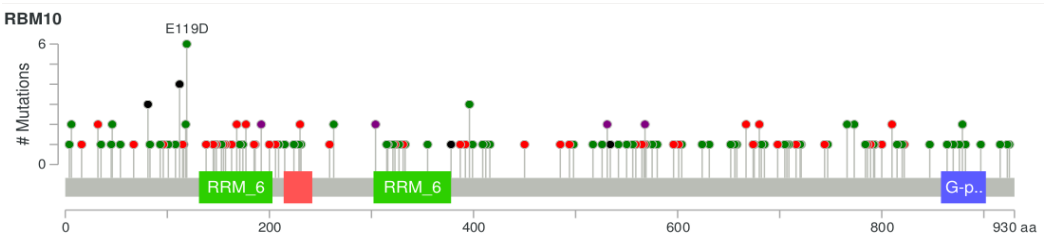

Figure 10: *RBM10* somatic mutations. Schematic lollipop representation of somatic mutations across the *RBM10* gene in TCGA pan-cancer studies (data retrieved from cBioportal). Truncating mutations are represented in black, missense mutations in green, and in-frame mutations in red.

So far, few studies have tried to shed light on the role of RBM10 in cancer, with some paradoxical results. Several reports have proposed a tumor suppressor role in lung (Bechara et al., 2013; Yin et al., 2018), ovarian (Bechara et al., 2013; Hernández et al., 2016; Wang et al., 2013), liver (Kunimoto et al., 2019), breast cancer (Martínez-Arribas, et al., 2006; Wang et al., 2012), and lymphoblastic leukemia (Wang et al., 2012) by reducing proliferation, cell colony formation, and decreasing xenograft tumor growth in mice. In lung adenocarcinoma. *RBM10* mutations are associated with decreased expression (Zhao et al., 2017) and an increased proliferative and colony formation

capacity of cancer cells, by regulating alternative splicing of *NUMB*, a component of the Notch signaling pathway that is frequently altered in lung cancer (Hernández, et al., 2016; Bechara et al., 2013). On the other hand, some studies have suggested oncogenic activity in small cell lung cancer (Loiselle et al, 2017) and lung adenocarcinoma (Sun et al., 2018), promoting proliferation or representing poor prognosis in patients. These contradictory findings might result not only from the specific effects of different mutations but also from different tissue-contexts, physiological expression levels, or the cooperation of RBM10 with other splicing factors, such as RBM5 (Loiselle et al., 2017).

RBM10 also has splicing-independent functions, for instance, it interacts with histone modifiers (e.g. 2A-DUB) (Zhu et al., 2007), centriole duplication regulatory proteins (e.g. the PLK4-STIL complex) (Kunimoto et al., 2020), and cellular localization of proteins (e.g. FilGAP) (Yamada et al., 2016). These interactions can translate into functional effects such as aberrant chromosomal division (Kunimoto et al., 2020) and cell spreading (Yamada et al., 2016). However, the mechanisms through which RBM10 affects tumorigenesis remain largely unknown.

3.4. *RBM10* and TARP syndrome

Using massively parallel sequencing, inactivating germline mutations in *RBM10* were identified associated with TARP syndrome (Talipes equinovarus, Atrial septal defect, Robin-sequence, and Persistence of the left superior vena cava, OMIM, #311900) (Johnston et al., 2010). TARP is a developmental disease that leads to an early death before or soon after birth (Kurpinski et al., 2003; Johnston et al., 2010; Gripp et al., 2011).

3.4.1. Epidemiology

TARP syndrome is a rare developmental disease with a low incidence, with less than 1 in 10^6 persons worldwide (Orphanet) and a diverse phenotype, that is almost invariably lethal, affecting males who either die prenatally or soon after birth. The first clinical studies reported that the affected children do not survive beyond 4 years (Johnston et al., 2010; Gripp et al., 2011; Johnston et al., 2014; Powis et al., 2017). However, later studies have reported 4 individuals surviving beyond infancy thanks to intensive care and effective management (Wang et al., 2013; Niceta et al., 2018; Hojland et al., 2018).

3.4.2. Genetics

TARP is an X-linked recessive disease. Several missense and nonsense mutations in *RBM10* have been described, for example, c.del159C (Gripp et al., 2011), c.1235G>A (Johnston et al., 2010), c.1893_1893insA (Johnston et al., 2010), and c.273_283delinsA (Hojland et al., 2018), suggesting that this disease has a diverse mutational spectrum and variable phenotypes. It is not known whether cells from TARP syndrome patients exhibit alterations in alternative splicing, raising the question that the role of RBM10 may go beyond alternative splicing (Niceta et al., 2019).

3.4.3. Clinical features

TARP syndrome was first described by Gorlin and colleagues in 1970, receiving the name of “Robin’s syndrome” since the affected newborns presented Pierre Robin syndrome in association with congenital heart malformations and clubfoot as main hallmarks. After the study of a 4-generation family with the disorder, the designation of TARP syndrome was proposed as an acronym after the four main features of patients (Talipes equinovarus, Atrial septal defect, Robin Pierre sequence) **(Fig. 11)** (Kurpinski et al., 2003):

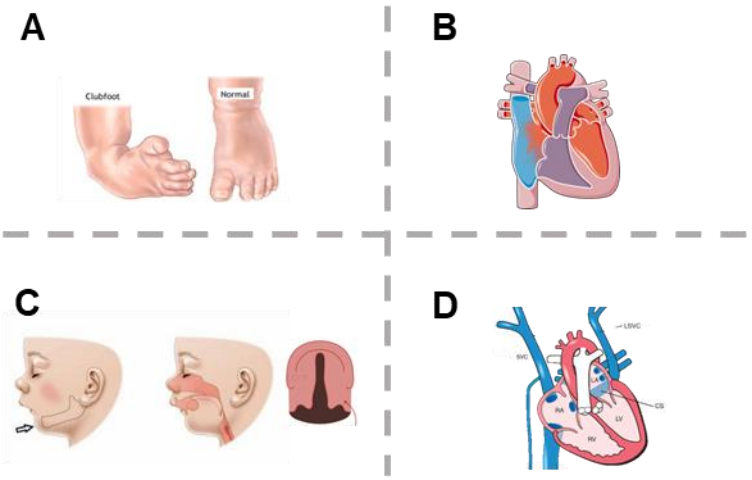

Figure 11: TARP syndrome main features. A. Talipes equinovarus or clubfoot. **B.** Atrial Septal Defect. **C.** Robin Sequence. **D.** Persistence of the left superior vena cava.

Atrial septal defects (ASD). The heart regulates blood flow through the coordinated contraction (systole) or relaxation (diastole) of its 4 chambers (2 atria, left and right and 2 ventricles, left and right) and through the opening or closing of the valves that connect the atria with the ventricles (atrioventricular valves) and the valves that connect the ventricles with the arteries (semilunar or sigmoid valves). In a normal heart cycle, deoxygenated blood is received into the right atrium from the superior vena cava and the inferior vena cava. At the same time, oxygenated blood from the lungs is received in the left atrium through four different pulmonary veins. Blood from the atria flows to the ventricles initially passively and finally actively by contraction of the atria (atrial systole). Deoxygenated blood flows into the right ventricle by crossing the opened tricuspid valve. Oxygenated blood flows into the left ventricle through the bicuspid or mitral valve. Tricuspid and mitral valves are known as atrioventricular valves. After this, blood is pumped out of the heart by the contraction of the ventricles (ventricular systole). From the right ventricle, deoxygenated blood is pumped into the pulmonary trunk through the pulmonary valve. The pulmonary trunk divides into two pulmonary arteries to reach the lungs, where the blood picks up oxygen. From the left ventricle, oxygenated blood is pumped into the aortic artery through the aortic valve to reach the different body tissues and supply them with oxygen. Both pulmonary and aortic valves are known as semilunar or sigmoid valves. Importantly, normal blood flow is allowed by the proper closure between the chambers and the function of the valves **(Fig. 12)**. The standard techniques used to assess heart function are electrocardiogram, echocardiography, and Magnetic Resonance Imaging (MRI).

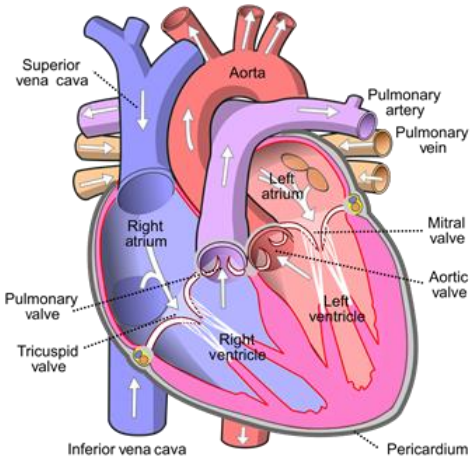

Figure 12: Normal heart structure and blood circulation. Blood is delivered into the right atrium by the superior and the inferior vena cava where it moves into the right ventricle by crossing the tricuspid valve. In the right atrium, blood is pumped into the pulmonary artery to go into the lungs to oxygenate. After this, oxygenated blood returns to the heart through the pulmonary veins into the left atrium where it is pushed into the left ventricle by crossing the mitral valve. Finally, blood is pumped out to the rest of the body through the aorta.

During development, there is a physiological communication between the atria, called *Foramen Ovale*, that allows blood to detour away from the lungs since blood is oxygenated in the placenta (Naqvi et al., 2018; Jensen et al., 2019). After birth this opening is no longer needed and, in the final stages of intrauterine development, it closes and generates a structure called *Fossa ovalis*, a remnant of the *Foramen Ovale*. If a small opening remains, it may not cause symptoms: many healthy adults have a leftover, called Patent Foramen Ovale, and live normally. However, larger defects in the upper heart chambers lead to ASD: the pressure difference between the two atria varies depending on the degree of the defect. When the ASD is small, the pressure in the left atrium is greater than in the right atrium, causing a left-to-right shunt (Dexter, 1956). When the septal defect is large, there is free communication between both atria and their respective venous systems and, during diastole, in their respective ventricles (Dexter, 1956). In patients with large (>2 cm^2) defects, the pressure difference is practically abolished. Large shunts generate a reduction in left ventricular filling pressures that will increase the left-to-right shunt, systemic venous congestion and will lead to a volume overload of the right ventricle, which gives rise to enlargement of right-sided cavities. This results in altered left ventricular geometry. On the other hand, reducing right ventricular filling pressures may decrease the left-to-right shunt and can lead to shunt reversal, causing cyanosis or low oxygen saturation (Le Gloan et al. 2018). In children with a large ASD (>10 mm), blood can move across the upper chambers from the left to the right atrium and out into the lung arteries, leading to a reduced life expectancy (Le Gloan et al. 2018). Significant ASD is associated with pulmonary

hypertension, congestive heart failure, and age-related increased mortality (Le Gloan et al. 2018; Campbell, 1970).

ASD is classified according to its location and nature of the embryological defect **(Fig. 13)**. If found in the middle of the atrial septum, it is called Secundum ASD; it represents 75% of all ASD. If found at the base of the wall, it is called Primum anomalies and it represents 15% of the cases; this is more common in congenital diseases such as Down's syndrome. ASD can also be found in the sinus venosus and coronary sinus, representing the remaining 10% (Lindsey and Hillis, 2007).

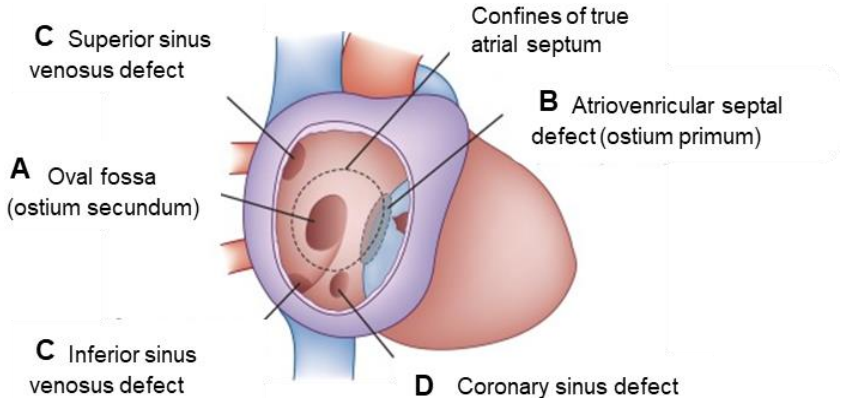

Figure 13: ASD classification according to its location. A. ASD in the middle of the septum of the ostium secundum. **B.** In the base of the septum of the ostium primum. **C.** In the sinus venosus. **D.** in the coronary sinus (Modified from Carabuena, 2018).

Persistence of the left superior vena cava (PLSVC). PLSVC refers to a rare anomalous pulmonary venous return present in 0.3-0.5% of individuals of the general population and 4.5% of individuals with congenital heart diseases (Tyrak et al., 2017; Zhong et al., 2015). It is a persistent remnant of a vessel that is present as a counterpart of the normal right-sided superior vena cava that, in general, disappears after birth (Saha et al., 2012). The PLSVC commonly drains into the right atrium through a dilated coronary sinus; when it drains directly to the left atrium, it causes a right-to-left cardiac shunt. Most individuals with PLSVC are asymptomatic. Only patients with unusual drainage and right-to-left shunting present with clinically significant disease. This drainage and anomalous venous return may lead to cardiac arrhythmias, decreased exercise tolerance, progressive fatigue, chest discomfort, palpitations, syncope, or cyanosis (Goyal et al., 2008). Importantly, almost 40% of patients with PLSVC have associated cardiac anomalies, such as ASD (Sarodia & Stoller, 2000) suggesting that both conditions can result from common causes.

Robin sequence. Also known as the Pierre Robin sequence, it is characterized by a set of abnormalities affecting the head and face: a smaller lower jaw (micrognathia), a tongue that is placed further back than normal (glossoptosis), and a soft, high-arched palate with an opening (cleft palate). It is believed that an underdeveloped lower jaw sets off the rest of the conditions, affecting the placement of the tongue, leading to a blockade of the airways and the formation of the palate during development. The combination of these features can lead to breathing and eating difficulties after birth. An isolated Pierre Robin sequence affects one in 14,000 persons (Cote et al., 2015; Giudice et al., 2018). In approximately 37% of the cases, the Robin sequence occurs as part of a syndrome with multiple malformations (Genetic and Rare Diseases Information Center, NIH, https://rarediseases.info.nih.gov/diseases).

Other clinical features. More recent studies have described a diverse range of signs and symptoms in subjects with TARP syndrome, suggesting that it is a pleiotropic condition with a wide phenotypic spectrum:

Table 3: Described features of TARP syndrome. Modified from Human Phenotype Ontology (https://hpo.jax.org/app/) and the Genetic and Rare Diseases Information Center (Genetic and Rare Diseases Information Center, NIH, https://rarediseases.info.nih.gov/diseases).

Medical Terms	Other Names
80%-99% of people present these features	
Atrial septal defect	An opening in the wall separating the top two chambers of the heart
Persistent left superior vena cava	
Pierre-Robin sequence	
Talipes equinovarus	Clubfeet
30%-79% of people present these features	
Cleft palate	Cleft roof of the mouth
Cyanosis	Blue discoloration of the skin
Failure to thrive	Faltering weight
Generalized hypotonia	Decreased muscle tone
Global developmental delay	
Glossoptosis	Retraction of the tongue
Hypertelorism	Wide-set eyes
Intellectual disability	Mental deficiency

Intrauterine growth retardation	Prenatal growth deficiency
Micrognathia	Little lower jaw
Rocker bottom foot	Rocker bottom feet
Sloping forehead	Inclined forehead
Underdeveloped supraorbital ridges	Flattened bony protrusion above eyes
Wide nasal bridge	Broad nasal bridge
5%-29% of people present these features	
Abnormal corpus callosum morphology	
Anteverted nares	Nasal tip, upturned
Apnea	
Broad-based gait	Wide based walk
Cerebellar hypoplasia	Small cerebellum
Clinodactyly	Permanent curving of the finger
Cryptorchidism	Undescended testes
Extramedullary hematopoiesis	
Finger syndactyly	
Hand polydactyly	Extra finger
Hearing impairment	Deafness
Horseshoe kidney	Horseshoe kidneys
Hydronephrosis	
Hypoplasia of proximal radius	
Low-set, posteriorly rotated ears	
Myopia	Close sighted
Optic atrophy	
Pectus excavatum	Funnel chest
Postaxial polydactyly	
Prominent antihelix	
Scoliosis	
Seizures	Seizure
Short palpebral fissure	Short opening between the eyelids
Short sternum	
Single transverse palmar crease	
Small earlobe	Small earlobes

Tetralogy of Fallot	
Thick eyebrow	Bushy eyebrows
Tongue nodules	
Widely patent fontanelles and sutures	
1%-4% of people present these features	
Abnormal hair pattern	Abnormal distribution of hair
Abnormality of the duodenum	
Alveolar ridge overgrowth	Overgrowth of the gum ridge
Athetoid cerebral palsy	
Pulmonary hypoplasia	Small lung
Percent of people who present these features is not available through HPO	
Abnormality of cardiovascular system morphology	
Cerebellar vermis hypoplasia	
Cutaneous syndactyly	
Deep palmar crease	Deep palm line
High palate	Elevated palate
Hypoplasia of the radius	Underdeveloped outer large forearm bone
Large fontanelles	Wide fontanelles
Low-set ears	Low set ears
Microtia	Small ears
Posteriorly rotated ears	Ears rotated toward the back of the head

4. OBJECTIVES

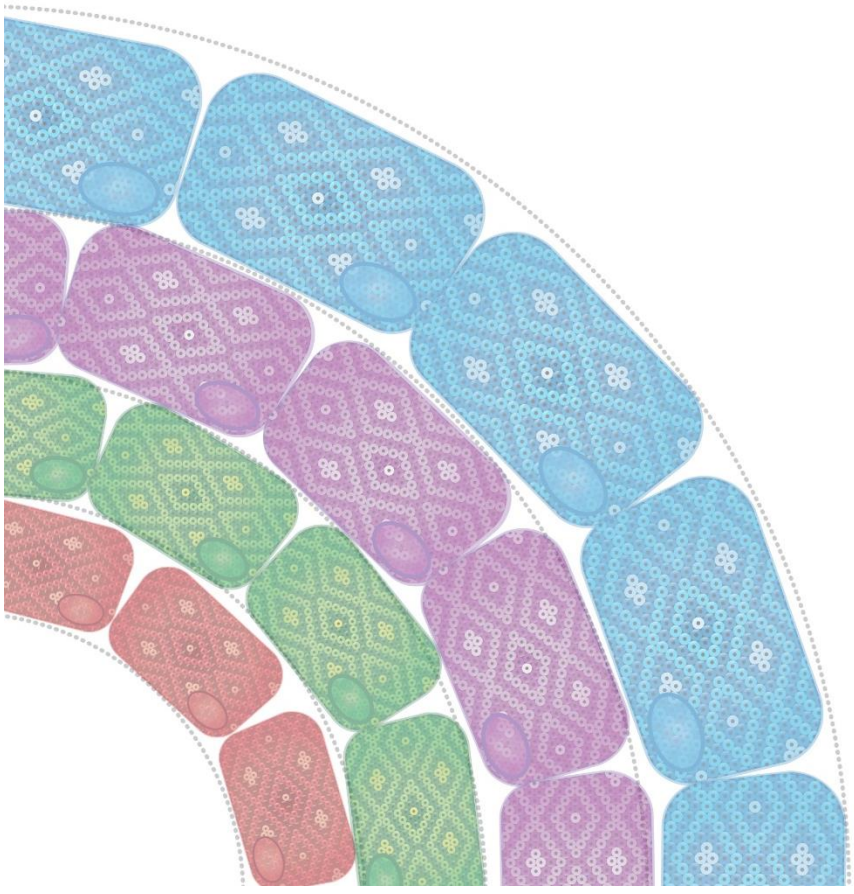

OBJECTIVES

RBM10 inactivating mutations have been reported recently in TARP syndrome - in the germline - and in BC - at the somatic level. However, little is known on how the mutations disrupt normal tissue homeostasis and contribute to tumor development.

I set out to study the role of *Rbm10,* in homeostatic conditions at the organismal level and in urothelial biology and tumorigenesis, leveraging on the generation of a new genetic mouse knockout model. My aims were:

1) To determine whether *Rbm10* is required for normal mouse development and whether *Rbm10* inactivation recapitulates TARP syndrome.

2) To assess the effect of *Rbm10* inactivation on adult tissue homeostasis.

3) To analyze how *Rbm10* inactivation affects urothelial biology.

4) To use the *Rbm10* conditional knockout mouse to model bladder cancer development.

1. MATERIALS AND METHODS

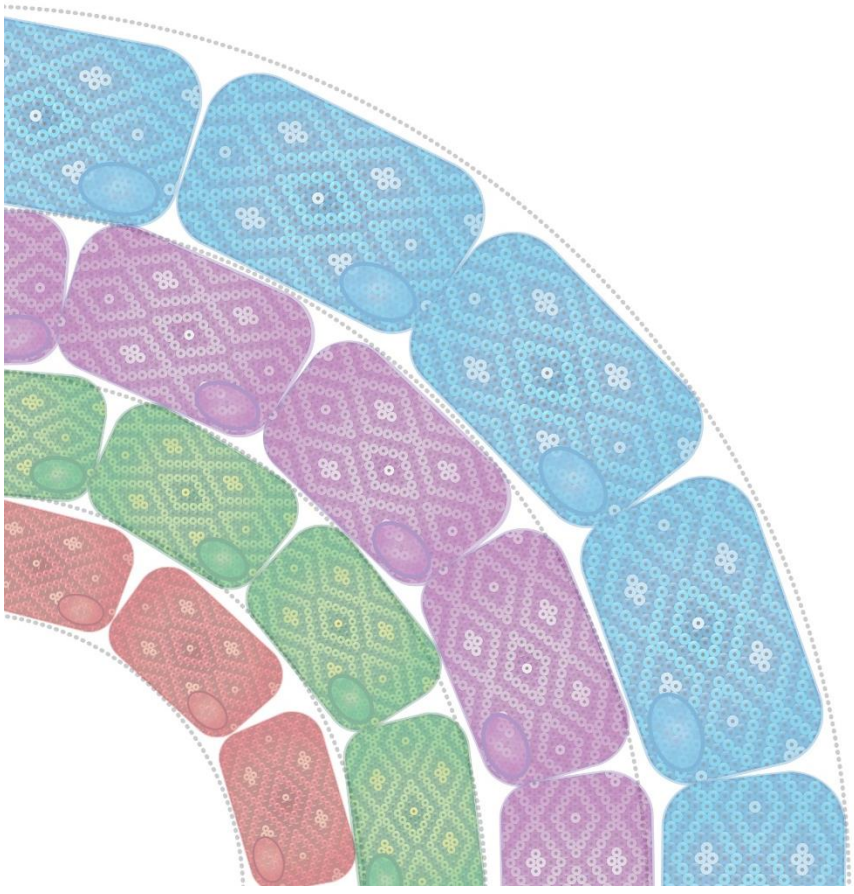

MATERIALS AND METHODS

5.1. Mouse strains and *in vivo* experiments.

The KOMP ES cell line Rbm10tm1a(KOMP)Mbp RRID:MMRRC_061232-UCD was obtained from the Mutant Mouse Resource and Research Center (University of California at Davis), an NIH-funded strain repository, donated by The KOMP Repository, originating from Kent Lloyd, UC Davis Mouse Biology Program. Positive clones were infected with adeno-FLP to remove the selection cassette and create the conditional allele. Cells were microinjected into C57BL/6BrdCrHsd-Tyrmorulae. Germline transmitting chimeras were screened by PCR (primers: forward (1) CCTGGTGTACAAAGTGAGTTCCAGC, reverse (1) CCACTATCTCCGCTCCTTCCTAACC, and reverse (2) CTACCTACATGGGACTGACTTCCCC) and selected to generate the colonies. Mice carrying the *Rbm10* conditional (c) KO allele were crossed with mice carrying a tamoxifen-inducible Cre-ERT2 allele [Tg. Ubiquitin C promoter (*Ubi)-CreERT2*] to isolate murine embryonic fibroblasts (MEF) and perform viability studies upon deletion in adult mice or with a constitutively active Cre [Tg. CMV immediate-early/enhancer chicken β actin hybrid promoter *(CAG)-Cre*], to assess embryonic lethality. Additionally, both strains were later crossed with Rosa26_ACTB-tdTomato_EGFP (*Rosa26 mT/mG*) strains to incorporate a reporter allele in heterozygosis. To induce recombination in adult animals, 6 week-old mice were fed for variable periods with a diet containing tamoxifen (TMX), as specified. For the experiments of embryo development or in adult mice, only males were used unless otherwise specified in the text. Using these strategies, the following mouse strains were generated:

Table 4. Mouse models used in this study

Name	Model alleles	Type of model
Rbm10 KO	Rbm10 lox/y; Tg. CAG-Cre	constitutive
Rbm10 KO	Rbm10 lox/y; Tg. Ubi-CreERT2; Rosa26 mT/mG	conditional
Kras Rbm10 KO*	Rbm10 lox/y; KRas+/LSL-G12Vgeo (Guerra et al., 2003); Tg. Ubi-CreERT2; Rosa26 mT/mG	conditional
Pik3ca Rbm10 KO*	Rbm10 lox/y; Pik3ca +/FLneoLH1047R-IRESGFRlucF (Renner & Carnero, 2009); Tg. Ubi-CreERT2; Rosa26 mT/mG	conditional
Trp53 KO Rbm10 KO	Rbm10 lox/y; Trp53lox/lox (Jonkers et al., 2001); Tg. Ubi-CreERT2; Rosa26 mT/mG	conditional

All strains were generated at the CNIO animal facility and mice were housed in a specific pathogen-free environment according to institutional guidelines. All crosses were maintained in a predominantly C57BL/6 background and littermates were used as controls

in the studies. All experiments were performed following the guidelines for Ethical Conduct in the Care and Use of Animals as stated in The International Guiding Principles for Biomedical Research involving Animals, developed by the Council for International Organizations of Medical Sciences (CIOMS), and approved by the institutional Ethics and Animal Welfare Committee (Instituto de Salud Carlos III, Madrid, Spain) and the Comunidad Autónoma de Madrid.

5.1.1. Echocardiography.

Studies were performed on E18.5 (embryonic days) embryos of *Rbm10 KO* pregnant mothers. Embryos/fetuses were imaged through the maternal abdominal wall with a Vevo 2100 ultrasound machine (VisualSonics, Canada) using a 40 MHz high-resolution linear transducer. All echocardiographic recordings were stored and analyzed offline in a blinded manner. To acquire images, hair was removed from the dam's abdomen and, afterwards, pregnant mice were lightly anesthetized using isoflurane (3% induction dose, 2.0-1.5% maintenance dose) plus oxygen (1 L/min). During the ultrasound recordings, the two laterally located uterine horns were manually palpated and scanned to determine the presence and position of the embryos/fetuses. In each individual embryo/fetus, the left and right side were established to detect the position of the heart. For morphological and functional assessment, bidimensional and M-mode echocardiography in short axis (SAX) and long axis (LAX) views of the left ventricle (LV) were performed. From the bidimensional SAX view, the end-systolic and end-diastolic ventricular internal area were traced to calculate fractional shortening. From the M-mode in LAX view, the end-systolic and end-diastolic ventricular internal diameter were measured and the ejection fraction was calculated. Afterwards, embryos were sacrificed by beheading according to ethical guidelines, fixed in 10% formalin, and decalcified. In addition, transthoracic echocardiography was performed blinded in mice of ages 6 and 10 months by an expert operator using a high-frequency ultrasound system (Vevo 2100, Visualsonics Inc., Canada) with a 40-MHz linear probe. Two-dimensional (2D) and M-mode (MM) echography were performed at a frame rate above 230 frames/sec, and pulse wave Doppler (PW) was acquired with a pulse repetition frequency of 40 kHz. Mice were lightly anesthetized with 0.5-2% isoflurane in oxygen, adjusting the isoflurane delivery trying to maintain the heart rate in 450±50 bpm. Mice were placed in a supine position using a heating platform and warmed ultrasound gel was used to maintain normothermia. A base apex electrocardiogram (ECG) was continuously monitored. Images were transferred to a computer and were analyzed off-line using the Vevo 2100 Workstation software.

Standard bidimensional (2D) and M-mode (MM) parasternal long and short axis views (LAX and SAX, respectively) were acquired for at least 10 cardiac cycles. Guided M-mode SAX imaging at the level of the papillary muscles was used to measure LV anterior wall,

internal diameter and posterior wall at the end of the diastole (LVAW,d; LVID,d and LVPW,d, respectively) and at maximum systole (LVAW,s; LVID,s and LVPW,s, respectively). From these parameters, LV systolic function was assessed by automatic calculation of fractional shortening (FS) using the equation: [(LVID,d – LVID,s) / LVID,d]x 100. Cardiac mass was also automatically obtained using the formula [1.053 x {(LVID,d + LVPW,d +IVS,d)3- LVID,d3}} x 0.8. A 4-chamber apical view was acquired to estimate right ventricle (RV) systolic function using the tricuspid annular plane systolic excursion (TAPSE), obtained from a MM view, measuring maximum lateral tricuspidal annulus movement.

The mitral valve inflow pattern was acquired using PW Doppler echography in the 4-chamber apical view to assess diastolic function. Early and late diastolic velocity peak waves (E and A, respectively), the E/A ratio, and the isovolumetric relaxation time (IVRT) were measured.

To evaluate pulmonary pressures, pulmonary artery (PA) flow was measured from the SAX, at the level of the aorta, optimized to visualize the PA valve crossing the aorta, and parallel to the ultrasound beams. Pulse wave Doppler was displayed at the beginning of the PA. The PA acceleration time (AT) and ejection time (ET) were measured, and the ratio was calculated (AT/ET).

5.1.2. Magnetic Resonance (MR) imaging analysis.

Decalcified-formalin-fixed *Rbm10 KO* E18.5 embryos were sent to Hospital Gregorio Marañón (Madrid) to perform an MRI. 3D T2-weighted MR images were acquired with a Biospin 7T (Bruker, Germany) with a Turbo RARE (Rapid Acquisition with Refocused Echoes) sequence with the following parameters: TR/TE = 1800/43.5 ms, rare factor = 16, 6 averages, matrix size 256 x 256 x 256, field of view 15 x 15 x 24 mm and a resolution of 0.059 x 0.059 x 0.094 mm with a total scan time of 13h 26min.

The size of the different regions of interest (ROIs) (e.g. whole body, eyeball, skull, sternum) were measured using the distance tool present in the Multimodality Workstation software (Pascau et al., 2006).

5.1.3. Micro Positron Emission Tomography-Computerized Tomography Scan (micro PET-CT scan).

Rbm10 KO adult mice were subject to CT scans at 60 weeks of age. In addition, *Kras* * *Rbm10 KO* having been with adenovirus-Cre were subjected to CT scans every two weeks until 50 weeks of age. Mice were anesthetized with a continuous flow of 1% to 3% isoflurane/oxygen mixture (2 L/min) and the chest area was imaged using the GE eXplore Locus micro-CT scanner (GE Healthcare, London, Canada). The isotropic resolution of this instrument is 45 µm. The micro-CT image acquisition consisted of 400 projections collected in one full rotation of the gantry in approximately 10 min. The image acquisition

was not respiratory-gated. The X-ray tube settings were 80 kV and 450 µA. The resulting raw data were reconstructed to a final image volume of 875 × 875 × 465 slices at (93 µm) 3 voxel dimensions.

5.1.4. TMX treatment of mice.

Conditional *Rbm10 KO, Kras* Rbm10, Trp53 KO Rbm10 KO* and *Pik3ca* Rbm10 KO* mice of 6 weeks of age were fed *ad libitum* with a TMX-containing diet to induce recombination of the indicated floxed alleles for 8 weeks. Mice were sacrificed at 80 weeks of age by CO_2 inhalation unless humane endpoint criteria were met at an earlier age.

5.1.5. Blood cell count.

Blood samples were collected in EDTA-tubes and blood cell numbers counted by LaserCell (CVM).

5.1.6. Adenovirus titration and infection.

All adenoviruses used in this study are serotype 5 adenoviruses with E1 deletion, Ad5CMVCre (the University of Iowa, VVC-U of Iowa-5). Stock titrations were used at $1x10^7$ pfu/ml. Viral stocks were aliquoted and stored at -80 ºC. Kras* *Rbm10 KO* mice of 8-10 weeks of age were infected intranasally with 60 µL of Ad5CMVCre and tumor development was followed up by CT scan. Mice were sacrificed at 50 weeks of age by CO_2 inhalation to perform tumor analysis, unless humane endpoint criteria were met at an earlier age.

5.2. Mouse urothelial organoids

5.2.1. Establishment of mouse urothelial organoids.

Mice of 8- to 12- weeks age were sacrificed by CO_2 inhalation; the bladder removed and turned inside-out to expose the surface. The urothelium was enzymatically digested with collagenase P (0.5 µg/mL) (Roche,11215809103) in Hank's Balanced Salt Solution (HBSS) (Life Technologies,14025050) in a thermoblock at 350 rpm at 37 ºC for 20 min. Collagenase P was later inactivated with 2mM EDTA and 50% FBS. The urothelium was scraped and the cell suspension was collected and filtered through a 70-µm strainer. The cell suspension was then centrifuged at 1200 rpm for 5 min at 4 ºC; the cell pellet was washed 2x with washing medium [Advanced DMEM F12 medium (Gibco, 12634010) + 1× HEPES (Gibco, 15630080) + 1× Glutamax (Gibco, 35050061)], and embedded in growth factor-reduced and phenol red-free Matrigel (Corning, 356231). Matrigel-cell suspensions (20 µl drops) were plated onto six-well plates and let solidify for 6 min in a humidified incubator at 37 ºC/5% CO_2. Wells were replenished with 2 mL of Complete Medium (CM) [Advanced DMEM/F12 medium (Gibco, 12634010), 1x penicillin/streptomycin,1× HEPES (Gibco, 15630080), 1× Glutamax (Gibco, 35050061), 50% WNT3A conditioned medium, 5% human RSPO1 conditioned medium, 1x N2 (Gibco, 17502048), 1 x B27 (Gibco, 12587010), 50 ng/ mL human recombinant EGF (Invitrogen, PHG0311L), 1 mM N-acetylcysteine (Sigma-Aldrich, 616-91-1), 50 µg/mL human Noggin (Peprotech, 120-10C)

and 1 μM LY2157299 (AxonChem, 700874-72-2), The ROCK inhibitor Y-27632 (10 μM) (Sigma-Aldrich, 129830-38-2)]. Cultures were expanded every 7-9 days to a 1:4 ratio. Matrigel was washed with phosphate-buffered saline (PBS). Afterwards, Matrigel was removed with 200ul/well of Cell Recovery solution (Corning, 354253) and chemically digested for 30 min at 37 ºC with 300 μL/well of Dispase II (10mg/mL) (Gibco, 17105041). The reaction was neutralized with 2 μM EDTA and 1 mL of washing medium and organoids were disaggregated with a syringe with a 21 G needle. The cell suspension was washed 2x with washing medium and centrifuged at 1200 rpm for 5 min at 4 ºC. Afterwards, the single cell pellet was embedded in ice-cold Matrigel to be plated onto six-well plates as previously described.

Table 5. List of reagents used for organoid culture

Reagents	Concentration	Source
Collagenase P	0.5μg/mL	**Roche**
Hank's Balanced Salt Solution	1x	**Life Technologies**
Advanced DMEM F12 medium	1x	**Gibco**
HEPES	1x	**Gibco**
GlutaMAX	1x	**Gibco**
Matrigel, growth factor-reduced and phenol red-free	1x	**Corning**
Cell Recovery Solution	1x	**Corning**
Dispase II	10mg/mL	**Gibco**
WNT3A conditioned medium	50%	**Homemade**
RSPO1 conditioned medium	5%	**Homemade**
N2	1x	**Gibco**
B27	1x	**Gibco**
Recombinant human EGF	50ng/mL	**Invitrogen**
N-acetylcysteine	1mM	**Sigma-Aldrich**
Recombinant human Noggin	50μg/mL	**Peprotech**

LY-2157299	1µM	**AxonChem**
Y-27632	10µM	**Sigma-Aldrich**
TryplE Express, no phenol-red	**1x**	**Gibco**

5.2.2. TMX treatment *in vitro*.

Organoids were treated with 2µM 4-OH-TMX in CM for 48h to induce recombination of floxed alleles. Recombination was assessed through the analysis of expression of mGFP or mTomato at the indicated time points.

5.2.3. FACS sorting.

At passage 4-5, organoids exposed to TMX and controls were disaggregated into single-cell suspensions as described previously. After centrifugation at 1200 rpm for 5 min, urothelial cells were resuspended (in 0.1% BSA/3mM EDTA + 100mg/mL normocin in PBS), filtered with FACS filters, and stained with DAPI to exclude dead cells. All samples were sorted to separate mGFP- and mTomato-expressing cells using a FACS ARIA Ilu sorter (BD Biosciences); at least 10,000 events were acquired.

5.2.4. Growth Factor dependency experiments.

After organoid dissociation, 2000 single cells were embedded in Matrigel (160 µL/well) and plated in 6-well plates. Growth was assessed by adding CM, CM-EGF, CM-WNT3A/RSPO1, and CM-EGF/WTN3A/RSPO1 for 7 days. Images were acquired at 1.25x magnification with a bright-field DMI600B microscope (Leica Microsystems). Cells were maintained at 37 ºC in a humidified environment in the presence of 5% CO_2 during imaging. Mosaic pictures of the entire well were taken and image stitching and quantification were done using ImageJ software.

5.2.5. Differentiation experiments.

After organoid dissociation, 4000 single-cells were embedded in Matrigel (160 µL/well) and plated in 6-well plates in CM for 7-9 days to generate new organoids. Later, Matrigel was removed with Dispase and Cell Recovery Solution, as described above, and organoids were replated in fresh Matrigel at a 1:2 ratio and Differentiation Medium (DM) [Advanced DMEM/F12 medium (Gibco, 12634010), 1x penicillin/streptomycin,1× HEPES (Gibco, 15630080), 1× Glutamax (Gibco, 35050061), N2 (Gibco, 17502048), 1 x B27 (Gibco, 12587010), 1 mM N-acetylcysteine ((Sigma-Aldrich, 616-91-1), The ROCK inhibitor Y-27632 (10 µM) (Sigma-Aldrich, 129830-38-2)] was added every 2-3 days for another 7 days. Images were acquired, and organoids were counted, as described above.

5.3. Human urothelial organoid experiments.

5.3.1. Establishment of human urothelial organoids.

Normal and tumor tissue samples were obtained from patients with BC undergoing transurethral resection (TUR) at Hospital Universitario “12 de Octubre” and Hospital Universitario “La Paz” (Madrid). Cell suspensions were generated by mincing tissue with a sterile blade and enzymatic digestion with 1:10 collagenase/hyaluronidase (StemCell Technologies, 7912) for 15 min at 37 ºC. Cell suspensions were washed with PBS, centrifuged at 1200 rpm for 5 min at 4 ºC, and resuspended in 1 mL of TryplE by pipetting up and down for 1 min. TryplE was later inactivated with Human Washing Medium [Hepatocyte Medium + 10% CS-FBS + 1× HEPES (Gibco, 15630080) + 1× Glutamax (Gibco, 35050061)] and filtered through a 100-µm strainer. The cell suspensions were centrifuged at 1200 rpm for 5 min at 4 ºC. Finally, cell pellets embedded in Matrigel (300 µL) were plated onto Matrigel pre-coated six-well plates and let solidify for 30 min at a humidified incubator at 37 ºC/5% CO_2. Wells were replenished with the organoid culture medium (2 mL) reported by the laboratory of Michael Shen (Columbia University, New York) (Lee et al., 2019) [Hepatocyte Medium (Corning, 355056) + 5% CS-FBS (Thermofisher Scientific, 12676029) + 1× HEPES (Gibco, 15630080) + 1× Glutamax (Gibco, 35050061) + EGF (Corning, 355056) + ROCK inhibitor Y-27632 (10 µM) (Sigma-Aldrich, 129830-38-2] and this was replaced every 2-3 days. Cultures were expanded every 2-3 weeks to a 1:2 ratio. Matrigel was washed with PBS and chemically digested for 30 min at 37 ºC with 300 µL/well of Dispase II solution (40mg/mL) (Gibco, 17105041). Cell suspensions were washed with PBS, centrifuged at 1200 rpm for 5 min at 4 ºC, and resuspended in 1 mL of TryplE by pipetting up and down for 1 min. TryplE was later inactivated and washed 2x with Human Washing Medium. Finally, cell pellets embedded in 300 µL of Matrigel were plated onto Matrigel pre-coated six-well plates and let solidify for 30 min at a humidified incubator at 37 ºC/5% CO2. Wells were replenished with 2 mL of human organoid culture medium every 2-3 days.

Table 6. List of reagents used for the culture of human organoids

Reagents	Concentration	Source
Collagenase/Hyaluronidase	1:10	**STEMCELL Technologies**
Hank's Balanced Salt Solution	1x	**Life Technologies**
Hepatocyte medium	1x	**Corning**

HEPES	1x	**Gibco**
GlutaMAX	1x	**Gibco**
Matrigel, growth factor-reduced and phenol red-free	1x	**Corning**
Cell Recovery Solution	1x	**Corning**
Dispase II	40mg/mL	**Gibco**
Recombinant human EGF	10ng/mL	**Invitrogen**
Normocin	100mg/mL	
Y-27632	10µM	**Sigma-Aldrich**
DBZ	2.5µM	**Tocris**
Heat-inactivated, charcoal-stripped FBS	5%	**Thermofisher Scientific**
TryplE Express, no phenol-red	1x	**Gibco**

5.3.2. Generation of an inducible RBM10 expression system.

5.3.4.1. RBM10 lentiviral cloning. The *RBM10* cDNA was amplified and Flag-tagged by PCR using the CloneAmp HiFi PCR Premix (Takara, 639298) and the following primers: CAGTTTAAACGATACGCGTATATGCGGCCGCACCATGCATATGGAGTATGAAAGAC GTGGTG and TAGAATCGAGACCGAGGAGAGGGTTAGGGATAGGCTTACCCTACTTGTCATCGTCA TCCT. The pLVX-Induc-Cherry-M2rtTA (kindly provided by Raúl Torres, Molecular Cytogenetics Unit, CNIO) was amplified by PCR by using the same system with the following primers: ATGCATGGTGCGGCCGCATA and GGTAAGCCTATCCCTAACCC. Both PCR products were column purified and ligated by homologous recombination by using the Gibson Assembly Cloning Kit (New England Biolabs, E5510S). Then, 2 µl of ligation products were used to transform One Shot Stbl3 chemically competent cells (ThermoFisher Scientific, C737303) using standard transformation protocols. The identity of the inserts was confirmed by enzymatic digestion with XhoI and Sanger sequencing.

5.3.4.2. RBM10 lentiviral production and cellular transduction. HEK293 -FT cells (ATCC, Rockville, MD) were used to produce lentiviral particles. In brief, cells were allowed to

reach 60% of confluence and transfected with the RBM10-pLVX-Induc-Cherry-M2rtTA plasmid (21 µg) together with psPAX (14 µg) and pCMV-VSVG (7 µg) helper plasmids using $CaCl_2$ 2 M HEPES Buffered Saline (HBS, pH 7.04). After 12 h, the supernatant was replaced with fresh medium. The supernatant was collected at 48 h and 72 h after transfection, filtered (0.45 µm), and added (1.5 ml) to the disaggregated cells at 50-60% confluence together with polybrene (hexadimethrine bromide, Sigma-Aldrich 107689) (5 µg/ml). Cells were incubated in the plate for 15 min at 37 ºC and centrifuged for 90 min at 1800 rpm The medium was replaced after overnight incubation at 37 ºC and after one week, cells were FACS-sorted to select mCherry-positive cells using a FACS ARIA Ilu sorter (BD Biosciences); at least 10,000 events were acquired. A week later, cells were trypsinized and embedded in Matrigel to generate new organoids.

5.3.4.3. RBM10 induction. To induce RBM10 expression, doxycycline (Sigma-Aldrich, D9891) (1µg/ml) was administered to mCherry-positive organoids. Pellets were collected 24-48h after induction. Expression of endogenous and ectopic RBM10 was assessed using western blotting with antibodies detecting RBM10 (Sigma-Aldrich, HPA034972) or FLAG (Sigma-Aldrich, F3165).

5.4. Human bladder cancer cell lines.

5.4.1. Cell lines.

ScaBER, RT4, and 96-1 urothelial BC cells were cultured in Dulbecco's modified Eagle's medium (DMEM) (Sigma-Aldrich, D5671), supplemented with 10% FBS (HyClone, Logan, UT, USA), 1% sodium pyruvate (Life Technologies, 11360070), and 1% penicillin/streptomycin (Gibco, 15140122). LWnt3a-producing cells - transfected with the Wnt3A cDNA (kindly provided by E. Battle, IRB Barcelona) - were used to produce Wnt3A conditioned medium. RSPO1 was obtained by isolating the conditioned medium of Expi293 (Life Technologies, A14527) cells transfected with a pOPINE-G-RSPO1-His6 plasmid (kindly provided by E. Battle) using the ExpiFectamine™ 293 Transfection Kit (ThermoFisher, A14525). The activity of both conditioned media was confirmed by analyzing the expression of *Axin2* in HeLa cells using RT-qPCR.

5.4.2. Generation of *RBM10* CRISPR/Cas9 KO cells.

RT4 urothelial cells were infected with a Cas9-expressing vector along with pspPAX packaging and pCMV-VSV-G envelope plasmids as described earlier; the transduced population was selected with blasticidin (1 µg/ml). After one week of selection, cells were allowed to grow for another week to pick Cas9-expressing clones. To target exon 3 of *RBM10,* guide RNAs (sgRNA) were designed (Table 7) to be introduced in a pKLV-U6gRNA-EF(BbsI)-PGKpuro2ABFP vector (Addgene, 62348). Cas9-expressing cells were infected with sgRBM10- pKLV-U6gRNA-EF(BbsI)-PGKpuro2ABFP plasmid,

pspPAX, and pCMV-VSV-G helper plasmids, and the infected population was selected with puromycin (2 µg/ml). After one week of selection, cells were allowed to grow for another week, trypsinized, FACS sorted into 96-well plates, and clonally expanded.

Table 7. Primers used to design sgRNAs

Primer Name	Forward sequence	Reverse sequence
sgRBM10 1	CACCGCGTTCATATCCTCGCGAGTAGT	TAAAACTACTCGCGAGGATATGAACG
sgRBM10 2	CACCGAGACCACGACTACCGGGACAGT	TAAAACTGTCCCGGTAGTCGTGGTCT
sgRBM10 3	CACCGCAGCCGAGACCACGACTACCGT	TAAAACGGTAGTCGTGGTCTCGGCTG

Table 8. Primers used to sequence *RBM10*

Primer Name	Primer Sequence (5'- 3')
1F_cDNA_RBM10	ATGAAAGACGTGGTGGTCGT
2F_cDNA_RBM10	ATGCGGAACAAATCTTCAGG
3F_cDNA_RBM10	AGGACAAGCAGACCCAACTG
4F_cDNA_RBM10	GTGCTGCTCCTGGCATCTAC
5F_cDNA_RBM10	ATAGCTTCCAGCCTATCAGCTC
6F_cDNA_RBM10	AGAGCCCAAGAGGAGGAAGT
1R_cDNA_RBM10	CGATAGTCCTGGTCCCGATA
2R_cDNA_RBM10	CAGTGGCAGTGTCTGCTGAT
3R_cDNA_RBM10	CATAGCCCTCATCCTGTTGG
4R_cDNA_RBM10	TGCTGGCTCTGAGCATTGTA
5R_cDNA_RBM10	AGAGCAGACAGGCCAGCTT
6R_cDNA_RBM10	AAGCGGGTCACCATTGTCT

5.4.3. Colony formation assays.

RT4 sgRBM10 KO isogenic cells were seeded ($3x10^4$/well) in 6-well plates in triplicates. After one week, cells were washed with PBS and fixed with PFA 4% o/n at 4 ºC. The day after, plates were washed with PBS, and stained with crystal violet/methanol for 5 min. After drying for 24h, plates were destained for 15 min with 10% acetic acid. The total volume was collected and diluted to 1:4 to measure absorbances at 590 nm.

5.5. Histopathology techniques.

5.5.1. Hematoxylin and eosin (HE) staining.

Samples from E18.5 embryos were embedded in paraffin and 3 µm sections were cut. Sections were deparaffinized, rehydrated in graded xylol and ethanol (70 to 100%), H-E stained, hydrated, and mounted.

5.5.2. Immunofluorescence (IF) and immunohistochemistry (IHC).

Organoids embedded in Matrigel were collected at day 7 days, fixed in 10% formalin, and embedded in paraffin. Immunofluorescence and immunohistochemistry analyses were performed using 3 µm sections. After deparaffinization and rehydration in xylol and ethanol (70 to 100%), antigen retrieval was performed by boiling in citrate buffer pH 6 for 10 min. For IF, sections were blocked with 3% BSA/0.1% Triton in PBS for 45 min at room temperature. Then, sections were incubated with primary antibodies overnight at 4 ºC. After washing with 0.1% Triton/PBS, specific secondary antibodies were added [Alexa Fluor 488-labeled goat anti-mouse Ig (A-11001), Alexa Fluor 555-labeled goat anti-rabbit Ig (A-21428); Alexa Fluor 488-labeled goat anti-chicken Ig (A-11039); Alexa Fluor 680-labeled goat anti-rabbit Ig (A-27042); all from Life Technologies] for 45 min (Table 9). Sections were washed 2x with PBS for 10 min and nuclei were counterstained with DAPI. Finally, sections were mounted in Prolong Gold Antifade Reagent (Life Technologies, P36930). Images were acquired using a confocal microscope (Leica, SP5) with a ×20 lens and ×40 immersion oil lens. For IHC, endogenous peroxidase was blocked with 3% H_2O_2 in methanol for 30 min at room temperature. Non-specific binding was reduced by blocking with 2% BSA in PBS for 45 min. Sections were incubated with primary antibodies overnight at 4 ºC . After washing with PBS x2, the secondary antibodies (Envision kit for mouse K4001 or rabbit K4003 Ig, Dako) were added for 45 min, washed, and 3,30-Diaminobenzidine tetrahydrochloride (DAB, Dako, K3468) was added as a chromogen to develop the reactions. Sections were lightly counterstained with hematoxylin for 4 min, dehydrated, and mounted. The antibodies used in this study are shown in Table 9. Histological images were acquired with a Nikon TE2000 microscope.

Table 9. List of primary and secondary antibodies used for IF and IHC.

Antibody	Dilution	Source
Alexa Fluor 488-labeled goat anti-mouse Ig	1:200	**Life Technologies**
Alexa Fluor 555-labeled goat anti-rabbit Ig	1:200	**Life Technologies**
Alexa Fluor 488-labeled goat anti-chicken Ig	1:200	**Life Technologies**
Alexa Fluor 680-labeled goat anti-rabbit Ig	1:200	**Life Technologies**

Rabbit monoclonal anti-RBM10	1:200	**Sigma-Aldrich**
Rabbit monoclonal anti- PPARγ	1:100	**Cell Signalling**
Rabbit polyclonal anti-Ki67	1:400	**Novocastra**
Rabbit monoclonal anti-FOXA1	1:100	**Abcam**
Mouse monoclonal anti-E-Cadherin	1:700	**BD Biosciences**
Rabbit monoclonal anti-Cleaved-caspase3	1:300	**Cell Signalling**
Rabbit polyclonal anti-KRT5	1:3000	**BioLegend**
Rabbit polyclonal anti-KRT14	1:3000	**BioLegend**
Mouse monoclonal anti-UPK3a	1:100	**Santa Cruz**
Mouse monoclonal anti-UPK1b	1:3000	**Dr. A. García-España**
Mouse monoclonal anti-KRT20	1:100	**Invitrogen**
Rabbit monoclonal anti-GATA3	**1:300**	**Sigma-Aldrich**

5.6. Molecular biology experiments.

5.6.1. Western blotting.

Cells were pelleted and washed with PBS. Whole cell extracts were prepared using RIPA buffer [0.05M Tris-HCl pH 7.5, 0.1% SDS, 0.15M NaCl, 1% Triton X-100, and 1% sodium deoxycholate] containing protease and phosphatase inhibitors (leupeptin, 10 µg/mL; aprotinin, 10 µg/mL; PMSF, 1 mM; orthovanadate, 1 mM; NaF,1 mM) (all from Sigma-Aldrich). Protein quantification was performed by the standard Bradford protocol and proteins (20µg) diluted in Laemmli buffer 1X were loaded onto polyacrylamide gels, fractionated by electrophoresis, and transferred to nitrocellulose membranes. After blocking, membranes were incubated with rabbit monoclonal anti-RBM10 and mouse monoclonal anti- β-Actin (Table 9) overnight at 4 ºC. After washing with 0.1% TBST in PBS, HRP-conjugated secondary antibodies were added, and incubated for 45 min at room temperature. The enhanced chemiluminescence system Luminata Classico HRP substrate (Merck-Millipore) was used to develop the reactions.

5.6.2. DNA extraction.

Genomic DNA was extracted from cells ($1x10^6$) using the Gentra Puregene Cell kit (Quiagen, 158388) following the manufacturer's guidelines. To extract genomic DNA from organoids, Matrigel was removed by adding dispase (500µl/well, 10mg/mL) (Gibco,

17105041) and incubating for 30 min at 37 ºC. Organoids were pelleted, the supernatant was removed and lysis buffer [100 mM Tris PH 8.0, 20 mM NaCl, 0.2% SDS, 5 mM EDTA, 200 µl/ml Proteinase K (PanReac AppliChem, A3830)] (500µl/well), was added for 3h at 56 ºC. After lysis, Phenol chloroform-isoamyl (500 µl) was added and mixed by vortexing, followed by a centrifugation for 15 min at 12000 rpm at 4 ºC. The supernatant was collected and 3M Na acetate (1:10 dilution) was added. Then, ethanol 100 % was added, mixed thoroughly, and centrifuged for 20 min at 12000 rpm The supernatant was removed by decantation and 1 ml of ethanol 70% was added, mixed, and samples were centrifuged for 10 min at 12000 rpm at 4 ºC. Ethanol was removed by decantation and tubes were spun-down 30 sec at 12000 rpm at 4 ºC to remove remaining ethanol.

5.6.3. RNA extraction and Real-Time quantitative PCR (RT-qPCR).

TRI Reagent ® (Sigma-Aldrich, T9424) and PureLinkTM RNA Mini Kit (Life Technologies, 12183020) were used to extract total RNA from cells/organoids. All samples were treated with DNase (Life Technologies, AM1906) before reverse transcription. Reverse transcription was performed with 200-1000 ng of RNA using the TaqMan® Reverse Transcription Reagents (Life Technologies, N8080234). Controls for genomic contamination were set with reaction mixes without RT. Real-time PCR was conducted using the 7900HT Real-Time PCR System (Applied Biosystems, Life Technologies) using GoTaq® qPCR Master Mix (Promega, TM318). Normalization was performed by using the ΔΔCt method using *Gapdh* expression as reference. Primer pairs were designed to achieve inter-exon amplicons of 200-250 bp (Table 10).

Table 10. List of primers used for RT-qPCR

Gene name	Forward (5'-3')	Reverse (5'-3')
Foxa1	TGGAGTTCATAGAGCCCAGG	**CATGAGAGCAACGACTGGAA**
Ki67	ATCATTGACCGCTCCTTTAGGT	**GCTCGCCTTGATGGTTCCT**
Krt5	ACATTAACAACCTCCGTAGACAG	**CGCTTGTTGATCTCATCCTC**
Krt10	GGGTAAAATCAAGGAGTGGT	**CTGCCCCTTAAGGTCCTCGA**
Krt14	AGGTGAAGATTCGGGACTGG	**GCTCCGTCTCAAACTTGGTC**
Krt20	CCTTGGAGATCAGCTTCCAC	**CCTGCGAATTGACAATGCTA**
PPARγ	CGCTGGGGTATTGGGTCG	**TTCAAATCTTGTCTGTCACACAGT**
Upk1a	GGCCTGACAGCAAAATAATGA	**GAGAAGCAGGAAGATGGCTT**

Upk1b	AATCAACAGGCCCTGGAAG	**GAAGAAGGCAGAGGAGACCA**
Upk2	GACAGCAGACCAGAGAGGCT	**ACACTGCCTGTCCAGACCTT**
Upk3a	AGTAGTGCTCAGTGGGACGC	**AGCGGCTCTTACGAGGTTTA**
Gapdh	**CCATGCCATCACTGCCAC**	**GGGTAGGAACACGGAAGG**

5.6.4. Bulk RNA-sequencing.

Three paired samples of *Rbm10 cKO* and *WT* organoids cultured in proliferation and differentiation conditions were analyzed. The quality of RNA was assayed by laboratory chip technology on an Agilent 2100 Bioanalyzer. PolyA+ RNA was isolated from total RNA (1 µg, RIN>9), randomly fragmented, converted to double-stranded cDNA for library preparation with the Illumina QuantSeq 3' mRNA-Seq Kit.

5.6.5. RNA-sequencing analysis.

Raw images generated by the sequencer were submitted to analysis, per-cycle base calling, and quality score assignment with Illumina's RTA (Real Time Analysis) integrated primary analysis software. Conversion of BCL (base calls) binary files to FASTQ format was subsequently performed with the Local Run Manager Generate FASTQ Analysis Module (Illumina). The Nextpresso version 1.9.2.2 analysis pipeline (Bioinformatics Unit, CNIO) was used to process the data with the version MGSCv376/mm8 of the mouse genome50.

Tophat was used for alignment (tophat-2.0.10.Linux_x86_64) using the following parameters: useGTF=" true", nTophatThreads="4", maxMultihits="20" readMismatches="3", segmentLength="25", segmentMismatches="1", spliceMismatches="0", reportSecondaryAlignments="false", bowtie="1", readEditDist="3", readGapLength="2", referenceIndexing="false", --no-coverage-search. Gene expression was quantified using cufflinks (version 2.2.1) using the following parameters: useGTF="true" nThreads="4" fragBiasCorrect="true", multiReadCorrect="false" library Normalization Method= "classic-fpkm", max Bundle Frags="500000", normalization= "compatibleHits", noEffectiveLengthCorrection="true", noLengthCorrection="false". Htseqcount was performed with the following settings: minaqual="0" featuretype= "exon" idattr= "gene_id". BBDuk preprocessing was performed for fastq files in *fastq; do echo $fq; outFastq=${fq/fastq/CLEAN.fastq}; /local/ljmartinezv/bbmap/bbduk.sh in=$fq out=${outFastq} ref=/local/ljmartinezv/bbmap/resources/polyA.fa.gz,/local/ljmartinezv/bbmap/resources/truseq.fa.gz k=13 ktrim=r useshortkmers=t mink=5 qtrim=r trimq=10 minlength=20; done

Differential expression analysis was done using Deseq2 using the following parameters: useCuffmergeAssembly="false", nThreads="2", fragBiasCorrect="true", multiReadCorrect="false", library Normalization Method="geometric" FDR="0.05" minAlignmentCount="10", seed="123L" FPKMthreshold="2", maxBundleFrags="5000000000", noEffectiveLengthCorrection="true", noLengthCorrection="false" dispersionMethod="pooled".
Normalized expression across all samples was calculated using Deseq using the following parameters: useCuffmergeAssembly="false", nThreads="2", outputFormat="simple-table" library Normalization Method="geometric", seed="123L" normalization="compatibleHits". BEDTools-Version-2.16.2 and samtools-0.1.19; bowtie-1.0.0 were also used to execute the software shown above.
Lists of differentially expressed genes (DEG) are provided in Table 11 and 12 for *Rbm10 KO* and *WT* organoids. Genes were ranked using the FDR q-value statistic to identify significant genes ($q < 0.05$) and then by fold change expression. Venn diagrams were used to assess any significant overlaps. GSEA (GSEA_Pre-ranked) was performed with MsigDB GO terms, BIOCARTA, KEGG, C6 Oncogenic signature and Reactome databases, using the standard settings, and with 1,000 permutations for Kolmogorov–Smirnoff correction for multiple testing. GSEA enrichment data were obtained and ranked according to FDR q value (significance threshold, $q < 0.25$). Heat maps of expression data were generated using R and GenePattern.

5.6.6. Additional bioinformatics analysis

Co-mutated gene analysis. Available data from the BLCA patients in TCGA database (2017) in cBioportal was used to determine RBM10 significant co-ocurrent genes according to adjusted p-value ($q < 0.05$) and was later filtered by using NIH ClinVar annotations (https://www.ncbi.nlm.nih.gov/clinvar/) to asses clinical significance. Heatmap of co-occurrence was generated using R.

Single cell data analysis. Single cell RNAseq data from 10X Genomics Chromium was preprocessed using Cell Ranger software. Features, barcodes and matrix files generated were loaded into Seurat v3 R toolkit for dowstream analysis using Read10X function. Low quality cells were filtered out according to their mitochondrial genes expression. Data normalization was carried out using sctransform function. Dimensionality reduction was performed by selection of significant principal components according to the stabilization of the elbow plot. Clustering analysis on these principle components was done by means of KNN graph construction (FindNeighbors function) and Louvain algorithm (FindClusters function) for different resolution levels. Cluster stabilization and consequent resolution level selection for downstream analysis was established according to clustree analysis.

Markers for every cluster compared to all remaining cells were found using FindAllMarkers function with Wilcoxon Rank Sum test. Visualization of the data was done by means of non linear dimensional reduction using RunUMAP function.

5.7. Quantification and statistical analysis.

All quantitative data are presented as mean ± standard error of the mean from ≥3 experiments or samples per data point. Comparisons of quantitative data between groups were performed using a non-parametric two-tailed Mann-Whitney U test to assess significance. For more than 2 groups, ANOVA was used. Violin plots represent the median and first and third quartiles (interquartile range) of the data; error bars were generated by GraphPad Prism version 6 software and represent the highest and lowest data within 1.5× interquartile range. All statistical analyses were performed with Excel, GraphPad Prism version 6 software, and R software. The Log-rank (Mantel–Cox) test was used to compare survival distributions. The Fisher exact test was used in the analysis of the distribution of categorical values within two groups. For in vitro and in vivo experiments, the sample size required was determined on the basis of prior pilot experiments. No formal sample size estimation analysis was conducted and the experiments were not randomized. Whenever possible, analyses were conducted blinded, as indicated in the text.

6.RESULTS

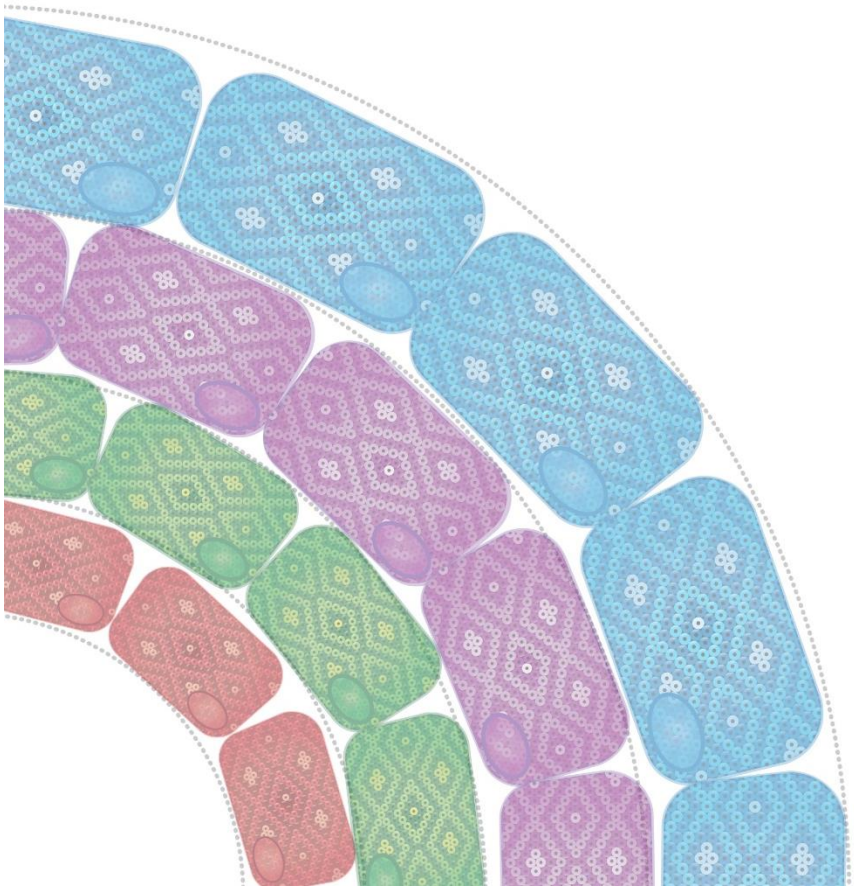

CHAPTER I

Role of *Rbm10* in mouse development and tissue homeostasis

6.1. Role of *Rbm10* in normal mouse development

6.1.1. *Rbm10* inactivation during embryo development leads to a male-lethal phenotype with partial penetrance

To determine the effect of *Rbm10* inactivation on mouse development, we used a constitutive knock-out allele making use of a Cre recombinase that is activated in the zygote (*Rbm10* null) (Sakai, et al. 1997). It is predicted that, upon recombination and excision of exon 3 of *Rbm10* **(Fig. 14A)**, cells would lack RBM10 protein expression. We envisioned that this model might recapitulate human TARP syndrome since germline *RBM10* mutations are predicted to cause loss of expression in patients. We confirmed that adult *Rbm10* null mice display extensive loss of RBM10 expression in a wide variety of tissues, where the residual protein was detected only in a few cells. Mice born with widespread RBM10 loss did not have reduced survival compared to control mice **(Fig. 14B, C)**. Nonetheless, the proportion of male adult *Rbm10* null mice born was lower than the expected mendelian rates, suggesting that some *Rbm10* null mice die during development, while in females this proportion was normal **(Fig.14D).**

We then collected embryos at E18.5 and found the expected WT:null and male:female ratios **(Fig. 14D),** demonstrating that *Rbm10* inactivation during embryo development leads to a male-lethal phenotype with partial penetrance. Therefore, we performed a comprehensive analysis of the *Rbm10* null embryos, focusing first on a search for TARP syndrome-associated defects.

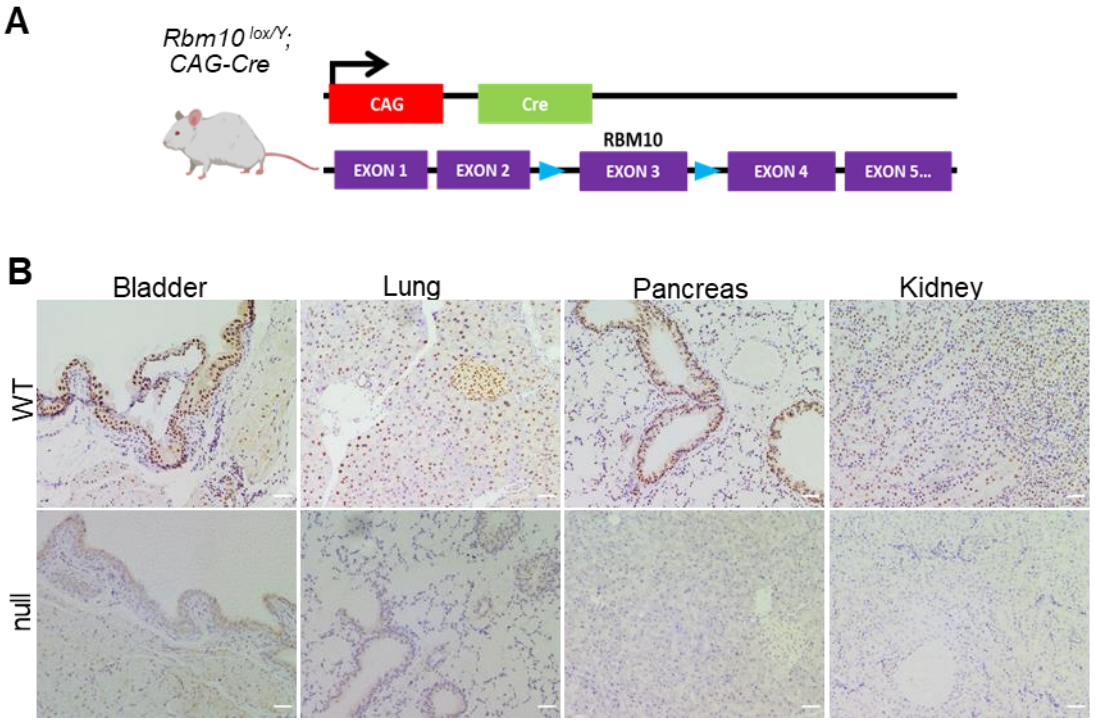

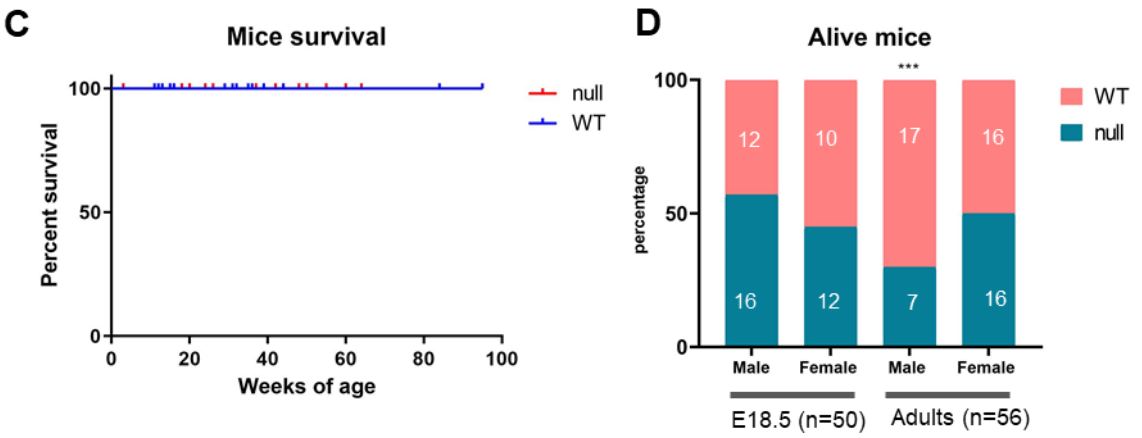

Figure 14: Generation of constitutive *Rbm10* null mice and survival analysis. A. Transgenic mouse line used to obtain homozygous *Rbm10* null mice. **B.** Representative images of RBM10 immunostaining of formalin-fixed paraffin-embedded tissues from 16 week-old *Rbm10* WT and null mice (scale bar, 50µm). **C.** Kaplan-Meier survival analysis of Rbm10 null (n=24) and *Rbm*10 WT (n=17) mice. **D**. Percentage of *Rbm*10 WT and null male and female mice that were alive at E18.5 (n=50) and at 30 weeks of age (n=56) (p-value < 0.001). The number of embryos/mice analyzed is annotated inside the bar graphs (*p≤0.05, **p≤ 0.01; Fisher's exact test).

6.1.2 Embryonic *Rbm10* inactivation causes a wide variety of heart defects

We designed a pipeline to characterize the defects leading *Rbm10* null embryos to early death and to find out their relatedness to the main features of TARP syndrome: atrial septal defect, cleft palate, and clubfoot. Persistence of the left superior vena cava was not assessed because the development of this anatomic structure differs in humans and mice, remaining patent only in the latter.

First, we assessed the heart function of E18.5 embryos by performing abdominal and uterine (not shown) echocardiography on the mothers in collaboration with Dr. M. Villalba (CNIC, Madrid) to measure the following parameters: heart rate, diastole, and systole area, blood flow ejection fraction, and fractional shortening. We could not detect significant differences between *Rbm10 WT* and null embryos, although a few individuals with outlier measurements of the abdominal heart area in diastole (p-value = 0.763), systole (p-value = 0.733), and heart rate (p-value = 0.110) were identified in the *Rbm10* null group **(Fig. 15A).**

We then performed MR imaging analysis of *Rbm10* null (n=15) and *Rbm10 WT* (n=11) embryos in collaboration with the team of Dr. M. Desco (CNIC, Madrid), and did not find any major abnormalities in vital organs nor were we able to detect heart septal defects **(Fig. 15B).** The results derived from this analysis will be discussed in the next section.

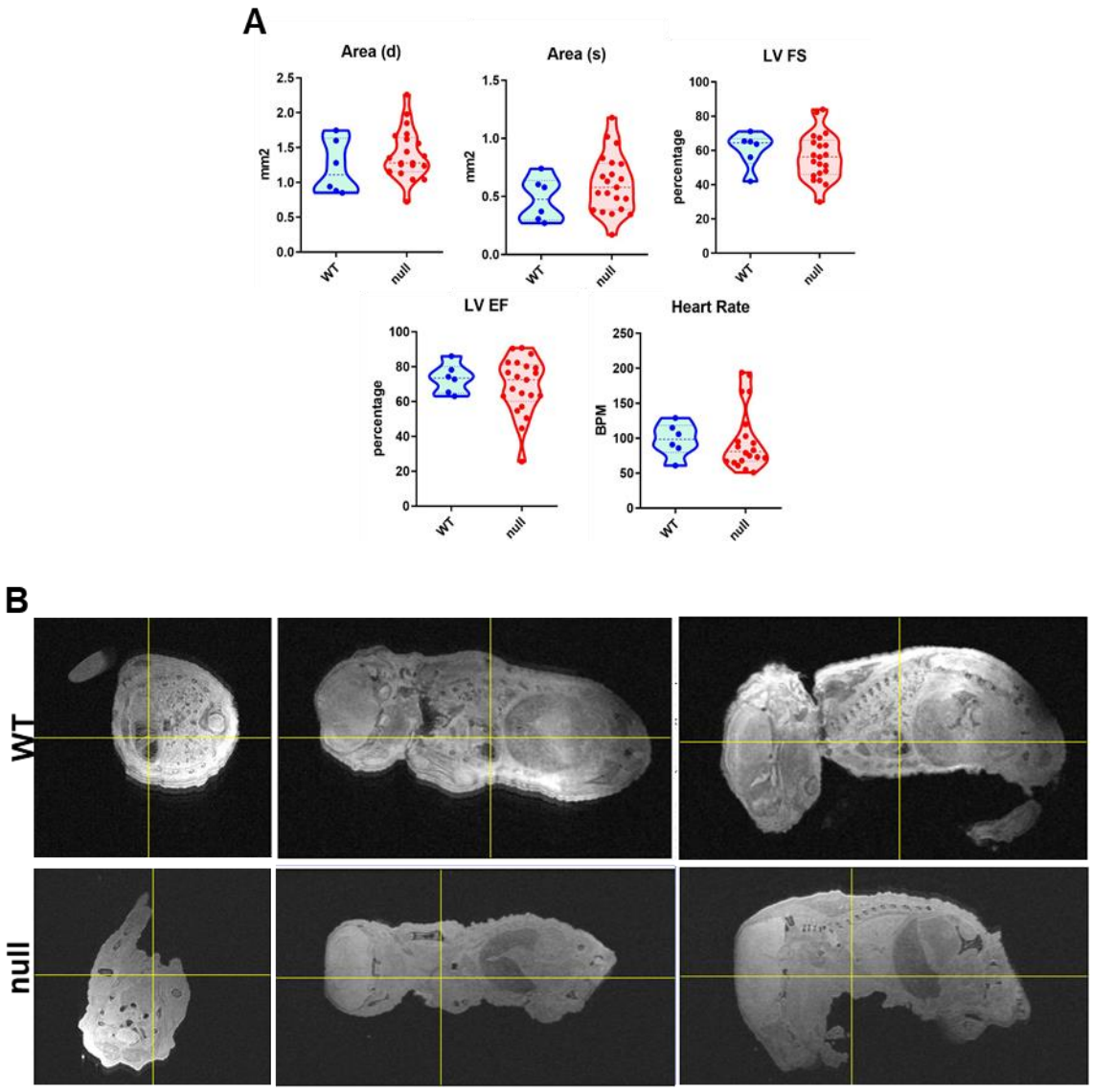

Figure 15: Echocardiography analysis of E18.5 *Rbm10 WT* and null embryos. A. Abdominal echocardiography findings showing normal diastole and systole displacements, blood flow injection (LV FS), blood flow ejection (LV EF), and heart rate. WT embryos (n=6) are represented in blue and null embryos (n=22) represented in red (Mann-Whitney test, dotted lines represent SD and mean) **B.** 3D T2-weighted MR images were acquired of *Rbm10* WT (n=11) and null (n=15) E18.5 embryos showing no differences in the heart or other vital organs including liver, lung kidney, and brain.

To further examine the heart phenotype, we performed a histological analysis of serial heart sections in collaboration with Dr. S. Martín-Puig (CNIC, Madrid). **Fig. 16** shows all the identified alterations. Forty-three percent of the *Rbm10* null embryos analyzed (13/30) presented severe heart septal defects **(Fig. 17B)**, compared to 1 out of 16 *Rbm10 WT* embryos (p-value = 0.016) **(Fig. 17A, 18A)**. Interventricular septal defects were detected in 2/30 *Rbm10* null embryos compared to 1/16 WT embryo (p-value = 1) **(Fig. 18B)**. Among other heart abnormalities, right atrium dilation was observed in 17/30 of the null versus 4/16 of the WT embryos (p-value = 0.062) **(Fig. 18C)**; right atrial hemorrhage and

communication were found exclusively in *Rbm10* null embryos with a frequency of 8/30 (p-value = 0.037) and 4/30 (p-value = 0.282), respectively **(Fig. 18D, E)**.

In addition, 3/30 and 4/30 of the *Rbm10* null embryos had valvular defects (p-value = 1) and a slimmer dorsal mesenchyme protrusion (p-value = 0.645), respectively, compared to 1/16 WT embryos; the differences were not statistically significant **(Fig. 18F, G)**. Occasional *Rbm10* null embryos (1/30) had deformed and hypomorphic ventricles, absence of the left atrium cavity, additional hemorrhages in the ventricles and valves, thinner apical sept, incomplete septum secundum, or filled ventricular chambers (data not shown). These occasional alterations were not observed in any of the WT embryos **(Fig. 16)**.

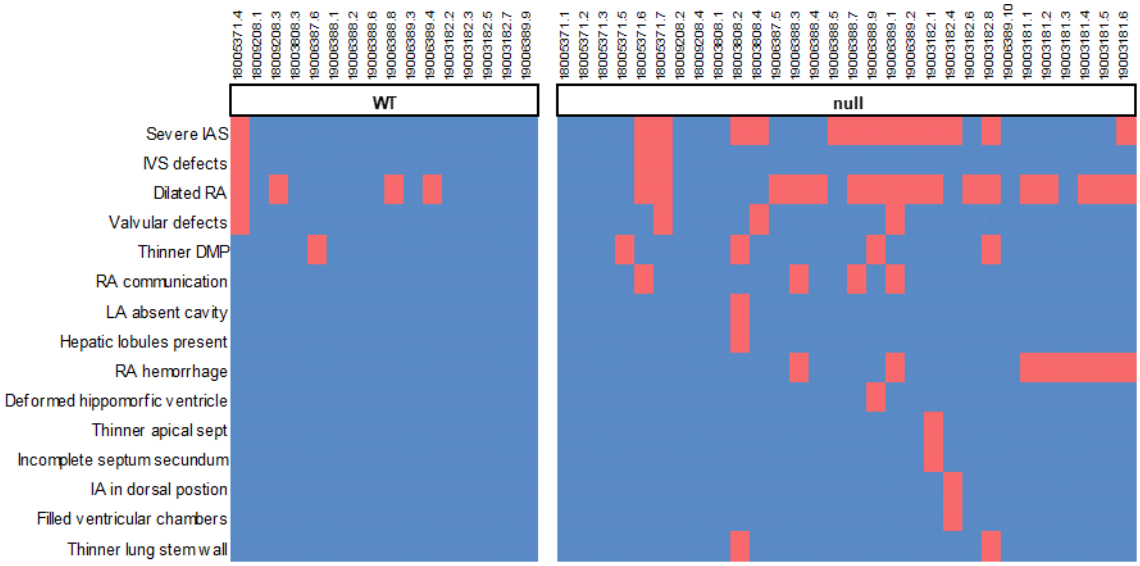

Figure 16: Contingency table of heart defects in E18.5 *Rbm10 WT* and null embryos. Summary of reported heart defects detected by histopathological analysis in *Rbm10 WT* (n=16) and null embryos (n=30).

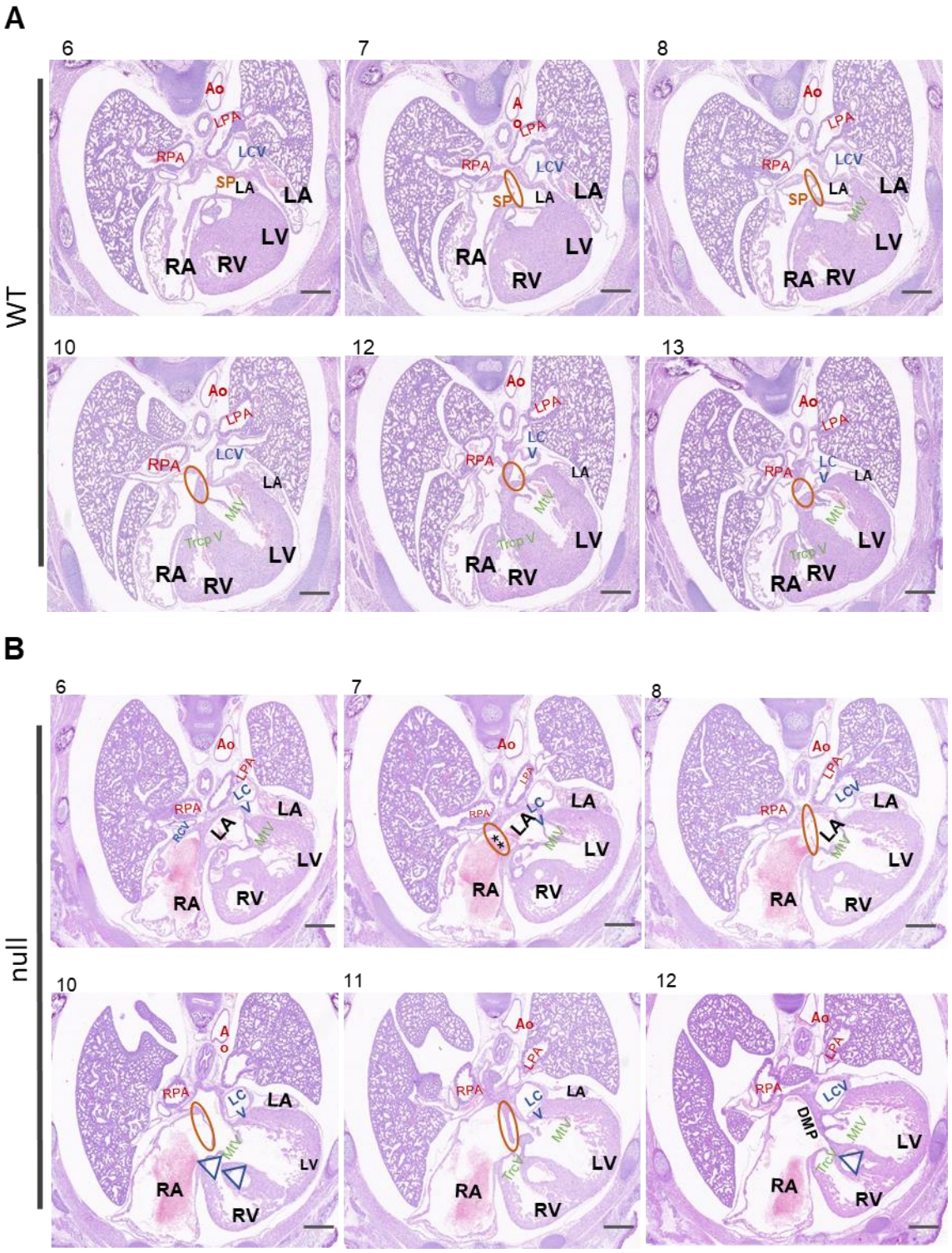

Figure 17: Histopathological analysis of the heart of E18.5 *Rbm10* WT and null embryos. **A.** and **B.** Transversal heart sections of WT and null embryos. DMP (Dorsal Mesenchymal Protrusion), RPA (Right Pulmonary Artery), LPA (Left Pulmonary Artery), LCV (Left Vena Cava), MtrV (Mitral Valve), TrcV (Tricuspid Valve), RV (Right Ventricle), LV (Left Ventricle), LA (Left Atria), RA (Right Atria), Ao (Aorta), PA (Pulmonary Artery), RCV (Right Vena Cava). Atrial defects are shown with ** inside red circles, Interventricular defects are shown with blue triangles (scale bar, 500µm).

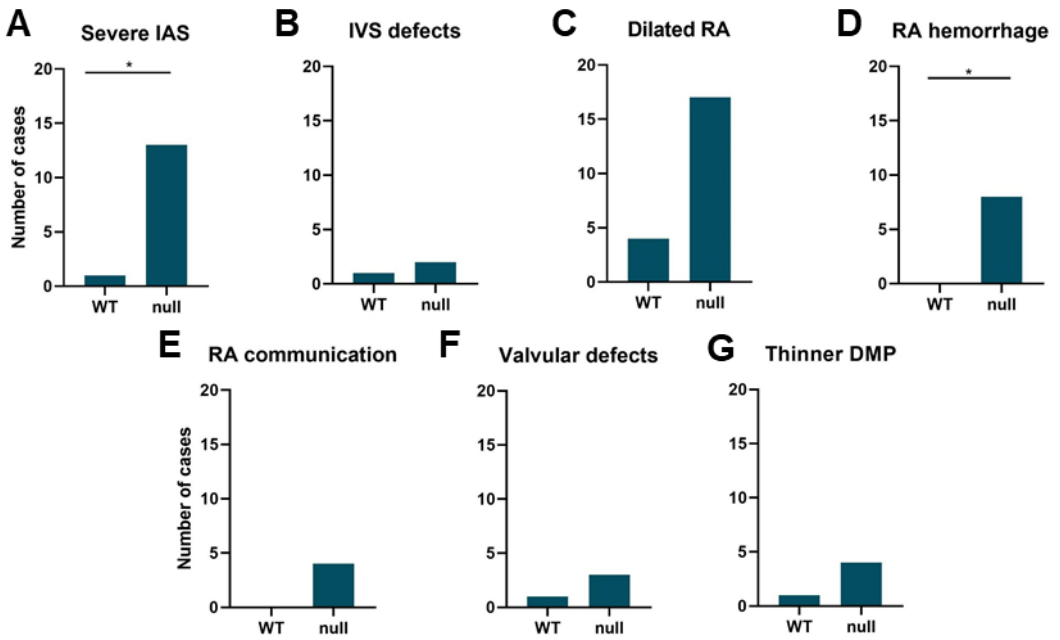

Figure 18: Quantification of histopathological analysis of the heart of E18.5 *Rbm10* WT and null embryos. Summary quantification of heart defects in *Rbm10 WT* (n=16) and null embryos (n=30): **A.** Severe IAS defects (p-value = 0.016) **B.** IVS defects (p-value = 1) **C.** Dilated RA (p-value = 0.062) **D.** RA hemorrhage (p-value = 0.037) **E.** RA communication (p-value = 0.282), **F.** valvular defects (p-value = 1) and **G**. thinner DMP (p-value = 0.645) (*p≤0.05; **p≤ 0.01; Fisher's exact test).

We found that 23/30 of *Rbm10* null E18.5 embryos presented heart defects (n=30). Eight of 18 male showed more than two severe heart defects and 6/18 presented more than three severe heart defects, compared to 3/12 and 2/12 of the *Rbm10* null females, (p-value = 0.715 and p-value = 0.683) respectively, indicating a slightly higher phenotype penetrance in males.

In summary, *Rbm10* null embryos presented a variety of heart abnormalities with a frequency higher than that of WT embryos. Some of them affect essential structures required for proper heart function, which have been described to be incompatible with survival and therefore are likely responsible for embryonic lethality.

6.1.3. Embryonic *Rbm10* inactivation causes craniofacial abnormalities

We also investigated the occurrence of the main craniofacial abnormalities reported in TARP syndrome by MR imaging. First, the size of *Rbm10* null (n=15) and *Rbm10 WT* (n=11) embryos was determined, along with sternum bone size since this tends to be smaller in TARP patients, showing no significant differences in both cases **(Fig. 19A, B)**. The size of the head was also normal, as determined by measuring the circumference from the occipital to frontal bones **(Fig. 19C)**. To rule out optic atrophy, the distance between the eyes and retinas and the volumes of both eyes were measured. While the

eye to retina distance was normal, eyes had significantly higher volume than those in WT embryos (p-value = 0.006) **(Fig. 19F)**. Finally, the distance between jaws and the distance between the jaw and tongue were measured to assess micrognathia; both appeared normal in both WT and null embryos **(Fig. 19H, I)**.

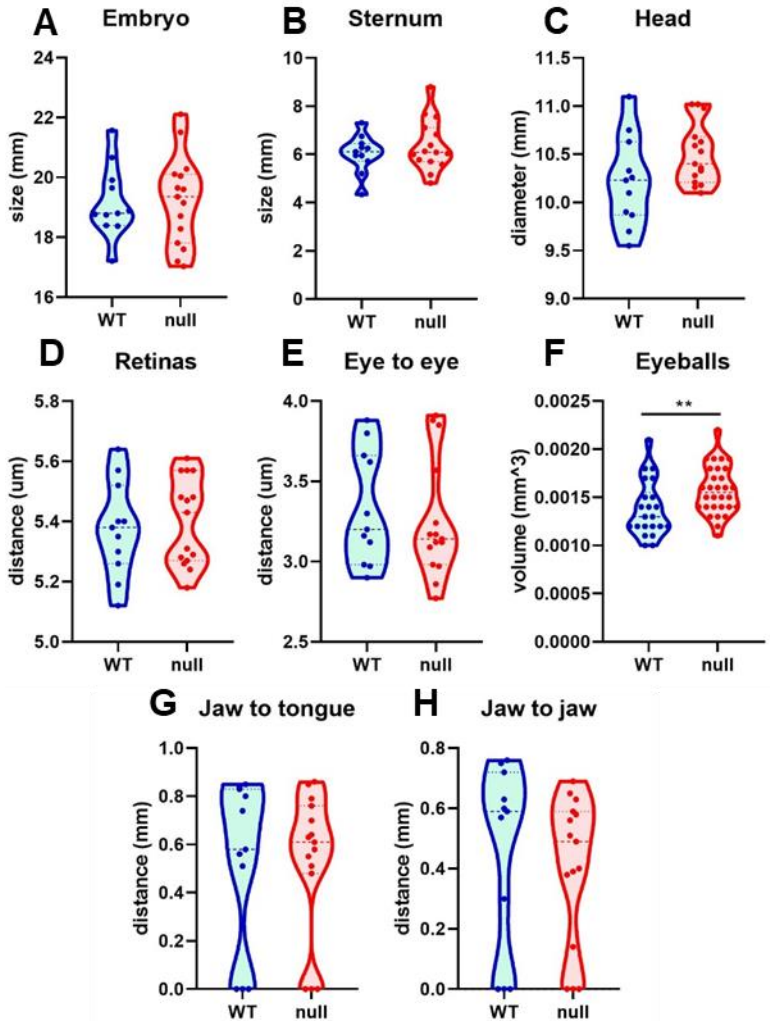

Figure 19: E18.5 *Rbm10* WT and null embryos measurements by MR. Measurements acquired by 3D T2-weighted MR images of *Rbm10* WT (n=11) and null (n=15) E18.5 embryos. **A.** Embryo size (p-value = 1) **B.** Sternum size (p-value=0.683) **C.** Occipital to frontal bone distance to determine head size (circumference) (p-value=0.111) **D.** Distance between retinas (p-value = 0.749) and **E.** Eye to eye distance (p-value = 0.618) **F.** Volume of both eyes (p-value = 0.006) and **G.** jaw to tongue distance (p-value = 0.9080) and **H.** the distance between the jaws (p-value = 0.388). WT embryos (n=11) are represented in blue and null embryos (n=15) represented in red. s stands for size, d for distance and v for volume (Mann-Whitney test, dotted lines represent SD and mean).

The occurrence of subtle craniofacial abnormalities was investigated at the histological level in *Rbm10* null (n=14) and *Rbm10 WT* (n=8) embryos in collaboration with Dr. M.C. Martínez (UCM, Madrid). The most prominent abnormalities occurred in the palate. We found that 9/14 *Rbm10* null embryos presented abnormal palate formation, compared to 3/8 *Rbm10 WT* embryos (p-value = 0.378) **(Fig. 20A)**. We also observed an increased

incidence of a primary cleft palate of 5/14 compared to 1/8 in WT embryos (p-value = 0.351). While these differences were not statistically significant, the cleft is considered to exist when it is greater than 20μm and in some of the *Rbm10* null embryos, we found clefts over 200 μm **(Fig. 20B).**

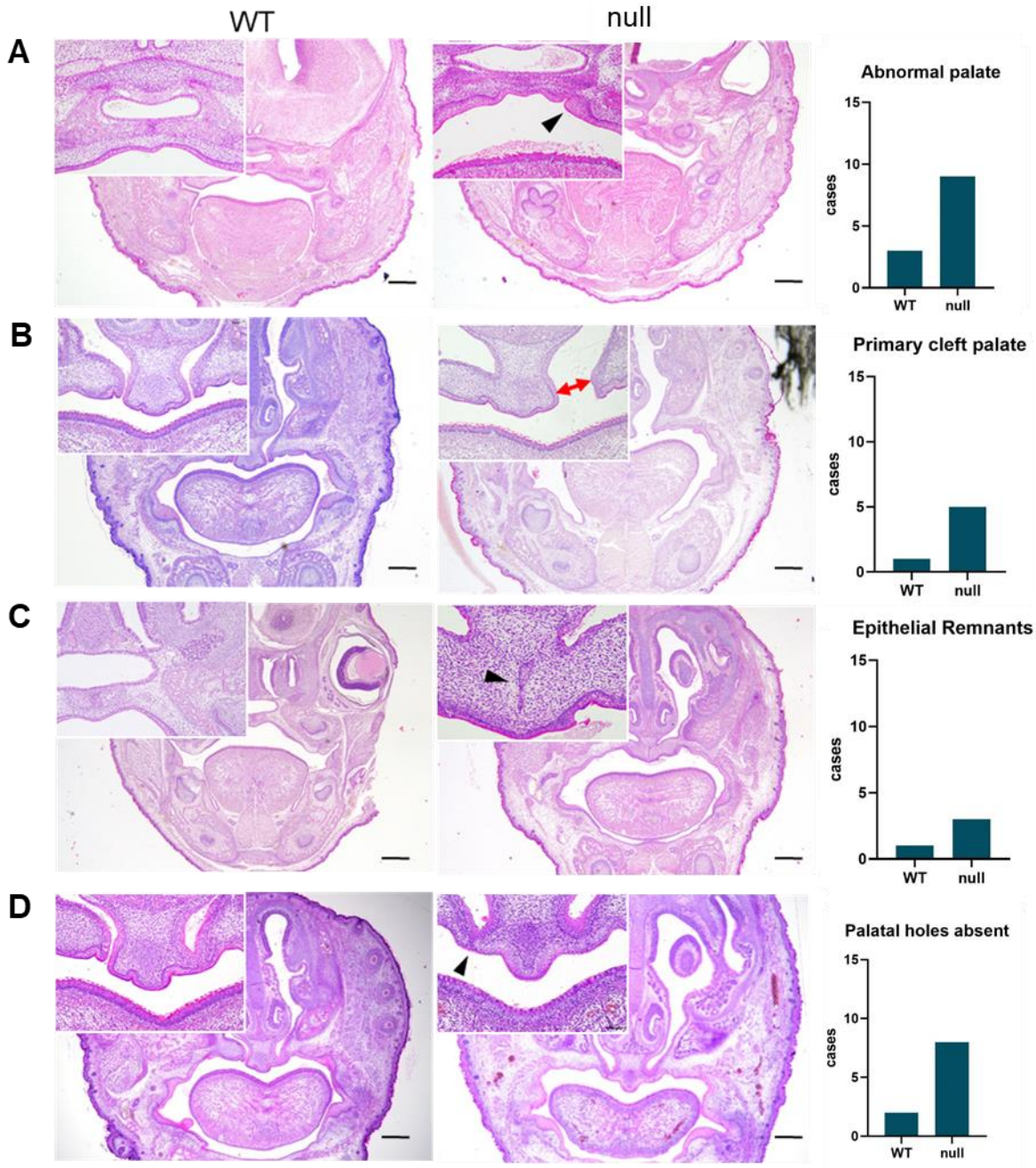

Figure 20: Histopathological analysis of the craniofacial region of E18.5 *Rbm10* WT and null embryos. Coronal head sections of WT (n=8) and null (n=14) embryos showing **A.** Abnormal morphology of the palate (p-value = 0.378) **B.** The presence of >20 μm clefts in the primary palate (p-value = 0.351) (red arrow points a cleft of 200μm) **C.** Epithelial remnants in the mesenchyme of the palate (p-value = 1) and **D.** Absence of palatal holes (p-value = 0.204). Head defects are shown with black arrows (scale bar 500μm) (*p≤0.05; **p≤ 0.01; Fisher's exact test).

Moreover, 3/14 of *Rbm10* null and 2/8 of WT embryos showed epithelial remnants which usually disappear at E15 **(Fig. 20C)** and 2/8 of *Rbm10* null embryos displayed abnormal palatal holes, compared to 8/14 of WT embryos that exhibit it (p-value = 0.2043) **(Fig. 20D)**.

Given the variable penetrance of the phenotypes described above, we assessed whether the heart and craniofacial abnormalities co-occurred in the same embryos. For this comparison, 14 *Rbm10* null and 8 *WT* embryos were analyzed. All of the *Rbm10* null embryos presenting heart defects also presented with head abnormalities, such as anterior cleft palate, epithelial remnants, abnormal palate, or absence of palatal holes (p-value< 0.001). By contrast, a few of the 8 *Rbm10 WT* embryos analyzed presented mild palate abnormalities - such as epithelial remnants or abnormal palate (mentioned above) - and only one of them presented a right atrium dilation. These findings are in agreement with the fact that 30% of *Rbm10* null male mice were lost before or during birth, as determined by the analysis described above, possibly due to the presence of multiple developmental abnormalities such as the ones described here. Overall, we conclude that the heart and head pathologies described in TARP syndrome are largely reproduced in *Rbm10* null embryos.

6.1.4 *Rbm10* null adult males present mild, non-lethal, alterations in heart function

Considering that a fraction of the *Rbm10* null males survived into adulthood, we assessed their health status. We followed mice closely by general CT scan bone CT scans and did not find any abnormalities **(Fig. 21A).** Given the embryonic heart phenotype, heart function was assessed by performing echocardiography in 3 month-old *Rbm10 WT* and null male mice **(Fig. 21B-J).**

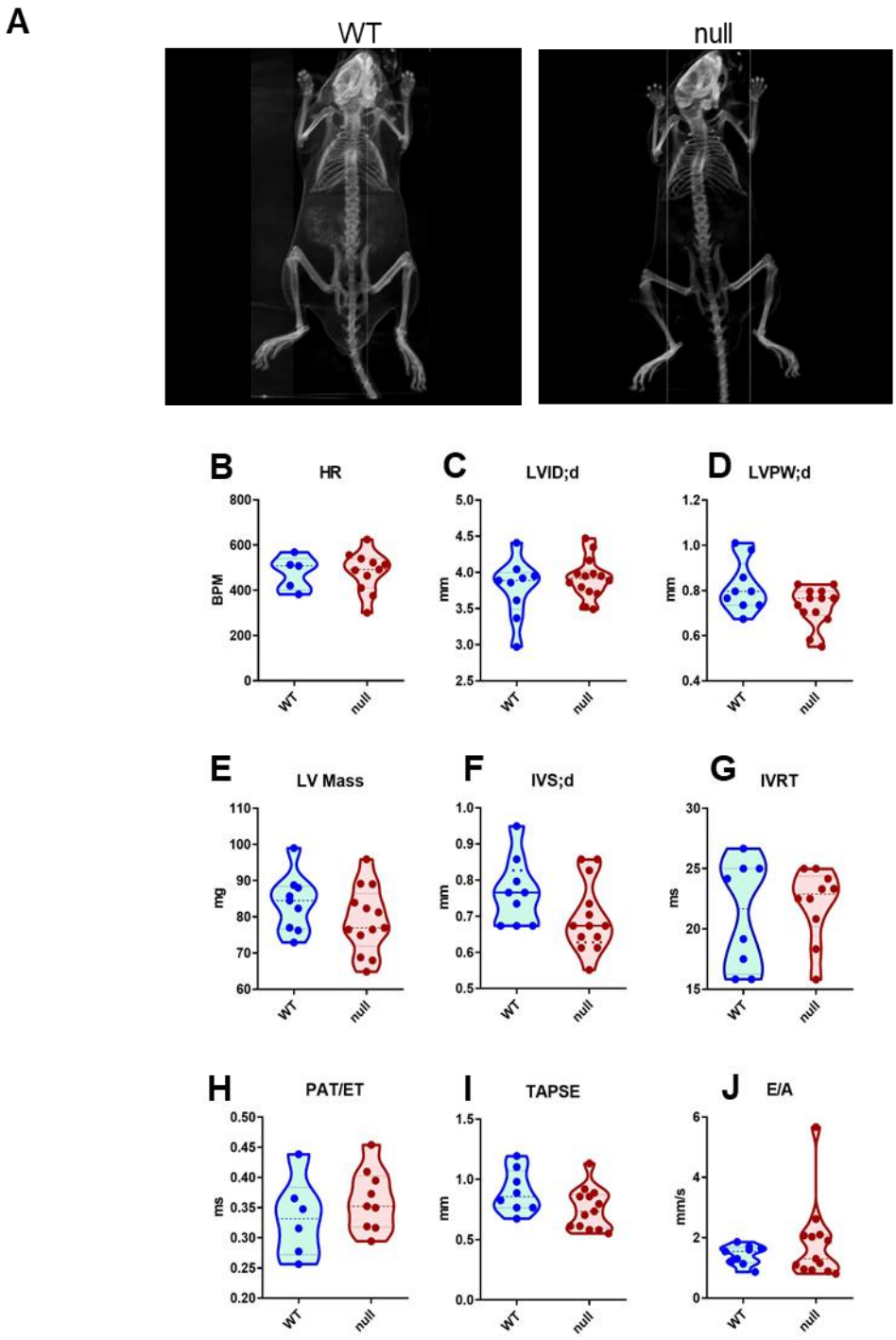

Figure 21: Health assessment of adult mice at 3 months of age. A. Bone CT of 16 week-old *Rbm10 WT* and null male mice (n=5/group). Graphs represent measurements mean +/- SD of **B.** Heart rate registered by beats per minute (BMP) (p-value = 1) **C.** Left ventricle internal diameter at the end of diastole (p-value = 0.546) **D.** Left ventricle posterior wall diameter at the end of diastole (p-value= 0.155) **E.** Corrected mass of the left ventricle (p-value = 0.270) **F.** Interventricular septum thickness in diastole (p-value = 0.0878) **G.** Isovolumic relaxation time (p-value = 0.984) **H.** Pulmonary pressures evaluation determined by pulmonary artery flow; acceleration (PAT) and ejection time (ET) (p-value = 0.272) **I.** Right ventricle systolic function determined by tricuspid annular plane systolic excursion (TAPSE) (p-value = 0.116) and **J.** Mitral valve function determined by early (E) and late (A) diastolic velocity peak waves (p-value= 0.756). WT mice (n=9) and null mice (n=14) (Mann-Whitney test, dotted lines represent mean and SD).

As shown in Figure 19, from a large series of cardiac parameters analyzed (heart rate, left ventricle internal diameter in diastole and systole, left ventricle posterior wall diameter, mass, and volume of the left ventricle, left ventricle ejection fraction and fractional shortening, interventricular septum thickness, isovolumic relaxation time, pulmonary artery flow, right ventricle systolic function, and mitral valve function), the only notable differences in *Rbm10* null mice were: 1) the occurrence of a slimmer, more dilated, left ventricle wall **(Fig. 21C-F)**; 2) the right ventricle presented an alteration related to systolic function by means of the measured variation during the cardiac cycle in the situation of the lateral portion of the annulus of the tricuspid valve without compromising mice survival **(Fig. 21I)**. The mitral valve and the pulmonary vein function had no significant alterations **(Fig. 21H & J)**. Overall, these differences did not affect the well-being of the mice.

6.2. Role of *Rbm10* in tissue homeostasis

6.2.1. *Rbm10* is dispensable during mouse adulthood

To determine whether *Rbm10* is required in adulthood, recombination and gene inactivation was induced using *Rbm10 KO* mice. Exon 3 of *Rbm10* was excised upon tamoxifen administration **(Fig. 22A)**. As controls, we used *Rbm10 WT* mice. In some experiments, the *Rosa26mTmG* allele was introduced to indirectly report on Cre recombinase activity. We administered a TMX-containing diet to 8 week-old mice for 2 months to induce systemic *Rbm10* recombination and avoid the potential outgrowth of unrecombined cells. We confirmed that adult male mice displayed extensive loss of RBM10 expression in a wide variety of tissues that appeared as histologically normal at 11 and 16 weeks of age. Few groups of cells were found to express RBM10 in the liver, pancreas, bladder, and lung **(Fig. 22B)**. In addition, we confirmed that RBM10 loss was maintained in 67 week-old mice, several weeks after treatment, where recombination levels were similar to recently treated mice (data not shown). Interestingly, we observed RBM10-expressing cell patches in the intestine in males and females, consisting of unrecombined clones. Females showed diverse levels of recombination, similar to our constitutive *Rbm10* KO model that looked histologically normal as well. Considering this, we performed all additional experiments in male mice. *Rbm10* inactivation did not affect survival: both *Rbm10 KO* (n= 24) and *WT* (n=30) mice survived up to 80 weeks of age without any detectable pathology resulting from *Rbm10* inactivation **(Fig. 23A)**. We followed a smaller cohort of TMX-treated mice (6 *Rbm10 KO* and 4 *Rbm10 WT* mice) for 10 weeks starting at 20 weeks of age with bi-weekly weight and monthly blood cell counts. We did not observe significant differences in either of these parameters between WT and KO mice **(Fig. 23C)**.

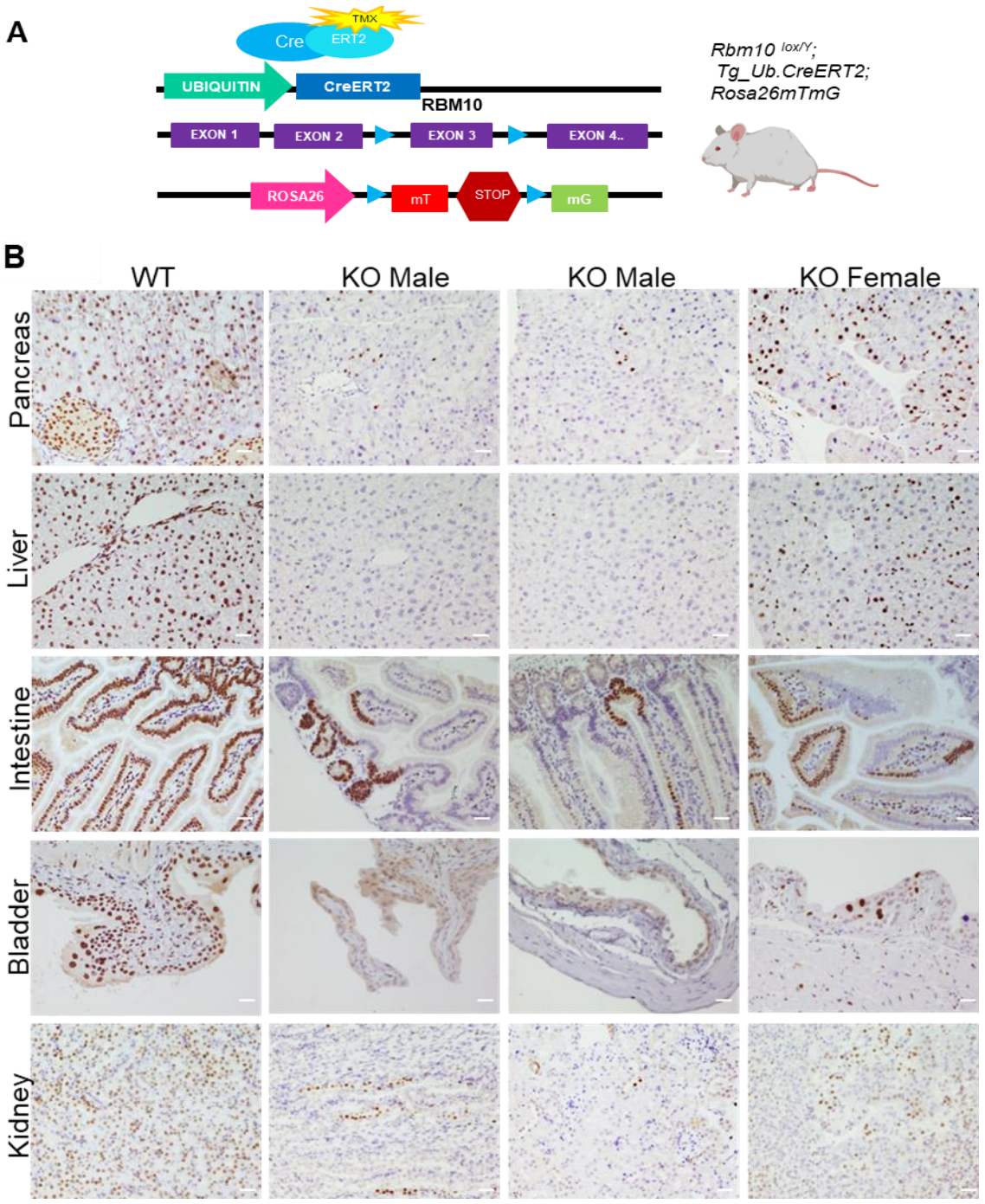

Figure 22: Generation of a conditional *Rbm10* KO mouse model. A. TMX inducible *Rbm10 KO* mouse strain **B.** Representative images of RBM10 immunostaining of formalin-fixed paraffin-embedded tissues from 11 week-old *Rbm10* WT and KO mice after 3 weeks of TMX treatment showing extensive loss of RBM10 expression, more so in male than in female mice (scale bar, 50µm).

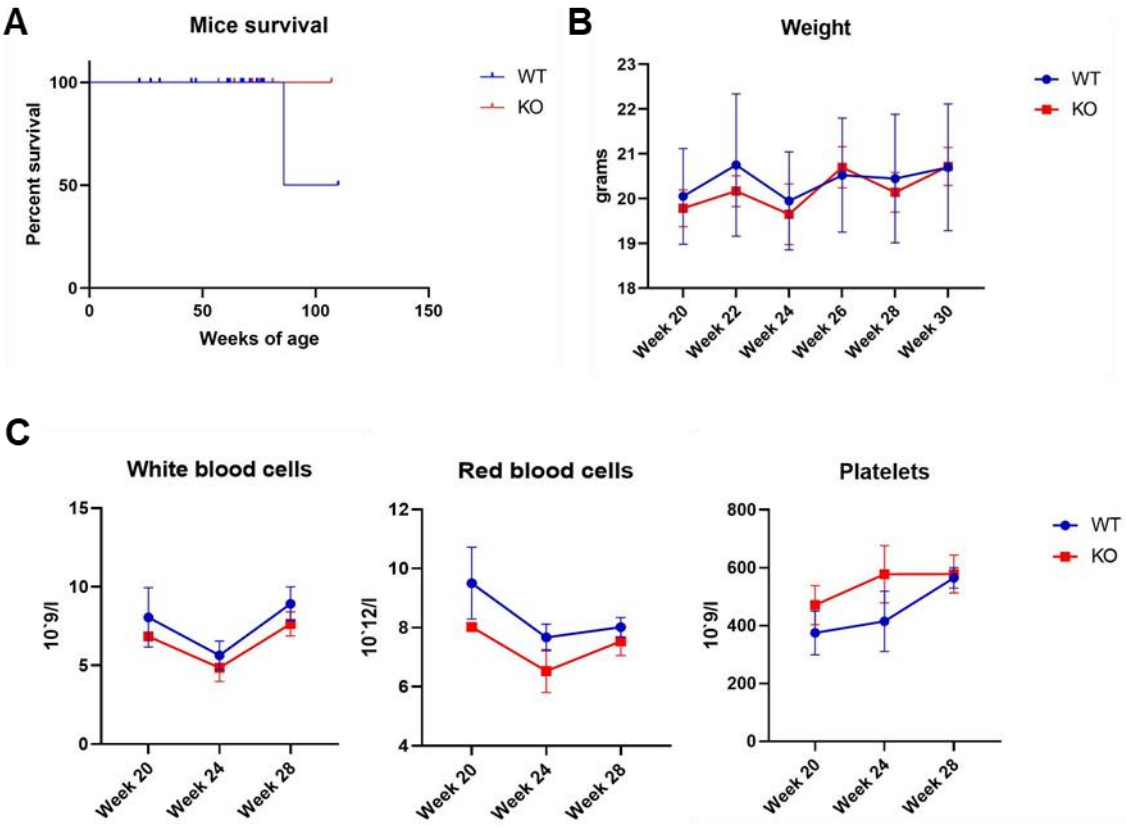

Figure 23: Effect of Rbm10 inactivation on the health status of adult mice. A. Kaplan-Meier survival analysis of *Rbm10 KO* (n=24; red line) vs. *Rbm10 WT* (n=30; blue line) male mice showing no significant difference in survival **B.** Weight (Median +/- SD) of *Rbm10 KO* (n=6; red) and WT (n=4; blue mice) was determined every two weeks, measurements started at 20 weeks of age during 10 weeks **C.** Blood cell counts of *Rbm10 KO* (n=6) and WT (n=4), determined on a monthly basis (Median +/- SD) month in TMX-treated mice, measurements started at 20 weeks of age during 8 weeks (blue circles represent WT mice and red squares KO mice).

Because our main interest is to assess the role of RBM10 in urothelial homeostasis and in bladder cancer, we analyzed the expression of RBM10 in the urothelium of TMX-treated mice with antibodies detecting a panel of urothelial markers. The expression of markers of stem cells (KRT14), basal/intermediate cells (KRT5), and umbrella cells (KRT20) in 16 week-old mice were similar in WT and KO mice **(Fig. 24)**. KRT14+ cells were found in the basal layer in both WT and KO mice; KRT5 was highly expressed across the basal/intermediate layers; KRT20 was found selectively in umbrella cells in the uppermost luminal layer.

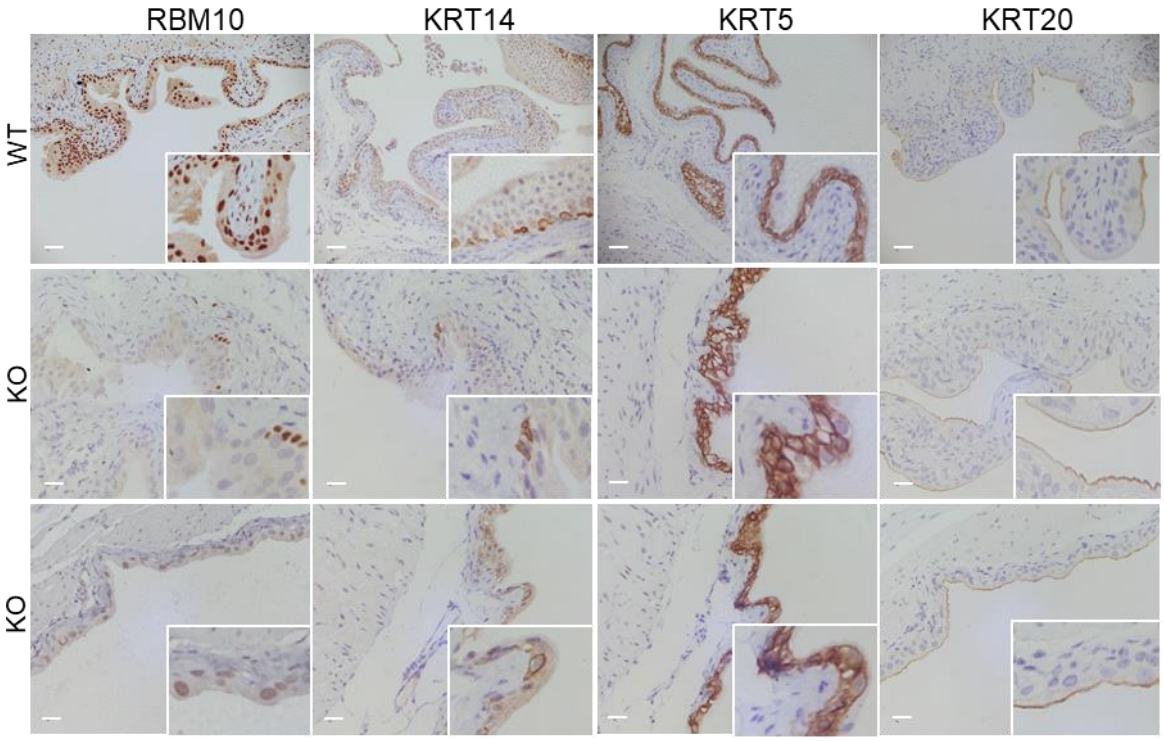

Figure 24: Urothelial marker expression in *Rbm10 WT* and *KO* mice. Representative brightfield microscopic images of immunohistochemical stainings of RBM10 and urothelial differentiation markers. Antibodies detecting KRT14 14, KRT5, and KRT20 label a subset of basal cells, the basal/intermediate layers, and the luminal layer, respectively (scale bar, 50µm).

Altogether, these results indicate that *Rbm10* inactivation in adult mice does not have a major impact on the well-being and histology of mice, suggesting that the gene is dispensable in adult homeostatic conditions.

CHAPTER II

Role of *Rbm10* in urothelial mouse biology

6.3. Role of *Rbm10* in urothelial mouse biology

6.3.1. *Rbm10 KO* mouse urothelial organoids show reduced proliferation and undergo differentiation in the absence of growth factors

Our laboratory has recently reported methods for the culture of mouse urothelial organoids and has demonstrated both their growth factor requirements and their ability to recapitulate the *in vivo* urothelial differentiation program (Santos et al., 2019). To determine the functional effects of *Rbm10* inactivation, I have generated organoids from urothelial cells of *Rbm10 KO* and control *Rbm10 WT* male mice.

In these studies, TMX (2µM) was added at passage 4 to induce recombination, which was tracked by the *Rosa26mTmG* reporter: unrecombined cells express Tomato, and recombined cells express GFP. After 48 h, TMX was removed from the medium and the expression of GFP was assessed in the organoids: Tomato expression was detected in a small proportion (5-30%) of organoids across the samples analyzed by fluorescence microscopy; within an organoid, all cells were homogeneous regarding reporter expression. Organoids were dissociated and cells were FACS-sorted to isolate enriched GFP-expressing and Tomato-expressing cells from both TMX-treated and control (-TMX) conditions. This allowed generating populations of only recombined or unrecombined cells: after sorting, a population of close to 100% GFP-positive cells was isolated **(Fig 25A)**. We then assessed RBM10 protein loss by immunofluorescence and western blot in *Rbm10 WT* and *Rbm10 KO* organoids and confirmed that, 12 days after TMX treatment, RBM10 protein expression was lost concomitantly to GFP expression **(Fig. 25B, C)**.

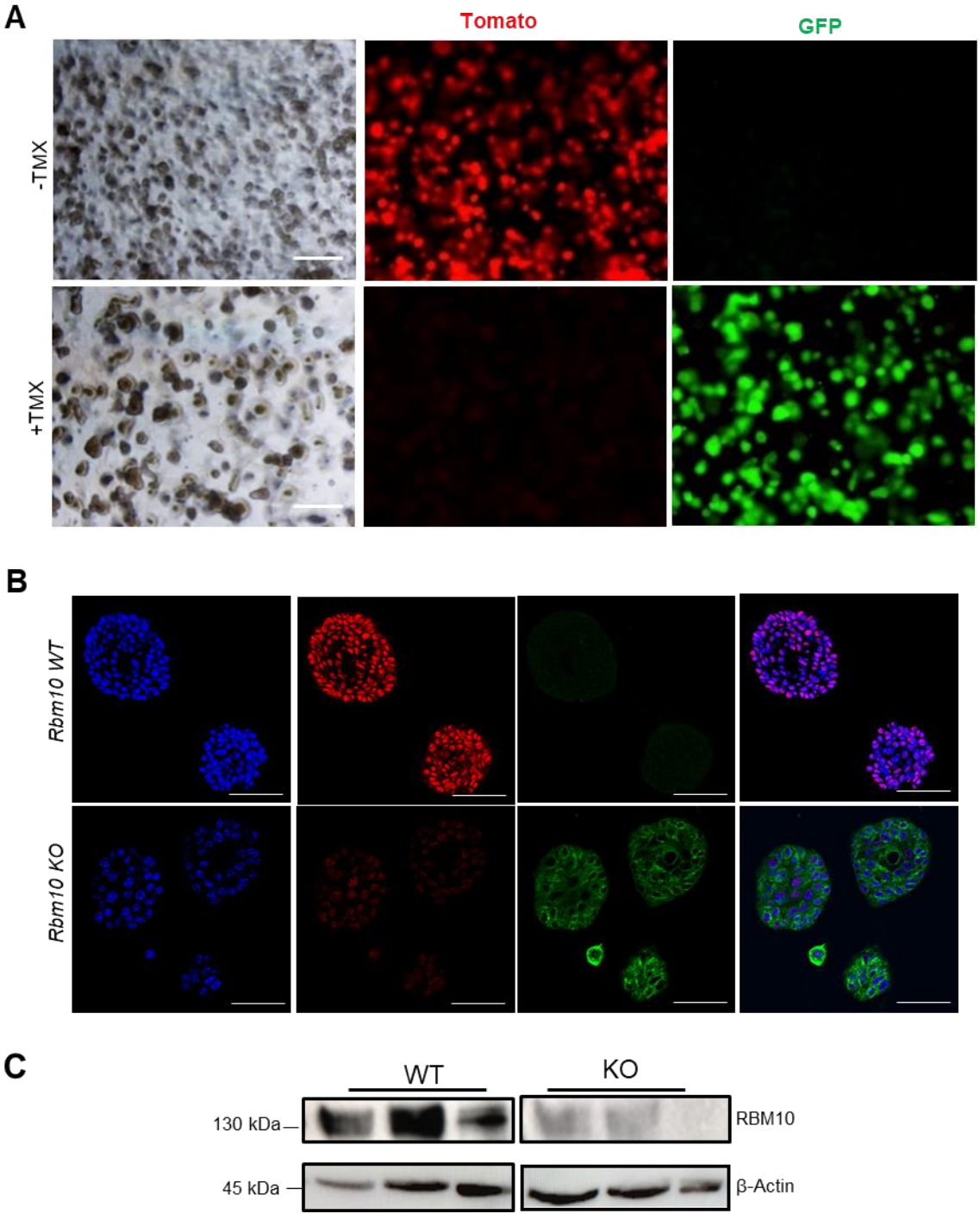

Figure 25: Establishment of *Rbm10 WT and KO* mouse urothelial organoids. A. Brightfield and fluorescent microscopy images of passage 6 FACs sorted *Rbm10 KO* and *Rbm10 WT* organoids after tamoxifen (2µM) or control DMSO addition onto urothelial cells for 48 hours, inducing GFP expression or maintaining Tomato expression, respectively (scale bar, 500µm) **B.** Immunofluorescence staining of sections of paraffin-embedded organoids 12 days after TMX or DMSO treatment, highlighting the nuclear expression with anti-RBM10 in *Rbm10 WT* organoids and with anti-GFP in membrane in *Rbm10 KO* organoids (n=4). DAPI staining is shown in blue (scale bar, 50µm) **C.** Western blot analysis of RBM10 and β-Actin on *Rbm10* WT and KO organoids protein extracts.

We then investigated whether *Rbm10* inactivation had an effect on the proliferative capacity of urothelial cells from 3 independent mice used to derive paired *Rbm10 WT* and *Rbm10 KO* organoids. We assessed proliferation by plating cells at 2000 cells/well in CM and quantified the number of organoids formed after 7 days by imaging analysis. *Rbm10 KO* organoids showed a significantly reduced capacity to proliferate despite the fact that they could be maintained uninterruptedly for >20 passages, suggesting that *Rbm10* inactivation is well tolerated by normal urothelial organoids **(Fig. 26A, B).**

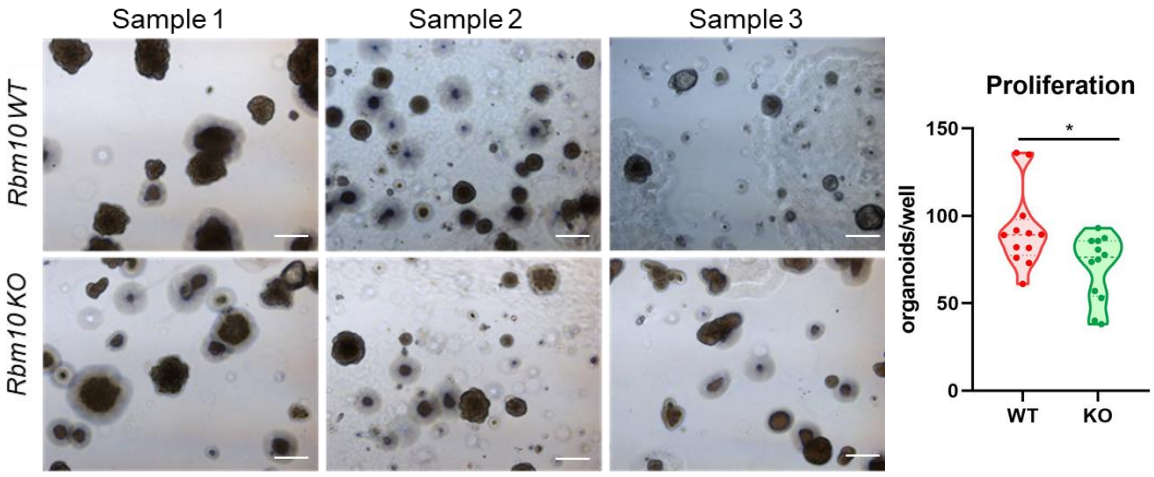

Figure 26: Growth capacity of *Rbm10 WT* and *KO* mouse urothelial organoids. Brightfield images of passage 8 *Rbm10 WT* and *Rbm10 KO* organoids (n=3) (Scale bar, 500µm) and corresponding quantification after 7 days in culture to determine proliferation potential (2000 cells/well) (p-value = 0.034). (Two-way ANOVA and paired T-test) *p≤0.05.

To assess the differentiation potential of *Rbm10* KO organoids, we induced differentiation by depleting all growth factors (medium without EGF, LY2157299, Noggin, WNT3A, and RSPO1), as previously described (Santos et al., 2019). Three independent organoid lines were cultured for 7 days in proliferative (P) or differentiated (D) conditions. Control WT organoids displayed an increase in size and lumen formation, as well as a thinner cell layer **(Fig. 27)**. To better characterize the phenotype in differentiation conditions, we quantified the proportion of cystic organoids and determined their area compared to differentiated WT conditions **(Fig. 28)**. In proliferation, the proportion of cystic organoids - compared to solid organoids - was significantly higher in *Rbm10 KO* cells when compared to WT (p-value = 0.009) **(Fig. 29A)**. There were no significant differences in the proportion of cystic *Rbm10 KO* vs. WT organoids in differentiation conditions (p-value = 1) **(Fig. 29A).** Moreover, *Rbm10 KO* organoids were significantly larger in proliferative conditions (p-value < 0.001) **(Fig. 29B)**. A similar trend was observed in differentiation conditions but the differences did not reach statistical significance (p-value = 0.053) **(Fig. 29C)**.

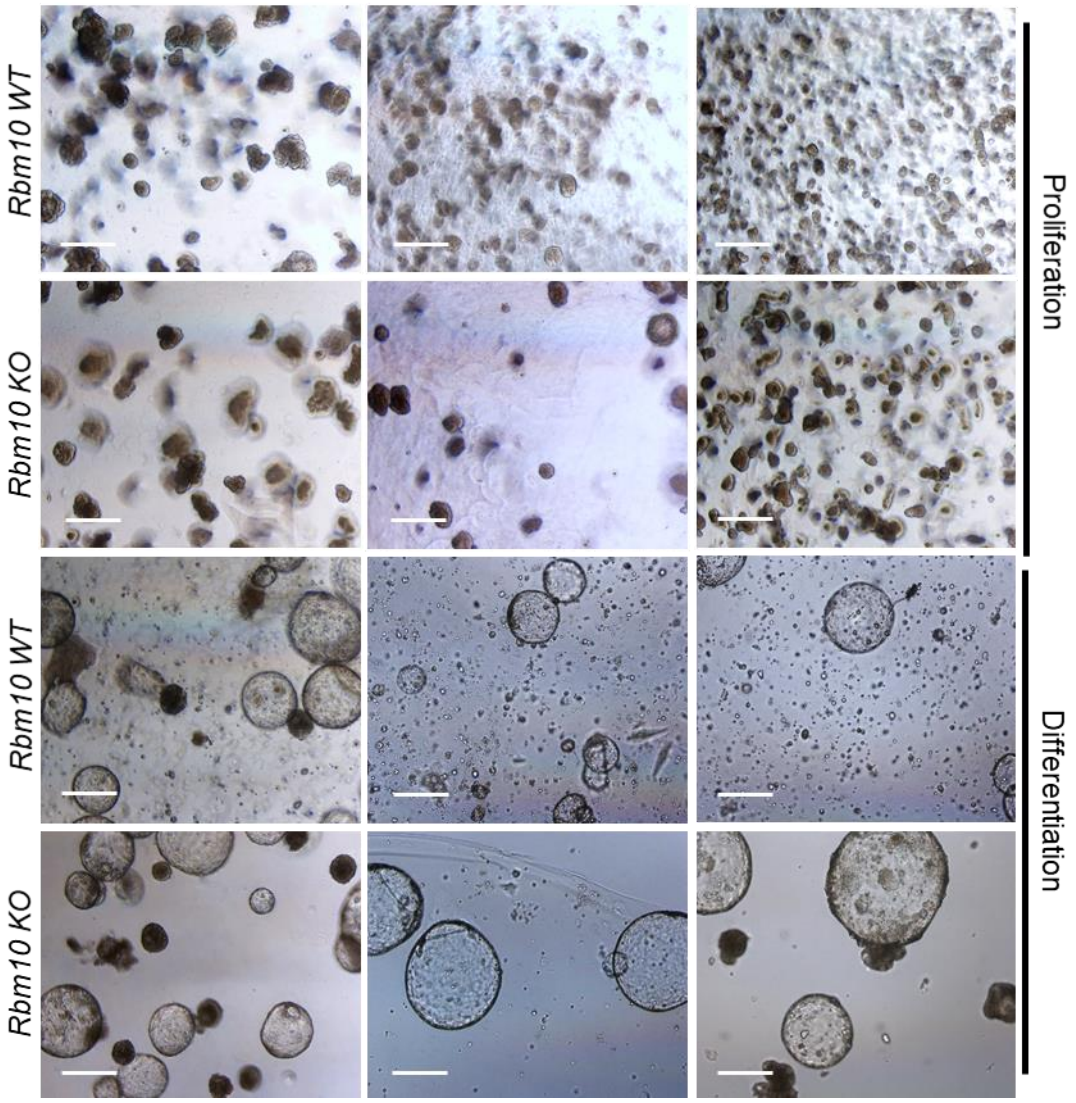

Figure 27: *Rbm10 WT* and *KO* mouse urothelial organoids in proliferative and differentiated conditions. Brightfield microscopy images of *Rbm10 WT* and *RBM10 KO* urothelial organoids plated in Matrigel in Complete Medium (CM) to promote proliferative conditions. After 7 days, differentiation was induced by changing the medium to differentiation medium (DM) (n= 3 WT & n= 3 KO), where images show size increase and lumen formation for the 3 different samples (scale bar, 500µm).

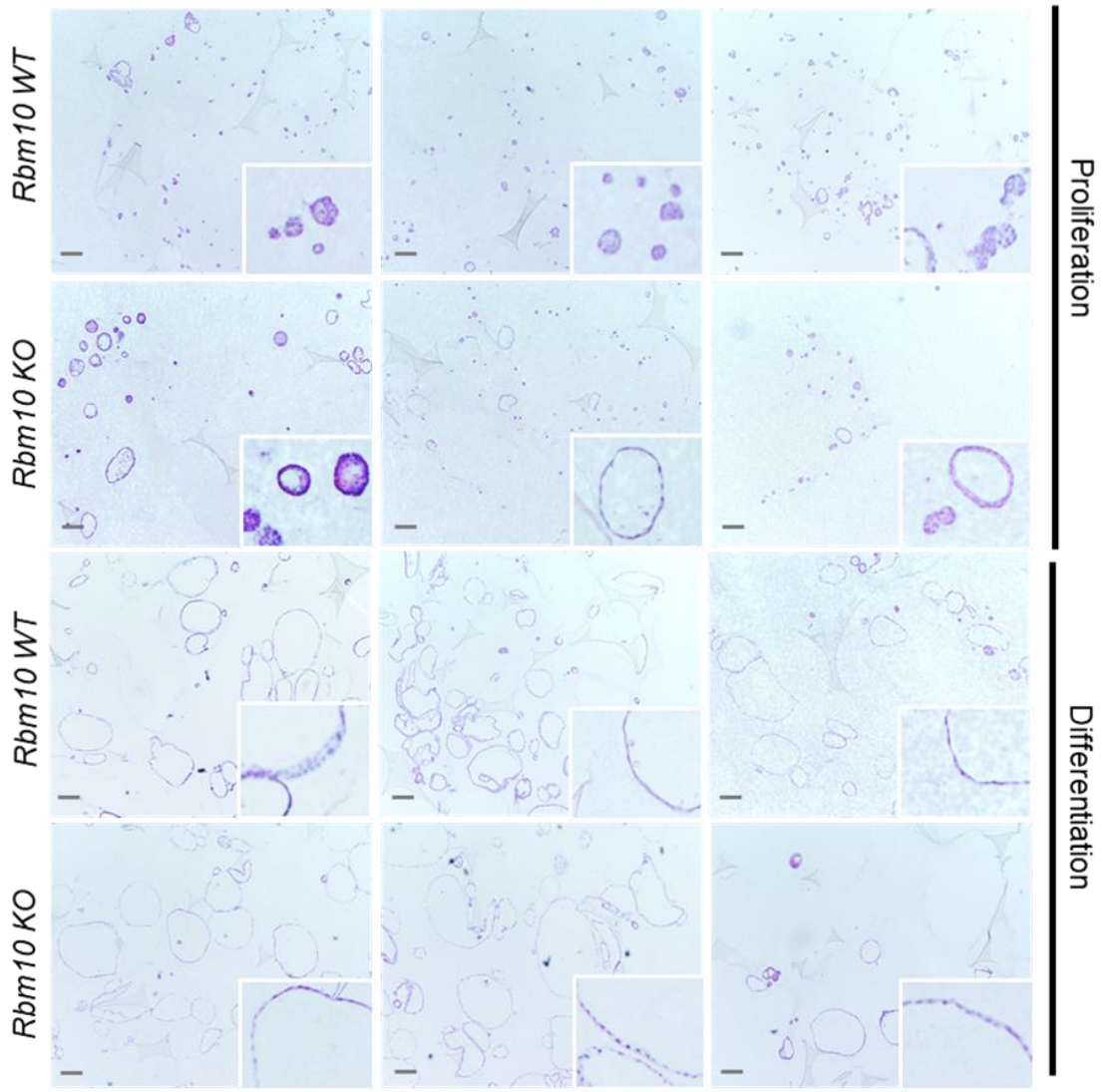

Figure 28: *Rbm10 WT* and *KO* mouse urothelial organoids HE staining in proliferative and differentiated conditions. Representative hematoxylin and eosin (HE) staining of *Rbm10 WT* and *RBM10 KO* organoids highlighting the increased size and cystic formation in differentiated organoids (n=3) (scale bar, 100µm).

In addition, we determined the diameter of the whole organoid, the thickness of the layers of cells forming the cystic structure, and the size of the lumen in cystic organoids found in both *Rbm10 WT* and *KO* organoids in P and D conditions **(Fig. 29C, D)**. In proliferation medium, we confirmed that *Rbm10 KO* organoids not only presented significantly larger diameter (p-value = 0.000) and lumen (p-value = 0.0034) but also that these occurred more frequently than in *Rbm10 WT* organoids **(Fig. 29D)** without showing significant differences in the thickness of cell layers **(Fig. 29E)**. In differentiation medium, the differences were more subtle and non-significant **(Fig. 29D)**.

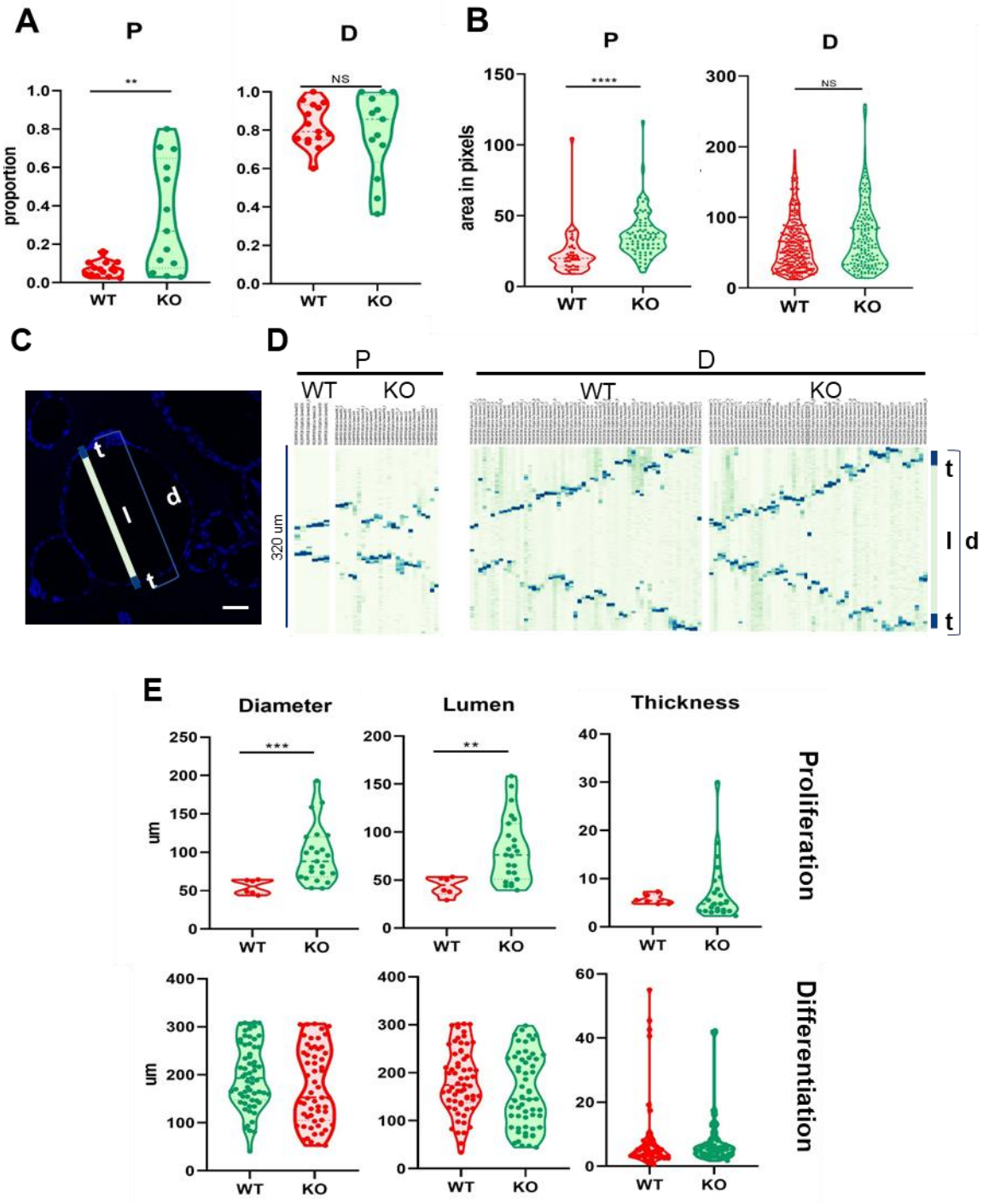

Figure 29: Quantification of differentiation capacity of *Rbm10 WT* and *KO* mouse urothelial organoids. **A.** Quantification showing the formation of cystic organoids in P and D both in WT and KO organoids, represented by the fold change when compared to the total number of organoids **B.** Quantification showing the area of cystic organoids in P and D both in WT and KO organoids, represented by the pixels occupied by the organoids **C.** Image of organoids displaying the features quantified in panel D; lumen (l), layers thickness (t) and diameter (d) (scale bar, 50µm) **D.** Signal distribution acquired by confocal microscopy displaying organoids features in P and D conditions; color code indicates the intensity of the signal: dark blue; high, light blue; intermediate and white; low **E.** Quantification of organoid features; diameter, lumen size and thickness (Mann-Whitney test) *p≤0.05, **p≤ 0.01, ***p≤ 0.001, ****p≤ 0.0001

6.3.2. Growth factor dependency assays reveal that *Rbm10 KO* mouse urothelial cells are less dependent on EGF and show higher EGFR expression

In order to determine whether *Rbm10 KO* and *WT* cells differ in their growth factor dependency, we performed organoid formation assays in medium depleted of one or more growth factors. We assessed growth as the number of organoids per well and the area occupied by organoids (Santos et al., 2019). *Rbm10 KO* and *WT* organoids were cultured in CM depleted of EGF, WNT3A/RSPO1, or all of them (**Fig. 30A**). *Rbm10 KO* organoids were significantly less EGF dependent than WT organoids when both parameters were considered **(Fig. 30B, C)**. In contrast, WNT3A/RSPO1 depletion did not significantly affect proliferation of *Rbm10 KO* organoids when compared to WT **(Fig. 30B, C)**. We observed dramatically reduced growth in both types of organoids when all 3 factors were absent **(Fig. 30A, B)**. To explore the observed less EGF-dependent phenotype, we analyzed EGFR expression using IHC: signal quantification showed that higher expression in *Rbm10 KO* organoids (p-value = 0.328) **(Fig. 30D)**.

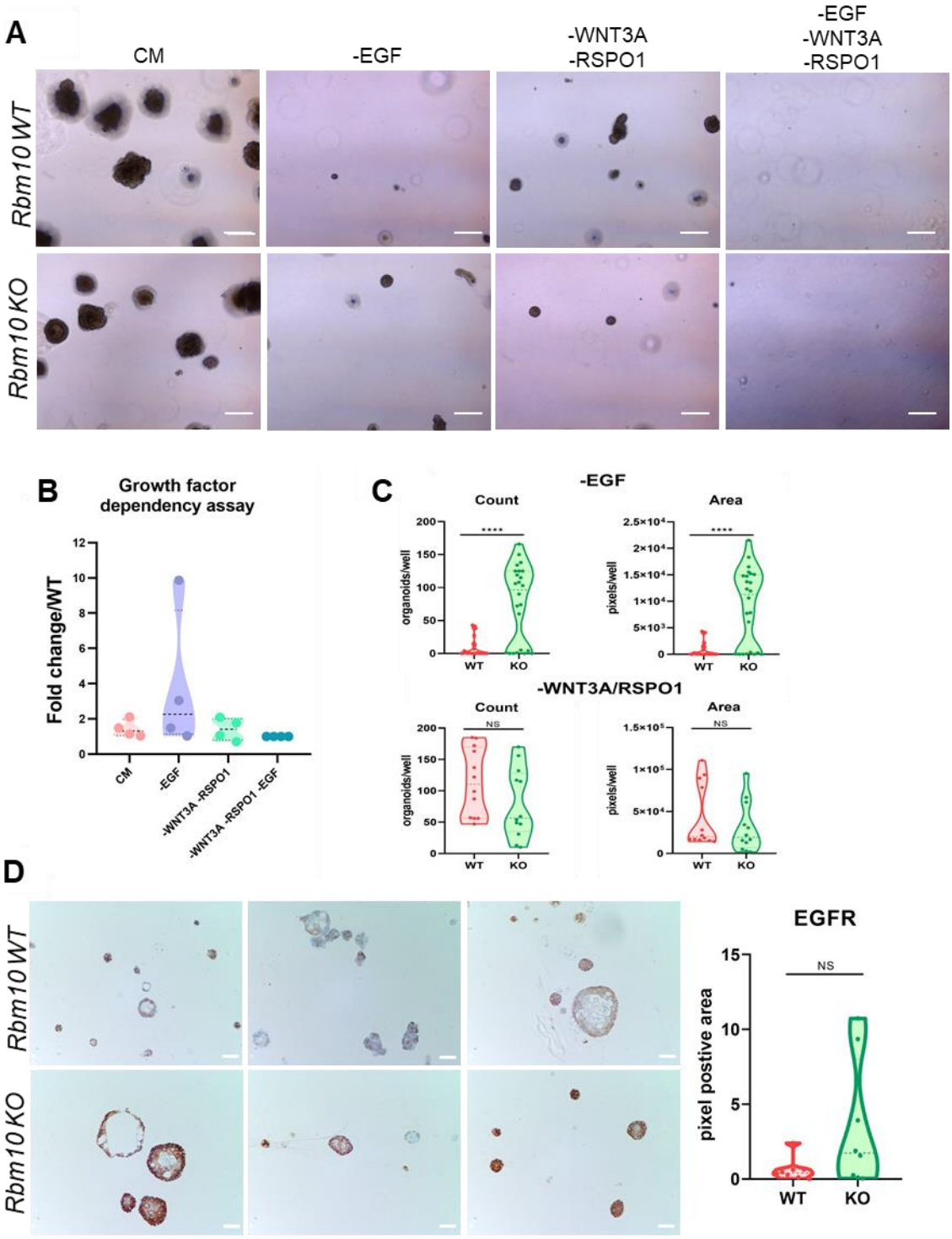

Figure 30: Growth factor dependency and EGFR expression in *Rbm10 WT* and *KO* mouse urothelial organoids. A. Brightfield images of passage 8 *Rbm10 WT* and *Rbm10 KO* urothelial organoids (n=3). Left panel shows organoids in CM as a control; central panel shows organoids in EGF-depleted medium; the right panel shows organoids in WNT3A/RSPO1-depleted medium (scale bar, 500µm) **B.** Quantification showing *Rbm10 KO* organoid growth in CM depleted from EGF, WNT3A/RSPO1, and both, represented by the fold-change compared to its paired WT control (n=4). **C.** Raw count (left panels) and area (right panels) of *Rbm10 WT* and *KO* organoids in CM without EGF and WNT3A/RSPO1 (n=4) (Student's T-test). *p≤0.05, **p≤ 0.01, ***p≤ 0.001, ****p≤ 0.0001 **D.** Immunohistochemical analysis of EGFR in *Rbm10 WT* and *Rbm10 KO* urothelial organoids (n=5) (scale bar, 500µm) and its corresponding quantification (p-value = 0.328, Mann-Whitney test).

6.3.3. Transcriptomic analysis indicate that *Rbm10* KO mouse urothelial organoids differentiate efficiently

To investigate whether *Rbm10* inactivation had a transcriptomic effect, we performed an RNA-Seq to acquire paired-end reads using two independent *Rbm10 WT* and *Rbm10 KO* paired organoids treated, or not, with TMX at passage 8 to induce *Rbm10* recombination (n=2/group). Therefore, the experiment consisted of two *Rbm10 KO* samples and 6 *Rbm10* unrecombined *WT* samples **(Fig. 31A)**.

Principal component analysis (PCA) showed that *Rbm10 KO* organoids clustered separately from *Rbm10 WT* organoids **(Fig. 31B)**. The normalized counts of *Rbm10* transcripts decreased when compared to WT **(Fig. 31C)**. Differential expression analysis using DESeq2 failed to show significantly differentially expressed genes (DEG) in *Rbm10 WT* organoids treated - or not - with TMX, indicating that TMX administration did not translate into major transcriptomic effects in urothelial cells. DEG analysis of *Rbm10 KO* (n=2) vs *WT* (n=6) organoids showed only 2 genes the expression of which was significantly different in both conditions, possibly as a result of reduced statistical power. For this reason, we performed an additional RNA-Seq experiment using *Rbm10 WT* and *Rbm10 KO* paired samples.

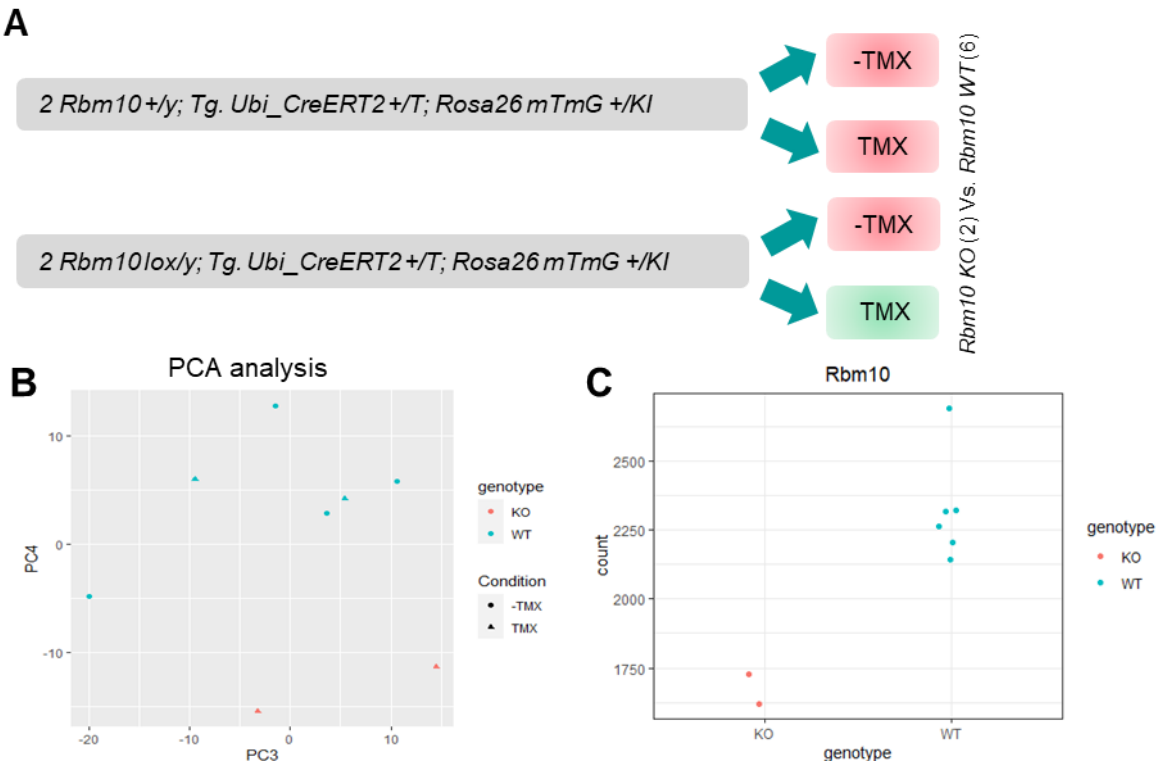

Figure 31: Preliminary RNA-Seq analysis of *Rbm10 KO* vs. *WT* organoids treated with or without TMX. A. Experimental design showing genotypes of the mice used to generate urothelial organoids and the corresponding treatment used to induce *Rbm10* recombination **B.** PCA analysis showing the distribution of and *Rbm10* WT (n=6) and *Rbm10 KO* (n=2) samples **C.** Normalized counts of *Rbm10* transcripts in WT (n=6) and KO (n=2) samples.

In order to gain statistical power and to determine whether *Rbm10* inactivation had an effect on organoids under P and D conditions, we performed a 3'-end RNA-Seq of 3 independent pairs of *Rbm10 WT* and *Rbm10 KO* organoids at passage 8 **(Fig. 32A)**. To evaluate inter and intragroup variability, we assessed the correlation of RPKM values of all samples. Pearson correlation matrix showed that *Rbm10 WT* organoids exhibited a higher correlation coefficient and were less heterogeneous than *Rbm10 KO* organoids **(Fig. 32B)**. We then asked the following questions: 1) do *Rbm10 KO* organoids undergo a similar differentiation program than WT organoids, 2) how *Rbm10 KO* organoids differ from *Rbm10 WT* organoids in proliferative conditions, and 3) how *Rbm10 KO* organoids differ from *Rbm10 WT* organoids in differentiated conditions **(Fig. 32C)**.

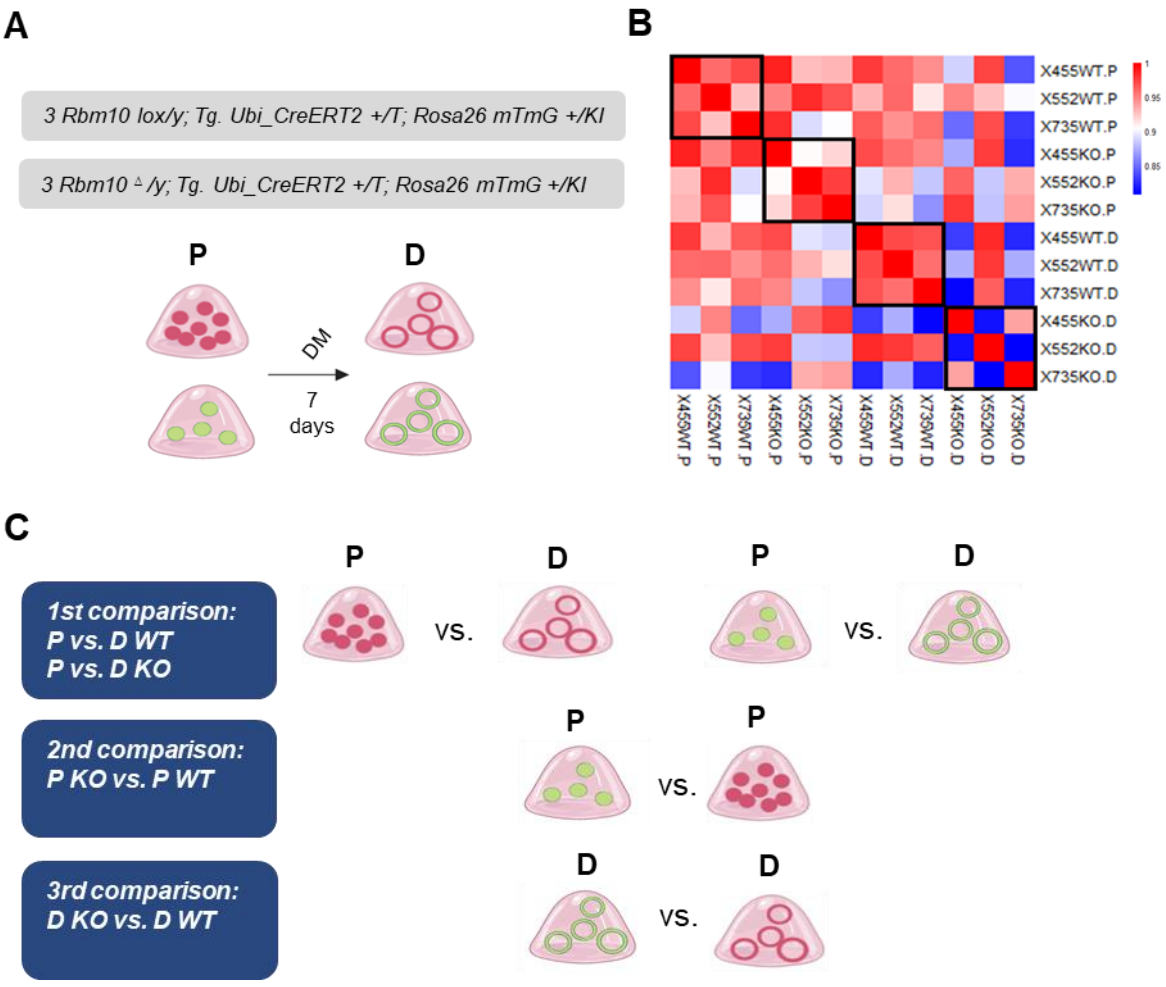

Figure 32: RNA-Seq analysis of *Rbm10 WT* and *KO* organoids in proliferative and differentiation conditions. A. RNA-Seq was performed using *Rbm10$^{lox/y}$;UbiCreERT2+/T; Rosa26mTmG$^{+/KI}$* organoids with or without TMX, to induce *Rbm10* recombination, both in P and D conditions **B.** Heatmap showing Pearson correlation among *Rbm10 WT* and *KO* organoids in P and D conditions **C.** Graphic representation of the comparisons.

To identify DEGs, I used DESeq2. In the P vs. D comparison of WT organoids, we observed that 249 genes were differentially expressed, 125 genes of which were up-regulated and 124 were down-regulated **(Fig. 33A)**. Sixty-eight percent of these genes (169/249) overlapped with those reported in normal urothelial organoids in D conditions by Santos et al., 2019. We then generated a signature with this 249 DEG (hereafter, WT Differentiation signature) and evaluated the enrichment scores of the up-regulated and down-regulated genes in this signature in *Rbm10 WT* and *KO* P and D organoids **(Fig. 33B)**. *Rbm10 WT* D organoids followed the expected trend, with significantly higher enrichment scores in the genes up-regulated of the WT Differentiation signature (p-value = 0.017) and a significantly decreased enrichment score of the down-regulated genes when compared with WT P organoids (p-value = 0.014). **(Fig. 33B)**. In differentiated *Rbm10 KO* organoids, a similar trend was observed for both the up-regulated and the down-regulated genes but the differences did not reach statistical significance (p-value=0.164 and p-value = 0.065, respectively), possibly due be due to the variability of the biological replicas **(Fig. 33B)**.

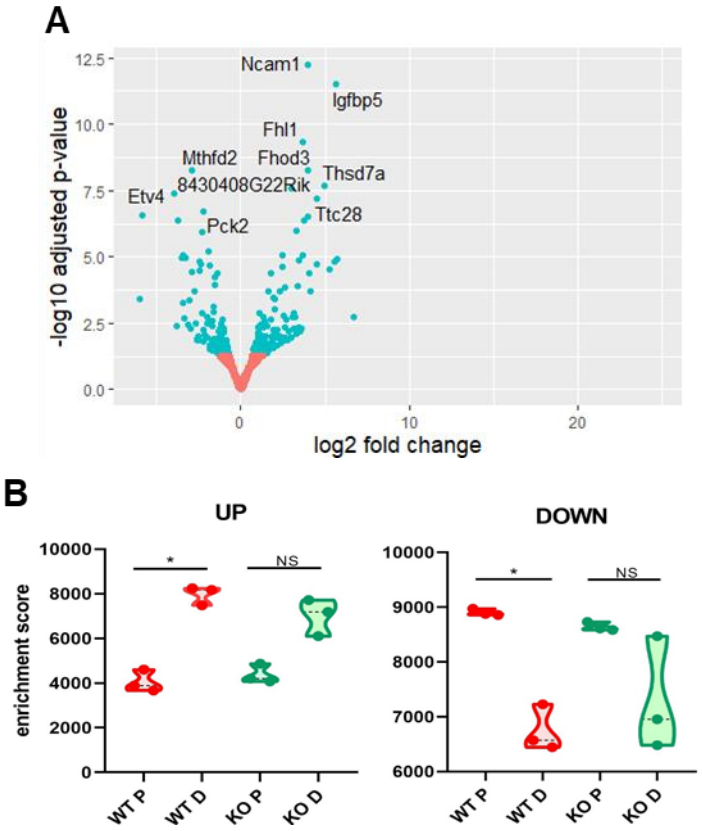

Figure 33: *Rbm10 WT* D DEGs compared to *Rbm10 WT* and KO organoids. A. Volcano plot representing significantly DEGs (blue) in *Rbm10 WT* organoids upon induction of differentiation (n=3) (adjusted p value ≤0.05) **B.** ssGSEA enrichment score of up-regulated genes (left) and down-regulated genes (right) from the WT Differentiation signature in *Rbm10 WT* and *KO* samples in P and D (n=3/group) (Paired T-test), *p≤0.05.

GSEA was also performed on the pre-ranked lists generated as an output from the first comparison: *Rbm10 WT* P vs. D conditions and *Rbm10 KO* P vs. D. We determined the enrichment scores for the urothelial differentiation signatures described by Robertson et al 2017, Tan et al 2019, and the signatures corresponding to DEGs of the three cell clusters identified by our group in a single cell RNA-Seq experiment using differentiated normal urothelial organoids. We observed significant (FDR <0.025) enrichment of Robertson and Tan *et al* signatures in both *Rbm10* WT and *KO* upon induction of differentiation, with similar NES scores and FDR values, suggesting an efficient urothelial differentiation **(Fig. 34A)**. We also observed significant enrichment of the signatures of the three cell clusters of differentiated organoids in *Rbm10 KO* samples **(Fig. 34A)**. We also checked the gene expression levels (normalized counts) of a panel of basal/intermediate and luminal markers in *Rbm10 WT* and *KO* organoids **(Fig. 34B)**: the expression pattern of basal/intermediate and luminal markers was similar in both conditions **(Fig. 34B)**. Of note, in *Rbm10 KO* P organoids, the basal levels of *Gata3, Upk1a, Upk1b*, and *Upk2* luminal markers were non-significantly higher than in WT P organoids, suggesting a more luminal-like phenotype **(Fig. 34B)**.

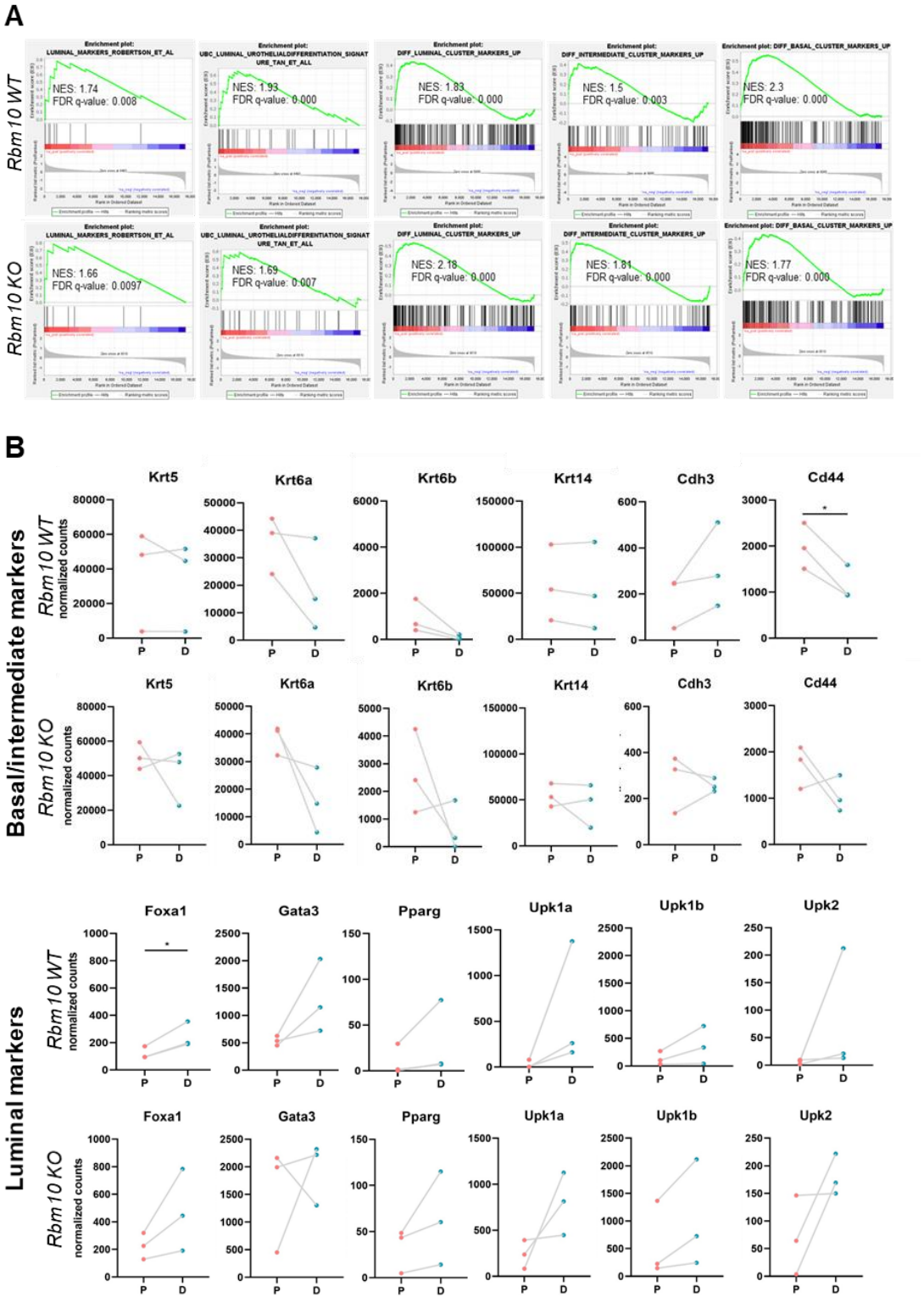

Figure 34: GSEA analysis of luminal signatures and expression of basal/intermediate and luminal markers in *Rbm10 WT* and *KO* organoids. A. Enrichment plots showing the up-regulation of luminal signatures in *Rbm10 WT* (top) and *KO* (bottom) D organoids. **B.** Graphs showing the expression (normalized counts) of a panel of basal (top) and luminal (bottom) urothelial markers in *Rbm10 WT* and *KO* organoids in P and D conditions. (Paired T-test) *p≤0.05.

To validate these findings, we determined the expression of selected differentiation markers (*Upk1a, Upk2, Gata3, Pparγ,* and *Foxa1*) using RT-qPCR and immunofluorescence. In agreement with the RNA-Seq analysis, the relative expression (fold-change when compared to WT) of luminal markers in proliferative conditions was higher in *Rbm10 KO* organoids, compared to WT organoids **(Fig. 35)**. In differentiation conditions, *Rbm10 KO* organoids showed less differences in the expression of *Upk1a* and *Upk2*, and higher expression of *Upk3a, Gata3, Pparγ,* and *Foxa1* **(Fig. 35)**.

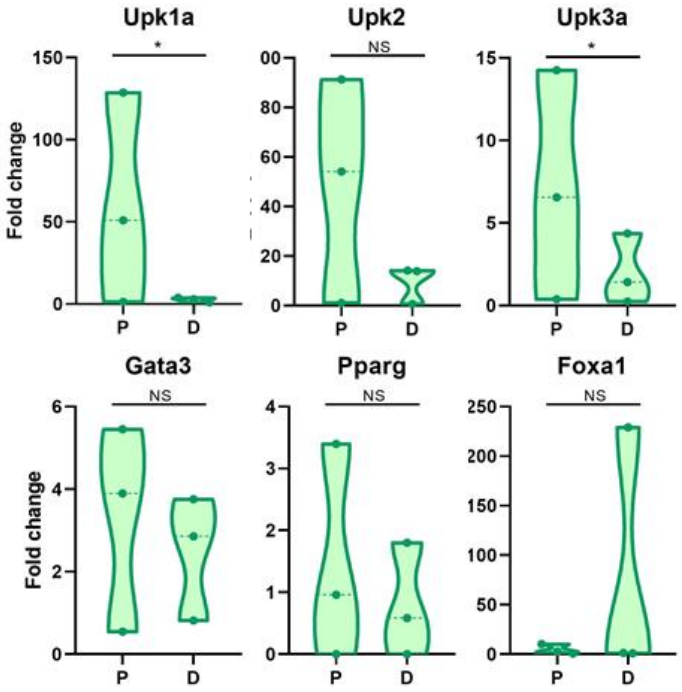

Figure 35: RNA luminal and basal/intermediate markers expression in *Rbm10 WT* and *KO* mouse urothelial organoids. RT-qPCR relative expression of *Krt5, Upk1a, Upk2, Gata3, Pparγ,* and *Foxa1* represented as fold change comparing paired *Rbm10 KO* Vs WT organoids in P and D (n =3/each group) (Two-way ANOVA) *p≤0.05.

By immunofluorescence, detection of basal/intermediate markers (KRT5, KRT6, and KRT16) was similar in proliferative conditions and decreased upon differentiation **(Fig. 36)**. Protein expression quantification showed decreased levels of KRT5 upon differentiation in both P and D, similar levels of UPK1A in all samples, and significantly increased levels of UPK3A in *Rbm10 KO* D organoids **(Fig. 36)**.

In summary: 1) the urothelial differentiation program was efficiently activated both in *Rbm10 WT* and *Rbm10 KO* organoids and 2) *Rbm10 KO* organoids expressed higher levels of luminal markers in proliferative conditions.

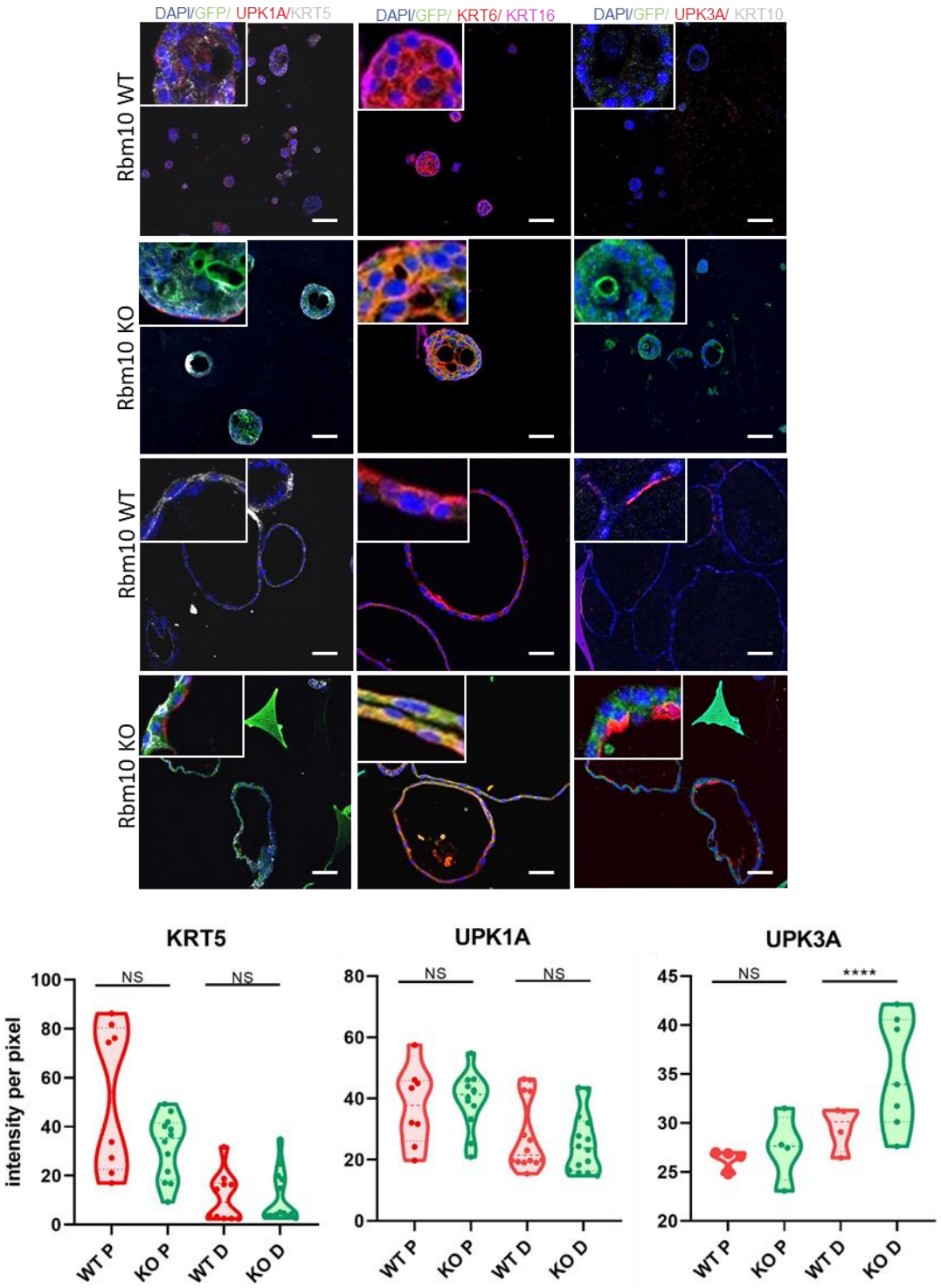

Figure 36: Luminal and basal/intermediate marker expression in *Rbm10 WT* and *KO* urothelial organoids. IF analysis of the expression of KRT5 and UPK1A (right), KRT6 and KRT16 (middle), and KRT10 and UPK3A (left) in 3 independent pairs *Rbm10 KO* and *WT* organoids in P and D (scale bar, 250µm); quantification of KRT5, UPK1A, and UPK3A by the IF intensity per pixel in 10x confocal microscope (Mann-Whitney test). *p≤0.05, **p≤ 0.01, ***p≤ 0.001, ****p≤ 0.0001.

6.3.4. *Rbm10 KO* urothelial organoids display a luminal-like phenotype with features of stratified epithelia

In the P KO vs. P WT comparison, 7 genes were significantly up-regulated, and 5 significantly down-regulated, in *Rbm10 KO* organoids **(Fig. 37A).** The function of these genes and their qualitative expression in human urothelium is summarized in Table 11.

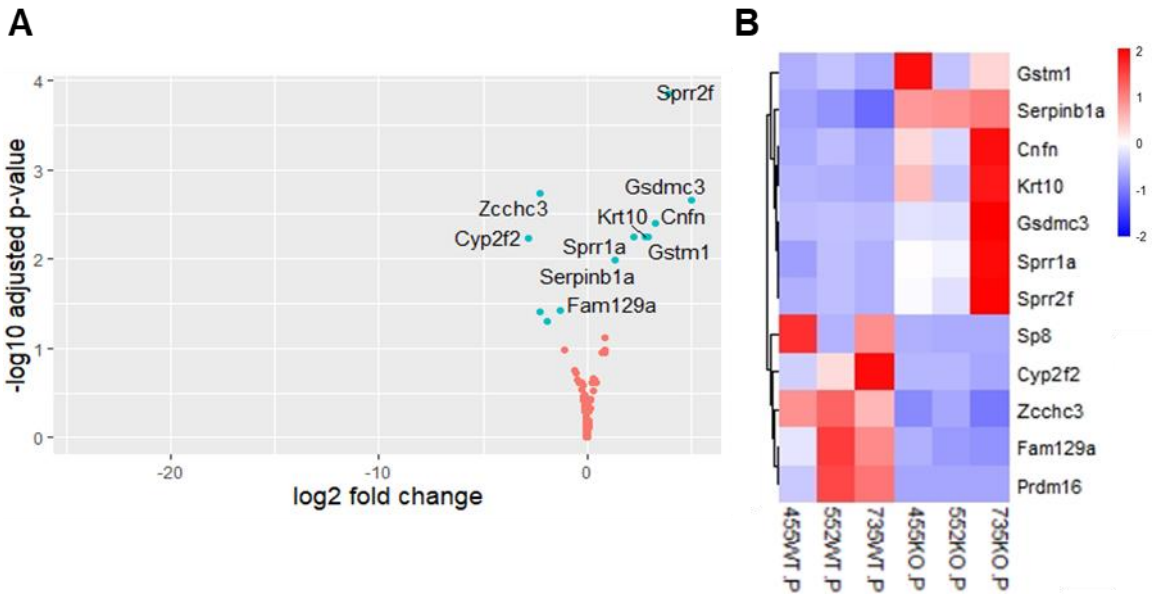

Figure 37: Differentially expressed genes in *Rbm10 KO* vs. WT organoids in proliferative conditions (DESeq2 analysis). A. Volcano plot of DEGs (blue) in *Rbm10 KO* organoids (adjusted p-value<0.05) (n=3) **B.** Heatmap representing normalized expression levels of DEG.

Gene	Function	Human urothelium
Gstm1	Glutathione S-transferase	luminal (high)
Serpinb1a	Proteinase inhibitor that protects against damage caused by inflammation	low
Cnfn	Is part of the insoluble cornified cell envelope of stratified squamous epithelia	very low
Krt10	Intermediate filament that composes cytoskeleton	low
Gsdmc3	N-terminal moiety promotes pyroptosis	very low
Sprr1a	Cross-linked envelope protein of keratinocytes	very low
Sprr2f	Cross-linked envelope protein of keratinocytes	not detected
Sp8	SP transcription factor family, essential for limb development	not detected
Cyp2f2	Xenobiotic metabolism	very low
Zcchc3	Involved in nucleic acid recognition and innate immune response	very low
Fam129a	Phosphorylation of proteins involved in translation regulation	medium
Prdm16	Zinc-finger transcription factor that displays histone methyltransferase activity	not detected

Table 11: Differentially expressed genes in *Rbm10 KO* vs. *WT* organoids in proliferative conditions. Functional information and qualitative RNA expression levels in human urothelium extracted from the Human Protein Atlas (https://www.proteinatlas.org/). Up-regulated genes shown in red and down-regulated genes shown in blue.

In the third comparison, we compared D KO vs. D WT organoids: 2 and 12 genes were significantly up- and down-regulated, respectively, in *Rbm10 KO* D organoids **(Fig. 38A).** The function of these genes and their qualitative RNA expression in the human urothelium is summarized in Table 12.

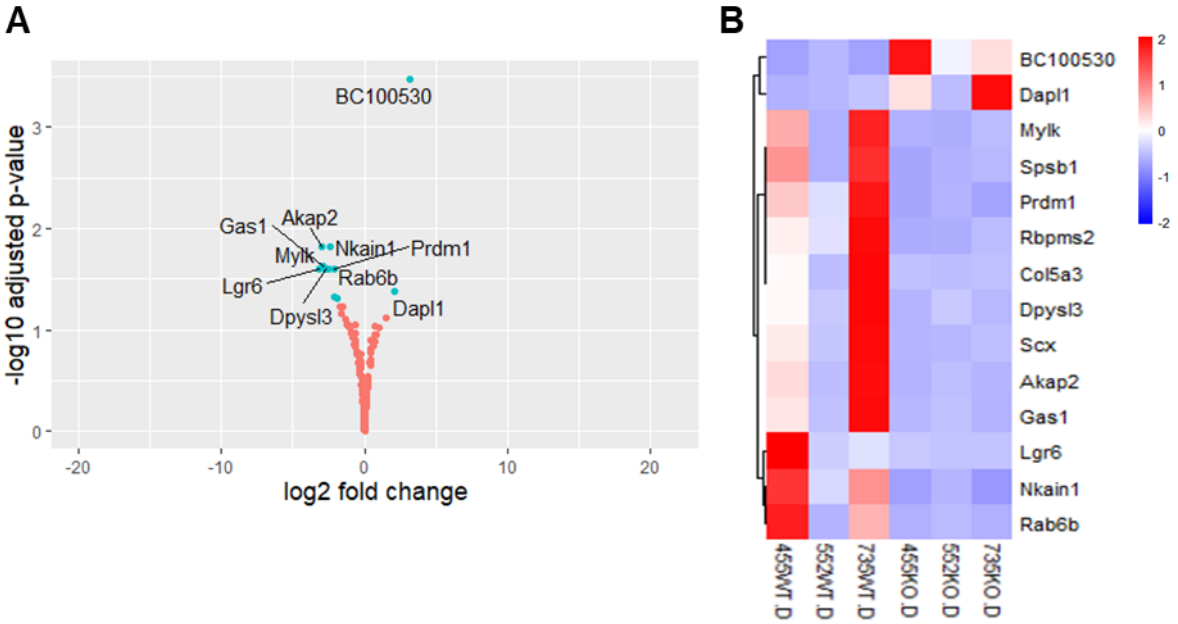

Figure 38: Differentially expressed genes in *Rbm10 KO* vs. WT organoids in differentiation conditions (DESeq2 analysis). A. Volcano plot of DEGs (blue) in *Rbm10 KO* organoids (adjusted p-value<0.05) (n=3) **B.** Heatmap representing normalized expression levels of DEG.

Gene	Function	Human urothelium
BC100530 (CstaA)	Protease inhibitor that is also related to keratinization	very low
Dapl1	Related to epithelial differentiation and apoptosis	very low
Spsb1	Involved in mediation of ubiquitination and proteasomal degradation	low
Prdm1	Repressor of beta-interferon gene expression	low
Rbpms2	RNA binding protein involved in the regulation of smooth muscle cell differentiation	very high
Col5a3	Collagen type part of the structure of the ECM	very low
Dpysl3	Involved in cell signaling for cytoskeleton remodeling	low
Scx	Plays an essential role in mesoderm formation	very low
Akap2	Regulatory subunit of protein kinase A involved in cAMP signaling	medium
Gas1	Involved in the regulation of cell growth	low
Lgr6	Receptor of R-spondins that potentiate the canonical Wnt signaling pathway	very low
Mylk	Kinase that phosphorylates myosin regulatory light chains	very high
Nkain1	Sodium/potassium-transporting ATPase interacting protein	very low
Rab6b	Member of the RAS oncogene family involved in protein metabolism	very low

Table 12: Differentially expressed genes in *Rbm10 KO* vs. *WT* organoids in differentiation conditions. Functional information and qualitative RNA expression levels in human urothelium extracted from the Human Protein Atlas (https://www.proteinatlas.org/). Up-regulated genes shown in red and down-regulated genes shown in blue.

To overcome the limitations resulting from the low number of DEGs in the comparisons described above, we performed GSEA using the pre-ranked gene list with the BIOCARTA, KEGG, REACTOME, and GO collections as well as selected gene signatures related to urothelial cancer. In the P KO vs. P WT comparison, our analysis showed significant up-regulation of urothelial luminal signatures (FDR <0.05) including genes such as *Upk1a, Upk2, Gata3, Foxa1, and Pparγ,* along with cornification and keratinization signatures, including genes as *Krt6b,* and *Egfr,* suggesting the enrichment of a luminal-like profile with stratified epithelium features in *Rbm10 KO* P organoids when compared with WT organoids **(Fig. 39)**. In agreement with these observations, KO P organoids displayed more cystic structures when compared to WT and at the same time, at a protein level, they exhibited higher EGFR levels **(Fig. 30D)**, which has been related to basal-squamous/squamous cell carcinomas subtypes (Sjodahl et al., 2012; Rebouissou et al., 2014). For this reason, we specifically assessed BIOCARTA, KEGG, and REACTOME gene signatures related to EGFR pathway activation in *Rbm10 KO* P organoids, where these were significantly enriched (FDR <0.25) **(Fig. 41)**. In parallel, in the P KO vs. P WT comparison, we observed the down-regulation in pathways related to cell cycle, DNA replication, RNA transcription, and translation with the significant down-regulation of several proteasome subunits and Origin Recognition Complex Subunit genes along with *Cdkn1a* and *E2F1* expression **(Fig. 39)**, which is in agreement with our previous observations in the proliferation assays **(Fig. 26).**

In our D WT vs. D KO comparison, we observed the significant enrichment of urothelial luminal signatures in *Rbm10 KO* organoids, including the up-regulation of luminal markers such as *Upk1b, Foxa1, Upk2, Pparγ,* and *Gata3.* However, the *Pparγ* signature was significantly down-regulated and reduced expression of *Col1a1, Tcf4, Tpm2, Cebpb,* and *Acta2* transcripts contributed to this pathway **(Fig. 40)**. Some of these genes code for proteins involved in differentiation *(Tcf4* and *Cebpb)* and others are related to the extracellular matrix (ECM) (*Col1a1*), intermediate filaments (*Vim*), or actin microfilaments *(Tpm2* and *Acta2*). We also observed a positive enrichment of signatures related to RNA translation and transcription, where genes related to DNA and RNA biology were significantly up-regulated **(Fig.40)**. By contrast, *Rbm10 KO* differentiated organoids show a negative enrichment in signatures related to the ECM structure and organization, as well as integrin interactions, where several collagen family member genes and integrins were significantly down-regulated **(Fig.40)**.

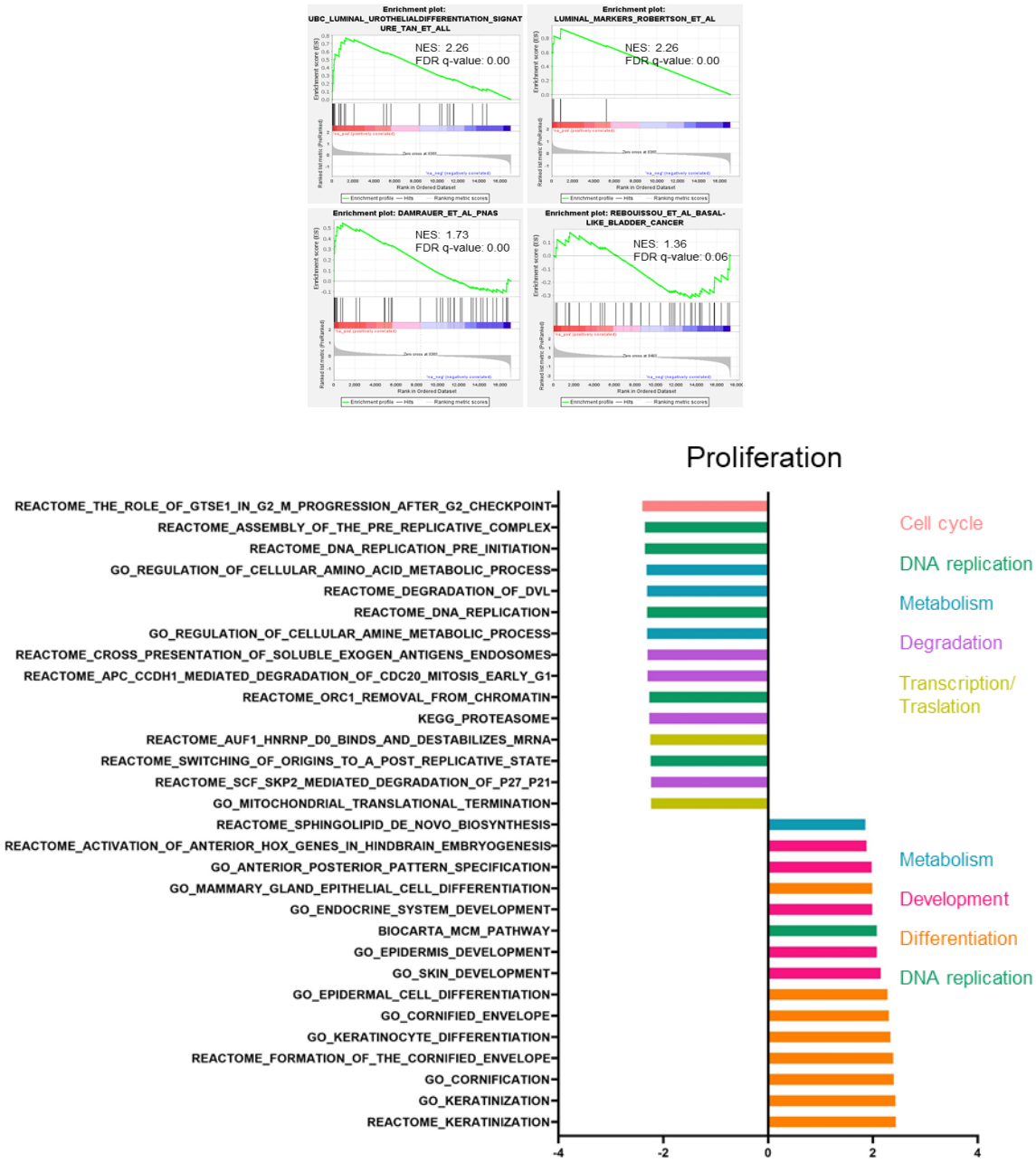

Figure 39: Enriched pathways identified by transcriptome analysis in *Rbm10 KO* vs. WT organoids in proliferation. Enrichment plots showing the up-regulation and the down-regulation of different pathways (top) and forest plot showing top 30 significantly enriched signatures (bottom) in *Rbm10 KO* organoids in proliferative conditions. FDR<0.05.

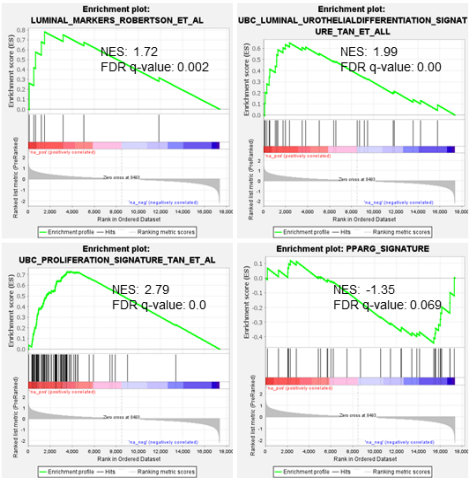

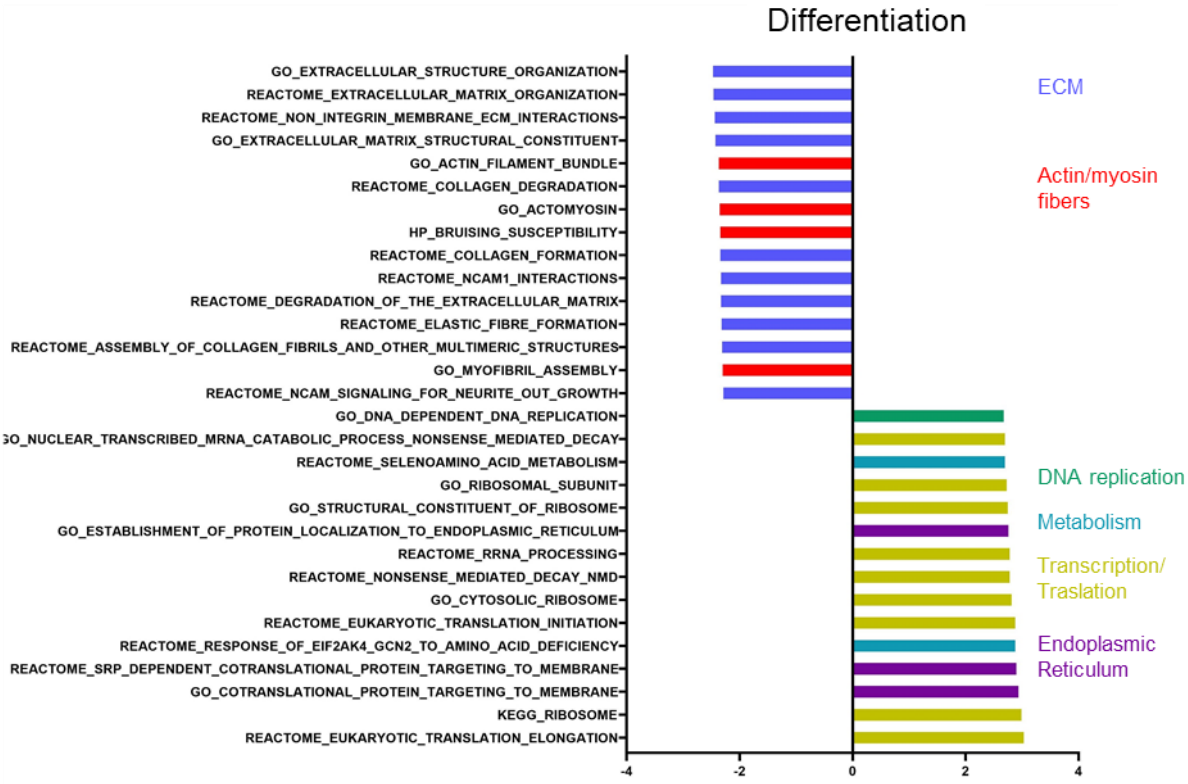

Figure 40: Enriched pathways identified by transcriptome analysis in *Rbm10 KO* vs. WT organoids in differentiation. Enrichment plots showing the up-regulation and the down-regulation of different pathways forest plot showing top 30 significantly enriched signatures (bottom) in *Rbm10 KO* organoids in differentiation conditions. FDR<0.05.

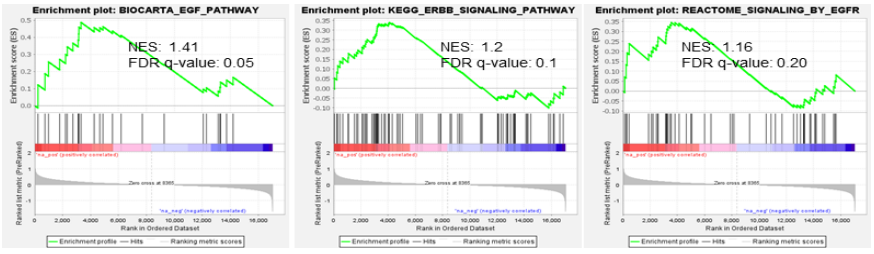

Figure 41: Enriched EGFR signaling pathways observed by transcriptome analysis in *Rbm10 KO* organoids. Enrichment plots related to EGF signaling pathway enrichment in *Rbm10 KO* organoids in proliferation conditions. FDR<0.25.

To acquire a deeper understanding of the changes described above in *Rbm10 KO* organoids, we investigated the expression of the DEGs with higher resolution taking advantage of the single cell RNA-Seq data from normal urothelial organoids reported by our group (Santos et al. 2019). In that study, dimensionality reduction and unsupervised clustering revealed 4 cell clusters in proliferative conditions (basal, basal proliferative, intermediate-low, and intermediate-high) and 3 cell clusters in differentiated conditions (basal, intermediate, and luminal) **(Fig. 42A)**. We observed that the DEG from our second comparison, *Rbm10 KO* Vs *WT* in P, were expressed across all the identified intermediate high, low, basal, and basal proliferative cell clusters. All the transcripts that were significantly up-regulated in *Rbm10 KO* P organoids, and detected in this experiment, were selectively enriched in the intermediate and luminal clusters, further supporting the enhanced urothelial differentiation in P organoids resulting from *Rbm10* inactivation **(Fig. 42A, B)**.

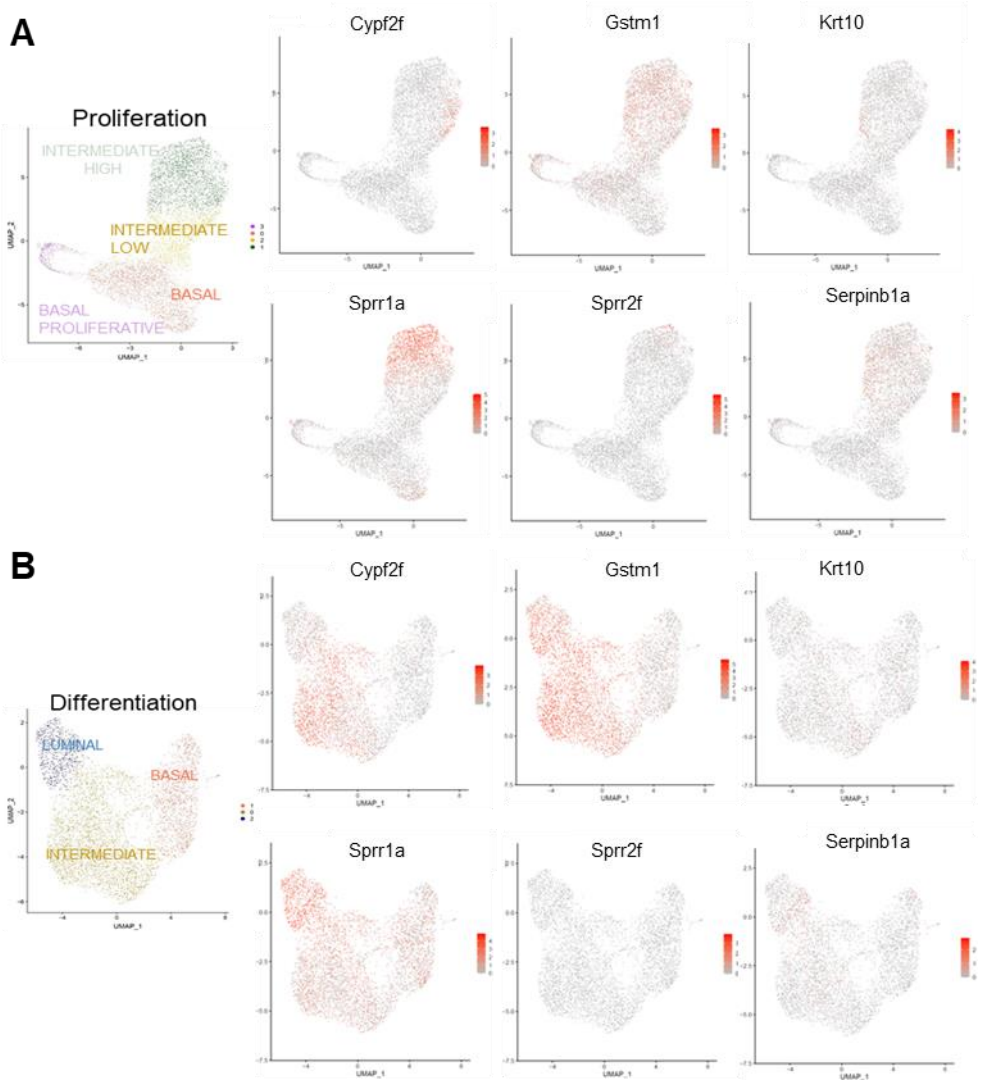

Figure 42: DEG of *Rbm10 KO* vs WT P organoids in scRNA-Seq data from normal urothelial organoids in proliferation (A) and differentiation (B) conditions.

In contrast to the above findings, the genes differentially expressed in *Rbm10 KO* vs *WT* organoids in differentiation conditions did not reveal consistent patterns of expression in the scRNA-Seq dataset **(Fig. 43)**.

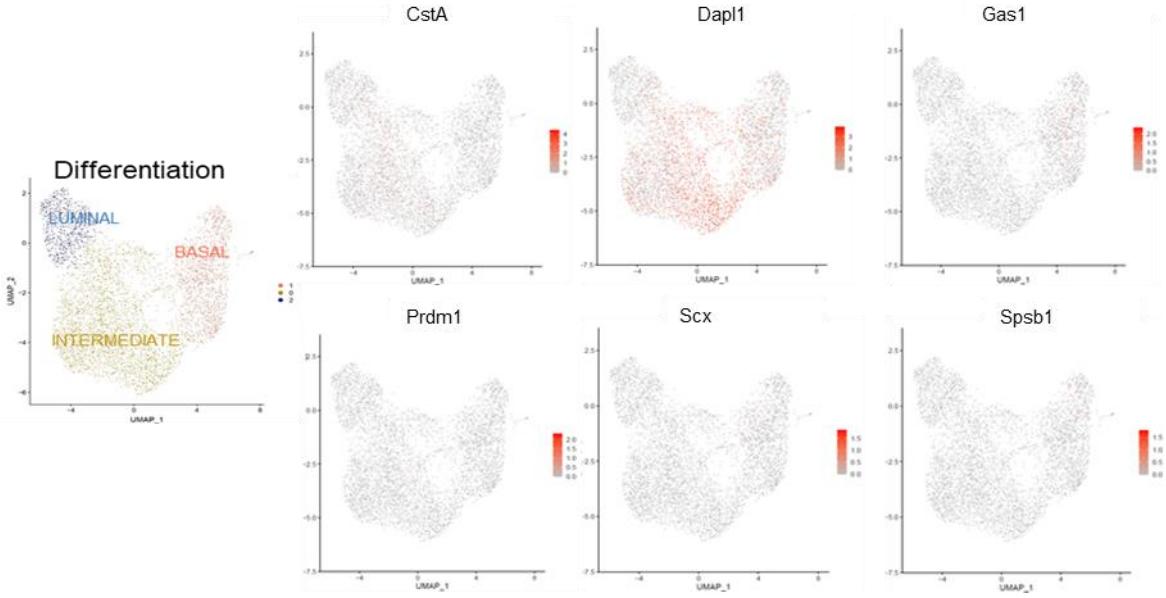

Figure 43: DEG of *Rbm10 KO* vs WT D organoids in scRNA-Seq data in normal urothelial organoids in differentiation.

To further assess the meaning of the DEG, we took advantage of the scRNA-Seq data of mouse normal urothelium published by Yu et al., 2019. Similar to the previous analysis, we compared the DEG of *Rbm10 KO* organoids in P and D to identify the clusters where these genes were expressed. Among the DEG in P, *Gstm1* and *Sprr1a* were highly expressed in all urothelial cell clusters **(Fig 44A)**. Similarly, *Krt10* was expressed in all clusters but at lower levels. *Cyp2f2* and *Gsdmc3* (not shown) were expressed in basal/intermediate clusters, as opposed to *Sprr2f,* found in luminal clusters. The other genes were expressed at low levels, precluding further analysis (data not shown). Among the DEG in D, most genes were expressed at low levels in urothelial clusters, except for *Dapl1*, found in basal/intermediate cells **(Fig. 44B)**. *Dpysl3, Akap2, Gas1,* and *Milk* were found mainly in mesenchymal cell clusters and at low levels in a subcluster of basal urothelial cells.

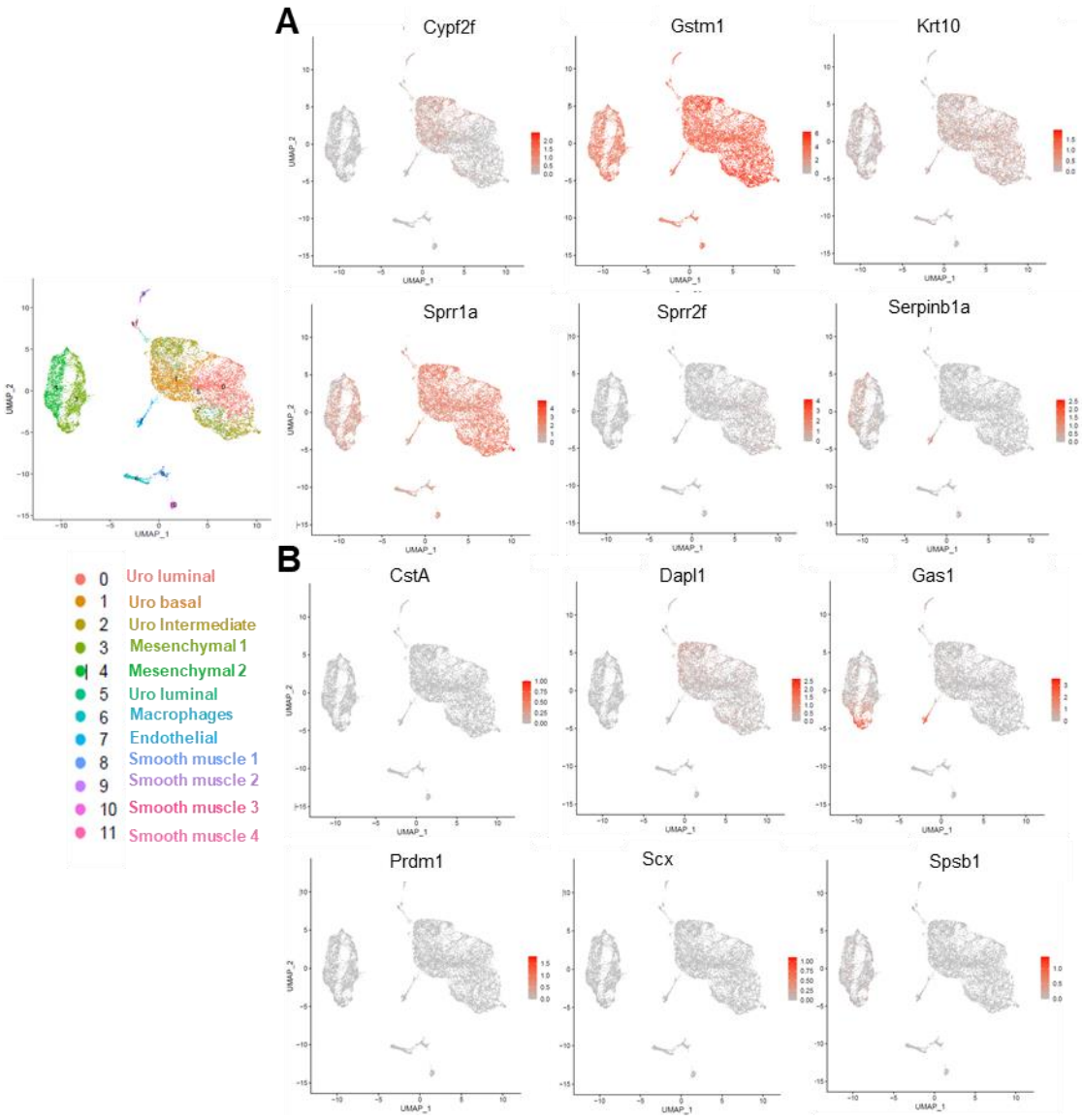

Figure 44: DEG of *Rbm10 KO* vs WT P and D organoids in scRNA-Seq data from mouse normal urothelium. A. DEG in Rbm10 KO organoids in proliferation **B.** DEG in Rbm10 KO organoids in differentiation**.**

In summary, *Rbm10 KO* organoids exhibit an enhanced luminal-like stratified epithelium phenotype, when compared with WT organoids, both under P and D conditions. The up-regulation of keratinization and cornification genes under proliferative conditions is suggestive of a differentiation process that is specific to stratified squamous epithelium, that has been previously described in normal urothelial organoids in proliferative conditions, which is also accompanied by a strong activation of the urothelial differentiation program in these organoids. These findings need to be validated at the gene and protein level.

CHAPTER III

RBM10 in bladder cancer

6.4. Role of *RBM10* in bladder cancer

6.4.1. *RBM10* is recurrently lost in bladder cancer, independently of stage or grade

A whole-exome sequencing experiment performed by our group identified recurrent mutations in several oncogenes and tumor suppressor genes in BC samples (Balbás-Martinez et al., 2013). In that study, *RBM10* mutations were found in tumors from both the papillary and non-papillary pathways. *RBM10* mutations have also been reported subsequently in 16/105 (16%) NMIBC tumors (cBioportal, MSK Eur Urol, 2017; Pietzak et al., 2017) and in 20/402 (5%) of MIBC tumors (cBioportal, TCGA PanCancer Atlas, Hoadley et al., 2018). Moreover, *RBM10* mutations have been reported in 3 to 6% of the cases in several other BC studies **(Fig. 45)**.

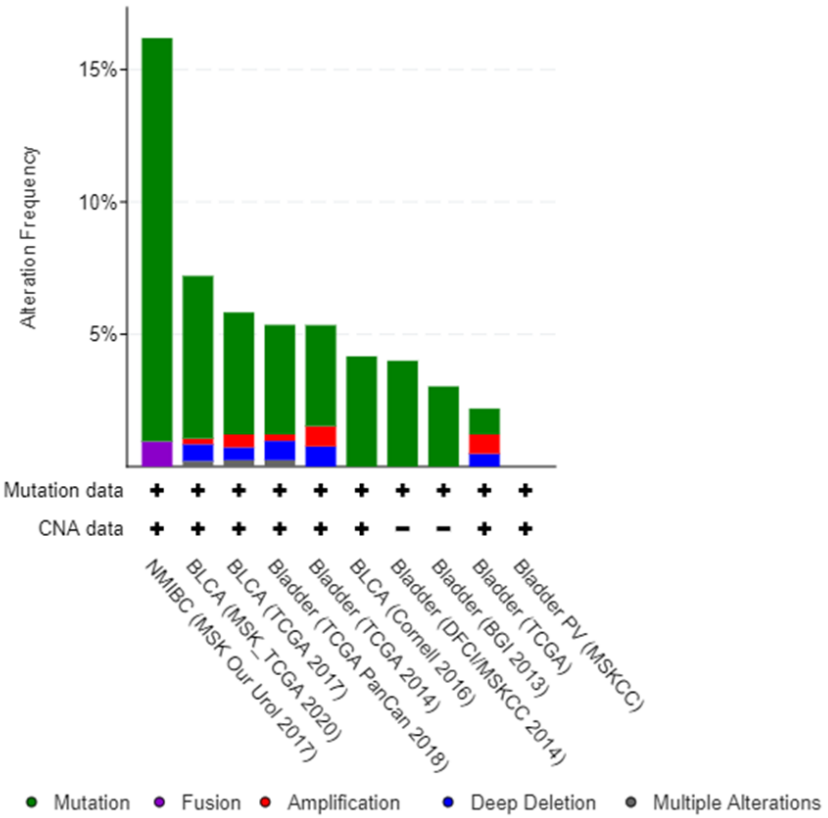

Figure 45: *RBM10* mutations in patients from different BC studies. Alteration frequency is represented by the percentage of reported RBM10 mutations in BC studies in cBioportal (https://www.cbioportal.org/).

At the outset of my project, there was very little information on the prevalence of *RBM10* mutations in BC. Therefore, we used IHC to assess the prevalence of loss of protein expression in 266 tumors covering the full spectrum of the disease, in collaboration with G. Sjödahl (U. Lund, Lund, Sweden) **(Fig. 46A)**. We identified 17 cases with undetectable RBM10, for a global frequency of 6.4%. This is likely an underestimate of

RBM10 alterations since missense mutations may not lead to loss of immunoreactivity. There were no significant differences in the prevalence of tumors showing RBM10 loss stratified by stage or grade **(Fig. 46B)**. Tumors were classified as UroA, UroB, GU, and infiltrated, according to the work of the Lund group (Sjödahl et al., 2012). Interestingly, the RBM10-null tumors were more frequent in the UroB group and there were no RBM10-negative tumors in the SCCL subgroup (0/25 SCCL tumors). These results suggest that *RBM10* is inactivated in a modest fraction of bladder tumors and that it is an early event during bladder cancer development.

These results are the foundation for the study of how *RBM10* inactivation contributes to BC development.

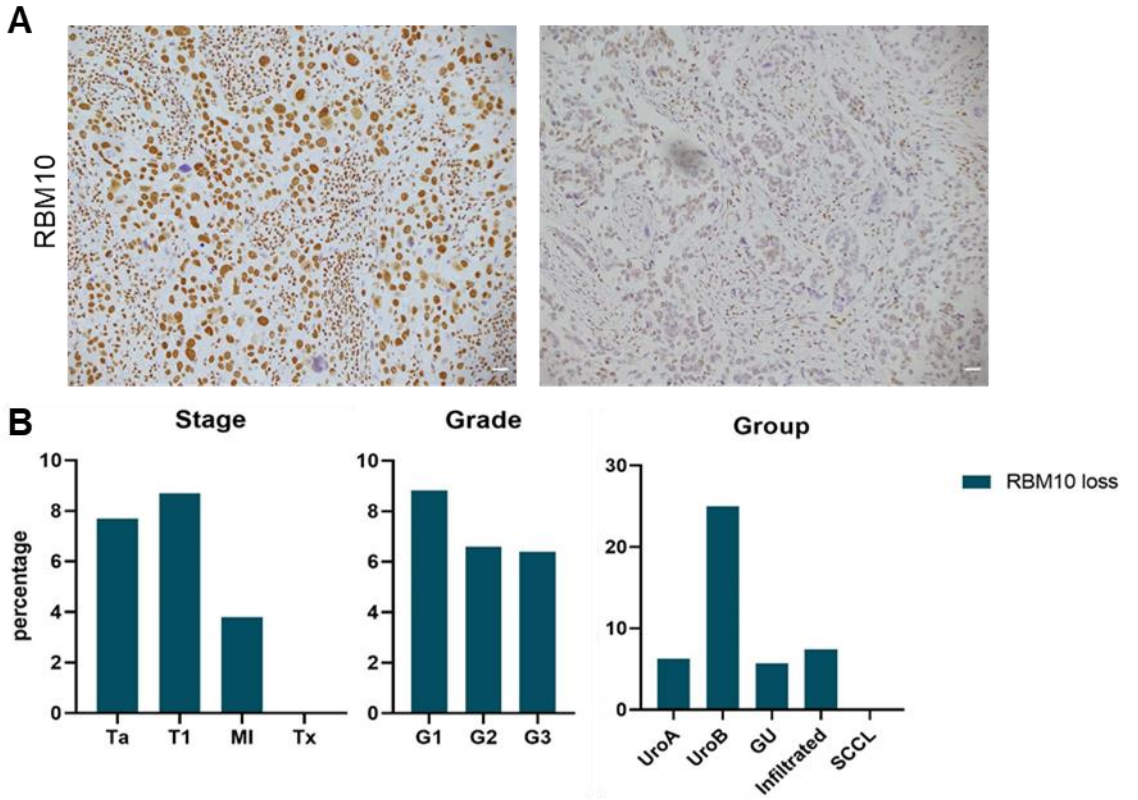

Group	RBM10 loss (%)
UroA	6,3
UroB	25
GU	5,7
Infiltrated	7,4
SCCL	0

Stage	RBM10 loss (%)
Ta	7,7
T1	8,7
MI	3,8
Tx	0

Grade	RBM10 loss (%)
G1	8,8
G2	6,6
G3	6,4

Figure 46: RBM10 loss of expression in bladder cancer TMAs. A. Representative images of RBM10 immunostaining in full sections from a bladder tumor harboring an *RBM10* truncating mutation (scale bar, 50µm) **B.** Frequency of loss of RBM10 expression in relationship with stage, grade, and tumor subgroup.

6.4.2. Co-occurrence of mutations in *RBM10* and other cancer genes in bladder cancer

To identify genes that might cooperate with *RBM10* inactivating mutations in BC, we performed a co-occurrence and mutual exclusivity analysis using the information available from the TCGA database (BLCA TCGA study, 2007). We focused on cases harboring *RBM10* inactivating mutations and filtered according to clinical relevance and pathogenicity scores according to ClinVar. **Fig. 47** shows the list of the top 10 genes co-mutated with *RBM10*. Some of these genes are frequently altered in BC (*KMT2C*, *TP53, ARID1A, STAG2,* and *PIK3CA),* either in NMIBC or in MIBC.

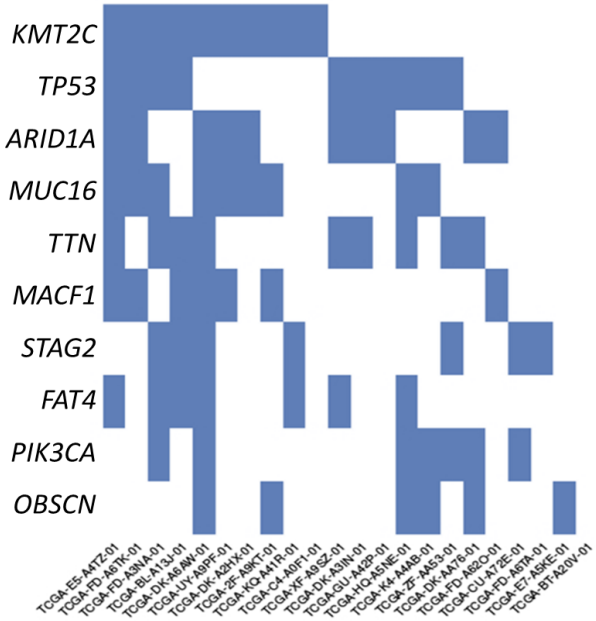

Figure 47: Data analysis to identify *RBM10* co-mutated genes. Top 10 co-mutated genes obtained from the 22 patients with *RBM10* inactivating mutations (TCGA Database) according to clinical relevance and pathogenicity scores and mouse strain generation.

6.4.3. Establishment of GEMMs to assess the functional cooperation of *Rbm10* inactivation with other BC genes

Based on the findings of genes co-mutated with *RBM10* in BC, we generated 3 additional conditional mouse strains to assess the functional cooperation with *Trp53*, *Kras*, and *Pik3ca*.

To assess cooperation between *Rbm10* and *Trp53,* we inactivated both genes in the urothelial luminal cells by using an allele driving CreERT2 expression from the *Upk3a* promoter. In addition, we generated two pan-cancer models with ubiquitous inducible activation of *Kras** or *Pi3kca** mutated alleles, along with *Rbm10* inactivation. In all cases, 6 weeks-old mice were fed a TMX-containing diet for 8 weeks. **Fig. 48** shows the Kaplan-Meier survival curves corresponding to the mice included in the three mouse experiments.

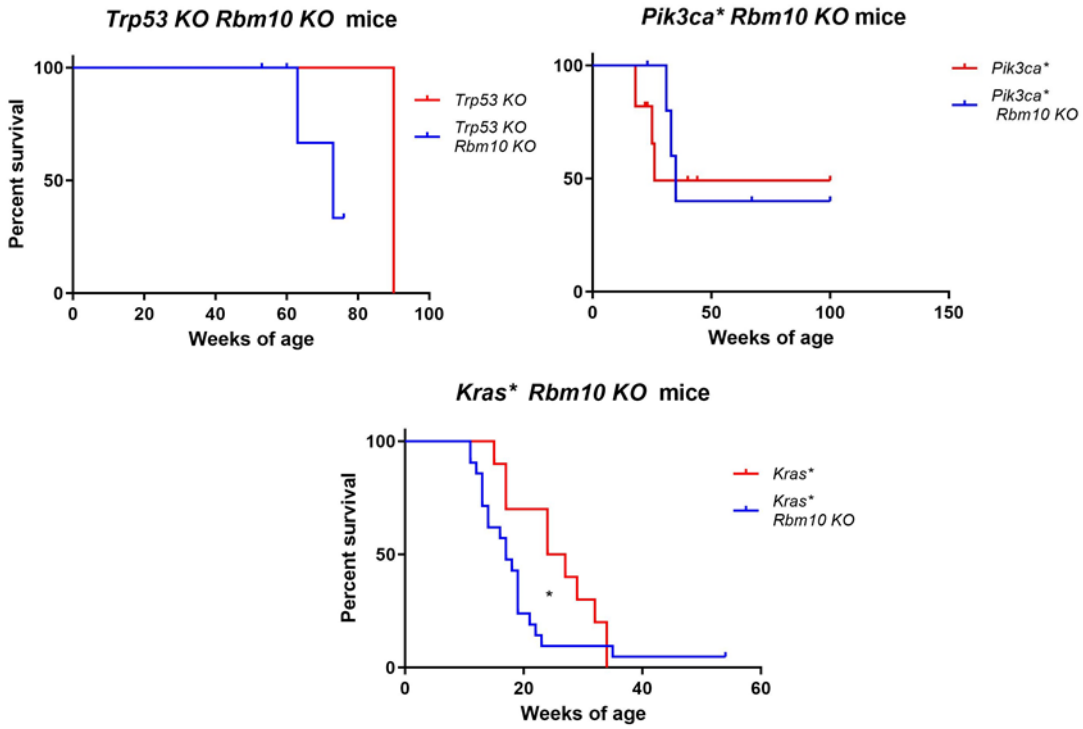

Figure 48: Survival curves of mice with *Rbm10 KO* in cooperation with *Tp53, Pi3kca* and *Kras*. Survival of TMX-induced *Trp53 KO Rbm10 KO* (n=7) and *Trp53* KO mice (n=3), *Pi3kca* Rbm10 KO* (n=5) and *Pi3kca** mice (n= 7), and *Kras* Rbm10 KO* (n=20) and *Kras** mice (n=10).

The preliminary analyses of cooperation of *Rbm10* and *Trp53* inactivation, based on a very small number of mice, do not provide evidence that inactivation of the two genes in the urothelium is sufficient for bladder tumor initiation. We observed similar results with *Rbm10* inactivation and *Pik3ca* activating mutations, although the number of mice is too low to reach a conclusion.

Mice in which ubiquitous inactivation of *Rbm10* was induced together with ubiquitous activation of mutant *Kras** showed a dramatic decrease in survival compared to mice with *Kras** activation alone (p-value = 0.022) **(Fig. 49A)**. Histopathological evaluation revealed that 2/3 *Kras** and 12/12 *Kras* Rbm10 KO* mice exhibited lung lesions. All mice showed stomach/oesophageal papillomas regardless of *Rbm10* status, which was likely the main cause of death. Regarding the lung, we observed a non-significant increase in the number (p-value = 0.1748) and size (p-value =0.1633) of tumors, as determined by the diameter, in *Kras* Rbm10 KO* mice compared to *Kras** mice **(Fig. 49B)**. Interestingly, 2 out of 12 *Kras* Rbm10* mice exhibited grade 2 adenomas.

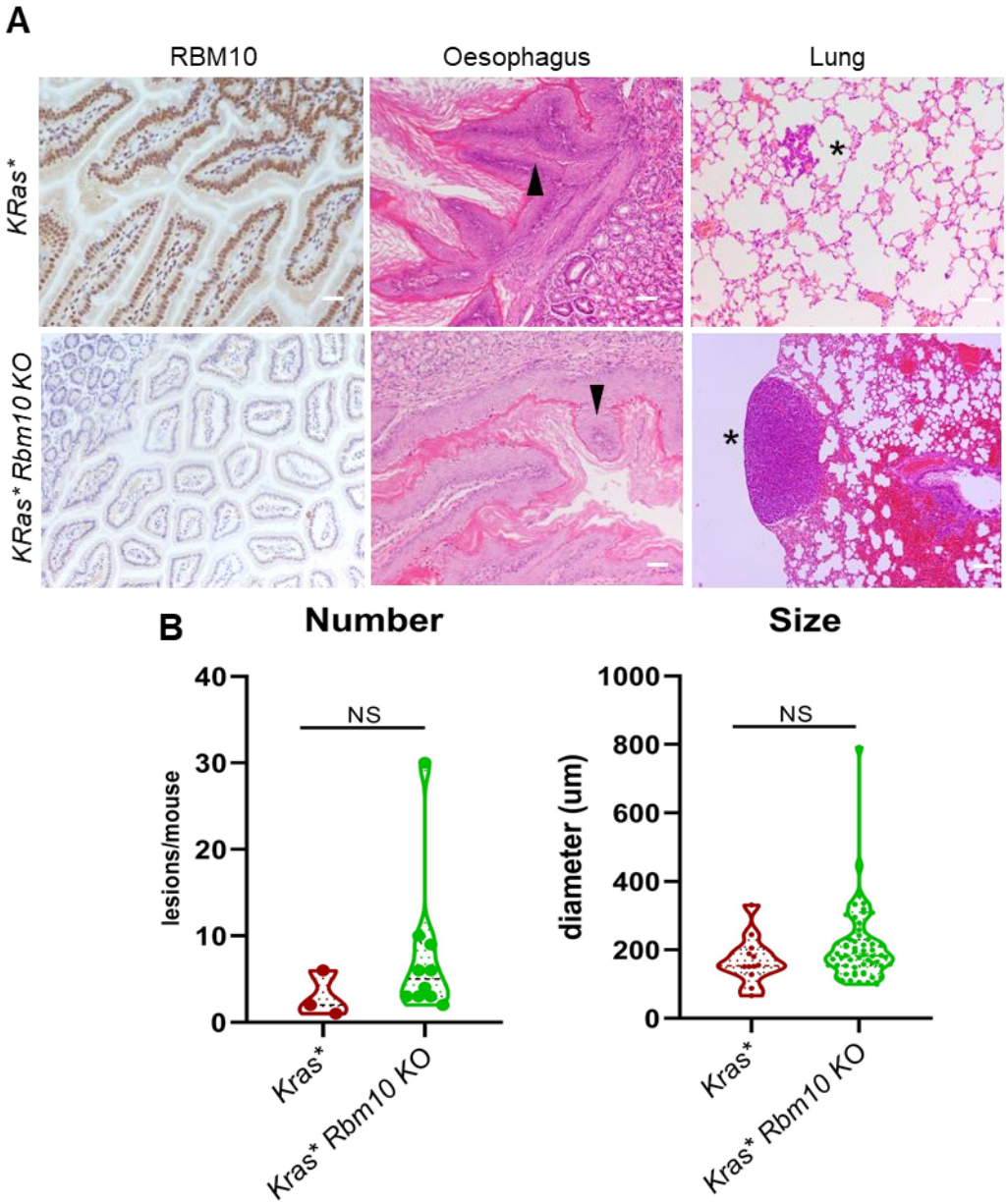

Figure 49: Histological assessment of the lung of *Kras* Rbm10 KO* mice. A. Representative images of RBM10 immunostaining in formalin-fixed paraffin-embedded tissues and HE staining of the oesophageal and lung sections from *Kras** (n =3) and *Kras* Rbm10 KO* mice (n=12) (arrows, papillomas; asterisks, lung lesions) (scale bar, 50µm) **B.** Number and size of lung tumors in *Kras** and *Kras* Rbm10 KO* mice (Mann-Whitey Test).

To bypass the mortality caused by the stomach/oesophageal papillomas and assess more precisely the cooperation of *Rbm10* inactivation with mutant *Kras* in the lung, I have induced recombination by administering adeno-cre intranasally. These mice are being followed using CT scan. In addition, I have generated urothelial organoids from these strains to assess how *Rbm10* inactivation and *Kras* activation cooperation at a functional level.

6.4.4. *RBM10 KO* in bladder cancer cells

To explore the role of *RBM10* inactivation in BC, we have used two different approaches: we have generated *RBM10 KO* clones derived from RT4 cells with the CRISPR/Cas9 system and we have obtained patient-derived *RBM10*-mutant BC organoids. In our first approach, we targeted the exon 3 of the human *RBM10* gene to generate a protein-truncating variant, as in our mouse models. We identified the stop codon introduced in the *RBM10* sequence in the three KO clones by Sanger sequencing and confirmed RBM10 protein loss by IHC and western blotting **(Fig. 50A-C)**.

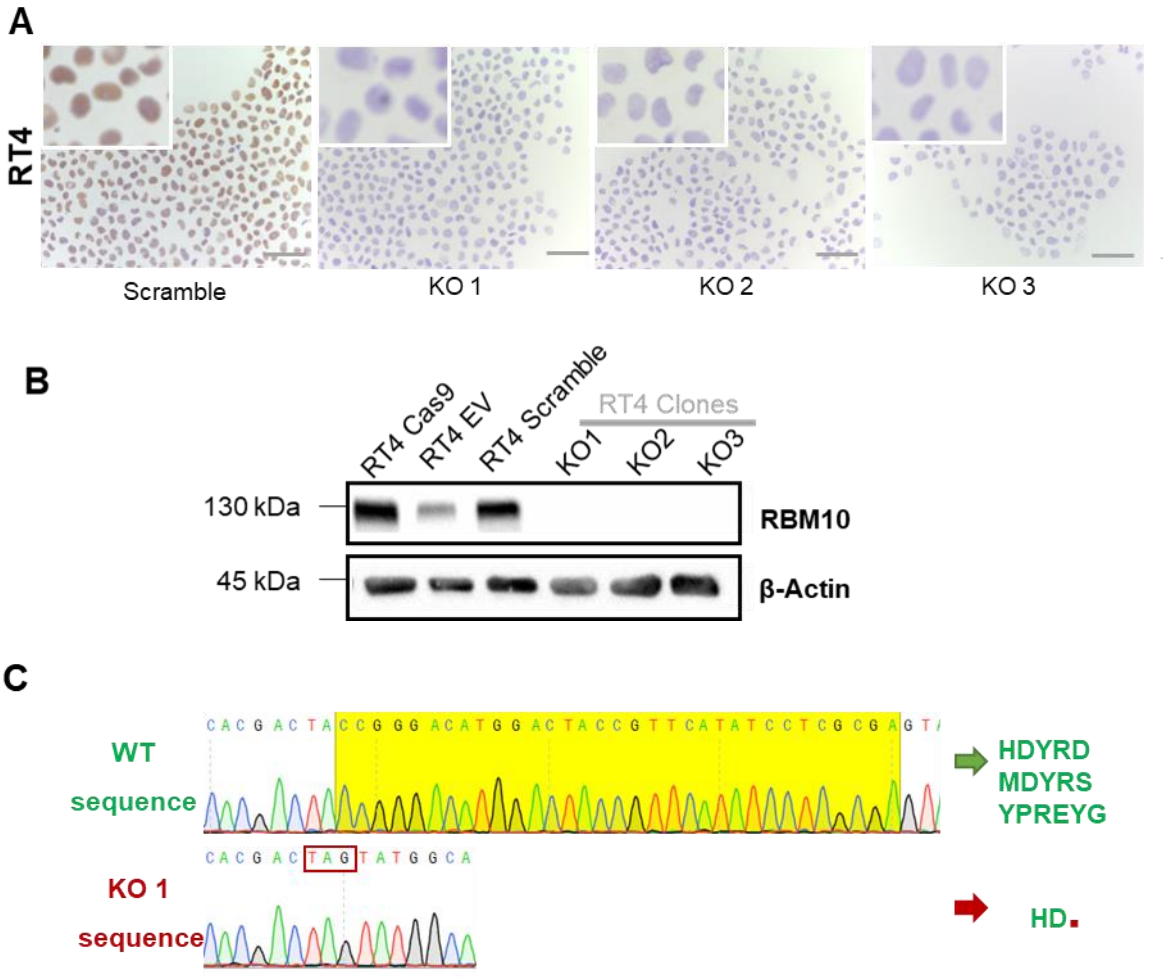

Figure 50: RT4 *RBM10 KO* clones establishment with CRISPR/Cas9 system. A. Representative images of RBM10 immunostaining in paraformaldehyde-fixed RT4 cell suspensions of RBM10 control (Scrambled), and *RBM10 KO* clones (scale bar, 100µm) **B.** Western blot analysis of RBM10 and β-Actin on *Rbm10* controls and KO clones protein extracts **C.** Sanger sequencing showing RBM10 WT sequence compared to RBM10 KO clone 1 where a premature stop codon was identified.

To investigate the effect of *RBM10* inactivation on cell growth, we performed clonogenic assays and determined the proliferation curves of the KO clones. We observed a decreased clonogenic potential in the RT4 KO clones when compared to the empty vector (EV) control **(Fig. 51A)**, however, we did not observe a significant difference in

the proliferation curves of these when compared to control **(Fig. 51B)**. Further analyses of these clones are being carried out in collaboration with T. Hoffmann and Dr. J. Valcárcel.

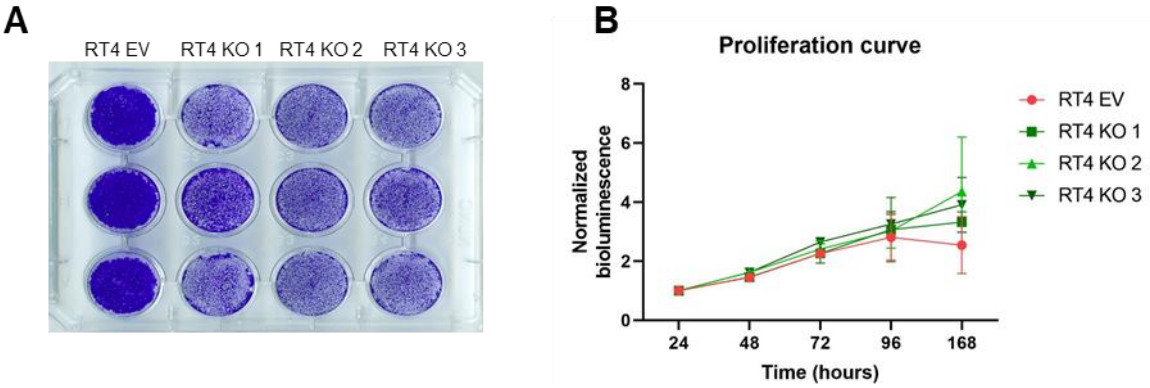

Figure 51: *RBM10 KO* clones clonogenic and proliferative potential. A. Representative image of the clonogenic assays performed with RT4 *RBM10* control and *RBM10 KO* clones **B.** Graph showing cell proliferation every 24 hours as determined by the emitted normalized bioluminescence in RT4 control and KO clones.

In our second approach, I have also generated a doxycycline-inducible system to reconstitute *RBM10* expression **(Fig. 52A)** and assess the cellular and molecular effects of exogenous expression of wild type RBM10 in mutant organoids. I have confirmed the suitability of the system by performing western blotting **(Fig. 52B)**. Finally, we are currently assessing the effects on proliferation, invasion, differentiation, growth factor dependency, and transcriptomic changes to identify and validate other altered splicing events that could help elucidate the role of RBM10 in tumorigenesis. These experiments are also being conducted in close collaboration with T. Hoffman and Dr. J. Valcárcel.

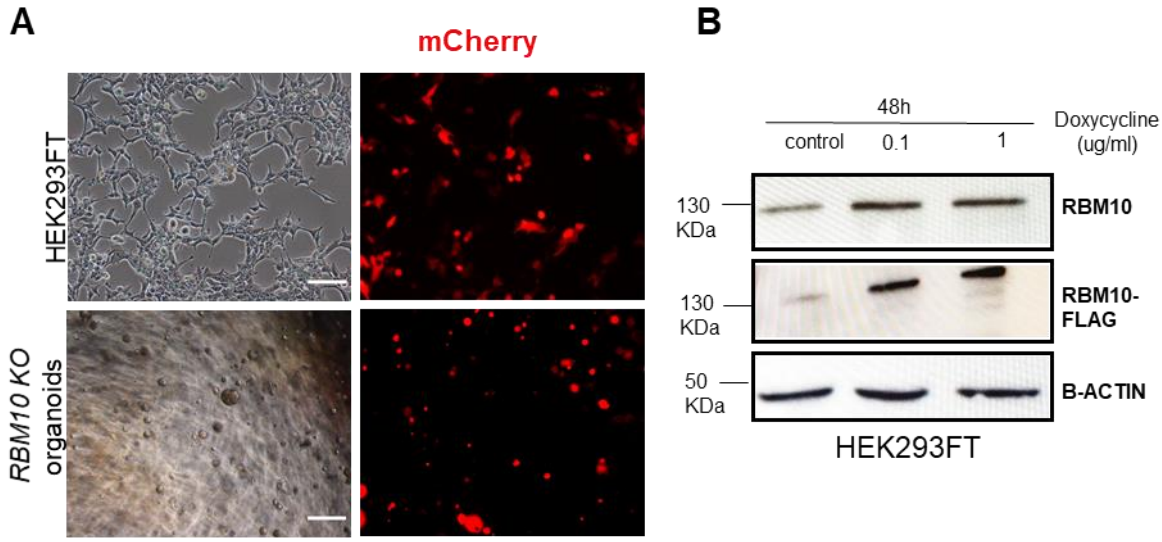

Figure 52: Establishment of an RBM10 inducible expression system. A. Representative imagines of HEK293FT cells (scale bar, 100µm) and patient-derived RBM10 mutant organoids (scale bar, 200µm) infected with an RBM10 inducible lentiviral plasmid and mCherry expression as an infection reporter **B.** Western blot analysis of endogenous RBM10, exogenous FLAG-tagged RBM10 and β-Actin on *Rbm10* controls and KO cell protein extracts after 48h of doxycycline induction *in vitro*.

7. DISCUSSION

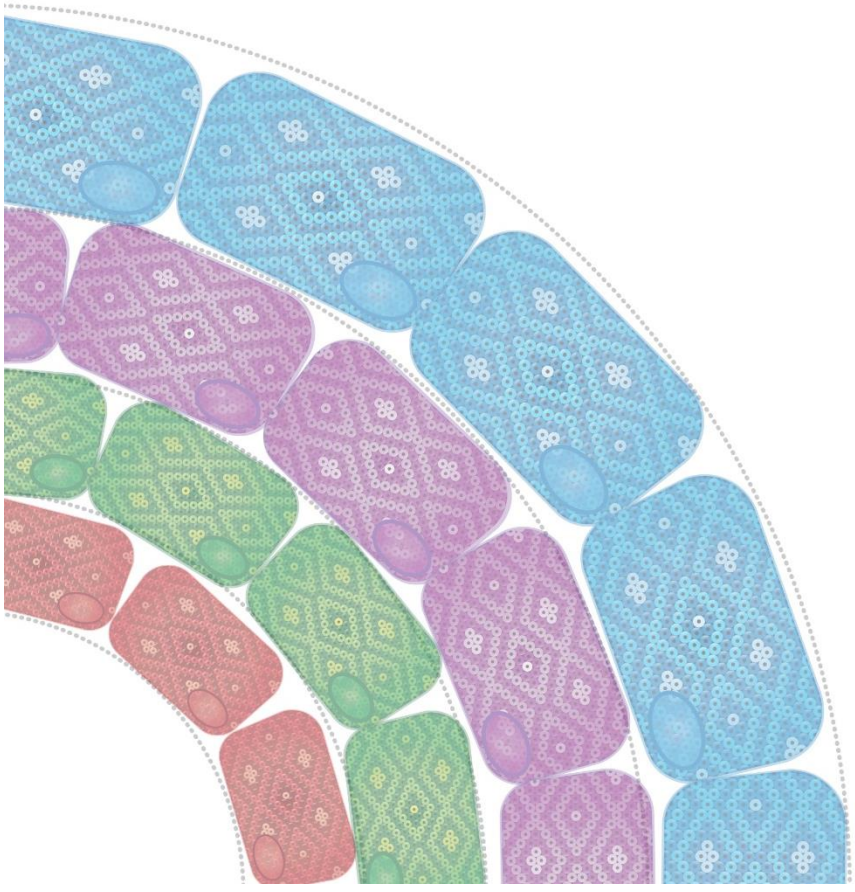

7.1. Germline *Rbm10* inactivation in mice leads to a male-lethal phenotype with partial penetrance

7.1.1. A new genetic mouse model to study the function of the splicing factor RBM10

As mentioned in the Introduction, *Rbm10* is one of many regulators of alternative splicing. While the general mechanisms of splicing are conserved across species, only 20% of the alternative splicing events of specific transcripts are conserved between humans and mice (Nurtdinov et al., 2003; Thanaraj et al., 2003). The cause of this low conservation has not been fully elucidated and likely results from the fact that many variables affect the regulation of splicing, including splicing factor structure and function, the sequence of the target exons, and the sequence of the introns, among others. Conservation of splicing events between mice and humans related to disease has been described in psoriasis, where disruption of several genes coding for splicing factor (e.g. *U2AF1, SRRM4,* and *DDX5*) has been linked to the disease (Li and Yu, 2018).

Genetic mouse models are powerful tools to study mechanisms of disease, provided functional conservation across species. Several strains have been generated with transgenic overexpression of genes coding for splicing factors, or with targeted deletions or knocked-in mutations. Most of the constitutive KO models generated present early embryonic lethality or severe defects in organogenesis, highlighting the essential functions of these proteins, known to be strictly non-redundant in certain cell types and developmental stages while in others they are dispensable (Moroy and Heyd, 2007). Knock-in models of other genes coding for splicing factors, such as *Prpf3/8/31,* have proven useful to recapitulate the main degenerative features found in retinitis pigmentosa patients (Graziotto, et al., 2011). Similarly, conditional mouse models with mutations in *Sf3b1, Srsf2*, and *U2af1* recapitulate - to a variable extent - the myelodysplastic syndromes associated with mutations in these genes in humans (Xu et al., 2019). Conditional knockout in the heart of *Sc35* and *Asf/Sf2*, two genes coding for SR proteins, has shown that - while not essential for cardiogenesis - they are crucial for heart function during adulthood (Xu et al., 2005; Ding et al., 2004).

TARP syndrome is a rare condition and the formal proof of the relevance of the pathogenic gene mutations/inactivation using genetic mouse models has not been acquired until now. A major question we posed at the beginning of my work was whether the differences in AS across species might hinder recapitulating TARP syndrome in our mouse model, based on the known lack of conservation of most splicing events between

mice and humans. The data presented in this study strongly suggest the conservation of *Rbm10* function in humans and mice. This might not be surprising considering that the murine RBM10 protein is 96% identical to the human RBM10 protein and the high conservation of intron-exon structure of the gene in both species (Johnston et al., 2010) **(Fig. 53)**. This finding strongly suggests that either the splicing events responsible for TARP syndrome are largely conserved or that the mechanism(s) through which *RBM10* mutations contribute to the developmental syndrome are not related to the function of the protein in splicing. *In situ* hybridization analysis of *Rbm10* at early stages of mouse embryo development (E9.5 and E10.5) shows high expression in branchial arches 1 and 2 and lower expression in the limbs (partially overlapping with the apical ectodermal ridge) and tail. These observations point to an important role of RBM10 in the development of structures derived from these regions and is consistent with the reported developmental defects resulting from loss of function *RBM10* mutations observed in TARP patients (Johnston et al., 2010).

Figure 53: Intron-exon structure of the *RBM10* gene in human and mouse genomes and derived splicing isoforms. Schematic representation of the *RBM10* locus and comparison of human and mouse reported protein-coding isoforms. Modified from Ensembl (http://www.ensembl.org/).

It is important to take into account that in our mouse model, Cre recombinase leads to the deletion of exon 3 of *Rbm10*, generating a premature stop codon. The resulting *Rbm10* transcripts are expected to undergo nonsense mediated decay (NMD), which in turn will lead to degradation of the mutant RNA and loss of RBM10 protein. We show that upon recombination, expression of RBM10 is widely lost in tissues of *Rbm10* KO mice. The fact that we have used an antibody against the N-terminus of the protein could be a limitation to our findings if an internal translation initiation site could give rise to a protein encompassing the C-terminus of the wild type species. Interestingly, to our

knowledge, there have been no reports on the loss of protein expression in tissues from patients with TARP syndrome.

In TARP syndrome, multiple non-sense and frameshift mutations predicted to be deleterious have been described (Johnston et al., 2010; Johnston et al., 2014; Wang et al., 2013; Powis et al., 2017; Hojland et al., 2018; Keappler et al., 2018), these alterations might be modeled in the *Rbm10 KO* mouse. Nevertheless, in described missense mutations, the functional impact on the annotated structure has not yet been described and might constitute a source of phenotypic variability no recapitulated in our KO mouse model.

The diversity of the mutations reported in patients could explain the substantial diversity in transcript variants, where the structural changes in the RBM10 protein can interfere with its normal functions. The functional impact of truncating mutations on RBM10 protein structure has been described in a few studies. In the study by Wang *et al*, the reported deleterious mutation of 1292 nt (ChrX: 46929367–46930658 bp, UCSC genomebrowser hg18), led to a loss of 239 amino acids, including the zinc finger domain, a portion of the G-patch domain, and a region with a nuclear localization signal, causing its mislocalization in the cytoplasm and leading unpaired splicing functions. A second study reported a deleterious mutation (c.1352_1353delAG. ChrX:47040717-47040718 bp, UCSC genome browser hg18) that resulted in the loss of several regions of the protein, including the OCRE, zinc finger, and G-patch domains (Powis et al., 2017). Of note, these domains are important for spliceosome assembly and recruitment of pre-mRNA (Bonnal et al., 2008). A third study revealed a frameshift mutation that led to a premature stop codon only for *RBM10* isoforms which include exon 4, leading to a loss-of-function in these variants. This exon is skipped in three out of five of the *RBM10* isoforms, hence the remaining transcripts that were unaffected may explain the survival of this patient into adulthood (Hojland et al., 2018). However, few studies have focused on the molecular and cellular impact of these mutations on disease pathogenesis. Therefore, increasing our knowledge and understanding of the mechanisms behind these alterations could shed light on the prediction of its clinical impact, having implications for prognosis and helping improve preventive diagnosis.

7.1.2. *Rbm10* constitutive KO embryos partially recapitulate human TARP syndrome

Gender-bias: penetrance in male and female mice. We first set out to generate hemizygous KO males since TARP syndrome is an X-linked inherited disease affecting males. Our initial observations pointed to a decrease in the expected KO:WT and

male:female ratios in adult mice, despite the fact that males were normal upon examination by CT Scan. We also generated *Rbm10* homozygous KO female embryos to evaluate phenotypic penetrance of *gene* inactivation in both genders, which was found to be lower. Male embryos presented a higher number of severe heart defects which could account for the decreased KO:WT and male:female ratios. We observed a 30% reduction of the *Rbm10 KO* male mice population, while the remaining 70% survived. In humans, survival into adulthood has been achieved, with multiple medical interventions, in a 28-year-old patient presenting ASD (Hojland et al., 2018) and in two teenage patients with a phenotype overlapping TARP syndrome (Wang et al., 2013). Nevertheless, the incidence of *RBM10* germline mutations in the adult population has not been reported to date. An *in silico* analysis of exome sequencing data from the gnomAD browser (https://gnomad.broadinstitute.org/) reveals that *RBM10* truncating mutations in healthy subjects must occur only exceptionally, although a variety of missense mutations have been identified. Their significance and/or association with milder forms of disease remain to be studied.

Males are more vulnerable to pathologies derived from mutations in genes on the X chromosome. Females who carry mutations are mosaic, having cells expressing one of the two sets of X-linked genes as a result of random chromosome inactivation by epigenetic silencing, serving as a mechanism of protection from severe clinical manifestations (Migeon, 2008). Different levels of mosaicism by X-inactivation have been reported in the heterozygous mothers of TARP patients without further clinical manifestations in them or their daughters (Johnston et al., 2014; Gripp et al., 2011; Hojland et al., 2018). In agreement with this notion, we have observed a mosaic pattern of RBM10 expression in various tissues from female mice, which could explain the milder heart and craniofacial phenotypes and the normal expected Mendelian ratio.

Cardiac phenotype. The constitutive *Rbm10* KO strain developed here has proven useful to recapitulate in E18.5 embryos two of the main features of TARP syndrome: the ASD - considered the main cause of lethality (Gripp et al., 2011). A detailed analysis of heart abnormalities has disclosed several other cardiac abnormalities that have been reported in clinical cases: heart chamber dilation (16%), atrial enlargement (12%), tricuspid and mitral valve abnormalities, and hemorrhages (Johnston et al., 2010; Johnston et al., 2014). In our model, the right atrium was dilated in >50% of the embryos, and hemorrhages occurred in 20% of individuals. Although we could not measure the function of the mitral valve in embryos due to technical limitations, we observed alterations in the lateral portion of the tricuspid valve in adult male mice. These

similarities with the human patients are remarkable, especially considering the phenotypic variability in cardiac phenotypes observed both in mice and in humans.

Craniofacial phenotypes. Craniofacial defects were also found with a higher incidence in *Rbm10 KO* embryos, mainly in the palate. However, the frequency of the abnormalities identified was often not significantly higher, possibly again due to the phenotypic variation. The absence of palatal holes, abnormal palate formation, and primary cleft palate highlights a certain level of conservation of *Rbm10* function in the development of the head region, as in humans. This was also reflected in the variable size of the cleft palate observed in *Rbm10 KO* embryos. An extended analysis of mutant embryos is warranted to reach more robust conclusions.

Other phenotypes. We did not observe the presence of *talipes equinovarus* (clubfoot) or bone malformations in adult mice by CT scan or during embryonic development by MR imaging. Of note, *talipes equinovarus* has been observed in other genetic mouse models with mutations in *Pitx1* (Dobbs et al., 2017). In our study, several explanations could account for this fact: 1) the mentioned variability, 2) the technical difficulties derived from sample fixation for visualization using MR imaging, 3) the relatively small number of analyzed animals, and 4) the fact that some of these features might be secondary - rather than primary - developmental defects. Of note, the absence of *talipes equinovarus* has been reported in TARP patients in three families (Johnston et al., 2014). In this report, some of the affected individuals also lacked the complete Robin sequence and some even lacked the cleft palate and ASD, emphasizing the intrinsic variability of the clinical phenotype which has been confirmed in more recent studies (Powis, et al.2017; Hojland et al. 2018).

We could not assess PLSVC, the fourth cardinal feature reported in 50% of TARP cases (Niceta et al., 2018), due to developmental differences between humans and mice. Normally, the right superior vena cava persists into adulthood in both species. However, in humans the left superior vena cava disappears after birth, whereas it persists postnatally in mice and both vena cavae independently empty into the right atrium (Manousiouthankis et al., 2014; Kaufman et al., 2004). As mentioned above, this feature is also subject to variability in human TARP patients.

Over the period of my thesis work, several reports have underscored that patients with TARP syndrome present additional abnormalities and that the phenotypes are pleiotropic. Therefore, the availability of the genetic mouse model described here offers the possibility of exploring in greater depth the developmental role of RBM10 given the very low incidence of TARP syndrome and the obvious ethical limitations related to

studies in patients. For these reasons, we are currently exploring whether milder, non-lethal, phenotypes may have been unnoticed in our analyses of embryos. In addition, in collaboration with J. M. Redondo (CNIC), we have set out to induce cardiac hypertrophy in 3 month-old knockout mice to reveal more subtle defects that might not have been detected without stress. This could be relevant to identify patients who are carriers of *RBM10* mutations who might present subtle congenital heart defects or altered cardiac function. Finally, in collaboration with E. Puelles (Instituto de Neurociencias, Alicante) we are currently assessing the occurrence of histological alterations in the central nervous system of *Rbm10 KO* male embryos.

In summary, we have generated the first genetic mouse model of TARP syndrome which largely recapitulates the features identified in patients and the variability of phenotype penetrance. This strain should be a valuable tool for the study of TARP syndrome and it should provide an improved understanding of the molecular basis of this condition.

7.1.3. On the molecular mechanism(s) involved in the developmental alterations resulting from *Rbm10* inactivation

Here, I have not addressed the cellular and molecular mechanisms responsible for the developmental abnormalities observed in *Rbm10* KO mice. This is, in part, due to the fact that our laboratory's main focus is on cancer. However, this is an important question that will need to be tackled in future studies. Embryonic development is a complex process and many of the genes/processes involved are conserved across species. It is, thus, conceivable that if the molecular processes are conserved, the models may provide clues for a better understanding of the pathogenesis of the defects and - possibly lead to improved therapeutic strategies.

Several observations made during our study have led us to consider the possibility that alterations in the processing of *Fgf8* transcripts might contribute to the phenotype of TARP syndrome. *FGF8* alterations have been linked to pathological conditions similar to those reported for TARP syndrome and in this study (Lewandoski et al., 2010; Moon and Capecchi, 2000; Frank et al., 2002; Hao et al., 2019; Trumpp et al., 1999; Becic et al., 2018; Imaizumi et al., 2018). A number of arguments are considered below:

- *Rbm10* and *Fgf8* have overlapping expression patterns in primary structures during development, as described for *Rbm10* by Johnston *et al* and for *Fgf8* (below).

- The deletion of *Fgf8* has been reported to cause abnormal cardiovascular structures leading to lethal malformations of the cardiac outflow tract, great vessels, and heart, mainly due to a failure to form arteries from the fourth pharyngeal arch during development (Frank et al., 2002).

- *Fgf8* loss of function also leads to abnormal craniofacial structures resembling human first arch syndromes (Frank et al., 2002; Trummp et al., 1999), altered limb formation lacking distal skeletal elements, or hypoplasia (Lewandoski et al., 2000; Moon and Capecchi, 2000). Mutations in *Fgf8* and other family members have been related to cleft lip and palate (Riley et al., 2007), all of which have been described in TARP syndrome.

- Two *Fgf8* splicing variants, *Fgf8a* and *Fgf8b*, have been demonstrated to have different activity and expression patterns across embryonic tissues (Fletcher et al., 2006; Inoue et al., 2006). Nevertheless, the molecular mechanisms involved in the regulation of *FGF8* splicing during embryogenesis in vertebrates have not been elucidated (Sunmonu et a., 2011).

FGF8 is involved in many critical processes during development by instructing growth and patterning. It belongs to the FGF family of secreted proteins that participate in progenitor cell specification, survival, proliferation, and differentiation. In particular, *FGF8* is expressed in the primitive streak and tail bud, the apical ectodermal ridge of the limb bud, the midbrain junction, and the anterior neural ridge (Crossley and Martin, 1995). It is considered to be secreted mainly by epithelial cells during the development of the first branchial arch and it is also expressed during development in the heart, limbs, kidney, CNS, and face, where it regulates multiple signaling pathways that are essential for proper early cardiogenesis, palatogenesis, odontogenesis, tongue development, salivary gland branching morphogenesis, and neuronal crest-derived tissues development (Eswarakumar et al., 2005; Trumpp et al., 1999; Haworth et al., 2007).

The function of *FGF8* has also been associated with that of *TBX1,* a transcription factor that controls elongation during development. *Tbx1* KO mice exhibit *Fgf8* down-regulation in the palate epithelium (Arnold et al., 2005). In humans, a role for *TBX1* has been described in the formation of the ventricular septum derived from the second heart field (Gittenberger-de Groot et al., 2014). FGF8 has also been associated with other morphogens, such as WNT1 - having overlapping domains in the development of the face (Frank et al., 2002) - or *Shh*, *Bmp2,* and other *Fgfs*, which present reduced or altered expression upon *Fgf8* deletion in the limbs (Lewandoski et al., 2000; Moon and Capecchi, 2000). In addition, positive feedback loops have been described involving, for

example, SHH as a regulator of FGF8 signaling in head ectoderm development (Haworth et al., 2007).

Nevertheless, other mechanisms have also been linked to atrial and ventricular septal defects, including mutations in *FAK*, *NODAL, GATA4, EGF,* and *TBX5* transcription factor/signaling pathways, among others (Doherty et al., 2010; Samarel, 2014; Gittenberger-de Groot et al., 2014; Yeh et al., 2017). In this regard, in collaboration with T. Hoffmann and J. Valcárcel, we have identified and validated altered splicing of *Fak* transcripts in *Rbm10 KO* mouse urothelial organoids, making this an interesting candidate for screening in the context of embryonic development in our KO embryos.

To confirm the validity of the hypotheses proposed above, several experiments can be proposed based on the fact that alternative splicing and isoform expression changes are frequent and variable across different tissues during development, pointing at it as an important developmental regulatory mechanism (Revil et al., 2010; Han et al., 2017; Grabowski et al., 2011). Specifically, the following approaches can be considered:

- RNA-Seq and alternative splicing analysis to identify putative alterations in *Rbm10* KO embryos, followed by RT-qPCR validation;

- *in situ* hybridization to confirm alternative splicing events at the individual cell level, given the fact that single cell RNA-Seq does not yet have the resolution to assess changes in alternative splicing;

- functional validation in cellular systems *in vitro*, by rescuing defects identified in cells from *Rbm10* KO mice, including effects on the migration, proliferation, and/or differentiation of progenitor cell populations.

Is also important to consider that *RBM10* might exhibit splicing-independent functions in developmental contexts, which have not been unveiled yet and could be addressed by using our mouse model.

7.1.4. *Rbm10* is dispensable during mouse adulthood

The reported mouse models for splicing factor genes study have mainly focused on introducing mutations by involved in hematopoietic related diseases through a variety of approaches (Li & Yu, 2019) and, in a few cases, introducing ubiquitous knockin mutations leading to retinopathies (Graziotto et al., 2011). To our knowledge, conditional

KO mouse models of splicing factor genes that have assessed gene inactivation in adult mice have not been reported.

The efficient recombination achieved in male mice in our *Rbm10* conditional KO mouse model allowed asking the question of relevance to adult homeostasis. Given the less consistent recombination achieved in females we focused on males. We did not observe significant differences in survival and at a histological level, the tissues analyzed looked normal. These findings highlight the importance of timing in the study of the role of splicing factors, where inactivation of *Rbm10* at an early developmental time point is lethal with incomplete penetrance while inactivation in adulthood did not result in an obvious phenotype. One caveat to this conclusion is the persistence of occasional unrecombined cells in tissues, but we did not observe obvious repopulation by these cells. One possibility is that the lack of a severe phenotype upon gene inactivation in homeostatic conditions is caused by postnatal - but not embryonic - redundancy in splicing factor functions. Another explanation could be that, in homeostatic conditions, altered splicing of its target transcripts does not have a severe functional impact on the cell and can be compensated by other cellular mechanisms. In addition, it is possible that RBM10 has functions other than its role in splicing and that these functions vary as a function of age.

7.2. RBM10 inactivation is an early event in bladder tumorigenesis

The concept of “field effect” has received support in bladder cancer, whereby some genetic alterations can be detected in tumor-free premalignant urothelium (Czerniak et al. 2000; Majewski et al., 2008; Thomsen et al., 2017; Strandgaard et al., 2020; Marzouka et al., 2020) (Piedrafita Bladder, et al., 2020). Multiple independent types of evidences support the notion that *RBM10* inactivation occurs early during bladder carcinogenesis:

1) Loss of RBM10 expression, used as a surrogate of inactivation mutations, occurs at a similar rate in BC regardless of all stage and grade;

2) We have observed loss of expression of RBM10 in histologically normal urothelium of tumors lacking RBM10 expression. These observations have been corroborated by our collaborators (A. Hartmann, Erlangen) who have found mosaic loss of RBM10 in large regions of histologically normal urothelium from full-bladder mappings of cystectomies from patients with MIBC;

3) Very recently, I. Martincorena's group has shown that inactivating *RBM10* mutations can be detected in normal urothelium of bladders from organ donors (without disease). *RBM10* is one of few genes for which mutant clones have been shown to undergo positive selection, indicating a functional effect (Lawson et al. 2020).

How RBM10 loss provides an advantage to mutant clones is not known. Current techniques do not allow assessing with sufficient robustness splicing changes at the single cell level or in microbiopsies of a small number of cells. Therefore, at the beginning of my project, T. Hoffmann and J. Valcárcel set out to investigate the splicing events associated with *RBM10* mutations in bladder tumors focusing on the UROMOL cohort of patients with NMIBC (Lindskrog et al., 2020). Because *RBM10* mutations leading to premature stop codons are predicted to lead to a down-regulation of transcript levels, they performed deep resequencing of 13 tumors (in collaboration with L. Dyrskjøt, Aarhus University, Denmark). This work, part of the Ph.D. thesis of T. Hoffmann, is summarized in **Box 1** and **Box 2**. *RBM10* mutations were associated with significant dysregulation of several splicing events in transcripts coding for proteins involved in cell cycle and chromosome segregation. The most significantly deregulated events implied *NDRG2, NCAPD3, MAPK10, SMC5, CRYZ, NCAPG2,* and *CENPX* mRNAs **(Box 1).** Some of these events have been shown to be altered also in our mouse urothelial organoids, as discussed below.

Box 1

Transcriptomic Analysis of Alternative Splicing in the UROMOL early stage bladder cancer cohort

The aim of this work was to analyze the alternative splicing (AS) profile of patient-derived bladder RNA sequencing data harboring RBM10 mutations. RBM10 is frequently mutated in bladder cancer and considered a cancer driver gene.

To achieve this, 13 tumor samples of the UROMOL cohort were re-sequenced in depth to allow AS quantification. 5 tumors with RBM10 wild-type status were then compared to 5 tumors with RBM10 alterations and the AS profiles were quantified using VAST-TOOLS (Irimia et al 2014). AS was quantified using the percentage spliced in (PSI), a measurement of inclusion of alternative sequences (Fig A). RBM10-mutated tumors showed altered patterns of AS in 391 events using a threshold of delta PSI (dPSI) of 10% between mutated and non-mutated tumors, mainly altering cassette exons rather than intron retention, alternative 3'ss or 5'ss events (Fig B). Notably, a high number of AS changes were shared with RNA sequencing data from human-derived-organoids comparing loss-of-function mutated organoids with RBM10 wild-type organoids (Fig C).

A

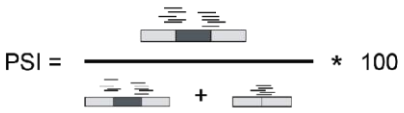

B

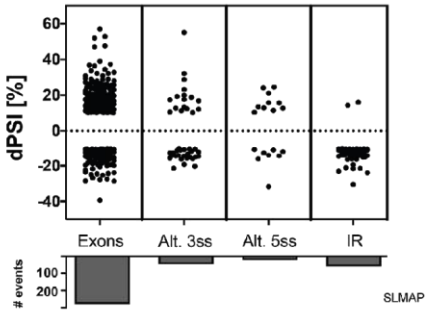

C

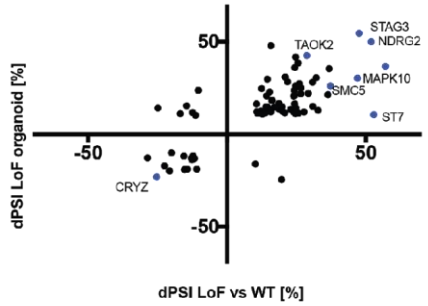

Next, the cassette exons found associated with RBM10 mutations in the tumors were analyzed more in detail. It was found that a significant fraction of those events were also altered in the TCGA late stage bladder cancer cohort. A number of those AS changes were also correlated with overall patient survival in the TCGA cohort when particular sets of PSI values were used as cut-offs. NDRG2 exon 6 is shown as an example: in the UROMOL cohort the PSI values for RBM10-mutated tumors were all higher than 50% and for RBM10 wild-type tumors PSI values were below 50% (Fig D).

D

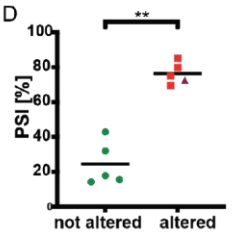

Using 48% as a cutoff, higher PSI values were associated with worse overall patient survival (Fig E). Similar observations were made for 9 other cassette exons linking RBM10 dependent exons with overall survival.

E

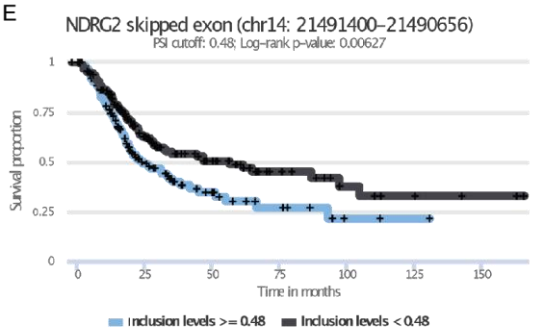

Further cassette exons were analyzed and certain common sequence/architectural features were found (summarized in Fig F). Additionally, CU-rich RNA binding motifs within the upstream intron were predicted using MEME and DREME algorithms (Fig G).

F

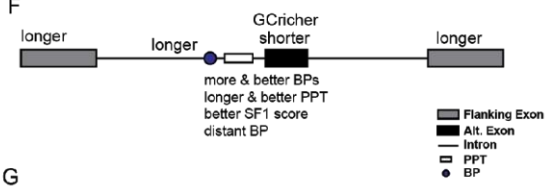

G

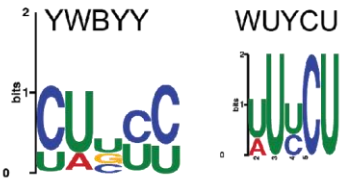

Box 2

Using those motifs, an RNA binding map was built, revealing that the motif was particularly enriched in exons displaying higher inclusion levels under conditions of RBM10 alterations (Fig H). Importantly, the enrichment in CU nucleotides was also observed in different CLIP studies (Bechara et al 2013, Wang et al 2013, Rodor et al 2016).

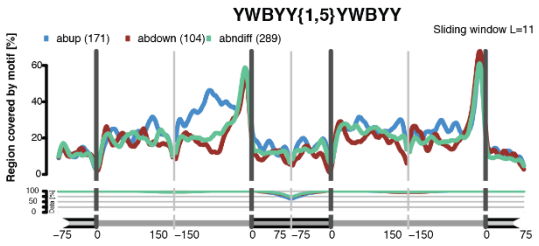

Analysis of differential gene expression of the whole UROMOL cohort comparing RBM10-mutated and wild-type tumors and analysis of GO-term enrichments found significant GO-term enrichments that were also enriched when GO-term analysis was performed on altered AS. The shared terms were:

- NUCLEAR_CHROMOSOME_SEGREGATION,
- CONDENSED_CHROMOSOME,
- REGULATION_OF_CELL_CYCLE_PROCESS and
-REGULATION_PROTEIN_COMPLEX_DISASSEMBLY

Additionally, a increased in absolute ploidy was observed in RBM10 mutated tumors within the TCGA cohort (Fig I) suggesting a potential function in correct execution of the cell cycle process and mitosis.

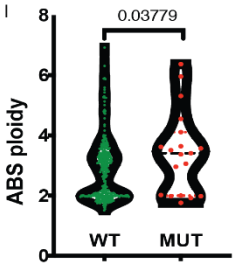

Next, RBM10 missense mutations were analyzed regarding their potential to alter AS to an extent similar to that of loss-of-function mutations. We observed remarkable differences between different missense mutations. This was interesting because missense mutations are frequent RBM10 mutations in bladder cancer, especially within the UROMOL cohort (Fig J).

Using different methods to predict the impact of individual missense mutations, we found that they showed distinct likelihood to impact protein structure/function (Fig K). Next, using computational imputation of missing values, we applied PCA analysis of AS patterns to the whole UROMOL cohort. Interestingly, we then found a high overlap between those mutations predicted to be deleterious, loss-of-function mutated tumors and RBM10 low expressing tumors (Fig L). Most interesting was the observation that many of those missense mutations were located within the second zinc finger domain of RBM10, suggesting that this poorly studied domain of RBM10 is mechanistically important for bladder cancer progression (Fig M).

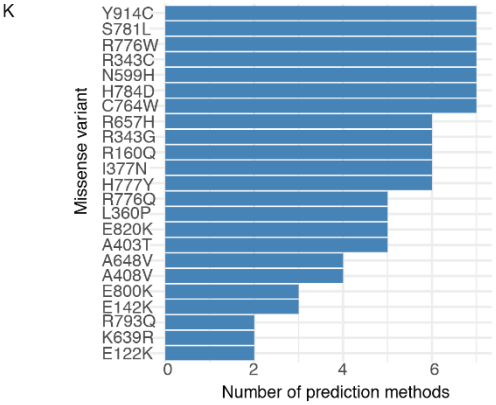

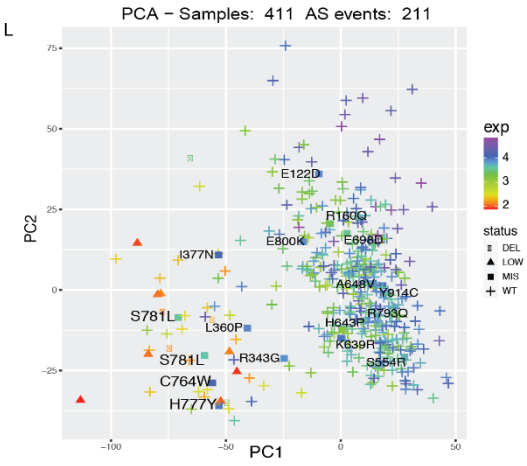

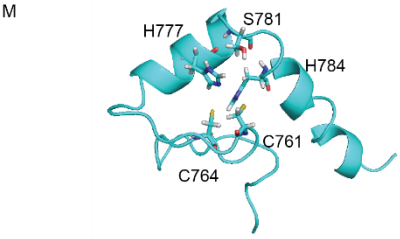

7.2.1. Rbm10 inactivation is not sufficient for bladder tumor development

In our conditional mouse model, ubiquitous *Rbm10* inactivation alone did not lead to tumors. We hypothesize that, as for many tumor suppressors, additional mutations need to accumulate for tumors to develop. The bioinformatic analysis of co-occurring mutations in BC samples led us to generated 3 additional conditional mouse strains to assess the cooperation of *Rbm10* with other tumor suppressors or oncogenes: *Kras* ^{G12V}, *Pik3ca* ^{H1047R}, and *Trp53*.

In two of these strains, *Pik3ca*; Rbm10 KO* and *Trp53 KO; Rbm10 KO*, we did not observe tumor development by introducing ubiquitous activation of knockin mutations in *Pik3ca* nor with the deletion of *Trp53* with an urothelial-specific promoter *Upk3a*. However, the number of mice analyzed is too small and this cohort is now being expanded. We obtained similar results with the *Trp53 KO; Rbm10 KO* model in 7 mice, in agreement with other studies in which the deletion in *p53* alone in *UPK3a* expressing cells has not been described as tumorigenic in the available bladder cancer mouse models.

Because *RBM10* mutations have also been reported in lung adenocarcinomas and in pancreatic tumors - both of which commonly harbor *KRAS* mutations - we opted for the use of an allele driving ubiquitous Cre expression. The tendency for an increased number of tumors of larger size in double mutant, but not in single mutant, mice argues for cooperation but the development of unrelated tumors complicates this analysis. To refine our observations, we have turned to selectively induce recombination in the lungs by administering adeno-Cre intranasally and we are currently following tumor development by CT scan. Overall, these findings indicate that the effect of *Rbm10* deletion on tumorigenesis is context-dependent (i.e. spatial, temporal, and genetic context) and the preliminary results suggest cooperation with mutant *Kras* in lung carcinogenesis. These findings are in agreement with other data supporting the cooperation of *RBM10* and *KRAS* mutations (Nanjo et al., 2020; Sun et al., 2018; Li et al., 2020, Zhao et al., 2017; Hernández et al., 2016).

Considering the fact that experiments with GEMMs are lengthy, the urothelium shows a low proliferation with turnover rates of 3-6 months, and the lack of tumors in mice harboring only *Rbm10* inactivation, we have undertaken two additional strategies: 1) to establish mouse cohorts of *Rbm10 KO* and *WT* male mice that are receiving BBN, a

urothelial-specific carcinogen and 2) to use organoids as a tool to better understand the role of RBM10 in urothelial biology.

7.2.2. Role of *Rbm10* in urothelial biology: an analysis using organoids

Organoids are powerful cellular tools to study the biology of normal epithelial cells which can often not be maintained permanently in 2D conditions. Their layered organization recapitulates better the complexity of the original tissue. Our group has demonstrated that, in proliferative conditions, normal urothelial organoids predominantly display a basal phenotype and that they are capable of activating the urothelial differentiation program upon removal of growth factors. Differentiated organoids have a distinct morphology, characterized by a reduced number of cell layers, a bigger lumen, the expression of higher levels of luminal markers such as *Upk1, Upk2, Upk3a, Foxa1,* and *Pparγ*, and they acquire barrier function, similar to the urothelium in the bladder (Santos et al., 2019).

An advantage of using normal urothelial organoids from the conditional KO mice is that the effect of *Rbm10* inactivation can be readily assessed upon induction of recombination *in vitro*. The *Rbm10 KO* organoid model was successfully established; to reduce variability, we restricted this work to male-derived organoids and isolated recombined cells using FACS, assuming first - and confirming later - that *Rbm10*-null cells were faithfully identified by the reporter. RBM10-null organoids showed almost normal growth, consistent with the lack of phenotype observed in adult KO mice. This agrees with the findings in normal bronchial and breast epithelial cells upon *RBM10* KD (Nanjo et al., 2020; Bechara et al., 2013) and has been shown in cells derived from mouse models for other splicing factor genes (Moroy & Heyd, 2007).

7.2.3 RBM10 and the EGF receptor pathway

Rbm10 KO organoids showed to be less proliferative than WT organoids. While this observation is somewhat unexpected for a tumor suppressor gene, studies with organoids have shown that normal cells can grow optimally - even better than transformed cells - in the rich medium used (Boj et al., 2015). These organoids are also less dependent on exogenous EGF and express higher levels of EGFR at the protein level. These phenotypes may be related to the altered splicing events of transcripts related to cell cycle and chromosome segregation **(Box 2)** and the down-regulated signatures in proliferative conditions in our GSEA analysis.

The EGF independence suggests the activation of a cell-autonomous EGFR activation, which is in agreement with our RNA-Seq data showing enrichment of EGFR signaling pathway associated-signatures, possibly through the endogenous production of EGF ligands. In pancreatic cancer, a subset of organoids acquires WNT/RSPO1 independence through the endogenous production of WNT ligands, in association with loss of "classical" ductal features (Seino et al., 2018). Other hypotheses include the possibility that *Rbm10* inactivation led to increased EGFR stability, making these organoids more sensitive to EGF or other receptor ligands. To test this hypothesis, we are currently performing proliferation assays in the presence of Erlotinib, an EGFR inhibitor. Alternatively, downstream pathway activation may lead to increased EGFR expression. An unexpected precedent for the latter has been described in mouse models of pancreatic cancer, where *Kras* mutations lead to the activation of an EGFR loop that renders cells extremely sensitive to *Egfr* genetic deletion (Navas et al., 2012). A link between RBM10 and EGFR has been very recently been described in lung cancer, where *RBM10* inactivation co-occurs with activating *EGFR* mutations: *RBM10* inactivation decreases EGFR inhibitor-mediated apoptosis (Nanjo et al., 2020). This significant co-occurrence is also found in lung adenocarcinoma tumors patients in the TCGA database (cBioportal, https://www.cbioportal.org/). Interestingly, RBM10 has been associated with the SRC family of tyrosine kinases, downstream targets of EGFR signaling, in the regulation of cell spreading in melanoma cells (Yamada et al., 2016) **(Fig. 43)**.

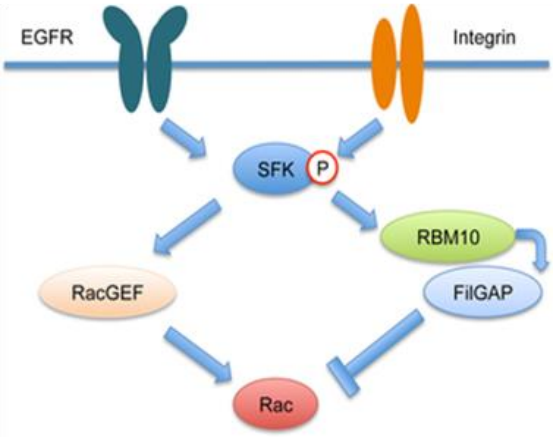

Figure 43: Association of RBM10 with EGFR downstream targets. Reported interaction of RBM10 with FilGAP through RAC1 in melanoma cell lines (Yamada et al,, 2016).

The EGFR pathway plays an essential role in urothelial proliferation and migration (Daher et al., 2003; Varley et al., 2005) and its activation - mainly through EGFR amplification and/or mutations in members of this receptor pathway. EGFR overactivation has been associated with the Basal/Squamous-like subgroup of MIBC

(Kamoun et al., 2020; Rebouissou et al., 2014). Unlike in lung adenocarcinoma, in MIBC tumors from the MSK/TCGA database, *RBM10* truncating mutations (4.3%) and *EGFR* amplifications (4.3%) are non-significant mutually exclusive (cBioportal: https://www.cbioportal.org/, MSK/TCGA database, 2020). Of note, I have found that RBM10 loss of expression is infrequent in MIBC with basal features, also suggesting distinct differences between lung and bladder cancer.

The candidate splicing events identified as altered in BC in association with *RBM10* mutations further point to the EGFR pathway. In the UROMOL and TCGA cohorts, RNA-Seq analysis has revealed changes in the splicing of *FAK*/*PTK2* and *ZDHHC20,* without changes in gene expression as determined by the normalized counts. *FAK* encodes a Ser-Thr kinase that regulates numerous signaling pathways; its dominant role has been reported in integrin signaling but it also participates in ERBB2 signaling and in the downstream activation of PI3K and AKT1, MAPK1/ERK2, and MAPK3/ERK1 signaling cascades **(Fig. 44)**. The effect of the predicted alteration in the *FAK* transcript variant is not known. High expression of *FAK* has been associated with poor prognosis in BC (Zhang et al., 2018) and has been related to an aggressive phenotype in several tumor types (Zhou et al., 2019).

ZDHHC20 encodes an enzyme that catalyzes palmitoylation of Cys residues in the C-terminus of EGFR, also regulating the duration of EGFR activation by internalization and degradation of this receptor (Runkle et al., 2017). Inhibition of ZDHHC20-mediated EGFR palmitoylation in breast, lung and kidney cancer cells reveals a dependence on EGFR signaling (Runkle et al., 2016). The predicted structure for the *ZDHHC20* transcript variant causes non-sense mediated decay through the inclusion of a poison exon, a type of highly conserved alternative exons containing premature termination codons. Importantly, RBM10 expression correlates with the inclusion of the poison exon in *ZDHHC20* transcript variants in BC, leading to lower levels of *ZDHHC20* mRNA, and being associated with shorter patient survival (T. Hoffman, doctoral thesis). We have successfully validated the deregulation of these two splicing events - identified through the transcriptomic analysis of human tumors - in *Rbm10 KO* organoids (data not shown), underscoring the usefulness of the *in vitro* mouse models. We plan to explore the biological effect of these splicing changes in various cellular models, including the mouse organoids. Specifically, we would address the effect on EGF dependency.

Considering this, our organoid system could be useful to reveal if the regulation of these mechanisms by *Rbm10* leads to the observed phenotype, less EGF dependency, and if the function of these variants is conserved between human and mice too.

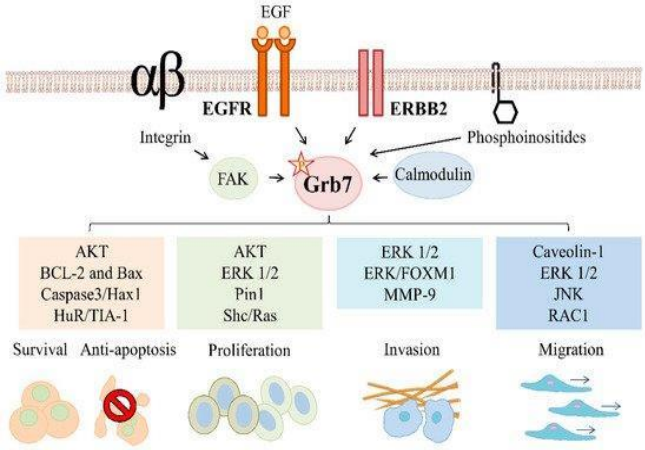

Figure 43: Association of RBM10 splicing targets that are mediators of the EGF family of receptors signaling. Reported role of FAK in the regulation of Grb7 and downstream targets involved in cell survival, proliferation, invasion and migration in cancer (Chu et al., 2019), from which *Bcl-2 (Bcl-x)* has been reported as RBM10 splicing targets in lung cancer cells (Nanjo et al., 2020) and RAC1 has been highlighted as a mediator in FilGAP: RBM10 interaction (Yamada et al,, 2016).

In summary, several aspects of the work reported here point to a functional relationship between RBM10 and the EGFR pathway that merits further work and could have therapeutic implications.

7.2.4. *Rbm10* inactivation leads to a luminal-like phenotype with stratified epithelium features in mouse urothelial organoids

The strong association of *RBM10* mutations with tumors with urothelial differentiation suggested its participation in this process. Therefore, we assessed the differentiation capacity of the *Rbm10 KO* organoids and confirmed that a canonical urothelial program can be activated upon growth factor depletion. This process was accompanied by morphological changes and up-regulation of luminal markers and signatures in organoids of both genotypes. Nevertheless, when we compared proliferative and differentiated *Rbm10 KO* organoids to WT organoids, *Rbm10 KO* organoids showed an enhanced luminal-like phenotype with up-regulation of several luminal markers, in agreement with the observations in human tumors. Intriguingly, there was an up-

regulation of markers related to stratified epithelia at the transcriptomic level. As described by Santos *et al*, normal urothelial organoids in proliferative conditions display a default squamous-like differentiation program while - in differentiated conditions - they activate the urothelial differentiation program. A mixed profile similar to what we observed in *Rbm10 KO* organoids in proliferation has been described in MIBC tumors, suggesting that these programs are not necessarily mutually exclusive (Font et al., 2020). We confirmed the expression of luminal and stratified epithelium markers in scRNAseq data from normal urothelial organoids, mainly in the intermediate and luminal cell clusters (Santos et al., 2019), hence, supporting our hypothesis. The fact that the *Rbm10 KO* organoids exhibit a luminal-like phenotype could be related to their reduced proliferation, even in a context of reduced EGF dependency and higher EGFR expression. Transcription factor motif analysis will be useful to determine specific pathway activation involving the up-regulation of both sets of luminal and stratified epithelial markers.

We found that the genes up-regulated in proliferation conditions (e.g. *Sprr2f, Cnfn, Sprr1a,* and *Krt10*) and *CstA* (up-regulated in differentiation) are directly linked to keratinization and cornified stratified squamous epithelia. In particular, KRT10 is rarely detectable in the healthy urothelium but low expression levels have been reported in proliferative and differentiated urothelial organoids (Liu, et al. 2019; Santos et al., 2019; Yu et al., 2019). *Gstm1*, which is also highly expressed in intermediate/luminal clusters from normal urothelial organoids in differentiation, was up-regulated in *Rbm10 KO* organoids. *GSMT1* is absent at the germline level in 50% of Caucasians and *GSTM1* nullity is associated with an increased risk of BC (Malats & Real, 2015). In tumors of the UROMOL and TCGA series, *GSTM1* expression is found exclusively in tumors with luminal phenotype, both in NMIBC and MIBC (M. Kalisz, our group, unpublished data). Importantly, of all tissues, the mouse bladder exhibits the highest levels of *Gstm1* expression, suggesting an important role of this gene in bladder homeostasis. *Gstm1* is also part of a PPARG-driven program in normal mouse bladder (Liu et al., 2018), which could account for the observed luminal-phenotype. *Pparγ* levels were non-significantly higher in both proliferative and differentiated KO organoids and enrichment scores of GSEA signatures of Pparγ signaling pathways were non-significant (M. Kalisz, unpublished data). Therefore, it remains to be established how *Rbm10* inactivation promotes up-regulation of differentiation markers.

Among the significantly down-regulated in *Rbm10 KO* organoids, we found other genes involved in xenobiotic metabolism, such as *Cyp2f2*. Its relevance has mainly been highlighted in the lung epithelium (Cruzan et al., 2009), linked to glutathione-regulated

metabolism (Shultz et al., 2001). A putative tumor suppressor, *Gas1,* involved in growth suppression by blocking entry to S phase, was also down-regulated in differentiated *Rbm10 KO* organoids. However, its role in BC has not been defined. *Dpys13*, coding for a protein involved in signaling for cytoskeleton remodeling, was down-regulated and is an unfavorable prognostic marker in urothelial cancer (https://www.proteinatlas.org/). The down-regulation of these genes and the mixed profile of luminal/stratified epithelium differentiation upon *Rbm10 KO*, suggest an enrichment of the urothelial differentiation program in these organoids and that *Rbm10* in this context might play an important role in activation of normal urothelial differentiation. One issue that remains to be determined is whether the findings related above refer to the concomitant expression of luminal and stratified differentiation markers in the same cells or in distinct cell populations. Multiplex IHC analyses and/or scRNA-Seq should help to answer this question.

Our RNA-Seq analyses have several limitations. First, the sequencing depth was not optimal to assess deregulated isoform expression, which could have been an important contribution to understand the mechanisms driving the phenotype we have observed. Second, the sequencing and library preparation methods used in the second round of RNA-Seq experiments (3´RNASeq using Lexogen libraries) considers the reads of the 3´ end only, which is an important limitation for the assessment of differential transcript expression, where whole transcript methods have higher detection rates regardless of the sequencing depth (Ma et al., 2019). Finally, a larger number of samples per condition would provide greater power to the experiments. In part, this is due to sample heterogeneity: in proliferative conditions, we identified wide ranges of expression for a number of significantly deregulated genes (e.g. *Sp8* and *Fam129a,* which showed low levels in one of the three KO samples analyzed). In normal urothelial organoids, the levels of expression of these genes were very low. Similarly, in normal urothelium, *Sp8* was expressed at very low levels and *Fam129a* was detected only in mesenchymal cell clusters. In differentiation conditions, one of the biological replicates of KO organoids had a clear outlier behavior. Similarly to proliferative conditions, when we tracked the expression of DEG in normal urothelial organoids, we observed that genes such as *Col5a3, Lrg6,* and *Rab6b* are barely expressed. In normal urothelium, *Col5a3* was expressed at low levels in mainly mesenchymal cells; *Lrg6* and *Rab6* were expressed in all cells at low levels as well. Nevertheless, the limitations of single-cell RNA sequencing need to be considered: it has a lower sensitivity and it is noisier and more complex than bulk-RNA-Seq (Chen et al., 2019). Most importantly, three factors can lie at the base of the heterogeneity of the biological replicas: 1) organoid cultures are inherently more heterogeneous than standard 2D cultures, 2) the differentiation protocol used may be

suboptimal and not all organoids in a given culture may engage in differentiation with similar efficiency or synchronously, and 3) there may be additional heterogeneity resulting from the *Rbm10* recombination step. Overall, increasing sample size would contribute to overcome some of these limitations, reduce background noise and false positive findings, and reduce false negatives through increased statistical power. Single cell RNA sequencing analysis may also provide additional information.

Despite sample heterogeneity, GSEA showed enrichment of gene signatures related to keratinization and cornification in proliferative conditions, consistent with our observations regarding up-regulation of stratified epithelium markers. In proliferation, there was also a negative enrichment in signatures related to cell cycle, DNA replication, metabolism, degradation, transcription, and translation. The down-regulation of genes related to the mentioned processes in these signatures agrees with the reduced proliferative phenotype of KO organoids. Conversely, in differentiation conditions these pathways were highly enriched, suggesting a more proliferative phenotype upon induction of differentiation. This finding contrasts with the higher enrichment scores in urothelial differentiation signatures.

It is possible that the use of organoids derived from *RBM10-mutant* human tumors may also provide key information about the deregulation of these processes. Rescue experiments with the inducible system that I have generated should shed light on the causal role of RBM10 loss in these processes.

7.2.5. RBM10 splicing regulation is conserved in human and mouse urothelial models.

Our collaborative efforts with the Valcárcel laboratory have provided a wider perspective on the role or *RBM10* in tumorigenesis. The transcriptomic analyses have considered both gene expression and splicing. Loss of function of RBM10 might not necessarily lead to changes in gene expression levels, although altered splicing could lead to transcript variants subject to non-sense mediated decay without changes in transcription. This could in turn affect the function or activity of the corresponding protein, as observed in other cancers (Bechara et al., 2013; Nanjo et al., 2020). In contrast, we would expect changes in alternative splicing upon loss of RBM10 function, assuming that this is a major mechanism through which this gene is involved in cancer. An important question concerns the degree of overlap of RBM10-dependent splicing events across species. In this regard, we have analyzed AS in human *RBM10* WT vs. mutant cells and in mouse *Rbm10* WT vs. null organoids. Consistent changes in AS, measured as the differential

percentage of spliced-in (dPSI) values, support that RBM10 loss does impact on splicing events, as identified in the RNA-Seq from the UROMOL cohort.

The consistent altered AS patterns in transcripts related to important cellular processes provide strong evidence of the validity of our findings, as are the rescue experiments performed **(Box 3).** The conservation of some of the AS changes between human and mouse urothelial cells and the findings related to TARP syndrome suggest that the function of RBM10 as an AS regulator is at least partially conserved between the two species and validates the models and tools that we have developed. Considering this, the findings regarding alterations in splicing events might help to outline future experiments to analyze the impact of these in normal cellular function.

Box 3

A subset of AS changes found altered in RBM10-mutated tumors of the UROMOL cohort was validated in cell-lines. Transient knock-down of RBM10 was performed in three different bladder cancer cell-lines (MGHU-3, Scaber & RT-4). Multiple events were validated as RBM10 targets. Fig N shows a representation of dPSIs from the knock-down of RBM10 in MGHU-3 and RT-4 cells against dPSIs derived from RNA sequencing data from the UROMOL cohort.

N

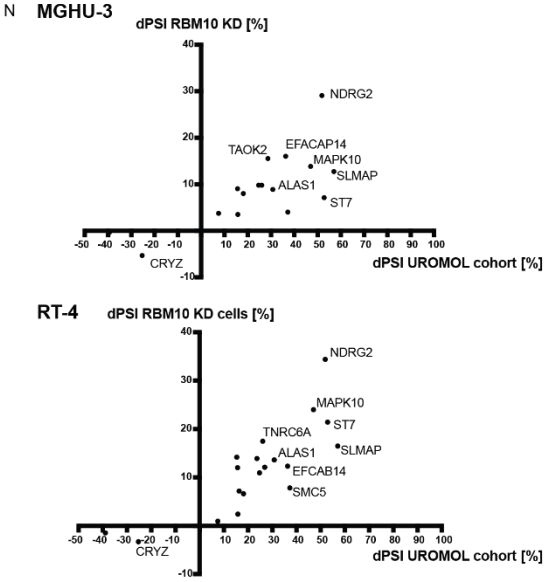

Additionally, AS events were validated in RT-4 knock-out cells which were generated by Ana Margarita Maldonado at the CNIO in collaboration with us (Fig O).

O

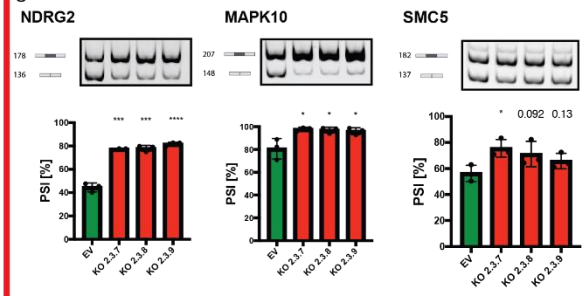

Further events were validated in human-derived organoids generated and grown at CNIO, whose RNA-seq sequencing had been analyzed (Fig P).

P

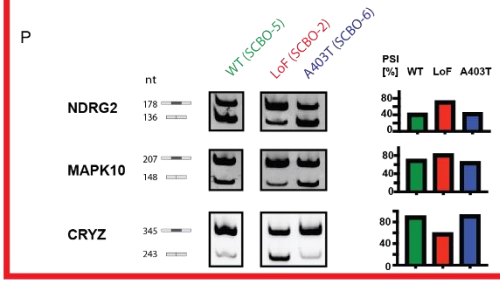

Next a subset of AS events that were conserved in mice was validated in mouse-derived organoids (Fig Q).

Q

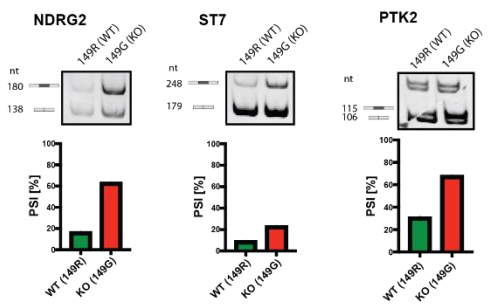

Lastly, cells were analyzed regarding potential phenotypes associated with alterations in RBM10 levels/activity. While shRNA-mediated RBM10 knock-down in several cell-lines and knock-out in the RT-4 cell-line showed no consistent effects (see clonogenic assays after successful knock-down of RBM10 in 97-1 cells in Fig R as an example), RBM10 overexpression using an inducible vector resulted in reduced colony growth, anoikis resistance and 3D growth (n=2, technical triplicates) (Fig S).

R

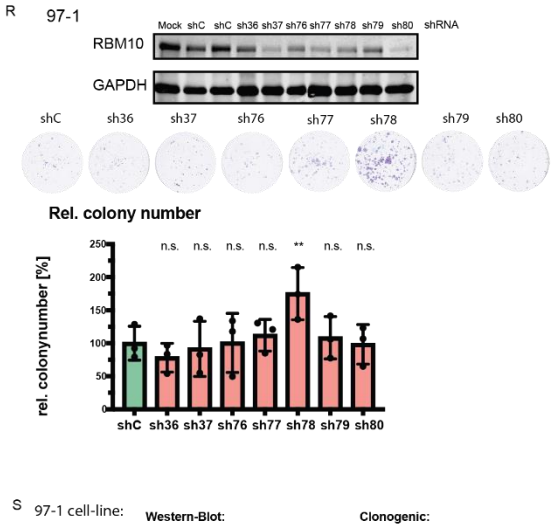

S

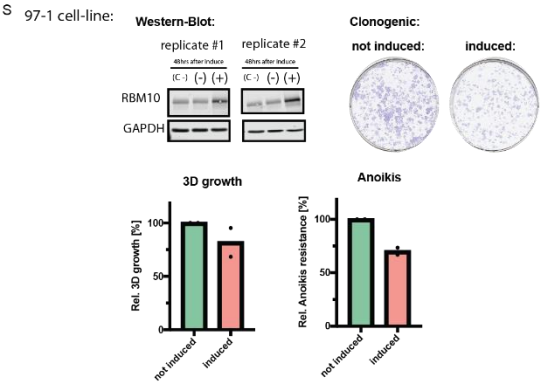

We have also established isogenic *RBM10 KO* and *KD* BC cells, although the results in proliferation and clonogenic assays are inconsistent due to unknown reasons that we believe are not related to experimental technical variation **(Box 3)**. It is possible that abnormal protein isoforms of RBM10 are expressed that could contribute to this variability.

The inducible RBM10 lentiviral expression plasmid that I have recently generated has allowed assessing the effect of *RBM10* overexpression on *RBM10 WT* bladder cancer cells, including a reduced clonogenic potential, 3D growth, and anoikis resistance **(Box 3)**. We are currently validating these findings using organoids established from human tumors harboring inactivating *RBM10* mutations (in collaboration with M. Shen, Columbia University, New York) in which we have reconstituted RBM10 expression to evaluate its impact on proliferation, growth factor dependence, differentiation, invasion, and tumor growth in xenograft models. Moreover, we have established additional BC organoid lines in which we are currently assessing *RBM10* mutational profile.

7.2.6. Closings

The current work provides a significant advance in knowledge. However, several aspects of the work require additional work or need to be explored:

- Assess more widely the existence of alterations in other tissues in the *Rbm10* constitutive KO embryos to acquire a more detailed description of their phenotype.
- Determine changes in splicing in mouse embryonic tissues affected by the deletion of *Rbm10* constitutive KO embryos in order to provide a mechanistic understanding of the observed alterations.
- Determine whether the cardiac function of surviving *Rbm10* constitutive KO mice is compromised in stress conditions, which could have possible implications in less severe forms of RBM10-related conditions.
- Acquire a deeper understanding of the mechanisms leading to reduced EGF dependency and explore whether this feature could be exploited at the therapeutic level.
- Validate the DEG identified through RNA-Seq and analyze changes in protein expression in mouse organoids, to determine whether the activation of urothelial and stratified transcriptomic signatures occur in the same or different cell populations.

- Evaluate the biological effects of the altered splicing changes in mouse and human organoids to identify the key events responsible for the contribution of RBM10 loss to tumor development.
- Evaluate the biological effects of RBM10 reconstitution in *RBM10* KO tumor organoids.
- Complete the analysis of the cooperation of *Rbm10* inactivation with mutations in oncogenes/tumor suppressor genes in mice to uncover how RBM10 contributes to cancer development.
- Understand how early RBM10 loss in tissues can lead to the positive selection of mutant clones.

8. CONCLUSIONS

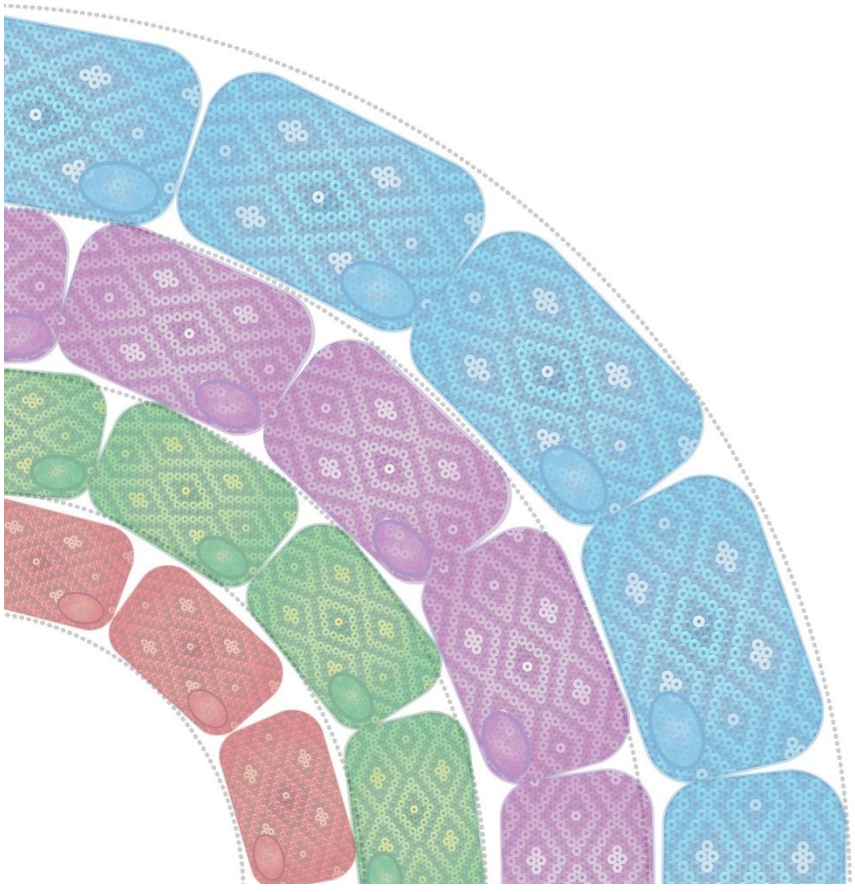

CONCLUSIONS

1) I have established the first *Rbm10* conditional knockout genetic mouse model.

2) RBM10 is required for normal embryonic development. Germline inactivation results in partial male lethality, recapitulating the main features of TARP syndrome in mice, including heart and craniofacial defects.

3) RBM10 is dispensable for homeostasis in adult mice.

4) *Rbm10* inactivation in normal mouse urothelial organoids leads to partial growth factor-independence (EGF) and up-regulation of signatures of urothelial and stratified differentiation.

5) *Rbm10* inactivation in normal mouse urothelial organoids results in changes in alternative splicing events identified in *RBM10*-mutant bladder cancers.

6) *Rbm10* inactivation is an early genetic alteration in bladder cancer; additional genetic alterations are required for tumor development.

7) The ensemble of the results strongly support the conservation of RBM10 function in humans and mice, including its role in alternative splicing, and validate the conditional mouse model for the study of human disease.

9. REFERENCES

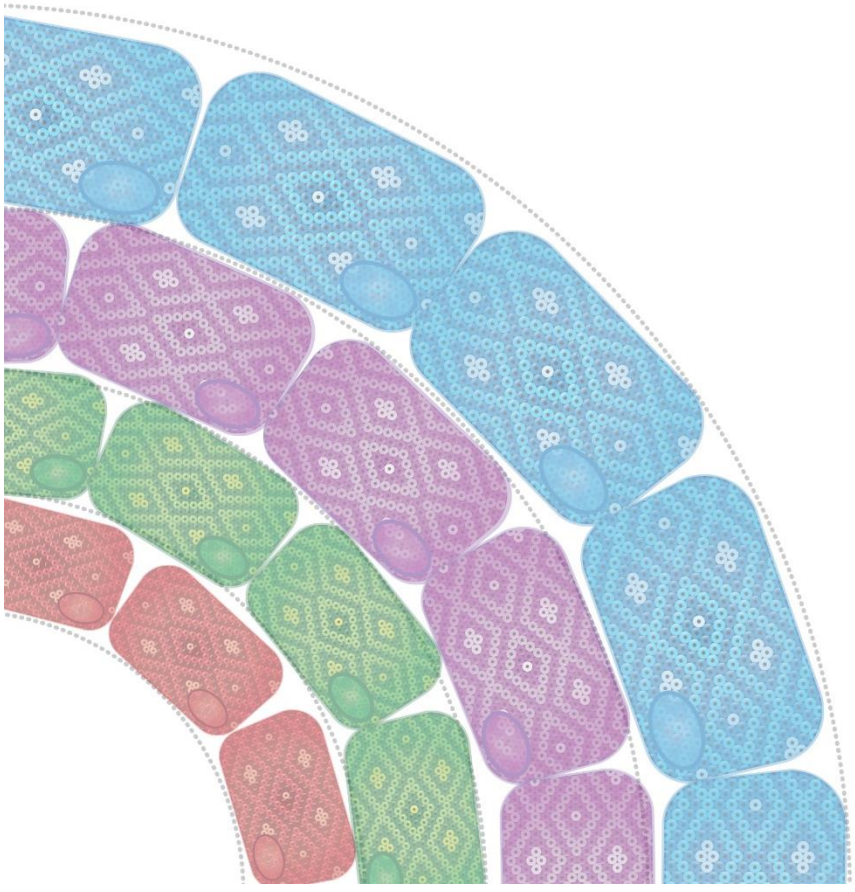

Aboulkassim, T. O., LaRue, H., Lemieux, P., Rousseau, F., & Fradet, Y. (2003). Alteration of the PATCHED locus in superficial bladder cancer. *Oncogene*, *22*(19), 2967–2971. https://doi.org/10.1038/sj.onc.1206513

Adams, J. M., & Cory, S. (n.d.). *Transgenic Models of Tumor Development*. http://science.sciencemag.org/

Ahmad, I., Morton, J. P., Singh, L. B., Radulescu, S. M., Ridgway, R. A., Patel, S., Woodgett, J., Winton, D. J., Taketo, M. M., Wu, X. R., Leung, H. Y., & Sansom, O. J. (2011). B-Catenin activation synergizes with PTEN loss to cause bladder cancer formation. *Oncogene*, *30*(2), 178–189. https://doi.org/10.1038/onc.2010.399

Ahmad, I., Patel, R., Liu, Y., Singh, L. B., Taketo, M. M., Wu, X. R., Leung, H. Y., & Sansom, O. J. (2011). Ras mutation cooperates with β-catenin activation to drive bladder tumourigenesis. *Cell Death and Disease*, *2*(3). https://doi.org/10.1038/cddis.2011.7

Ahmad, I., Singh, L. B., Foth, M., Morris, C. A., Taketo, M. M., Wu, X. R., Leung, H. Y., Sansom, O. J., & Iwata, T. (2011). K-Ras and β-catenin mutations cooperate with Fgfr3 mutations in mice to promote tumorigenesis in the skin and lung, but not in the bladder. *DMM Disease Models and Mechanisms*, *4*(4), 548–555. https://doi.org/10.1242/dmm.006874

Alifrangis, C., McGovern, U., Freeman, A., Powles, T., & Linch, M. (n.d.). Molecular and histopathology directed therapy for advanced bladder cancer. *Nature Reviews Urology*. https://doi.org/10.1038/s41585

Allory, Y., Beukers, W., Sagrera, A., Flández, M., Marqués, M., Márquez, M., Van Der Keur, K. A., Dyrskjot, L., Lurkin, I., Vermeij, M., Carrato, A., Lloreta, J., Lorente, J. A., Carrillo-De Santa Pau, E., Masius, R. G., Kogevinas, M., Steyerberg, E. W., Van Tilborg, A. A. G., Abas, C., … Real, F. X. (2014). Telomerase reverse transcriptase promoter mutations in bladder cancer: High frequency across stages, detection in urine, and lack of association with outcome. *European Urology*, *65*(2), 360–366. https://doi.org/10.1016/j.eururo.2013.08.052

Al-Zalabani, A. H., Stewart, K. F. J., Wesselius, A., Schols, A. M. W. J., & Zeegers, M. P. (2016). Modifiable risk factors for the prevention of bladder cancer: a systematic review of meta-analyses. In *European Journal of Epidemiology* (Vol. 31, Issue 9, pp. 811–851). Springer Netherlands. https://doi.org/10.1007/s10654-016-0138-6

Antoni, S., Ferlay, J., Soerjomataram, I., Znaor, A., Jemal, A., & Bray, F. (2017). Bladder Cancer Incidence and Mortality: A Global Overview and Recent Trends. In *European Urology* (Vol. 71, Issue 1, pp. 96–108). Elsevier B.V. https://doi.org/10.1016/j.eururo.2016.06.010

Arima, Y., Ogura, H., Katsunuma, K., Tanaka, Y., Murakami, M., Atsumi, T., Nakajima, K., Kamimura, D., Suzuki, H., Jiang, J.-J., Ohara, O., Hasegawa, Y., Ohki, T., Ota, M., Okuyama, Y., & Nakagawa, I. (2017). Rbm10 regulates inflammation development via alternative splicing of Dnmt3b. *International Immunology*, *29*(12), 581–591. https://doi.org/10.1093/intimm/dxx067

Aveyard, J.S.; Skilleter, A.; Knowles, M. A. (1999). Somatic mutation of PTEN in bladder carcinoma. *British Journal of Cancer*, *80*, 904–908.

Balbás-Martínez, C., Rodríguez-Pinilla, M., Casanova, A., Domínguez, O., Pisano, D. G., Gómez, G., Lloreta, J., Lorente, J. A., Malats, N., & Real, F. X. (2013). ARID1A Alterations Are Associated with FGFR3-Wild Type, Poor-Prognosis, Urothelial Bladder Tumors. *PLoS ONE*, *8*(5). https://doi.org/10.1371/journal.pone.0062483

Balbás-Martínez, C., Sagrera, A., Carrillo-De-Santa-Pau, E., Earl, J., Márquez, M., Vazquez, M., Lapi, E., Castro-Giner, F., Beltran, S., Bayés, M., Carrato, A., Cigudosa, J. C., Domínguez, O., Gut, M., Herranz, J., Juanpere, N., Kogevinas, M., Langa, X., López-Knowles, E., … Real, F. X. (2013). Recurrent inactivation of STAG2 in bladder cancer is not associated with aneuploidy. *Nature Genetics*, *45*(12), 1464–1469. https://doi.org/10.1038/ng.2799

Baranello, L., Kouzine, F., & Levens, D. (2014). CTCF and cohesin cooperate to organize the 3D structure of the mammalian genome. In *Proceedings of the National Academy of Sciences of the United States of America* (Vol. 111, Issue 3, pp. 889–890). National Academy of Sciences. https://doi.org/10.1073/pnas.1321957111

Bartfeld, S., Bayram, T., Van De Wetering, M., Huch, M., Begthel, H., Kujala, P., Vries, R., Peters, P. J., & Clevers, H. (2015). In vitro expansion of human gastric epithelial stem cells and their responses to bacterial infection. *Gastroenterology*, *148*(1), 126-136.e6. https://doi.org/10.1053/j.gastro.2014.09.042

Bechara, E. G., Sebestyén, E., Bernardis, I., Eyras, E., & Valcárcel, J. (2013). RBM5, 6, and 10 differentially regulate NUMB alternative splicing to control cancer cell proliferation. *Molecular Cell*, *52*(5), 720–733. https://doi.org/10.1016/j.molcel.2013.11.010

Becic, T., Kero, D., Vukojevic, K., Mardesic, S., & Saraga-Babic, M. (2018). Growth factors FGF8 and FGF2 and their receptor FGFR1, transcriptional factors Msx-1 and MSX-2, and apoptotic factors p19 and RIP5 participate in the early human limb development. *Acta Histochemica*, *120*(3), 205–214. https://doi.org/10.1016/j.acthis.2018.01.008

Behzadnia, N., Golas, M. M., Hartmuth, K., Sander, B., Kastner, B., Deckert, J., Dube, P., Will, C. L., Urlaub, H., Stark, H., & Lührmann, R. (2007). Composition and three-dimensional EM structure of double affinity-purified, human prespliceosomal A complexes. *EMBO Journal*, *26*(6), 1737–1748. https://doi.org/10.1038/sj.emboj.7601631

Ben-David, U., Ha, G., Tseng, Y. Y., Greenwald, N. F., Oh, C., Shih, J., McFarland, J. M., Wong, B., Boehm, J. S., Beroukhim, R., & Golub, T. R. (2017). Patient-derived xenografts undergo mouse-specific tumor evolution. *Nature Genetics*, *49*(11), 1567–1575. https://doi.org/10.1038/ng.3967

Benedict, W. F., Lerner, S. P., Zhou, J., Shen, X., Tokunaga, H., & Czerniak, B. (n.d.). *Level of retinoblastoma protein expression correlates with p16 (MTS-1/INK4A/CDKN2) status in bladder cancer*. http://www.stockton-press.co.uk/onc

Bernardo, C., Eriksson, P., Marzouka, N. al dain, Liedberg, F., Sjödahl, G., & Höglund, M. (2019). Molecular pathology of the luminal class of urothelial tumors. *Journal of Pathology*, *249*(3), 308–318. https://doi.org/10.1002/path.5318

Bertaux-Skeirik, N., Centeno, J., Feng, R., Schumacher, M. A., Shivdasani, R. A., & Zavros, Y. (2016). Co-culture of gastric organoids and immortalized stomach mesenchymal cells. *Methods in Molecular Biology*, *1422*, 23–31. https://doi.org/10.1007/978-1-4939-3603-8_3

Bessonov, S., Anokhina, M., Will, C. L., Urlaub, H., & Lührmann, R. (2008). Isolation of an active step I spliceosome and composition of its RNP core. *Nature*, *452*(7189), 846–850. https://doi.org/10.1038/nature06842

Billerey, C., Chopin, D., Lè Ne Aubriot-Lorton, M.-H., Ricol, D., Gil Diez De Medina, S., Bas, ‡, Rhijn, V., Bralet, M.-P., Lefrere-Belda, M.-A., Lahaye, J.-B., Abbou, C. C., Bonaventure, J., Zafrani, E. S., Van Der Kwast, T., Thiery, J. P., & Radvanyi, F. (2001). Short Communication Frequent FGFR3 Mutations in Papillary Non-Invasive Bladder (pTa) Tumors. In *American Journal of Pathology* (Vol. 158, Issue 6).

Biselli-Chicote, P. M., Oliveira, A. R. C. P., Pavarino, E. C., & Goloni-Bertollo, E. M. (2012). VEGF gene alternative splicing: Pro- and anti-angiogenic isoforms in cancer. In *Journal of Cancer Research and Clinical Oncology* (Vol. 138, Issue 3, pp. 363–370). https://doi.org/10.1007/s00432-011-1073-2

Biton, A., Bernard-Pierrot, I., Lou, Y., Krucker, C., Chapeaublanc, E., Rubio-Pérez, C., López-Bigas, N., Kamoun, A., Neuzillet, Y., Gestraud, P., Grieco, L., Rebouissou, S., deReyniès, A., Benhamou, S., Lebret, T., Southgate, J., Barillot, E., Allory, Y., Zinovyev, A., & Radvanyi, F. (2014). Independent Component Analysis Uncovers the Landscape of the Bladder Tumor Transcriptome and Reveals Insights into Luminal and Basal Subtypes. *Cell Reports*, *9*(4), 1235–1245. https://doi.org/10.1016/j.celrep.2014.10.035

Blinova, E., Roshchin, D., Kogan, E., Samishina, E., Demura, T., Deryabina, O., Suslova, I., Blinov, D., Zhdanov, P., Osmanov, U., Nelipa, M., & Kaprin, A. (2019). Patient-Derived Non-Muscular Invasive Bladder Cancer Xenografts of Main Molecular Subtypes of the Tumor for Anti-Pd-l1 Treatment Assessment. *Cells*, *8*(6), 526. https://doi.org/10.3390/cells8060526

Boers, S. N., & Bredenoord, A. L. (2018). Consent for governance in the ethical use of organoids comment. In *Nature Cell Biology* (Vol. 20, Issue 6, pp. 642–645). Nature Publishing Group. https://doi.org/10.1038/s41556-018-0112-5

Boj, S. F., Hwang, C. Il, Baker, L. A., Chio, I. I. C., Engle, D. D., Corbo, V., Jager, M., Ponz-Sarvise, M., Tiriac, H., Spector, M. S., Gracanin, A., Oni, T., Yu, K. H., Van Boxtel, R., Huch, M., Rivera, K. D., Wilson, J. P., Feigin, M. E., Öhlund, D., … Tuveson, D. A. (2015). Organoid models of human and mouse ductal pancreatic cancer. *Cell*, *160*(1–2), 324–338. https://doi.org/10.1016/j.cell.2014.12.021

Bonnal, S., Vigevani, L., & Valcárcel, J. (2012). The spliceosome as a target of novel antitumour drugs. In *Nature Reviews Drug Discovery* (Vol. 11, Issue 11, pp. 847–859). https://doi.org/10.1038/nrd3823

Bray, F., Ferlay, J., Soerjomataram, I., Siegel, R. L., Torre, L. A., & Jemal, A. (2018). Global cancer statistics 2018: GLOBOCAN estimates of incidence and mortality worldwide for 36 cancers in 185 countries. *CA: A Cancer Journal for Clinicians*, *68*(6), 394–424. https://doi.org/10.3322/caac.21492

Brooks, A. N., Choi, P. S., De Waal, L., Sharifnia, T., Imielinski, M., Saksena, G., Sekhar, P. C., Sivachenko, A., Rosenberg, M., Chmielecki, J., Lawrence, M. S., DeLuca, D. S., Getz, G., & Meyerson, M. (2014). A pan-cancer analysis of transcriptome changes associated with somatic mutations in U2AF1 reveals commonly altered splicing events. *PLoS ONE*, *9*(1). https://doi.org/10.1371/journal.pone.0087361

Bubenik, J., Baresova, M., Viklick~~, V., Jakoubkova, J., Sainerova, H., & Donner, J. (1973). ESTABLISHED CELL LINE OF URINARY BLADDER CARCINOMA (T24) CONTAINING TUMOUR-SPECIFIC ANTIGEN. In *Int. J. Cancer* (Issue 11).

Byrne, A. T., Alférez, D. G., Amant, F., Annibali, D., Arribas, J., Biankin, A. V., Bruna, A., Budinská, E., Caldas, C., Chang, D. K., Clarke, R. B., Clevers, H., Coukos, G., Dangles-Marie, V., Gail Eckhardt, S., Gonzalez-Suarez, E., Hermans, E., Hidalgo, M., Jarzabek, M. A., … Trusolino, L. (2017). Interrogating open issues in cancer precision medicine with patient-derived xenografts. In *Nature Reviews Cancer* (Vol. 17, Issue 4, pp. 254–268). Nature Publishing Group. https://doi.org/10.1038/nrc.2016.140

Cairns, P., Mao, L., Merlo, A., Lee, D. J., Schwab, D., Eby, Y., Tokino, K., Van Der Riet, P., Blaugrund, J. E., Sidransky, D., Kamb, A., Liu, Q., Harshman, K., Tavtigian, S., Cordon-Cardo, C., & Skolnick, M. H. (1994). Rates of p16 (MTS1) mutations in primary tumors with 9p loss. In *Science* (Vol. 265, Issue 5170, pp. 415–417). https://doi.org/10.1126/science.8023167

Campbell, M. (1970). Natural history of atrial septal defect. In *British Heart Journal* (Vol. 32, 820-826).

Cancer, U. I. U. A. (2009). *TNM Classification of Malignant Tumours*.

Cappellen, D.; De Oliveira, C.; Ricol, D.; Gil, S., Bourdin, J., Sastre-Garau, X.; Chopin, D.; Thiery, J.P.; Radvanyi, F. (1999). Frequent activating mutations of FGFR3 in human bladder and cervix carcinomas. *Nature Genetics*, *23*, 18–19.

Carabuena, J. M. (2018). Atrial septal defect. In *Consults in Obstetric Anesthesiology* (pp. 75–76). Springer International Publishing. https://doi.org/10.1007/978-3-319-59680-8_18

Cattaneo, C. M., Dijkstra, K. K., Fanchi, L. F., Kelderman, S., Kaing, S., van Rooij, N., van den Brink, S., Schumacher, T. N., & Voest, E. E. (2020). Tumor organoid–T-cell coculture systems. *Nature Protocols*, *15*(1), 15–39. https://doi.org/10.1038/s41596-019-0232-9

Chakrabarti, J., Holokai, L., Syu, L. J., Steele, N., Chang, J., Dlugosz, A., & Zavros, Y. (2018). Mouse-Derived Gastric Organoid and Immune Cell Co-culture for the Study of the Tumor Microenvironment. In *Methods in Molecular Biology* (Vol. 1817, pp. 157–168). Humana Press Inc. https://doi.org/10.1007/978-1-4939-8600-2_16

Chen, G., Ning, B., & Shi, T. (2019). Single-cell RNA-seq technologies and related computational data analysis. In *Frontiers in Genetics* (Vol. 10, Issue APR). Frontiers Media S.A. https://doi.org/10.3389/fgene.2019.00317

Cheng, H. L., Liu, H. S., Lin, Y. J., Chen, H. H. W., Hsu, P. Y., Chang, T. Y., Ho, C. L., Tzai, T. S., & Chow, N. H. (2005). Co-expression of RON and MET is a prognostic indicator for patients with transitional-cell carcinoma of the bladder. *British Journal of Cancer*, *92*(10), 1906–1914. https://doi.org/10.1038/sj.bjc.6602593

Cheng, J., Huang, H., Zhang, Z.-T., Shapiro, E., Pellicer, A., Sun, T.-T., & Wu, X.-R. (2002). Overexpression of Epidermal Growth Factor Receptor in Urothelium Elicits Urothelial Hyperplasia and Promotes Bladder Tumor Growth 1. In *CANCER RESEARCH* (Vol. 62).

Cheng, L., Montironi, R., Davidson, D. D., & Lopez-Beltran, A. (2009). Staging and reporting of urothelial carcinoma of the urinary bladder. *Modern Pathology*, *22*, S70–S95. https://doi.org/10.1038/modpathol.2009.1

Choi, W., Porten, S., Kim, S., Willis, D., Plimack, E. R., Hoffman-Censits, J., Roth, B., Cheng, T., Tran, M., Lee, I. L., Melquist, J., Bondaruk, J., Majewski, T., Zhang, S., Pretzsch, S., Baggerly, K., Siefker-Radtke, A., Czerniak, B., Dinney, C. P. N., & McConkey, D. J. (2014). Identification of Distinct Basal and Luminal Subtypes of Muscle-Invasive Bladder Cancer with Different Sensitivities to Frontline Chemotherapy. *Cancer Cell*, *25*(2), 152–165. https://doi.org/10.1016/j.ccr.2014.01.009

Chu, P.-Y., Tai, Y.-L., & Shen, T.-L. (2019). Grb7, a Critical Mediator of EGFR/ErbB Signaling, in Cancer Development and as a Potential Therapeutic Target. *Cells*, *8*(5), 435. https://doi.org/10.3390/cells8050435

Collisson, E. A., Campbell, J. D., Brooks, A. N., Berger, A. H., Lee, W., Chmielecki, J., Beer, D. G., Cope, L., Creighton, C. J., Danilova, L., Ding, L., Getz, G., Hammerman, P. S., Hayes, D. N., Hernandez, B., Herman, J. G., Heymach, J. V., Jurisica, I., Kucherlapati, R., … Cheney, R. (2014). Comprehensive molecular profiling of lung adenocarcinoma: The cancer genome atlas research network. *Nature*, *511*(7511), 543–550. https://doi.org/10.1038/nature13385

Cooper, T. A., Wan, L., & Dreyfuss, G. (2009). *RNA and Disease*. Cell, 136(4), 777-793.

Corrigan, D. J., Luchsinger, L. L., De Almeida, M. J., Williams, L. J., Strikoudis, A., & Snoeck, H. W. (2018). PRDM16 isoforms differentially regulate normal and leukemic hematopoiesis and inflammatory gene signature. *Journal of Clinical Investigation*, *128*(8), 3250–3264. https://doi.org/10.1172/JCI99862

Corsini, L., Bonnal, S., Basquin, J., Hothorn, M., Scheffzek, K., Valcárcel, J., & Sattler, M. (2007). U2AF-homology motif interactions are required for alternative splicing regulation by SPF45. *Nature Structural and Molecular Biology*, *14*(7), 620–629. https://doi.org/10.1038/nsmb1260

CÔté, A., Fanous, A., Almajed, A., & Lacroix, Y. (2015). Pierre Robin sequence: Review of diagnostic and treatment challenges. In *International Journal of Pediatric Otorhinolaryngology* (Vol. 79, Issue 4, pp. 451–464). Elsevier Ireland Ltd. https://doi.org/10.1016/j.ijporl.2015.01.035

Crossley, P.H.; Martin, G. R. (1995). The mouse Fgf8 gene encodes a family of polypeptides and is expressed in regions that direct outgrowth and pattering in the developing embryo. *Development*, 439–451.

Cruzan, G., Bus, J., Banton, M., Gingell, R., & Carlson, G. (2009). Mouse specific lung tumors from CYP2F2-mediated cytotoxic metabolism: An endpoint/toxic response where data from multiple chemicals converge to support a mode of action. *Regulatory Toxicology and Pharmacology*, *55*(2), 205–218. https://doi.org/10.1016/j.yrtph.2009.07.002

Czerniak, B., Li, L., Chaturvedi, V., Ro, J. Y., Johnston, D. A., Hodges, S., & Benedict, W. F. (2000). Genetic Modeling of Human Urinary Bladder Carcinogenesis. In *Genes Chromosomes Cancer* (Vol. 27).

Damrauer, J. S., Hoadley, K. A., Chism, D. D., Fan, C., Tignanelli, C. J., Wobker, S. E., Yeh, J. J., Milowsky, M. I., Iyer, G., Parker, J. S., & Kim, W. Y. (2014). Intrinsic subtypes of high-grade bladder cancer reflect the hallmarks of breast cancer biology. *Proceedings of the National Academy of Sciences of the United States of America*, *111*(8), 3110–3115. https://doi.org/10.1073/pnas.1318376111

Darman, R. B., Seiler, M., Agrawal, A. A., Lim, K. H., Peng, S., Aird, D., Bailey, S. L., Bhavsar, E. B., Chan, B., Colla, S., Corson, L., Feala, J., Fekkes, P., Ichikawa, K., Keaney, G. F., Lee, L., Kumar, P., Kunii, K., MacKenzie, C., … Buonamici, S. (2015). Cancer-Associated SF3B1 Hotspot Mutations Induce Cryptic 3' Splice Site Selection through Use of a Different Branch Point. *Cell Reports*, *13*(5), 1033–1045. https://doi.org/10.1016/j.celrep.2015.09.053

David, C. J., & Manley, J. L. (2010). Alternative pre-mRNA splicing regulation in cancer: Pathways and programs unhinged. In *Genes and Development* (Vol. 24, Issue 21, pp. 2343–2364). https://doi.org/10.1101/gad.1973010

De La Peña, F. A., Kanasaki, K., Kanasaki, M., Tangirala, N., Maeda, G., & Kalluri, R. (2011). Loss of p53 and acquisition of angiogenic microRNA profile are insufficient to facilitate progression of bladder urothelial carcinoma in situ to invasive carcinoma. *Journal of Biological Chemistry*, *286*(23), 20778–20787. https://doi.org/10.1074/jbc.M110.198069

DeBoever, C., Ghia, E. M., Shepard, P. J., Rassenti, L., Barrett, C. L., Jepsen, K., Jamieson, C. H. M., Carson, D., Kipps, T. J., & Frazer, K. A. (2015). Transcriptome Sequencing Reveals Potential Mechanism of Cryptic 3' Splice Site Selection in SF3B1-mutated Cancers. *PLoS Computational Biology*, *11*(3). https://doi.org/10.1371/journal.pcbi.1004105

Deckert, J., Hartmuth, K., Boehringer, D., Behzadnia, N., Will, C. L., Kastner, B., Stark, H., Urlaub, H., & Luhrmann, R. (2006). Protein Composition and Electron Microscopy Structure of Affinity-Purified Human Spliceosomal B Complexes Isolated under Physiological Conditions. *Molecular and Cellular Biology*, *26*(14), 5528–5543. https://doi.org/10.1128/mcb.00582-06

Ding, J. H., Xu, X., Yang, D., Chu, P. H., Dalton, N. D., Ye, Z., Yeakley, J. M., Cheng, H., Xiao, R. P., Ross, J., Chen, J., & Fu, X. D. (2004). Dilated cardiomyopathy caused by tissue-specific ablation of SC35 in the heart. *EMBO Journal*, *23*(4), 885–896. https://doi.org/10.1038/sj.emboj.7600054

Dobbs, M. B., & Gurnett, C. A. (2017). The 2017 ABJS Nicolas Andry Award: Advancing Personalized Medicine for Clubfoot Through Translational Research. *Clinical Orthopaedics and Related Research*, *475*(6), 1716–1725. https://doi.org/10.1007/s11999-017-5290-0

Dobek, G. L., & Godbey, W. T. (2010). An orthotopic model of murine bladder cancer. *Journal of Visualized Experiments*, *48*. https://doi.org/10.3791/2535

Dobruch, J., Daneshmand, S., Fisch, M., Lotan, Y., Noon, A. P., Resnick, M. J., Shariat, S. F., Zlotta, A. R., & Boorjian, S. A. (2016). Gender and Bladder Cancer: A Collaborative Review of Etiology, Biology, and Outcomes. In *European Urology* (Vol. 69, Issue 2, pp. 300–310). Elsevier B.V. https://doi.org/10.1016/j.eururo.2015.08.037

Doherty, J. T., Conlon, F. L., Mack, C. P., & Taylor, J. M. (2010). Focal adhesion kinase is essential for cardiac looping and multichamber heart formation. *Genesis*, *48*(8), 492–504. https://doi.org/10.1002/dvg.20650

Donohower, L.A.; Harvey, M.; Slagle, B.L; McArthur, M.J.; Montgomery, C.A.; Butel, J.S.; Bradley, A. (1992). Mice deficient for p53 are developmentally normal but susceptible to spontaneous tumors. *Nature*, *356*(19), 215–221.

Drost, J., Van Jaarsveld, R. H., Ponsioen, B., Zimberlin, C., Van Boxtel, R., Buijs, A., Sachs, N., Overmeer, R. M., Offerhaus, G. J., Begthel, H., Korving, J., Van De Wetering, M., Schwank, G., Logtenberg, M., Cuppen, E., Snippert, H. J., Medema, J. P., Kops, G. J. P. L., & Clevers, H. (2015). Sequential cancer mutations in cultured human intestinal stem cells. *Nature*, *521*(7550), 43–47. https://doi.org/10.1038/nature14415

Duarte, A. A., Gogola, E., Sachs, N., Barazas, M., Annunziato, S., R De Ruiter, J., Velds, A., Blatter, S., Houthuijzen, J. M., Van De Ven, M., Clevers, H., Borst, P., Jonkers, J., & Rottenberg, S. (2018). BRCA-deficient mouse mammary tumor organoids to study cancer-drug resistance. *Nature Methods*, *15*(2), 134–140. https://doi.org/10.1038/nmeth.4535

Earl, J., Rico, D., Carrillo-de-Santa-Pau, E., Rodríguez-Santiago, B., Méndez-Pertuz, M., Auer, H., Gómez, G., Grossman, H. B., Pisano, D. G., Schulz, W. A., Pérez-Jurado, L. A., Carrato, A., Theodorescu, D., Chanock, S., Valencia, A., & Real, F. X. (2015). The UBC-40 Urothelial Bladder Cancer cell line index: A genomic resource for functional studies. *BMC Genomics*, *16*(1). https://doi.org/10.1186/s12864-015-1450-3

Ersig, D., Elmajian, D., Groshen, S., Freeman, J., Stein, J., Chen, S., Nichols, P.; Skinner, D., Jones, P.A., Cote, R. J. (1994). Accumulation of nuclear p53 and tumor progression in bladder cancer. *The New England Journal of Medicine*, *331*(19), 1259–1264.

Eswarakumar, V. P., Lax, I., & Schlessinger, J. (2005). Cellular signaling by fibroblast growth factor receptors. *Cytokine and Growth Factor Reviews*, *16*(2 SPEC. ISS.), 139–149. https://doi.org/10.1016/j.cytogfr.2005.01.001

Fei, L. R., Huang, W. J., Wang, Y., Lei, L., Li, Z. H., Zheng, Y. W., Wang, Z., Yang, M. Q., Liu, C. C., & Xu, H. T. (2019). PRDM16 functions as a suppressor of lung

adenocarcinoma metastasis. *Journal of Experimental and Clinical Cancer Research*, *38*(1). https://doi.org/10.1186/s13046-019-1042-1

Feng, L., Gu, C., Jia, M., Wu, T., Sun, W., & Sun, X. (2018). Functional role of RBM10 in lung adenocarcinoma proliferation. *International Journal of Oncology*. https://doi.org/10.3892/ijo.2018.4643

Feng, X., Yan, N., Sun, W., Zheng, S., Jiang, S., Wang, J., Guo, C., Hao, L., Tian, Y., Liu, S., & Sun, M. Z. (2019). miR-4521-FAM129A axial regulation on ccRCC progression through TIMP-1/MMP2/MMP9 and MDM2/p53/Bcl2/Bax pathways. *Cell Death Discovery*, *5*(1). https://doi.org/10.1038/s41420-019-0167-5

Ferreira, P. G., Jares, P., Rico, D., Gómez-López, G., Martínez-Trillos, A., Villamor, N., Ecker, S., González-Pérez, A., Knowles, D. G., Monlong, J., Johnson, R., Quesada, V., Djebali, S., Papasaikas, P., López-Guerra, M., Colomer, D., Royo, C., Cazorla, M., Pinyol, M., … Guigó, R. (2014). Transcriptome characterization by RNA sequencing identifies a major molecular and clinical subdivision in chronic lymphocytic leukemia. *Genome Research*, *24*(2), 212–226. https://doi.org/10.1101/gr.152132.112

Filippini, D., Agosto, S. D., Delfino, P., Simbolo, M., Piro, G., Rusev, B., Veghini, L., Cantù, C., Lupo, F., Ugel, S., De Sanctis, F., Bronte, V., Milella, M., Tortora, G., Scarpa, A., Carbone, C., & Corbo, V. (2019). Immunoevolution of mouse pancreatic organoid isografts from preinvasive to metastatic disease. *Scientific Reports*, *9*(1), 12286. https://doi.org/10.1038/s41598-019-48663-7

Fleischmann, A., Rotzer, D., Seiler, R., Studer, U. E., & Thalmann, G. N. (2011). Her2 amplification is significantly more frequent in lymph node metastases from urothelial bladder cancer than in the primary tumours. *European Urology*, *60*(2), 350–357. https://doi.org/10.1016/j.eururo.2011.05.035

Fletcher, R. B., Baker, J. C., & Harland, R. M. (2006). FGF8 spliceforms mediate early mesoderm and posterior neural tissue formation in Xenopus. *Development*, *133*(9), 1703–1714. https://doi.org/10.1242/dev.02342

Font, A., Domènech, M., Benítez, R., Rava, M., Marqués, M., Ramírez, J. L., Pineda, S., Domínguez-Rodríguez, S., Gago, J. L., Badal, J., Carrato, C., López, H., Quer, A., Castellano, D., Malats, N., & Real, F. X. (2020). Immunohistochemistry-based taxonomical classification of bladder cancer predicts response to neoadjuvant chemotherapy. *Cancers*, *12*(7), 1–13. https://doi.org/10.3390/cancers12071784

Frank, D. U., Fotheringham, L. K., Brewer, J. A., Muglia, L. J., Tristani-Firouzi, M., Capecchi, M. R., & Moon, A. M. (2002). An Fgf8 Mouse Mutant Phenocopies Human 22q11 Deletion Syndrome NIH Public Access. In *Development* (Vol. 129).

Gao, J., Huang, H. Y., Pak, J., Cheng, J., Zhang, Z. T., Shapiro, E., Pellicer, A., Sun, T. T., & Wu, X. R. (2004). p53 deficiency provokes urothelial proliferation and synergizes with activated Ha-ras in promoting urothelial tumorigenesis. *Oncogene*, *23*(3), 687–696. https://doi.org/10.1038/sj.onc.1207169

Garcia-España, A., Salazar, E., Sun, T.-T., Wu, X.-R., & Pellicer, A. (2005). Differential Expression of Cell Cycle Regulators in Phenotypic Variants of Transgenically Induced Bladder Tumors: Implications for Tumor Behavior. In *Cancer Res* (Vol. 65, Issue 4). www.aacrjournals.org

Gilbert, W. (1978). Why genes in pieces? *Nature*, *271*(9), 501.

Gilmour, D., Rembold, M., & Leptin, M. (2017). From morphogen to morphogenesis and back. In *Nature* (Vol. 541, Issue 7637, pp. 311–320). Nature Publishing Group. https://doi.org/10.1038/nature21348

Gittenberger-De Groot, A. C., Calkoen, E. E., Poelmann, R. E., Bartelings, M. M., & Jongbloed, M. R. M. (2014). Morphogenesis and molecular considerations on congenital cardiac septal defects. In *Annals of Medicine* (Vol. 46, Issue 8, pp. 640–652). Informa Healthcare. https://doi.org/10.3109/07853890.2014.959557

Giudice, A., Barone, S., Belhous, K., Morice, A., Soupre, V., Bennardo, F., Boddaert, N., Vazquez, M. P., Abadie, V., & Picard, A. (2018). Pierre Robin sequence: A comprehensive narrative review of the literature over time. In *Journal of Stomatology, Oral and Maxillofacial Surgery* (Vol. 119, Issue 5, pp. 419–428). Elsevier Masson SAS. https://doi.org/10.1016/j.jormas.2018.05.002

Glisovic, T., Bachorik, J. L., Yong, J., & Dreyfuss, G. (n.d.). *RNA-binding proteins and post-transcriptional gene regulation*.

Godwin, J. L., Hoffman-Censits, J., & Plimack, E. (2018). Recent developments in the treatment of advanced bladder cancer. In *Urologic Oncology: Seminars and Original Investigations* (Vol. 36, Issue 3, pp. 109–114). Elsevier Inc. https://doi.org/10.1016/j.urolonc.2017.12.018

Goyal, S. K., Punnam, S. R., Verma, G., & Ruberg, F. L. (2008). Persistent left superior vena cava: A case report and review of literature. *Cardiovascular Ultrasound*, *6*. https://doi.org/10.1186/1476-7120-6-50

Grabowski, P. (2011). Alternative splicing takes shape during neuronal development. In *Current Opinion in Genetics and Development* (Vol. 21, Issue 4, pp. 388–394). https://doi.org/10.1016/j.gde.2011.03.005

Graziotto, J. J., Farkas, M. H., Bujakowska, K., Deramaudt, B. M., Zhang, Q., Nandrot, E. F., Inglehearn, C. F., Bhattacharya, S. S., & Pierce, E. A. (2011). Three gene-targeted mouse models of RNA splicing factor RP show late-onset RPE and retinal degeneration. *Investigative Ophthalmology and Visual Science*, *52*(1), 190–198. https://doi.org/10.1167/iovs.10-5194

Gripp, K. W., Hopkins, E., Johnston, J. J., Krause, C., Dobyns, W. B., & Biesecker, L. G. (2011). Long-term survival in TARP syndrome and confirmation of RBM10 as the disease-causing gene. *American Journal of Medical Genetics, Part A*, *155*(10), 2516–2520. https://doi.org/10.1002/ajmg.a.34190

Grippo, P. J., & Sandgren, E. P. (n.d.). *Highly Invasive Transitional Cell Carcinoma of the Bladder in a Simian Virus 40 T-Antigen Transgenic Mouse Model*.

Gü Nther, J. H., Jurczok, A., Wulf, T., Brandau, S., Deinert, I., Jocham, D., & Böhle, A. (1999). Optimizing Syngeneic Orthotopic Murine Bladder Cancer (MB49) 1. In *CANCER RESEARCH* (Vol. 59).

Habuchi, T., Luscombe, M., Elder, P. A., & Knowles, M. A. (1998). Structure and Methylation-Based Silencing of a Gene (DBCCR1) within a Candidate Bladder Cancer Tumor Suppressor Region at 9q32-q33. In *GENOMICS* (Vol. 48).

Haferlach, T., Nagata, Y., Grossmann, V., Okuno, Y., Bacher, U., Nagae, G., Schnittger, S., Sanada, M., Kon, A., Alpermann, T., Yoshida, K., Roller, A., Nadarajah, N., Shiraishi, Y., Shiozawa, Y., Chiba, K., Tanaka, H., Koeffler, H. P., Klein, H. U., … Ogawa, S. (2014). Landscape of genetic lesions in 944 patients with myelodysplastic syndromes. *Leukemia*, *28*(2), 241–247. https://doi.org/10.1038/leu.2013.336

Han, H., Braunschweig, U., Gonatopoulos-Pournatzis, T., Weatheritt, R. J., Hirsch, C. L., Ha, K. C. H., Radovani, E., Nabeel-Shah, S., Sterne-Weiler, T., Wang, J., O'Hanlon, D., Pan, Q., Ray, D., Zheng, H., Vizeacoumar, F., Datti, A., Magomedova, L., Cummins, C. L., Hughes, T. R., … Blencowe, B. J. (2017). Multilayered Control of Alternative Splicing Regulatory Networks by Transcription Factors. *Molecular Cell*, *65*(3), 539-553.e7. https://doi.org/10.1016/j.molcel.2017.01.011

Hao, Y., Tang, S., Yuan, Y., Liu, R., & Chen, Q. (2019). Roles of FGF8 subfamily in embryogenesis and oral-maxillofacial diseases (Review). In *International Journal of Oncology* (Vol. 54, Issue 3, pp. 797–806). Spandidos Publications. https://doi.org/10.3892/ijo.2019.4677

Hao, Y. Q., Su, Z. Z., Lv, X. J., Li, P., Gao, P., Wang, C., Bai, Y., & Zhang, J. (2015). RNA-binding motif protein 5 negatively regulates the activity of Wnt/β-catenin signaling in cigarette smoke-induced alveolar epithelial injury. *Oncology Reports*, *33*(5), 2438–2444. https://doi.org/10.3892/or.2015.3828

Hartmann, A., Schlake, G., Zaak, D., Hungerhuber, E., Hofstetter, A., Hofstaedter, F., & Knuechel, R. (2002). Occurrence of Chromosome 9 and p53 Alterations in Multifocal Dysplasia and Carcinoma in Situ of Human Urinary Bladder 1. In *CANCER RESEARCH* (Vol. 62). www.iarc.fr.

He, C., Zhou, F., Zuo, Z., Cheng, H., & Zhou, R. (2009). A global view of cancer-specific transcript variants by subtractive transcriptome-wide analysis. *PLoS ONE*, *4*(3). https://doi.org/10.1371/journal.pone.0004732

Hedegaard, J., Lamy, P., Nordentoft, I., Algaba, F., Høyer, S., Ulhøi, B. P., Vang, S., Reinert, T., Hermann, G. G., Mogensen, K., Thomsen, M. B. H., Nielsen, M. M., Marquez, M., Segersten, U., Aine, M., Höglund, M., Birkenkamp-Demtröder, K., Fristrup, N., Borre, M., … Dyrskjøt, L. (2016). Comprehensive Transcriptional Analysis of Early-Stage Urothelial Carcinoma. *Cancer Cell*, *30*(1), 27–42. https://doi.org/10.1016/j.ccell.2016.05.004

Hegele, A., Kamburov, A., Grossmann, A., Sourlis, C., Wowro, S., Weimann, M., Will, C. L., Pena, V., Lührmann, R., & Stelzl, U. (2012). Dynamic Protein-Protein Interaction Wiring of the Human Spliceosome. *Molecular Cell*, *45*(4), 567–580. https://doi.org/10.1016/j.molcel.2011.12.034

Hernández, J., Bechara, E., Schlesinger, D., Delgado, J., Serrano, L., & Valcárcel, J. (2016). Tumor suppressor properties of the splicing regulatory factor RBM10. *RNA Biology*, *13*(4), 466–472. https://doi.org/10.1080/15476286.2016.1144004

Hernández, S., López-Knowles, E., Lloreta, J., Kogevinas, M., Amorós, A., Tardón, A., Carrato, A., Serra, C., Malats, N., & Real, F. X. (2006). Prospective study of FGFR3 mutations as a prognostic factor in nonmuscle invasive urothelial bladder

carcinomas. *Journal of Clinical Oncology*, *24*(22), 3664–3671. https://doi.org/10.1200/JCO.2005.05.1771

Hicks, M. J., Mueller, W. F., Shepard, P. J., & Hertel, K. J. (2010). Competing Upstream 5' Splice Sites Enhance the Rate of Proximal Splicing. *Molecular and Cellular Biology*, *30*(8), 1878–1886. https://doi.org/10.1128/mcb.01071-09

Hidalgo, M., Amant, F., Biankin, A. V., Budinská, E., Byrne, A. T., Caldas, C., Clarke, R. B., de Jong, S., Jonkers, J., Mælandsmo, G. M., Roman-Roman, S., Seoane, J., Trusolino, L., & Villanueva, A. (2014). Patient-derived Xenograft models: An emerging platform for translational cancer research. *Cancer Discovery*, *4*(9), 998–1013. https://doi.org/10.1158/2159-8290.CD-14-0001

Hoadley, K. A., Yau, C., Hinoue, T., Wolf, D. M., Lazar, A. J., Drill, E., Shen, R., Taylor, A. M., Cherniack, A. D., Thorsson, V., Akbani, R., Bowlby, R., Wong, C. K., Wiznerowicz, M., Sanchez-Vega, F., Robertson, A. G., Schneider, B. G., Lawrence, M. S., Noushmehr, H., … Laird, P. W. (2018). Cell-of-Origin Patterns Dominate the Molecular Classification of 10,000 Tumors from 33 Types of Cancer. *Cell*, *173*(2), 291-304.e6. https://doi.org/10.1016/j.cell.2018.03.022

Højland, A. T., Lolas, I., Okkels, H., Lautrup, C. K., Diness, B. R., Petersen, M. B., & Nielsen, I. K. (2018). First reported adult patient with TARP syndrome: A case report. *American Journal of Medical Genetics, Part A*, *176*(12), 2915–2918. https://doi.org/10.1002/ajmg.a.40638

Hu, J. L., Todhunter, M. E., LaBarge, M. A., & Gartner, Z. J. (2018). Opportunities for organoids as new models of aging. *Journal of Cell Biology*, *217*(1), 39–50. https://doi.org/10.1083/jcb.201709054

Huan, W., Zhang, J., Li, Y., & Zhi, K. (2019). Involvement of DHX9/YB-1 complex induced alternative splicing of Krüppel-like factor 5 mRNA in phenotypic transformation of vascular smooth muscle cells. *Am J Physiol Cell Physiol*, *317*, 262–269. https://doi.org/10.1152/ajpcell.00067.2019.-Phenotypic

Huang, L., Holtzinger, A., Jagan, I., Begora, M., Lohse, I., Ngai, N., Nostro, C., Wang, R., Muthuswamy, L. B., Crawford, H. C., Arrowsmith, C., Kalloger, S. E., Renouf, D. J., Connor, A. A., Cleary, S., Schaeffer, D. F., Roehrl, M., Tsao, M. S., Gallinger, S., … Muthuswamy, S. K. (2015). Ductal pancreatic cancer modeling and drug screening using human pluripotent stem cell- and patient-derived tumor organoids. *Nature Medicine*, *21*(11), 1364–1371. https://doi.org/10.1038/nm.3973

Huch, M., Dorrell, C., Boj, S. F., Van Es, J. H., Li, V. S. W., Van De Wetering, M., Sato, T., Hamer, K., Sasaki, N., Finegold, M. J., Haft, A., Vries, R. G., Grompe, M., & Clevers, H. (2013). In vitro expansion of single Lgr5 + liver stem cells induced by Wnt-driven regeneration. *Nature*, *494*(7436), 247–250. https://doi.org/10.1038/nature11826

Huch, M., & Koo, B. K. (2015). Modeling mouse and human development using organoid cultures. In *Development (Cambridge)* (Vol. 142, Issue 18, pp. 3113–3125). Company of Biologists Ltd. https://doi.org/10.1242/dev.118570

Humphrey, P. A., Moch, H., Cubilla, A. L., Ulbright, T. M., & Reuter, V. E. (2016). The 2016 WHO Classification of Tumours of the Urinary System and Male Genital

Organs—Part B: Prostate and Bladder Tumours. *European Urology*, *70*(1), 106–119. https://doi.org/10.1016/j.eururo.2016.02.028

Hung, K.-Y., & Tarn, W.-Y. (2018). *RBM4 Modulates Radial Migration via Alternative Splicing of Dab1 during Cortex Development*. https://doi.org/10

Hurst, C. D., Alder, O., Platt, F. M., Droop, A., Stead, L. F., Burns, J. E., Burghel, G. J., Jain, S., Klimczak, L. J., Lindsay, H., Roulson, J. A., Taylor, C. F., Thygesen, H., Cameron, A. J., Ridley, A. J., Mott, H. R., Gordenin, D. A., & Knowles, M. A. (2017). Genomic Subtypes of Non-invasive Bladder Cancer with Distinct Metabolic Profile and Female Gender Bias in KDM6A Mutation Frequency. *Cancer Cell*, *32*(5), 701-715.e7. https://doi.org/10.1016/j.ccell.2017.08.005

Hurst, C. D., Platt, F. M., & Knowles, M. A. (2014). Comprehensive mutation analysis of the TERT promoter in bladder cancer and detection of mutations in voided urine. In *European Urology* (Vol. 65, Issue 2, pp. 367–369). https://doi.org/10.1016/j.eururo.2013.08.057

Hurst, C. D., Platt, F. M., Taylor, C. F., & Knowles, M. A. (2012). Novel tumor subgroups of urothelial carcinoma of the bladder defined by integrated genomic analysis. *Clinical Cancer Research*, *18*(21), 5865–5877. https://doi.org/10.1158/1078-0432.CCR-12-1807

Imagawa, E., Konuma, T., Cork, E. E., Diaz, G. A., & Oishi, K. (2020). A novel missense variant in RBM10 can cause a mild form of TARP syndrome with developmental delay and dysmorphic features. *Clinical Genetics*. https://doi.org/10.1111/cge.13835

Imaizumi, K., Fujimori, K., Ishii, S., Otomo, A., Hosoi, Y., Miyajima, H., Warita, H., Aoki, M., Hadano, S., Akamatsu, W., & Okano, H. (2018). Rostrocaudal areal patterning of human PSC-derived cortical neurons by FGF8 signaling. *ENeuro*, *5*(2). https://doi.org/10.1523/ENEURO.0368-17.2018

Inoue, A., Paulo Takahashi, K., Kimura, M., Watanabe, T., & Morisawa, S. (1996). Molecular cloning of a RNA binding protein, S1-1. In *Nucleic Acids Research* (Vol. 24, Issue 15).

Inoue, A., Yamamoto, N., Kimura, M., Nishio, K., Yamane, H., & Nakajima, K. (2014). RBM10 regulates alternative splicing. *FEBS Letters*, *588*(6), 942–947. https://doi.org/10.1016/j.febslet.2014.01.052

Inoue, F., Nagayoshi, S., Ota, S., Islam, M. E., Tonou-Fujimori, N., Odaira, Y., Kawakami, K., & Yamasu, K. (2006). Genomic organization, alternative splicing, and multiple regulatory regions of the zebrafish fgf8 gene. *Development Growth and Differentiation*, *48*(7), 447–462. https://doi.org/10.1111/j.1440-169X.2006.00882.x

Irimia, M., Penny, D., & Roy, S. W. (2007). Coevolution of genomic intron number and splice sites. In *Trends in Genetics* (Vol. 23, Issue 7, pp. 321–325). https://doi.org/10.1016/j.tig.2007.04.001

Jabs, J., Zickgraf, F. M., Park, J., Wagner, S., Jiang, X., Jechow, K., Kleinheinz, K., Toprak, U. H., Schneider, M. A., Meister, M., Spaich, S., Sütterlin, M., Schlesner, M., Trumpp, A., Sprick, M., Eils, R., & Conrad, C. (2017). Screening drug effects in

patient-derived cancer cells links organoid responses to genome alterations. *Molecular Systems Biology*, *13*(11), 955. https://doi.org/10.15252/msb.20177697

Jacks, T., Fazeli, A., Schmitt, E. M., Bronsont, R. T., Goodell, M. A., & Weinberg, R. A. (1992). *Effects of an Rb mutation in the mouse*.

James, C. G., Ulici, V., Tuckermann, J., Michael, T. M., & Beier, F. (2007). Expression profiling of Dexamethasone-treated primary chondrocytes identifies targets of glucocorticoid signalling in endochondral bone development. *BMC Genomics*, *8*. https://doi.org/10.1186/1471-2164-8-205

Jensen, B., Wang, T., & Moorman, A. F. M. (2019). Evolution and Development of the Atrial Septum. *Anatomical Record*, *302*(1), 32–48. https://doi.org/10.1002/ar.23914

Jeromin, S., Weissmann, S., Haferlach, C., Dicker, F., Bayer, K., Grossmann, V., Alpermann, T., Roller, A., Kohlmann, A., Haferlach, T., Kern, W., & Schnittger, S. (2014). SF3B1 mutations correlated to cytogenetics and mutations in NOTCH1, FBXW7, MYD88, XPO1 and TP53 in 1160 untreated CLL patients. *Leukemia*, *28*(1), 108–117. https://doi.org/10.1038/leu.2013.263

Jiang, L., Liu, L., Zhang, J., Chen, Y., Liu, B., Tang, N., Ji, Y., Yu, L., Luo, L., Xie, S., Li, L., & Zhang, Y. (2017). Increased cell apoptosis in human lung adenocarcinoma and in vivo tumor growth inhibition by RBM10, a tumor suppressor gene. *Oncology Letters*, *14*(4), 4663–4669. https://doi.org/10.3892/ol.2017.6765

Johnston, J. J., Sapp, J. C., Curry, C., Horton, M., Leon, E., Cusmano-Ozog, K., Dobyns, W. B., Hudgins, L., Zackai, E., & Biesecker, L. G. (2014). Expansion of the TARP syndrome phenotype associated with de novo mutations and mosaicism. *American Journal of Medical Genetics, Part A*, *164*(1), 120–128. https://doi.org/10.1002/ajmg.a.36212

Johnston, J. J., Teer, J. K., Cherukuri, P. F., Hansen, N. F., Loftus, S. K., Chong, K., Mullikin, J. C., & Biesecker, L. G. (2010). Massively Parallel Sequencing of Exons on the X Chromosome Identifies RBM10 as the Gene that Causes a Syndromic Form of Cleft Palate. *American Journal of Human Genetics*, *86*(5), 743–748. https://doi.org/10.1016/j.ajhg.2010.04.007

Juanpere, N., Agell, L., Lorenzo, M., De Muga, S., López-Vilaró, L., Murillo, R., Mojal, S., Serrano, S., Lorente, J. A., Lloreta, J., & Hernández, S. (2012). Mutations in FGFR3 and PIK3CA, singly or combined with RAS and AKT1, are associated with AKT but not with MAPK pathway activation in urothelial bladder cancer. *Human Pathology*, *43*(10), 1573–1582. https://doi.org/10.1016/j.humpath.2011.10.026

Kaeppler, K. E., Stetson, R. C., Lanpher, B. C., & Collura, C. A. (2018). Infant male with TARP syndrome: Review of clinical features, prognosis, and commonalities with previously reported patients. *American Journal of Medical Genetics, Part A*, *176*(12), 2911–2914. https://doi.org/10.1002/ajmg.a.40645

Kahles, A., Lehmann, K. Van, Toussaint, N. C., Hüser, M., Stark, S. G., Sachsenberg, T., Stegle, O., Kohlbacher, O., Sander, C., Caesar-Johnson, S. J., Demchok, J. A., Felau, I., Kasapi, M., Ferguson, M. L., Hutter, C. M., Sofia, H. J., Tarnuzzer, R., Wang, Z., Yang, L., … Rätsch, G. (2018). Comprehensive Analysis of

Alternative Splicing Across Tumors from 8,705 Patients. *Cancer Cell*. https://doi.org/10.1016/j.ccell.2018.07.001

Kamat, A. M., Hahn, N. M., Efstathiou, J. A., Lerner, S. P., Malmström, P. U., Choi, W., Guo, C. C., Lotan, Y., & Kassouf, W. (2016). Bladder cancer. In *The Lancet* (Vol. 388, Issue 10061, pp. 2796–2810). Lancet Publishing Group. https://doi.org/10.1016/S0140-6736(16)30512-8

Kamoun, A., de Reyniès, A., Allory, Y., Sjödahl, G., Robertson, A. G., Seiler, R., Hoadley, K. A., Groeneveld, C. S., Al-Ahmadie, H., Choi, W., Castro, M. A. A., Fontugne, J., Eriksson, P., Mo, Q., Kardos, J., Zlotta, A., Hartmann, A., Dinney, C. P., Bellmunt, J., … Weinstein, J. (2020). A Consensus Molecular Classification of Muscle-invasive Bladder Cancer[Formula presented]. *European Urology*, *77*(4), 420–433. https://doi.org/10.1016/j.eururo.2019.09.006

Kassouf, W., Black, P. C., Tuziak, T., Bondaruk, J., Lee, S., Brown, G. A., Adam, L., Wei, C., Baggerly, K., Bar-Eli, M., McConkey, D., Czerniak, B., & Dinney, C. P. (2008). Distinctive Expression Pattern of ErbB Family Receptors Signifies an Aggressive Variant of Bladder Cancer. *Journal of Urology*, *179*(1), 353–358. https://doi.org/10.1016/j.juro.2007.08.087

Kaufman, M. H., & Richardson, L. (2005). 3D reconstruction of the vessels that enter the right atrium of the mouse heart at Theiler Stage 20. *Clinical Anatomy*, *18*(1), 27–38. https://doi.org/10.1002/ca.10242

Kelemen, O., Convertini, P., Zhang, Z., Wen, Y., Shen, M., Falaleeva, M., & Stamm, S. (2013). Function of alternative splicing. In *Gene* (Vol. 514, Issue 1, pp. 1–30). https://doi.org/10.1016/j.gene.2012.07.083

Kersten, K., Visser, K. E., Miltenburg, M. H., & Jonkers, J. (2017). Genetically engineered mouse models in oncology research and cancer medicine. *EMBO Molecular Medicine*, *9*(2), 137–153. https://doi.org/10.15252/emmm.201606857

Kinde, I., Munari, E., Faraj, S. F., Hruban, R. H., Schoenberg, M., Bivalacqua, T., Allaf, M., Springer, S., Wang, Y., Diaz, L. A., Kinzler, K. W., Vogelstein, B., Papadopoulos, N., & Netto, G. J. (2013). TERT promoter mutations occur early in urothelial neoplasia and are biomarkers of early disease and disease recurrence in urine. *Cancer Research*, *73*(24), 7162–7167. https://doi.org/10.1158/0008-5472.CAN-13-2498

Klinck, R., Bramard, A., Inkel, L., Dufresne-Martin, G., Gervais-Bird, J., Madden, R., Paquet, É. R., Koh, C. S., Venables, J. P., Prinos, P., Jilaveanu-Pelmus, M., Wellinger, R., Rancourt, C., Chabot, B., & Elela, S. A. (2008). Multiple alternative splicing markers for ovarian cancer. *Cancer Research*, *68*(3), 657–663. https://doi.org/10.1158/0008-5472.CAN-07-2580

Knowles, M. A., & Hurst, C. D. (2015). Molecular biology of bladder cancer: New insights into pathogenesis and clinical diversity. In *Nature Reviews Cancer* (Vol. 15, Issue 1, pp. 25–41). Nature Publishing Group. https://doi.org/10.1038/nrc3817

Kompier, L. C., Lurkin, I., van der Aa, M. N. M., van Rhijn, B. W. G., van der Kwast, T. H., & Zwarthoff, E. C. (2010). FGFR3, HRAS, KRAS, NRAS AND PIK3CA mutations in bladder cancer and their potential as biomarkers for surveillance and therapy. *PLoS ONE*, *5*(11). https://doi.org/10.1371/journal.pone.0013821

Kong, X., Ball, A. R., Pham, H. X., Zeng, W., Chen, H.-Y., Schmiesing, J. A., Kim, J.-S., Berns, M., & Yokomori, K. (2014). Distinct Functions of Human Cohesin-SA1 and Cohesin-SA2 in Double-Strand Break Repair. *Molecular and Cellular Biology*, *34*(4), 685–698. https://doi.org/10.1128/mcb.01503-13

Krüger, S., Weitsch, G., Büttner, H., Matthiensen, A., Böhmer, T., Marquardt, T., Sayk, F., Feller, A. C., & Böhle, A. (2002). HER2 overexpression in muscle-invasive urothelial carcinoma of the bladder: Prognostic implications. *International Journal of Cancer*, *102*(5), 514–518. https://doi.org/10.1002/ijc.10731

Kunimoto, H., Inoue, A., Kojima, H., Yang, J., Zhao, H., Tsuruta, D., & Nakajima, K. (2020). RBM10 regulates centriole duplication in HepG2 cells by ectopically assembling PLK4-STIL complexes in the nucleus. *Genes to Cells*, *25*(2), 100–110. https://doi.org/10.1111/gtc.12741

Kurokawa, K., Akaike, Y., Masuda, K., Kuwano, Y., Nishida, K., Yamagishi, N., Kajita, K., Tanahashi, T., & Rokutan, K. (2014). Down-regulation of serine/arginine-rich splicing factor 3 induces G1 cell cycle arrest and apoptosis in colon cancer cells. *Oncogene*, *33*(11), 1407–1417. https://doi.org/10.1038/onc.2013.86

Kurpinski, K. T., Magyari, P. A., Gorlin, R. J., Ng, D., & Biesecker, L. G. (2003). Designation of the TARP syndrome and linkage to Xp11.23-q13.3 without samples from affected patients. *American Journal of Medical Genetics*, *120A*(1), 1–4. https://doi.org/10.1002/ajmg.a.10201

Lapointe, E., Roy, J. G., Chabot, B., Klinck, R., Hunt, S. C., Durand, M., Ybazeta, G., Knee, J. M., Loiselle, J. J., Stein, L., Tessier, S. J., Beauvais, A., Sutherland, L. C., Kalatskaya, I., Thibault, P., & Kothary, R. (2017). Splicing arrays reveal novel RBM10 targets, including SMN2 pre-mRNA. *BMC Molecular Biology*, *18*(1). https://doi.org/10.1186/s12867-017-0096-x

Lapuk, A. V., Volik, S. V., Wang, Y., & Collins, C. C. (2014). The role of mRNA splicing in prostate cancer. In *Asian Journal of Andrology* (Vol. 16, Issue 4, pp. 515–521). Medknow Publications. https://doi.org/10.4103/1008-682X.127825

Lawson, A. R. J., Abascal, F., Coorens, T. H. H., Hooks, Y., O'neill, L., Latimer, C., Raine, K., Sanders, M. A., Warren, A. Y., Mahbubani, K. T. A., Bareham, B., Butler, T. M., Harvey, L. M. R., Cagan, A., Menzies, A., Moore, L., Colquhoun, A. J., Turner, W., Thomas, B., … Martincorena, I. (2020). Extensive heterogeneity in somatic mutation and selection in the human bladder. *Science*, *370*, 75–82. http://science.sciencemag.org/

Lee, S. H., Hu, W., Matulay, J. T., Silva, M. V., Owczarek, T. B., Kim, K., Chua, C. W., Barlow, L. M. J., Kandoth, C., Williams, A. B., Bergren, S. K., Pietzak, E. J., Anderson, C. B., Benson, M. C., Coleman, J. A., Taylor, B. S., Abate-Shen, C., McKiernan, J. M., Al-Ahmadie, H., … Shen, M. M. (2018). Tumor Evolution and Drug Response in Patient-Derived Organoid Models of Bladder Cancer. *Cell*, *173*(2), 515-528.e17. https://doi.org/10.1016/j.cell.2018.03.017

Leoni, G., Le Pera, L., Ferrè, F., Raimondo, D., & Tramontano, A. (2011). Coding potential of the products of alternative splicing in human. *Genome Biology*, *12*(1). https://doi.org/10.1186/gb-2011-12-1-r9

Lerner, S. P., & Robertson, A. G. (2016). Molecular Subtypes of Non-muscle Invasive Bladder Cancer. In *Cancer Cell* (Vol. 30, Issue 1, pp. 1–3). Cell Press. https://doi.org/10.1016/j.ccell.2016.06.012

Lewandoski, M., Sun, X., & Martin, G. R. (2000). *Fgf8 signalling from the AER is essential for normal limb development*. http://genetics.nature.com/supplementary_info/

Li, J., & Yu, P. (2018). Genome-wide transcriptome analysis identifies alternative splicing regulatory network and key splicing factors in mouse and human psoriasis. *Scientific Reports*, *8*(1). https://doi.org/10.1038/s41598-018-22284-y

Li, Z., Xue, Q., Xu, J., Zhang, P., & Ding, B. (2020). The role of RBM10 mutations in the development, treatment, and prognosis of lung adenocarcinoma. *Cell Cycle*. https://doi.org/10.1080/15384101.2020.1829801

Lin, C., Yin, Y., Stemler, K., Humphrey, P., Kibel, A. S., Mysorekar, I. U., & Ma, L. (2013). Constitutive β-catenin activation induces male-specific tumorigenesis in the bladder urothelium. *Cancer Research*, *73*(19), 5914–5925. https://doi.org/10.1158/0008-5472.CAN-12-4198

Lindgren, D., Sjödahl, G., Lauss, M., Staaf, J., Chebil, G., Lövgren, K., Gudjonsson, S., Liedberg, F., Patschan, O., Månsson, W., Fernö, M., & Höglund, M. (2012). Integrated genomic and gene expression profiling identifies two major genomic circuits in urothelial carcinoma. *PLoS ONE*, *7*(6). https://doi.org/10.1371/journal.pone.0038863

Lindsey, J. B., & Hillis, L. D. (2007). Clinical update: atrial septal defect in adults. In *Lancet* (Vol. 369, Issue 9569, pp. 1244–1246). Elsevier Limited. https://doi.org/10.1016/S0140-6736(07)60576-5

Lindskrog, S., Prip, F., Lamy, P., Taber, A., Groeneveld, C., Birkenkamp-Demtroder, K., Jensen, J., Strandgaard, T., Nordentoft, I., Christensen, E., Sokac, M., Birkbak, N., Maretty, L., Hermann, G., Petersen, A., Weyerer, V., Grimm, M.-O., Horstmann, M., Sjodahl, G., … Dyrskjot, L. (2020). *An integrated multi-omics analysis identifies clinically relevant molecular subtypes of non-muscle-invasive bladder cancer*. https://doi.org/10.1101/2020.06.19.20054809

Liu, C., Tate, T., Batourina, E., Truschel, S. T., Potter, S., Adam, M., Xiang, T., Picard, M., Reiley, M., Schneider, K., Tamargo, M., Lu, C., Chen, X., He, J., Kim, H., & Mendelsohn, C. L. (2019). Pparg promotes differentiation and regulates mitochondrial gene expression in bladder epithelial cells. *Nature Communications*, *10*(1). https://doi.org/10.1038/s41467-019-12332-0

Logothetou-Rellaa, H., Neslandb, J. M., Karayiannisc, A., & Dimopoulosc, C. (1988). Growth Characteristics of Cultured Human Normal Bladder Epithelial Cells: A Comparison with Urothelial Carcinoma Cell Cultures. In *Eur Urol* (Vol. 15).

Loiselle, J. J., Roy, J. G., & Sutherland, L. C. (2017). RBM10 promotes transformation-associated processes in small cell lung cancer and is directly regulated by RBM5. *PLoS ONE*, *12*(6). https://doi.org/10.1371/journal.pone.0180258

Loiselle, J. J., & Sutherland, L. C. (2018). RBM10: Harmful or helpful-many factors to consider. *Journal of Cellular Biochemistry*, *119*(5), 3809–3818. https://doi.org/10.1002/jcb.26644

López-Knowles, E., Hernández, S., Malats, N., Kogevinas, M., Lloreta, J., Carrato, A., Tardón, A., Serra, C., & Real, F. X. (2006). PIK3CA mutations are an early genetic alteration associated with FGFR3 mutations in superficial papillary bladder tumors. *Cancer Research*, *66*(15), 7401–7404. https://doi.org/10.1158/0008-5472.CAN-06-1182

Lukong, K. E., Chang, K. wei, Khandjian, E. W., & Richard, S. (2008). RNA-binding proteins in human genetic disease. In *Trends in Genetics* (Vol. 24, Issue 8, pp. 416–425). https://doi.org/10.1016/j.tig.2008.05.004

Ma, F., Fuqua, B. K., Hasin, Y., Yukhtman, C., Vulpe, C. D., Lusis, A. J., & Pellegrini, M. (2019). A comparison between whole transcript and 3' RNA sequencing methods using Kapa and Lexogen library preparation methods 06 Biological Sciences 0604 Genetics. *BMC Genomics*, *20*(1). https://doi.org/10.1186/s12864-018-5393-3

Majewski, T., Lee, S., Jeong, J., Yoon, D. S., Kram, A., Kim, M. S., Tuziak, T., Bondaruk, J., Lee, S., Park, W. S., Tang, K. S., Chung, W., Shen, L., Ahmed, S. S., Johnston, D. A., Grossman, H. B., Dinney, C. P., Zhou, J. H., Harris, R. A., … Czerniak, B. (2008). Understanding the development of human bladder cancer by using a whole-organ genomic mapping strategy. *Laboratory Investigation*, *88*(7), 694–721. https://doi.org/10.1038/labinvest.2008.27

Majewski, T., Yao, H., Bondaruk, J., Chung, W., Lee, S., Lee, J. G., Zhang, S., Cogdell, D., Yang, G., Choi, W., Dinney, C., Grossman, H. B., Logothetis, C., Scherer, S. E., Guo, C. C., Zhang, L., Wei, P., Weinstein, J. N., Issa, J. P., … Czerniak, B. (2019). Whole-Organ Genomic Characterization of Mucosal Field Effects Initiating Bladder Carcinogenesis. *Cell Reports*, *26*(8), 2241-2256.e4. https://doi.org/10.1016/j.celrep.2019.01.095

Makeyev, E. V., Zhang, J., Carrasco, M. A., & Maniatis, T. (2007). The MicroRNA miR-124 Promotes Neuronal Differentiation by Triggering Brain-Specific Alternative Pre-mRNA Splicing. *Molecular Cell*, *27*(3), 435–448. https://doi.org/10.1016/j.molcel.2007.07.015

Makishima, H., Visconte, V., Sakaguchi, H., Jankowska, A. M., Kar, S. A., Jerez, A., Przychodzen, B., Bupathi, M., Guinta, K., Afable, M. G., Sekeres, M. A., Padgett, R. A., Tiu, R. V., & Maciejewski, J. P. (2012). Mutations in the spliceosome machinery, a novel and ubiquitous pathway in leukemogenesis. *Blood*, *119*(14), 3203–3210. https://doi.org/10.1182/blood-2011-12-399774

Malats, N., & Real, F. X. (2015). Epidemiology of Bladder Cancer. In *Hematology/Oncology Clinics of North America* (Vol. 29, Issue 2, pp. 177–189). W.B. Saunders. https://doi.org/10.1016/j.hoc.2014.10.001

Manfredi, J. J. (2010). The Mdm2-p53 relationship evolves: Mdm2 swings both ways as an oncogene and a tumor suppressor. In *Genes and Development* (Vol. 24, Issue 15, pp. 1580–1589). https://doi.org/10.1101/gad.1941710

Manousiouthakis, E., Mendez, M., Garner, M. C., Exertier, P., & Makita, T. (2014). Venous endothelin guides sympathetic innervation of the developing mouse heart. *Nature Communications*, *5*. https://doi.org/10.1038/ncomms4918

Martinez-Arribas, F., Agydo, D., Pollan, M., Gómez-Esquer, F., Díaz-Gil, G., Lucas, R., & Schneider, J. (2006). Positive correlation between the expression of X-chromosome RBM genes (RBMX, RBM3, RBM10) and the proapoptotic Bax gene in human breast cancer. *Journal of Cellular Biochemistry*, *97*(6), 1275–1282. https://doi.org/10.1002/jcb.20725

Marzouka, N. A. D., Lindgren, D., Eriksson, P., Sjödahl, G., Bernardo, C., Liedberg, F., Axelson, H., & Höglund, M. (2020). Recurring urothelial carcinomas show genomic rearrangements incompatible with a direct relationship. *Scientific Reports*, *10*(1). https://doi.org/10.1038/s41598-020-75854-4

Meeks, J. J., & Lerner, S. P. (2017). Molecular Landscape of Non-Muscle Invasive Bladder Cancer. In *Cancer Cell* (Vol. 32, Issue 5, pp. 550–551). Cell Press. https://doi.org/10.1016/j.ccell.2017.08.015

Miedzybrodzka, Z. (2003). Congenital talipes equinovarus (clubfoot): a disorder of the foot but not the hand. In *J. Anat* (Vol. 202).

Migeon, B. R. (2008). X inactivation, female mosaicism, and sex differences in renal diseases. In *Journal of the American Society of Nephrology* (Vol. 19, Issue 11, pp. 2052–2059). https://doi.org/10.1681/ASN.2008020198

Mitra, A. P., Birkhahn, M., & Cote, R. J. (2007). p53 and retinoblastoma pathways in bladder cancer. In *World Journal of Urology* (Vol. 25, Issue 6, pp. 563–571). https://doi.org/10.1007/s00345-007-0197-0

Miura, S., & Suzuki, A. (2017). Generation of Mouse and Human Organoid-Forming Intestinal Progenitor Cells by Direct Lineage Reprogramming. *Cell Stem Cell*, *21*(4), 456-471.e5. https://doi.org/10.1016/j.stem.2017.08.020

Moch, H., Cubilla, A. L., Humphrey, P. A., Reuter, V. E., & Ulbright, T. M. (2016). The 2016 WHO Classification of Tumours of the Urinary System and Male Genital Organs—Part A: Renal, Penile, and Testicular Tumours. *European Urology*, *70*(1), 93–105. https://doi.org/10.1016/j.eururo.2016.02.029

Mohan, N., Kumar, V., Kandala, D. T., Kartha, C. C., & Laishram, R. S. (2018). A Splicing-Independent Function of RBM10 Controls Specific 3′ UTR Processing to Regulate Cardiac Hypertrophy. *Cell Reports*, *24*(13), 3539–3553. https://doi.org/10.1016/j.celrep.2018.08.077

Moon, A. M., Capecchi, M. R., & Genet, N. (2000). Fgf8 is required for outgrowth and patterning of the limbs NIH Public Access Author Manuscript. In *Nat Genet* (Vol. 26, Issue 4).

Möröy, T., & Heyd, F. (2007). The impact of alternative splicing in vivo: Mouse models show the way. In *RNA* (Vol. 13, Issue 8, pp. 1155–1171). Cold Spring Harbor Laboratory Press. https://doi.org/10.1261/rna.554607

Morrison, C. D., Liu, P., Woloszynska-Read, A., Zhang, J., Luo, W., Qin, M., Bshara, W., Conroy, J. M., Sabatini, L., Vedell, P., Xiong, D., Liu, S., Wang, J., Shen, H.,

Li, Y., Omilian, A. R., Hill, A., Head, K., Guru, K., … Trump, D. L. (2014). Whole-genome sequencing identifies genomic heterogeneity at a nucleotide and chromosomal level in bladder cancer. *Proceedings of the National Academy of Sciences of the United States of America*, *111*(6). https://doi.org/10.1073/pnas.1313580111

Mullenders, J., de Jongh, E., Brousali, A., Roosen, M., Blom, J. P. A., Begthel, H., Korving, J., Jonges, T., Kranenburg, O., Meijer, R., & Clevers, H. C. (2019). Mouse and human urothelial cancer organoids: A tool for bladder cancer research. *Proceedings of the National Academy of Sciences of the United States of America*, *116*(10), 4567–4574. https://doi.org/10.1073/pnas.1803595116

Nanjo, S., Wu, W., Karachaliou, N., Blakely, C. M., Suzuki, J., Ali, S., Lucas Kerr, D., Olivas, V., Shue, J., Rotow, J., Mayekar, M., Haderk, F., Chatterjee, N., Urisman, A., Kirichok, Y., Tan, D. S. W., Rosell, R., Okimoto, R. A., & Bivona, T. G. (n.d.). *Title: Deficiency of the splicing factor RBM10 limits EGFR inhibitor response in EGFR mutant lung cancer*. https://doi.org/10.1101/2020.10.26.356352

Naqvi, N., McCarthy, K. P., & Ho, S. Y. (2018). Anatomy of the atrial septum and interatrial communications. In *Journal of Thoracic Disease* (Vol. 10, pp. S2837–S2847). AME Publishing Company. https://doi.org/10.21037/jtd.2018.02.18

Nassar, A. H., Umeton, R., Kim, J., Lundgren, K., Harshman, L. C., Van Allen, E. M., Preston, M. A., Dong, F., Bellmunt, J., Mouw, K. W., Choueiri, T. K., Sonpavde, G., & Kwiatkowski, D. J. (2018). Mutational analysis of 472 urothelial carcinoma across grades and anatomic sites. *Clinical Cancer Research*. https://doi.org/10.1158/1078-0432.CCR-18-3147

Navas, C., Hernández-Porras, I., Schuhmacher, A. J., Sibilia, M., Guerra, C., & Barbacid, M. (2012). EGF Receptor Signaling Is Essential for K-Ras Oncogene-Driven Pancreatic Ductal Adenocarcinoma. *Cancer Cell*, *22*(3), 318–330. https://doi.org/10.1016/j.ccr.2012.08.001

Neal, J. T., Li, X., Zhu, J., Giangarra, V., Grzeskowiak, C. L., Ju, J., Liu, I. H., Chiou, S. H., Salahudeen, A. A., Smith, A. R., Deutsch, B. C., Liao, L., Zemek, A. J., Zhao, F., Karlsson, K., Schultz, L. M., Metzner, T. J., Nadauld, L. D., Tseng, Y. Y., … Kuo, C. J. (2018). Organoid Modeling of the Tumor Immune Microenvironment. *Cell*. https://doi.org/10.1016/j.cell.2018.11.021

NICE. (2017). Bladder cancer: diagnosis and management of bladder cancer. In *BJU International* (Vol. 120, Issue 6, pp. 755–765). Blackwell Publishing Ltd. https://doi.org/10.1111/bju.14045

Niceta, M., Barresi, S., Pantaleoni, F., Capolino, R., Dentici, M. L., Ciolfi, A., Pizzi, S., Bartuli, A., Dallapiccola, B., Tartaglia, M., & Digilio, M. C. (2018). TARP syndrome: Long-term survival, anatomic patterns of congenital heart defects, differential diagnosis and pathogenetic considerations. *European Journal of Medical Genetics*. https://doi.org/10.1016/j.ejmg.2018.09.001

Nie, J., & Hashino, E. (2017). Organoid technologies meet genome engineering. *EMBO Reports*, *18*(3), 367–376. https://doi.org/10.15252/embr.201643732

Nilsen, T. W., & Graveley, B. R. (2010). Expansion of the eukaryotic proteome by alternative splicing. In *Nature* (Vol. 463, Issue 7280, pp. 457–463). https://doi.org/10.1038/nature08909

Nishiyama, N., Arai, E., Nagashio, R., Fujimoto, H., Hosoda, F., Shibata, T., Tsukamoto, T., Yokoi, S., Imoto, I., Inazawa, J., & Kanai, Y. (2011). Copy number alterations in urothelial carcinomas: Their clinicopathological significance and correlation with DNA methylation alterations. *Carcinogenesis*, *32*(4), 462–469. https://doi.org/10.1093/carcin/bgq274

Nordentoft, I., Lamy, P., Birkenkamp-Demtröder, K., Shumansky, K., Vang, S., Hornshøj, H., Juul, M., Villesen, P., Hedegaard, J., Roth, A., Thorsen, K., Høyer, S., Borre, M., Reinert, T., Fristrup, N., Dyrskjøt, L., Shah, S., Pedersen, J. S., & Ørntoft, T. F. (2014). Mutational context and diverse clonal development in early and late bladder cancer. *Cell Reports*, *7*(5), 1649–1663. https://doi.org/10.1016/j.celrep.2014.04.038

Nozima, B. H., Mendes, T. B., Da Silva Pereira, G. J., Araldi, R. P., Miazato Iwamura, E. S., Smaili, S. S., Griz Carvalheira, G. M., & Cerutti, J. M. (2019). FAM129A regulates autophagy in thyroid carcinomas in an oncogene-dependent manner. *Endocrine-Related Cancer*, *26*(1), 227–238. https://doi.org/10.1530/ERC-17-0530

Nurtdinov, R. N., Artamonova, I. I., Mironov, A. A., & Gelfand, M. S. (2003). Low conservation of alternative splicing patterns in the human and mouse genomes. *Human Molecular Genetics*, *12*(11), 1313–1320. https://doi.org/10.1093/hmg/ddg137

Obeng, E. A., Stewart, C., & Abdel-Wahab, O. (2019). Altered RNA processing in cancer pathogenesis and therapy. In *Cancer Discovery* (Vol. 9, Issue 11, pp. 1493–1510). American Association for Cancer Research Inc. https://doi.org/10.1158/2159-8290.CD-19-0399

Pablo Baeza-Centurion, A., Miñ ana, B., rn Schmiedel, J. M., Valcá rcel, J., Lehner Correspondence, B., Baeza-Centurion, P., & Lehner, B. (2019). Combinatorial Genetics Reveals a Scaling Law for the Effects of Mutations on Splicing In Brief A quantitative, predictive model for alternative splicing decisions explains the probability of exon inclusion in the context of natural and disease-associated . *Cell*, *176*, 549–563. https://doi.org/10.1016/j.cell.2018.12.010

Pällmann, N., Livgård, M., Tesikova, M., Zeynep Nenseth, H., Akkus, E., Sikkeland, J., Jin, Y., Koc, D., Kuzu, O. F., Pradhan, M., Danielsen, H. E., Kahraman, N., Mokhlis, H. M., Ozpolat, B., Banerjee, P. P., Uren, A., Fazli, L., Rennie, P. S., Jin, Y., & Saatcioglu, F. (2019). Regulation of the unfolded protein response through ATF4 and FAM129A in prostate cancer. *Oncogene*, *38*(35), 6301–6318. https://doi.org/10.1038/s41388-019-0879-2

Pan, C. X., Zhang, H., Tepper, C. G., Lin, T. Y., Davis, R. R., Keck, J., Ghosh, P. M., Gill, P., Airhart, S., Bult, C., Gandara, D. R., Liu, E., & De Vere White, R. W. (2015). Development and characterization of bladder cancer patient- derived xenografts for molecularly guided targeted therapy. *PLoS ONE*, *10*(8). https://doi.org/10.1371/journal.pone.0134346

Pan, Q., Shai, O., Lee, L. J., Frey, B. J., & Blencowe, B. J. (2008). Deep surveying of alternative splicing complexity in the human transcriptome by high-throughput sequencing. *Nature Genetics*, *40*(12), 1413–1415. https://doi.org/10.1038/ng.259

Papaemmanuil, E., Gerstung, M., Malcovati, L., Tauro, S., Gundem, G., Van Loo, P., Yoon, C. J., Ellis, P., Wedge, D. C., Pellagatti, A., Shlien, A., Groves, M. J., Forbes, S. A., Raine, K., Hinton, J., Mudie, L. J., McLaren, S., Hardy, C., Latimer, C., … Campbell, P. J. (2013). Clinical and biological implications of driver mutations in myelodysplastic syndromes. *Blood*, *122*(22), 3616–3627. https://doi.org/10.1182/blood-2013-08-518886

Papasaikas, P., & Valcárcel, J. (2016). The Spliceosome: The Ultimate RNA Chaperone and Sculptor. In *Trends in Biochemical Sciences* (Vol. 41, Issue 1). https://doi.org/10.1016/j.tibs.2015.11.003

Pascau, J., Vaquero, J., Abella, M., Cacho, R., Lage, E., & Desco, M. (n.d.). *MULTIMODALITY WORKSTATION FOR SMALL ANIMAL IMAGE VISUALIZATION AND ANALYSIS*.

Pauli, C., Hopkins, B. D., Prandi, D., Shaw, R., Fedrizzi, T., Sboner, A., Sailer, V., Augello, M., Puca, L., Rosati, R., McNary, T. J., Churakova, Y., Cheung, C., Triscott, J., Pisapia, D., Rao, R., Mosquera, J. M., Robinson, B., Faltas, B. M., … Rubin, M. A. (2017). Personalized in vitro and in vivo cancer models to guide precision medicine. *Cancer Discovery*, *7*(5), 462–477. https://doi.org/10.1158/2159-8290.CD-16-1154

Piedrafita, G., Fernández, L. C., & Real, F. X. (2020). Mutations in non-tumoral human urothelium: Disease prelude or epilogue? In *Bladder Cancer* (Vol. 6, Issue 3, pp. 249–252). IOS Press BV. https://doi.org/10.3233/BLC-200363

Pietzak, E. J., Bagrodia, A., Cha, E. K., Drill, E. N., Iyer, G., Isharwal, S., Ostrovnaya, I., Baez, P., Li, Q., Berger, M. F., Zehir, A., Schultz, N., Rosenberg, J. E., Bajorin, D. F., Dalbagni, G., Al-Ahmadie, H., Solit, D. B., & Bochner, B. H. (2017). Next-generation Sequencing of Nonmuscle Invasive Bladder Cancer Reveals Potential Biomarkers and Rational Therapeutic Targets. *European Urology*, *72*(6), 952–959. https://doi.org/10.1016/j.eururo.2017.05.032

Platt, F. M., Hurst, C. D., Taylor, C. F., Gregory, W. M., Harnden, P., & Knowles, M. A. (2009). Spectrum of phosphatidylinositol 3-kinase pathway gene alterations in bladder cancer. *Clinical Cancer Research*, *15*(19), 6008–6017. https://doi.org/10.1158/1078-0432.CCR-09-0898

Plimack, E. R., Dunbrack, R. L., Brennan, T. A., Andrake, M. D., Zhou, Y., Serebriiskii, I. G., Slifker, M., Alpaugh, K., Dulaimi, E., Palma, N., Hoffman-Censits, J., Bilusic, M., Wong, Y. N., Kutikov, A., Viterbo, R., Greenberg, R. E., Chen, D. Y. T., Lallas, C. D., Trabulsi, E. J., … Ross, E. A. (2015). Defects in DNA Repair Genes Predict Response to Neoadjuvant Cisplatin-based Chemotherapy in Muscle-invasive Bladder Cancer. *European Urology*, *68*(6), 959–967. https://doi.org/10.1016/j.eururo.2015.07.009

Ploeg, M., Aben, K. K. H., & Kiemeney, L. A. (2009). The present and future burden of urinary bladder cancer in the world. *World Journal of Urology*, *27*(3), 289–293. https://doi.org/10.1007/s00345-009-0383-3

Powis, Z., Hart, A., Cherny, S., Petrik, I., Palmaer, E., Tang, S., & Jones, C. (2017). Clinical diagnostic exome evaluation for an infant with a lethal disorder: Genetic diagnosis of TARP syndrome and expansion of the phenotype in a patient with a newly reported RBM10 alteration. *BMC Medical Genetics*, *18*(1). https://doi.org/10.1186/s12881-017-0426-3

Puzio-Kuter, A. M., Castillo-Martin, M., Kinkade, C. W., Wang, X., Shen, T. H., Matos, T., Shen, M. M., Cordon-Cardo, C., & Abate-Shen, C. (2009). Inactivation of p53 and Pten promotes invasive bladder cancer. *Genes and Development*, *23*(6), 675–680. https://doi.org/10.1101/gad.1772909

Rabbitts, T. H. (2001). Tumor Necrosis Factor (TNF). In *Encyclopedia of Genetics* (p. 2081). Elsevier. https://doi.org/10.1006/rwgn.2001.1627

Rampias, T., Vgenopoulou, P., Avgeris, M., Polyzos, A., Stravodimos, K., Valavanis, C., Scorilas, A., & Klinakis, A. (2014). A new tumor suppressor role for the Notch pathway in bladder cancer. *Nature Medicine*, *20*(10), 1199–1205. https://doi.org/10.1038/nm.3678

Rasheed, S., Gardner, M. B., Rongey, R. W., Nelson-Rees, W. A., & Arnstein, P. (1977). *Human Bladder Carcinoma: Characterization of Two New Tumor Cell Lines and Search for Tumor Viruses1, 2, 3 J NATL CANCER INST* (Vol. 58, Issue 4). https://academic.oup.com/jnci/article-abstract/58/4/881/908786

Rebouissou, S., Bernard-Pierrot, I., De Reyniès, A., Lepage, M.-L., Krucker, C., Chapeaublanc, E., Hérault, A., Kamoun, A., Caillault, A., Letouzé, E., Elarouci, N., Neuzillet, Y., Denoux, Y., Molinié, V., Vordos, D., Laplanche, A., Maillé, P., Soyeux, P., Ofualuka, K., … Radvanyi, F. (n.d.). *EGFR as a potential therapeutic target for a subset of muscle-invasive bladder cancers presenting a basal-like phenotype*. www.ScienceTranslationalMedicine.org

Rebouissou, S., Hérault, A., Letouzé, E., Neuzillet, Y., Laplanche, A., Ofualuka, K., Maillé, P., Leroy, K., Riou, A., Lepage, M. L., Vordos, D., De La Taille, A., Denoux, Y., Sibony, M., Guyon, F., Lebret, T., Benhamou, S., Allory, Y., & Radvanyi, F. (2012). CDKN2A homozygous deletion is associated with muscle invasion in FGFR3-mutated urothelial bladder carcinoma. *Journal of Pathology*, *227*(3), 315–324. https://doi.org/10.1002/path.4017

Revil, T., Gaffney, D., Dias, C., Majewski, J., & Jerome-Majewska, L. A. (2010). Alternative splicing is frequent during early embryonic development in mouse. *BMC Genomics*, *11*(1). https://doi.org/10.1186/1471-2164-11-399

Riley, B. M., Mansilla, M. A., Ma, J., Daack-Hirsch, S., Maher, B. S., Raffensperger, L. M., Russo, E. T., Vieira, A. R., Dodé, C., Mohammadi, M., Marazita, M. L., & Murray, J. C. (2007). *Impaired FGF signaling contributes to cleft lip and palate*. www.pnas.org/cgi/content/full/

Ringuette-Goulet, C., Bolduc, S., & Pouliot, F. (2018). Modeling human bladder cancer. *World Journal of Urology*, *36*(11), 1759–1766. https://doi.org/10.1007/s00345-018-2369-5

Robertson, A. G., Groeneveld, C. S., Jordan, B., Lin, X., McLaughlin, K. A., Das, A., Fall, L. A., Fantini, D., Taxter, T. J., Mogil, L. S., Lindskrog, S. V., Dyrskjøt, L., McConkey, D. J., Svatek, R. S., de Reyniès, A., Castro, M. A. A., & Meeks, J. J.

(2020). Identification of Differential Tumor Subtypes of T1 Bladder Cancer. *European Urology*, *78*(4), 533–537. https://doi.org/10.1016/j.eururo.2020.06.048

Robertson, A. G., Kim, J., Al-Ahmadie, H., Bellmunt, J., Guo, G., Cherniack, A. D., Hinoue, T., Laird, P. W., Hoadley, K. A., Akbani, R., Castro, M. A. A., Gibb, E. A., Kanchi, R. S., Gordenin, D. A., Shukla, S. A., Sanchez-Vega, F., Hansel, D. E., Czerniak, B. A., Reuter, V. E., … Zwarthoff, E. C. (2017). Comprehensive Molecular Characterization of Muscle-Invasive Bladder Cancer. *Cell*, *171*(3), 540-556.e25. https://doi.org/10.1016/j.cell.2017.09.007

Rochel, N., Krucker, C., Coutos-Thévenot, L., Osz, J., Zhang, R., Guyon, E., Zita, W., Vanthong, S., Hernandez, O. A., Bourguet, M., Badawy, K. Al, Dufour, F., Peluso-Iltis, C., Heckler-Beji, S., Dejaegere, A., Kamoun, A., de Reyniès, A., Neuzillet, Y., Rebouissou, S., … Bernard-Pierrot, I. (2019). Recurrent activating mutations of PPARγ associated with luminal bladder tumors. *Nature Communications*, *10*(1). https://doi.org/10.1038/s41467-018-08157-y

Rodor, J., FitzPatrick, D. R., Eyras, E., & Cáceres, J. F. (2017). The RNA-binding landscape of RBM10 and its role in alternative splicing regulation in models of mouse early development. *RNA Biology*, *14*(1), 45–57. https://doi.org/10.1080/15476286.2016.1247148

Roskoski, R. (2015). Src protein-tyrosine kinase structure, mechanism, and small molecule inhibitors This paper is dedicated to the memory of Prof. Donald F. Steiner (1930-2014) - Advisor, mentor, and discoverer of proinsulin. In *Pharmacological Research* (Vol. 94, pp. 9–25). Academic Press. https://doi.org/10.1016/j.phrs.2015.01.003

Rossi, G., Manfrin, A., & Lutolf, M. P. (2018). Progress and potential in organoid research. In *Nature Reviews Genetics*. https://doi.org/10.1038/s41576-018-0051-9

Ruan, J. L., Hsu, J. W., Browning, R. J., Stride, E., Yildiz, Y. O., Vojnovic, B., & Kiltie, A. E. (2019). Mouse Models of Muscle-invasive Bladder Cancer: Key Considerations for Clinical Translation Based on Molecular Subtypes. In *European Urology Oncology* (Vol. 2, Issue 3, pp. 239–247). Elsevier B.V. https://doi.org/10.1016/j.euo.2018.08.014

Runkle, K. B., Kharbanda, A., Stypulkowski, E., Cao, X. J., Wang, W., Garcia, B. A., & Witze, E. S. (2016). Inhibition of DHHC20-Mediated EGFR Palmitoylation Creates a Dependence on EGFR Signaling. *Molecular Cell*, *62*(3), 385–396. https://doi.org/10.1016/j.molcel.2016.04.003

Saha, S., Paoletti, S., Robertson, D. Persistent left superior vena cava considerations in fetal, pediatric and adult populations. AJUM, 2, 61-66 (2012).

Sakai, K., & Miyazaki, J.-I. (1997). A Transgenic Mouse Line That Retains Cre Recombinase Activity in Mature Oocytes Irrespective of the cre Transgene Transmission. In *BIOCHEMICAL AND BIOPHYSICAL RESEARCH COMMUNICATIONS* (Vol. 237).

Samarel, A. M. (2014). Focal adhesion signaling in heart failure. In *Pflugers Archiv European Journal of Physiology* (Vol. 466, Issue 6, pp. 1101–1111). Springer Verlag. https://doi.org/10.1007/s00424-014-1456-8

Sampath, J., & Pelus, L. M. (2007). Alternative Splice Variants of Survivin as Potential Targets in Cancer. In *Current Drug Discovery Technologies* (Vol. 4).

Sanchez-Carbayo, M., Socci, N. D., Jose Lozano, J., Haab, B. B., & Cordon-Cardo, C. (2006). Profiling Bladder Cancer Using Targeted Antibody Arrays. *Am J Pathol*, *168*, 93–103. https://doi.org/10.2353/ajpath.2006

Santos, C. P., Lapi, E., Martínez de Villarreal, J., Álvaro-Espinosa, L., Fernández-Barral, A., Barbáchano, A., Domínguez, O., Laughney, A. M., Megías, D., Muñoz, A., & Real, F. X. (2019). Urothelial organoids originating from Cd49fhigh mouse stem cells display Notch-dependent differentiation capacity. *Nature Communications*, *10*(1), 4407. https://doi.org/10.1038/s41467-019-12307-1

Sato, T., Stange, D. E., Ferrante, M., Vries, R. G. J., Van Es, J. H., Van Den Brink, S., Van Houdt, W. J., Pronk, A., Van Gorp, J., Siersema, P. D., & Clevers, H. (2011). Long-term expansion of epithelial organoids from human colon, adenoma, adenocarcinoma, and Barrett's epithelium. *Gastroenterology*, *141*(5), 1762–1772. https://doi.org/10.1053/j.gastro.2011.07.050

Sato, T., Vries, R. G., Snippert, H. J., Van De Wetering, M., Barker, N., Stange, D. E., Van Es, J. H., Abo, A., Kujala, P., Peters, P. J., & Clevers, H. (2009). Single Lgr5 stem cells build crypt-villus structures in vitro without a mesenchymal niche. *Nature*, *459*(7244), 262–265. https://doi.org/10.1038/nature07935

Seiler, M., Peng, S., Agrawal, A. A., Palacino, J., Teng, T., Zhu, P., Smith, P. G., Caesar-Johnson, S. J., Demchok, J. A., Felau, I., Kasapi, M., Ferguson, M. L., Hutter, C. M., Sofia, H. J., Tarnuzzer, R., Wang, Z., Yang, L., Zenklusen, J. C., Zhang, J. (Julia), … Yu, L. (2018). Somatic Mutational Landscape of Splicing Factor Genes and Their Functional Consequences across 33 Cancer Types. *Cell Reports*. https://doi.org/10.1016/j.celrep.2018.01.088

Seino, T., Kawasaki, S., Shimokawa, M., Tamagawa, H., Toshimitsu, K., Fujii, M., Ohta, Y., Matano, M., Nanki, K., Kawasaki, K., Takahashi, S., Sugimoto, S., Iwasaki, E., Takagi, J., Itoi, T., Kitago, M., Kitagawa, Y., Kanai, T., & Sato, T. (2018). Human Pancreatic Tumor Organoids Reveal Loss of Stem Cell Niche Factor Dependence during Disease Progression. *Cell Stem Cell*, *22*(3), 454-467.e6. https://doi.org/10.1016/j.stem.2017.12.009

Shao, W., & Wang, T. (n.d.). *Transcript assembly improves expression quantification of transposable 1 elements in single cell RNA-seq data*. https://doi.org/10.1101/2020.07.31.231027

Sharpless, N. E., & DePinho, R. A. (2006). The mighty mouse: Genetically engineered mouse models in cancer drug development. In *Nature Reviews Drug Discovery* (Vol. 5, Issue 9, pp. 741–754). https://doi.org/10.1038/nrd2110

Shorning, B. Y., Griffiths, D., & Clarke, A. R. (2011). Lkb1 and Pten synergise to suppress mTOR-Mediated tumorigenesis and epithelial-mesenchymal transition in the mouse bladder. *PLoS ONE*, *6*(1). https://doi.org/10.1371/journal.pone.0016209

Shultz, M. A., Morin, D., Chang, A.-M., & Buckpitt, A. (2001). *Metabolic Capabilities of CYP2F2 with Various Pulmonary Toxicants and Its Relative Abundance in Mouse Lung Subcompartments*. http://jpet.aspetjournals.org

Sjödahl, G. (2018). Molecular subtype profiling of urothelial carcinoma using a subtype-specific immunohistochemistry panel. In *Methods in Molecular Biology* (Vol. 1655, pp. 53–64). Humana Press Inc. https://doi.org/10.1007/978-1-4939-7234-0_5

Sjödahl, G., Lauss, M., Gudjonsson, S., Liedberg, F., Halldén, C., Chebil, G., Månsson, W., Höglund, M., & Lindgren, D. (2011). A systematic study of gene mutations in urothelial carcinoma; inactivating mutations in tsc2 and pik3r1. *PLoS ONE*, *6*(4). https://doi.org/10.1371/journal.pone.0018583

Sjödahl, G., Lauss, M., Lövgren, K., Chebil, G., Gudjonsson, S., Veerla, S., Patschan, O., Aine, M., Fernö, M., Ringnér, M., Månsson, W., Liedberg, F., Lindgren, D., & Höglund, M. (2012). A molecular taxonomy for urothelial carcinoma. *Clinical Cancer Research*, *18*(12), 3377–3386. https://doi.org/10.1158/1078-0432.CCR-12-0077-T

Smith, A. B., Deal, A. M., Woods, M. E., Wallen, E. M., Pruthi, R. S., Chen, R. C., Milowsky, M. I., & Nielsen, M. E. (2014). Muscle-invasive bladder cancer: Evaluating treatment and survival in the National Cancer Data Base. *BJU International*, *114*(5), 719–726. https://doi.org/10.1111/bju.12601

Strandgaard, T., Nordentoft, I., Lamy, P., Christensen, E., Thomsen, M. B. H., Jensen, J. B., & Dyrskjøt, L. (2020). Mutational Analysis of Field Cancerization in Bladder Cancer. *Bladder Cancer*, *6*(3), 253–264. https://doi.org/10.3233/blc-200282

Sun, X., Jia, M., Sun, W., Feng, L., Gu, C., & Wu, T. (2018). Functional role of RBM10 in lung adenocarcinoma proliferation. *International Journal of Oncology*. https://doi.org/10.3892/ijo.2018.4643

Sun, Y., Bao, Y., Han, W., Song, F., Shen, X., Zhao, J., Zuo, J., Saffen, D., Chen, W., Wang, Z., You, X., & Wang, Y. (2017). Autoregulation of RBM10 and cross-regulation of RBM10/RBM5 via alternative splicing-coupled nonsense-mediated decay. *Nucleic Acids Research*, *45*(14), 8524–8540. https://doi.org/10.1093/nar/gkx508

Sutherland, L. C., Rintala-Maki, N. D., White, R. D., & Morin, C. D. (2005). RNA Binding Motif (RBM) proteins: A novel family of apoptosis modulators? In *Journal of Cellular Biochemistry* (Vol. 94, Issue 1, pp. 5–24). https://doi.org/10.1002/jcb.20204

Sutherland, L. C., Thibault, P., Durand, M., Lapointe, E., Knee, J. M., Beauvais, A., Kalatskaya, I., Hunt, S. C., Loiselle, J. J., Roy, J. G., Tessier, S. J., Ybazeta, G., Stein, L., Kothary, R., Klinck, R., & Chabot, B. (2017). Splicing arrays reveal novel RBM10 targets, including SMN2 pre-mRNA. *BMC Molecular Biology*, *18*(1). https://doi.org/10.1186/s12867-017-0096-x

Tan, T. Z., Rouanne, M., Tan, K. T., Huang, R. Y. J., & Thiery, J. P. (2019). Molecular Subtypes of Urothelial Bladder Cancer: Results from a Meta-cohort Analysis of 2411 Tumors. *European Urology*, *75*(3), 423–432. https://doi.org/10.1016/j.eururo.2018.08.027

Tang, Y., Horikawa, I., Ajiro, M., Robles, A. I., Fujita, K., Mondal, A. M., Stauffer, J. K., Zheng, Z. M., & Harris, C. C. (2013). Down-regulation of splicing factor SRSF3 induces p53β, an alternatively spliced isoform of p53 that promotes cellular senescence. *Oncogene*, *32*(22), 2792–2798. https://doi.org/10.1038/onc.2012.288

Thanaraj, T. A., Clark, F., & Muilu, J. (2003). Conservation of human alternative splice events in mouse. *Nucleic Acids Research*, *31*(10), 2544–2552. https://doi.org/10.1093/nar/gkg355

Thiselton, D. L., McDowall, J., Brandau, O., Ramser, J., D'Esposito, F., Bhattacharya, S. S., Ross, M. T., Hardcastle, A. J., & Meindl, A. (2002). An integrated, functionally annotated gene map of the DXS8026-ELK1 interval on human Xp11.3-Xp11.23: Potential hotspot for neurogenetic disorders. *Genomics*, *79*(4), 560–572. https://doi.org/10.1006/geno.2002.6733

Thomsen, M. B. H., Nordentoft, I., Lamy, P., Vang, S., Reinert, L., Mapendano, C. K., Høyer, S., Ørntoft, T. F., Jensen, J. B., & Dyrskjøt, L. (2017). Comprehensive multiregional analysis of molecular heterogeneity in bladder cancer. *Scientific Reports*, *7*(1). https://doi.org/10.1038/s41598-017-11291-0

Tirosh, I., Berman, J., & Barkai, N. (2007). The pattern and evolution of yeast promoter bendability. In *Trends in Genetics* (Vol. 23, Issue 7, pp. 318–321). https://doi.org/10.1016/j.tig.2007.03.015

Tract, U., Elliott, A. Y., Cleveland, P., Cervenka, J., Castro, A. E., Stein, N., Hakala, T. R., & Fraley, E. E. (1974). Characterization of a Cell Line From Human Transitional Cell Cancer of the. In *JOURNAL OF THE NATIONAL CANCER INSTITUTE* (Vol. 53, Issue 5). https://academic.oup.com/jnci/article-abstract/53/5/1341/932467

Trumpp, A., Depew, M. J., Rubenstein, J. L. R., Michael Bishop, J., Martin, G. R., & Hooper, G. W. (1999). Cre-mediated gene inactivation demonstrates that FGF8 is required for cell survival and patterning of the first branchial arch. *Genes and Development*, *13*, 3136–3148. www.genesdev.org

Tyrak, K. W., Hołda, J., Hołda, M. K., Koziej, M., Piatek, K., & Klimek-Piotrowska, W. (2017). Persistent left superior vena cava. *Cardiovascular Journal of Africa*, *28*(3), e1-E4. https://doi.org/10.5830/CVJA-2016-084

Van Allen, E. M., Mouw, K. W., Kim, P., Iyer, G., Wagle, N., Al-Ahmadie, H., Zhu, C., Ostrovnaya, I., Kryukov, G. V., O'connor, K. W., Sfakianos, J., Garcia-Grossman, I., Kim, J., Guancial, E. A., Bambury, R., Bahl, S., Gupta, N., Farlow, D., Qu, A., … Rosenberg, J. E. (2014). Somatic ERCC2 mutations correlate with cisplatin sensitivity in muscle-invasive urothelial carcinoma. *Cancer Discovery*, *4*(10), 1140–1153. https://doi.org/10.1158/2159-8290.CD-14-0623

Van De Wetering, M., Francies, H. E., Francis, J. M., Bounova, G., Iorio, F., Pronk, A., Van Houdt, W., Van Gorp, J., Taylor-Weiner, A., Kester, L., McLaren-Douglas, A., Blokker, J., Jaksani, S., Bartfeld, S., Volckman, R., Van Sluis, P., Li, V. S. W., Seepo, S., Sekhar Pedamallu, C., … Clevers, H. (2015). Prospective derivation of a living organoid biobank of colorectal cancer patients. *Cell*, *161*(4), 933–945. https://doi.org/10.1016/j.cell.2015.03.053

Vasconcelos-Nobrega, C.; Colaco, A.; Lopes, C.; Oliveira, P. A. (2012). BBN as an Urothelial Carcinogen. *In Vivo*, *26*, 727–740.

Végran, F., Boidot, R., Oudin, C., Riedinger, J. M., Bonnetain, F., & Lizard-Nacol, S. (2006). Overexpression of caspase-3s splice variant in locally advanced breast carcinoma is associated with poor response to neoadjuvant chemotherapy.

Clinical Cancer Research, *12*(19), 5794–5800. https://doi.org/10.1158/1078-0432.CCR-06-0725

Venables, J. P., Klinck, R., Bramard, A., Inkel, L., Dufresne-Martin, G., Koh, C. S., Gervais-Bird, J., Lapointe, E., Froehlich, U., Durand, M., Gendron, D., Brosseau, J. P., Thibault, P., Lucier, J. F., Tremblay, K., Prinos, P., Wellinger, R. J., Chabot, B., Rancourt, C., & Elela, S. A. (2008). Identification of alternative splicing markers for breast cancer. *Cancer Research*, *68*(22), 9525–9531. https://doi.org/10.1158/0008-5472.CAN-08-1769

Wang, C. Y., Xu, Z. Bin, Wang, J. P., Jiao, Y., & Zhang, B. (2017). Rb deficiency accelerates progression of carcinoma of the urinary bladder in vivo and in vitro through inhibiting autophagy and apoptosis. *International Journal of Oncology*, *50*(4), 1221–1232. https://doi.org/10.3892/ijo.2017.3889

Wang, E. T., Sandberg, R., Luo, S., Khrebtukova, I., Zhang, L., Mayr, C., Kingsmore, S. F., Schroth, G. P., & Burge, C. B. (2008). Alternative isoform regulation in human tissue transcriptomes. *Nature*, *456*(7221), 470–476. https://doi.org/10.1038/nature07509

Wang, K., Bacon, M. L., Tessier, J. J., Rintala-Maki, N. D., Tang, V., & Sutherland, L. C. (2012). RBM10 Modulates Apoptosis and Influences TNF-α Gene Expression. *Journal of Cell Death*, *5*, JCD.S9073. https://doi.org/10.4137/jcd.s9073

Wang, L. H., Wu, C. F., Rajasekaran, N., & Shin, Y. K. (2019). Loss of tumor suppressor gene function in human cancer: An overview. In *Cellular Physiology and Biochemistry* (Vol. 51, Issue 6, pp. 2647–2693). S. Karger AG. https://doi.org/10.1159/000495956

Wang, L., Šuštić, T., Leite de Oliveira, R., Lieftink, C., Halonen, P., van de Ven, M., Beijersbergen, R. L., van den Heuvel, M. M., Bernards, R., & van der Heijden, M. S. (2017). A Functional Genetic Screen Identifies the Phosphoinositide 3-kinase Pathway as a Determinant of Resistance to Fibroblast Growth Factor Receptor Inhibitors in FGFR Mutant Urothelial Cell Carcinoma [Figure presented]. *European Urology*, *71*(6), 858–862. https://doi.org/10.1016/j.eururo.2017.01.021

WANG, Y., LIU, J., HUANG, B., XU, Y.-M., LI, J., HUANG, L.-F., LIN, J., ZHANG, J., MIN, Q.-H., YANG, W.-M., & WANG, X.-Z. (2015). Mechanism of alternative splicing and its regulation. *Biomedical Reports*, *3*(2), 152–158. https://doi.org/10.3892/br.2014.407

Wang, Y., Gogol-Döring, A., Hu, H., Fröhler, S., Ma, Y., Jens, M., Maaskola, J., Murakawa, Y., Quedenau, C., Landthaler, M., Kalscheuer, V., Wieczorek, D., Wang, Y., Hu, Y., & Chen, W. (2013). Integrative analysis revealed the molecular mechanism underlying RBM10-mediated splicing regulation. *EMBO Molecular Medicine*, *5*(9), 1431–1442. https://doi.org/10.1002/emmm.201302663

Warrick, J. I., Sjödahl, G., Kaag, M., Raman, J. D., Merrill, S., Shuman, L., Chen, G., Walter, V., & DeGraff, D. J. (2019). Intratumoral Heterogeneity of Bladder Cancer by Molecular Subtypes and Histologic Variants [Figure presented]. *European Urology*, *75*(1), 18–22. https://doi.org/10.1016/j.eururo.2018.09.003

Weeber, F., Ooft, S. N., Dijkstra, K. K., & Voest, E. E. (2017). Tumor Organoids as a Pre-clinical Cancer Model for Drug Discovery. In *Cell Chemical Biology* (Vol. 24,

Issue 9, pp. 1092–1100). Elsevier Ltd. https://doi.org/10.1016/j.chembiol.2017.06.012

Weinstein, J. N., Akbani, R., Broom, B. M., Wang, W., Verhaak, R. G. W., McConkey, D., Lerner, S., Morgan, M., Creighton, C. J., Smith, C., Cherniack, A. D., Kim, J., Pedamallu, C. S., Noble, M. S., Al-Ahmadie, H. A., Reuter, V. E., Rosenberg, J. E., F.Bajorin, D., Bochner, B. H., … Eley, G. (2014). Comprehensive molecular characterization of urothelial bladder carcinoma. *Nature*, *507*(7492), 315–322. https://doi.org/10.1038/nature12965

Williams, S. V., Hurst, C. D., & Knowles, M. A. (2013). Oncogenic FGFR3 gene fusions in bladder cancer. *Human Molecular Genetics*, *22*(4), 795–803. https://doi.org/10.1093/hmg/dds486

Wołącewicz, M., Hrynkiewicz, R., Grywalska, E., Suchojad, T., Leksowski, T., Roliński, J., & Niedźwiedzka-Rystwej, P. (2020). Immunotherapy in bladder cancer: Current methods and future perspectives. *Cancers*, *12*(5). https://doi.org/10.3390/cancers12051181

Woldu, S. L., Bagrodia, A., & Lotan, Y. (2017). Guideline of guidelines: non-muscle-invasive bladder cancer. *BJU International*, *119*(3), 371–380. https://doi.org/10.1111/bju.13760

Xerri, L., Parc, P., Brousset, P., Schlaifer, D., Hassoun, J., Reed, J. C., Krajewski, S., & Birnbaum, D. (1996). Predominant expression of the long isoform of Bcl-x (Bcl-xL) in human lymphomas. *Brithis Journal of Haematology*, *92*, 900–906.

Xu, J. J., Smeets, M. F., Tan, S. Y., Wall, M., Purton, L. E., & Walkley, C. R. (2019). Modeling human RNA spliceosome mutations in the mouse: not all mice were created equal. In *Experimental Hematology* (Vol. 70, pp. 10–23). Elsevier Inc. https://doi.org/10.1016/j.exphem.2018.11.001

Xu, X., & Fu, X. D. (2005). Conditional knockout mice to study alternative splicing in vivo. *Methods*, *37*(4), 387–392. https://doi.org/10.1016/j.ymeth.2005.07.019

Xu, X., Yang, D., Ding, J. H., Wang, W., Chu, P. H., Dalton, N. D., Wang, H. Y., Bermingham, J. R., Ye, Z., Liu, F., Rosenfeld, M. G., Manley, J. L., Ross, J., Chen, J., Xiao, R. P., Cheng, H., & Fu, X. D. (2005). ASF/SF2-regulated CaMKIIδ alternative splicing temporally reprograms excitation-contraction coupling in cardiac muscle. *Cell*, *120*(1), 59–72. https://doi.org/10.1016/j.cell.2004.11.036

Yamada, H., Tsutsumi, K., Nakazawa, Y., Shibagaki, Y., Hattori, S., & Ohta, Y. (2016). Src family tyrosine kinase signaling regulates FilGAP through association with RBM10. *PLoS ONE*, *11*(1). https://doi.org/10.1371/journal.pone.0146593

Ye, J., Beetz, N., O'Keeffe, S., Tapia, J. C., Macpherson, L., Chen, W. V., Bassel-Duby, R., Olson, E. N., & Maniatis, T. (2015). HnRNP U protein is required for normal pre-mRNA splicing and postnatal heart development and function. *Proceedings of the National Academy of Sciences of the United States of America*, *112*(23), E3020–E3029. https://doi.org/10.1073/pnas.1508461112

Yeh, C. C., Fan, Y., Yang, Y. L., & Mann, M. J. (2017). Atrial ERK1/2 activation in the embryo leads to incomplete Septal closure: A novel mouse model of atrial Septal

defect. *Journal of Biomedical Science*, *24*(1). https://doi.org/10.1186/s12929-017-0392-2

Yin, L. L., Wen, X. M., Li, M., Xu, Y. M., Zhao, X. F., Li, J., & Wang, X. W. (2018). A gene mutation in RNA-binding protein 10 is associated with lung adenocarcinoma progression and poor prognosis. *Oncology Letters*, *16*(5), 6283–6292. https://doi.org/10.3892/ol.2018.9496

Yoshida, K., Sanada, M., Shiraishi, Y., Nowak, D., Nagata, Y., Yamamoto, R., Sato, Y., Sato-Otsubo, A., Kon, A., Nagasaki, M., Chalkidis, G., Suzuki, Y., Shiosaka, M., Kawahata, R., Yamaguchi, T., Otsu, M., Obara, N., Sakata-Yanagimoto, M., Ishiyama, K., … Ogawa, S. (2011). Frequent pathway mutations of splicing machinery in myelodysplasia. *Nature*, *478*(7367), 64–69. https://doi.org/10.1038/nature10496

Yoshida, T., Sopko, N. A., Kates, M., Liu, X., Joice, G., Mcconkey, D. J., & Bivalacqua, T. J. (2018). Three-dimensional organoid culture reveals involvement of Wnt/β-catenin pathway in proliferation of bladder cancer cells. In *Oncotarget* (Vol. 9, Issue 13). www.impactjournals.com/oncotarget

Zhang, J., & Manley, J. L. (2013). Misregulation of pre-mRNA alternative splicing in cancer. In *Cancer Discovery* (Vol. 3, Issue 11, pp. 1228–1237). https://doi.org/10.1158/2159-8290.CD-13-0253

Zhang, Z.-T., Pak, J., Huang, H.-Y., Shapiro, E., Sun, T.-T., Pellicer, A., & Wu, X.-R. (2001). Role of Ha-ras activation in super®cial papillary pathway of urothelial tumor formation. In *Oncogene* (Vol. 20). www.nature.com/onc

Zhang, Z.-T., Pak, J., Shapiro, E., Sun, T.-T., & Wu, X.-R. (1999). Urothelium-specific Expression of an Oncogene in Transgenic Mice Induced the Formation of Carcinoma in Situ and Invasive Transitional Cell Carcinoma 1. In *CANCER RESEARCH* (Vol. 59).

Zhao, J., Saffen, D., Han, W., Chen, W., You, X., Zuo, J., Song, F., Wang, Z., Sun, Y., Wang, Y., Bao, Y., & Shen, X. (2017). Autoregulation of RBM10 and cross-regulation of RBM10/RBM5 via alternative splicing-coupled nonsense-mediated decay. *Nucleic Acids Research*, *45*(14), 8524–8540. https://doi.org/10.1093/nar/gkx508

Zhao, J., Sun, Y., Huang, Y., Song, F., Huang, Z., Bao, Y., Zuo, J., Saffen, D., Shao, Z., Liu, W., & Wang, Y. (2017). Functional analysis reveals that RBM10 mutations contribute to lung adenocarcinoma pathogenesis by deregulating splicing. *Scientific Reports*, *7*. https://doi.org/10.1038/srep40488

Zheng, S., Damoiseaux, R., Chen, L., & Black, D. L. (2013). A broadly applicable high-throughput screening strategy identifies new regulators of Dlg4 (Psd-95) alternative splicing. *Genome Research*, *23*(6), 998–1007. https://doi.org/10.1101/gr.147546.112

Zhong, Y. L., Long, X. M., Jiang, L. Y., He, B. F., Lin, H., Luo, P., & Jiang, W. (2015). Surgical Treatment of Dextroversion, Isolated Persistent Left Superior Vena Cava Draining into the Left Atrium. *Journal of Cardiac Surgery*, *30*(10), 767–770. https://doi.org/10.1111/jocs.12611

Zhou, Z., & Fu, X. D. (2013). Regulation of splicing by SR proteins and SR protein-specific kinases. In *Chromosoma* (Vol. 122, Issue 3, pp. 191–207). https://doi.org/10.1007/s00412-013-0407-z

Zhu, P., Zhou, W., Wang, J., Puc, J., Ohgi, K. A., Erdjument-Bromage, H., Tempst, P., Glass, C. K., & Rosenfeld, M. G. (2007). A Histone H2A Deubiquitinase Complex Coordinating Histone Acetylation and H1 Dissociation in Transcriptional Regulation. *Molecular Cell*, *27*(4), 609–621. https://doi.org/10.1016/j.molcel.2007.07.024

Zhu, S., Yu, W., Yang, X., Wu, C., & Cheng, F. (2020). Traditional Classification and Novel Subtyping Systems for Bladder Cancer. In *Frontiers in Oncology* (Vol. 10). Frontiers Media S.A. https://doi.org/10.3389/fonc.2020.00102

Ziebold, U., Reza, T., Caron, A., & Lees, J. A. (2001). E2F3 contributes both to the inappropriate proliferation and to the apoptosis arising in Rb mutant embryos. *Genes and Development*, *15*(4), 386–391. https://doi.org/10.1101/gad.858801

Zieger, K., Dyrskjøt, L., Wiuf, C., Jensen, J. L., Andersen, C. L., Jensen, K. M. E., & Ørntoft, T. F. (2005). Role of activating fibroblast growth factor receptor 3 mutations in the development of bladder tumors. *Clinical Cancer Research*, *11*(21), 7709–7719. https://doi.org/10.1158/1078-0432.CCR-05-1130

Zuiverloon, T. C. M., De Jong, F. C., Costello, J. C., & Theodorescu, D. (2018). Systematic Review: Characteristics and Preclinical Uses of Bladder Cancer Cell Lines. In *Bladder Cancer* (Vol. 4, Issue 2, pp. 169–183). IOS Press. https://doi.org/10.3233/BLC-180167